Silentium: Silent Delivery Drone DSE 2018

Technical Report · July 2018
DOI: 10.13140/RG.2.2.18190.25929

13 authors, including:

Jose Ignacio de Alvear Cardenas
Delft University of Technology
1 PUBLICATION **0** CITATIONS
SEE PROFILE

Francesco Avallone
Delft University of Technology
53 PUBLICATIONS **169** CITATIONS
SEE PROFILE

Yvonne Eggers
Delft University of Technology
1 PUBLICATION **0** CITATIONS
SEE PROFILE

Joost Ellerbroek
Delft University of Technology
75 PUBLICATIONS **250** CITATIONS
SEE PROFILE

Silentium

DSE 2018: A Silent Delivery Drone

J. I. de Alvear Cárdenas
Y. Eggers
F. van Hoorn
L. Jou Ferrer
E. Oosterhof
R. Stikker
L. Terenzi
R. Veder
L. A. H. Velthausz
M. van der Waals

Technische Universiteit Delft

TU Delft

This page was intentionally left blank

Silentium

DSE 2018: A Silent Delivery Drone

by

José Ignacio de Alvear Cárdenas	4463196
Yvonne Eggers	4444922
Flip van Hoorn	4303717
Laura Jou Ferrer	4456734
Edzer Oosterhof	4387821
Roelof Stikker	4476883
Lorenzo Terenzi	4465156
Rano Veder	4460464
Lars A.H. Velthausz	4442253
Max van der Waals	4437322

Project duration:	April 23, 2018 – July 6, 2018	
Tutor	Francesco Avallone	AWEP - Wind Energy Section
Coaches	Eirini Tsiangou	ASM - Structural Integrity and Composites
	Joost Ellerbroek	C&S - Air Traffic Management

TU Delft

Executive Summary

In order to avoid delays due to traffic, major delivery companies like Amazon, DHL and UPS are developing drones for the delivery of parcels. Since the noise of current drones is perceived to be disturbing, a need for silent delivery drones is arising. This report comprises the detailed design process performed by the enterprise Silentium to arrive at such a system and the following paragraphs summarise the steps taken.

Market Analysis A business model has been made in order to define a value proposition of the Silentium company, its position in the shipping industry and lastly a market analysis.

The current package delivery industry has a rather slow and expensive process for the last part of package delivery. This is where Silentium can bring value to both big sized retailers and shipping companies. Drones can have a revolutionary effect on the last step of the delivery in densely populated areas. An analysis of the competitors has been made in order to have a reliable and competitively priced product. Several start-ups and mature companies have been analysed, such as Matternet, UPS and Amazon. It has been established that the target market will include big retailers and shipping companies, as smaller ventures have non-standardised and other cheap ways to deliver their products. Next, the market volume and the potential growth was determined. The current total cost of parcel delivery globally is approximately 70 Billion Euros, with growth rates of 7-10 % for established markets and up to 300 % in 2015 for developing markets such as in India [23]. From the daily products delivered an estimated 86 million parcels could potentially be delivered with the use of drones [22]. However, there are some potential drawbacks which could limit the growth of the market such as regulations and public acceptance of delivery drones [23].

To estimate the volume of the market some assumptions have been made:

- 50 % of last-mile delivery operations can be performed using a drone
- On average a drone will deliver 3 packages with an autonomy of 30 km
- Travel time for the deliveries is 1 hour, assuming 30 km/h speed plus extra time for operations
- 7 hours per day of operational time

Using these assumptions an estimated number of 1.5 million delivery drones could be used worldwide. Since they have to be replaced every 3 years, the production rate should be 500,000 per year. Assuming a market share of 20%, this leads to 100,000 drones to be produced by Silentium every year.

Project Sustainability Before the detailed design of the drone could be started, it was important to establish how sustainability would be implemented during the final phase of the project. A Work Flow Diagram including focus points for sustainability was created.

Operations When designing a system it also has to be considered how it can be operated and if it e.g. requires additional infrastructure as this is essential for the success of the product. From the base station, the drone will be initialised, packages will be loaded and the delivery will be tracked. A route will be determined before take-off, by making use of a routing algorithm which takes into account all constraints posed by the design of the drone.

The drone takes off vertically to 60 m altitude, transitions to forward climb until it reaches 120 m, cruises to the destination at 18.75 $\mathrm{m\,s^{-1}}$, loiters and finally descends for delivery. The delivery can be performed on top of a building, in a garden or at a designated location in the neighbourhood, depending on the area. Before delivery, two messages will be sent to the package recipient, one notifying that the drone left the depot and one notifying that the drone will arrive in a few minutes. A third message is sent when delivery is completed. Customers should sign up for the service using an app on their phone, so a landing spot can be determined by using GPS locations.

Requirements First, the user and stakeholder requirements were established taking into account the wishes and needs of the customer and of all stakeholders. Subsequently, a Functional Flow Diagram (FFD) and a Functional Breakdown Structure (FBS) were presented which provide a detailed overview of the functions that have to be performed by the drone. The diagrams helped in the generation o the system requirements. In order to be able to give specifications about the mass and power available per subsystem in the subsystem requirements, a technical budget breakdown was performed next. From the preliminary sizing was derived a technical budget breakdown which indicates how much power and mass were available per subsystem during the detailed design phase. With those numbers established, the subsystem requirements could be derived and finally, the approach used for contingency planning was explained. This was necessary since the methods used for the estimation of the technical budget are generally inaccurate throughout the

duration of the project but have a decreasing level of uncertainty the further the design progresses. Consequently, the contingencies factors chosen for both mass and power were 25%, 15%, and 10% for the conceptual phase, the preliminary phase and the current, detailed phase, respectively.

Conceptual Design Summary In order to provide a good starting point for the detailed design of the delivery drone, the steps taken leading to the final phase of the project were summarised. A trade-off between the possible configurations for the delivery drone was made. Based on this, 4 concepts were created which were then sized to determine more of their respective performance characteristics. Comparing these, the most suitable design was chosen which was then used as a basis for the detailed design. The four designs included a fixed wing, a flying wing, a flying with integrated propellers and a tilt-wing concept. The criteria used for the trade-off were mass, dimensions, aerodynamic and stability characteristics, noise, cost, risk, reliability, availability, maintainability and safety. Comparing the concepts w.r.t to the trade-off criteria yielded that the flying wing is the most suitable one for the delivery drone due to its low mass, favourable stability characteristics and low risk. Finally, a sensitivity analysis was performed in which the weights of the trade-off criteria were varied. This was done to simulate the uncertainty in the methods used for the trade-off. It could be shown that the flying wing would win the trade-off for all possible, realistic combination of weights proving that it is a robust design and that it can indeed be used a basis for the detailed design.

Detailed Design: Data Handling and Communication The detailed design was started with the Data Handling and Communication Subsystem as it provides a good overview of the interaction between all the components. In this part of the report, all electrical components that will be used for the drone were selected. In order to comply with the requirements, all of them were off-the-shelf. These components included batteries and a Power Distribution Board (PDB), to provide and distribute power and a processing unit. Furthermore, a flight controller was added to process the information from the sensors and send commands to the Electronic Speed Controllers (ESC) in order to adjust the path or the attitude. The sensors included Inertial Measurement Units, obstacle avoidance sensors, a camera and a pitot tube. For communication with the base station, it was decided to use a mobile broadband chip (including GPS), because of the favourable up- and downlink capabilities when compared to radio communication. Finally, the ESCs and the motors were selected.

Detailed Design: Aerodynamics The aerodynamic analysis has been of key importance given that it has defined the shape and size of the final system. The main wing aerofoil combines two candidates, namely the SD 7090 at the root and he Fauvel 14, aerofoil with reflex, at the tip to obtain favourable stability characteristics.

Furthermore, with the aim of storing all the subsystems within the vehicle, it was decided to include a fuselage which can also provide lift to make the design more sustainable. It was decided to use the NACA 4424 aerofoil at the root of the fuselage (thicker than required in order to house multiple subsystems) and the NACA 4421 aerofoil at the tip of the fuselage.

Finally, the drag and interference of the propellers in front of the wing with the lifting surface were studied. For this analysis, the zero-lift drag, the induced drag and the interference drag of the propellers were researched. In the end, it was concluded that all propeller generate 8.53 N of additional drag during cruise. The last form of drag is a function of the angle of attack and the downwash angle gradient, which was found to have a value of 0.74 N which has been included in the 8.53N.

As a result, the final wing design has a lift-over-drag ratio during cruise of 8 [-], lower than the L/D of 12 [-] required by the sizing process. It also has a moment coefficient during cruise of -0.136 [-], moment which is counteracted by the control surfaces generating trim drag.

Detailed Design: Stability The stability analysis of the aircraft was required as input for the control analysis and the design of the corresponding control surfaces. Both situations, before and after the payload is deployed had to be considered, since this causes a shift in the location of the c.g.

First of all, the longitudinal static stability was analysed. The neutral point, which coincides with the aerodynamic centre of the wing, should be located behind the centre of gravity. It was found that the centre of gravity was located at 0.368 m w.r.t. the nose with the payload and 0.358 m without the payload. Since the location of the centre of gravity, including the static margin, was lower than the location of the neutral point, the aircraft was considered longitudinally statically stable.

Secondly, the longitudinal dynamic stability was studied. A stability analysis was run using the XFLR5 tool which showed the design stable.

Thirdly, for the lateral static stability was ensured that the wing was weathervane stable, roll and yaw damped.

Fourthly, as with the longitudinal dynamic stability, the lateral eigenmotions were studied. In order to ensure this stability, the dihedral angle of the wing was increased to 22°.

Finally, the stability during Vertical Take-Off and Landing (VTOL) operations was analysed. It was concluded that a thrust differential must exist between the front and aft propellers in order to counteract the moment caused by the different distances, from the two propulsion groups to the centre of gravity. As a result, the front propellers must generate more thrust.

Final Planform and Aerodynamic and Stability Characteristics The final wing planform is presented in Figure 1 and the geometry characteristics are summarised in Table 1.

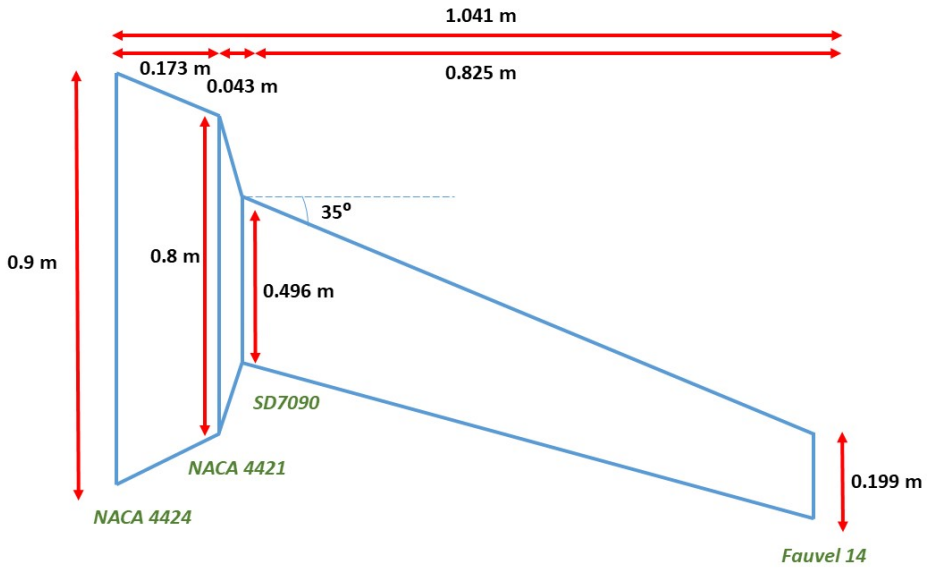

Figure 1: Planform of the final flying wing. The different aerofoils are indicated in green at the locations where they start along the span.

Parameter	Value
Span [m]	2.08
Taper ratio [-]	0.36
Sweep [°]	35
Root chord [m]	0.556
Tip chord [m]	0.199
Surface area [m]	0.786
Aspect ratio [-]	5.504
Dihedral [°]	22

Table 1: Final planform geometry characteristics.

Detailed Design: Structure From the flight envelope, it could be derived that the load factor to design for was 3.75. However, since the general loads are relatively low for the choice of the material, priority was given to cost and stiffness over strength. The material selected is Nylon 6 with a density of 1.15 $\mathrm{kg\,dm^{-1}}$, a Young modulus of 2.23 GPa and a yield strength of 67.6 MPa. The most suitable structure was found to be a wing box where only the skin carries the load. The thickness of the skin varies both spanwise and chordwise since it was optimised to minimise weight while avoiding structural instabilities and an unfeasible design from a manufacturing point of view. Using a boom idealisation, the highest stresses in the structure were found to be 18 MPa, the expected lifetime 3 years and the total mass 2.87 kg.

Detailed Design: Control The design presented in this report can be regarded as unconventional in terms of control systems. There are many resources to be found for both the control of multicopters and fixed-wing drones, but the combination of both in one system is relatively new. The choice was made to only design control systems for the VTOL and fixed wing flight phases individually and not for the transition between them due to the time constraints.

The design of the control systems was done by first modelling the non-linear dynamic behaviour of the drone during fixed-wing flight and VTOL flight. Using multiple assumptions, the models could be simplified, which allowed for easier simulation.

Finally, the program Simulink was used to design the actual control systems and simulate the total system. The VTOL flight of the drone is controlled by supplying the controller with the desired position and heading as a function of time ($x(t)$, $y(t)$, $z(t)$ and $\psi(t)$). The fixed wing flight is controlled by supplying the control system with the required velocity, altitude and heading (u, z and ψ).

Detailed Design: Navigation One of the challenges encountered during the design process of the navigation subsystem is the fact that it has to be able to fly autonomously. Its 3 main tasks were consequently position and attitude determination, obstacle avoidance and finding the landing spot. Furthermore, it had to be single-point failure free.

While GPS-signal is frequently lost in urban areas, it was still decided to use it as the primary means of position determination since it is light and cheap Signals of Opportunity (SoP), which is a technology using signals present in urban areas such as WiFi, cellular reception etc. for navigation, was chosen to take over the position determination when GPS-signal is unavailable. Furthermore, barometers and a pitot tube were required since GPS cannot determine the altitude and velocity accurately. It was decided to use an inertial measurement unit (IMU) including magnetometers for the attitude determination.

Since the drone flies at a higher horizontal than vertical velocity, the sensors used for obstacle detection in the horizontal direction needed a larger range. Consequently, it was decided to use a laser scanner with a range of 40 m for the sides of the drone and ultrasonic sensors which are much cheaper and lighter but only have a range of about 5 m, for the top and bottom.

Finally, it was planned to position a camera which can operate during day and night time at the bottom of the drone. This enables the system to find its final destination by comparing the ground below it with a picture of the landing spot using image recognition.

Detailed Design: Propulsion and Noise The design of the propulsion subsystem was based on an aerofoil selection leading to a blade design and motor selection. It was constantly tried to reduce parameters related to noise where possible.

The blade of the propeller utilises two aerofoils, given the large variations of Reynolds number over the blades: GOE225 was selected for high Reynolds numbers ($75,000$) and the Wortmann FX 60-126/1 for low Reynolds numbers ($\leq 75,000$). The propeller has been designed on the basis of the Adkins-Liebeck [3] design procedure. This is an approach that optimises a planform with respect to the power required. The method is based on the blade element momentum theory, which considers the momentum equation for a blade section and integrates it over the span to yield the blade performance. The design point has been determined such that it reduces the parameters that relate to noise production. For the VTOL propeller 2500 RPM with 3 blades were selected and for the FW propeller, 2400 RPM with 2 blades. The twist has been reduced to facilitate lower inflow velocities.

The propeller is required to produce a noise level of less than 65 dBA at 7.5 metres distance, in order to comply to Dutch noise regulations for loading and unloading businesses. In addition, the average sound experienced by citizens has to be below 40 dBA. The maximum instantaneous noise level is expected to be defined by the takeoff and landing phase, whereas the maximum average noise level is assumed to be defined by the noise during cruise phase, as the average sound will not be affected by a single delivery taking place. The noise radiation of the designed propeller was initially estimated by taking the shaft power, the number of blades, the propeller diameter, the rotational velocity, the observer distance, and the number of blades as input parameters. Using this method, the noise was estimated to be 55 dBA, at 7.5 meters during hover, and 25 dBA during cruise, at an altitude of 120 meters. After verifying the hover case with a higher-fidelity model, the noise was found to be 60 dBA, which is still significantly below the requirement. The power required, however, was found to be more than budgeted for, which means that either the number of packages that can be delivered needs to be reduced, or the depth of discharge of the batteries needs to be increased, which leads to an increase in cost.

Detailed Design: Payload Mechanism A mechanism which can safely transport and release parcels while complying with several constraints on cost and mass had to be designed. It has to carry up to 4 parcels with a maximum total mass

of 2.5 kg and a size of 210 x 297 x 105 mm (w x l x h).

The payload bay is separated into 8 equal units of 105 x 74.25 x 105 mm (w x l x h), where a unit can have a maximum mass of 500 g. A suction mechanism is used with eight silicon suction cups of 30 mm diameter equally distributed over the units. Eight micro vacuum pumps, operating at -400 mbar, ensure quick and continuous vacuum of the suction cups. The soft silicon suction cups and relatively low-pressure difference limit any damage done to the packaging of the parcels.

To ensure safe transport and smooth airflow along the underside of the fuselage, hatches are used which open when the drone has landed. Two linear servos are used to open and close the hatches. The servos are also able to withstand a maximum static force of 200 N in case of failure of the holding mechanism. The complete system has a mass of 480 g.

Detailed Design: Auxiliary Systems Several systems which could not clearly be allocated to one specific subsystem had to be designed. These included the landing gear, an emergency landing system and safety lights.

For the landing gear, it was important to ensure the stability of the drone when landed while keeping the weight and cost low. The best option was found to be four carbon fibre rods which are retracted by means of small servos, which are integrated into the rods used for the attachment of the propellers to the main body. The rods have a length of 280 mm which resulted in a ground clearance of 78 mm for the horizontal propeller. Small fairings at the ends of the rods were used to ensure smooth airflow around the landing gear when in cruise.

A safety mechanism was needed to reduce the risk of harming people or animals in case of failure of the propulsive system. A ballistic parachute was used which can deploy in one second, making it effective even at low altitudes. A comparison was made between different off-the-shelf parachutes, which showed that the Galaxy Sky GBS 10/150 was the best option. It has a mass of 405 g and costs 1044 euros. When deployed, the parachute slows the drone down to a descent speed of 4.8 $\mathrm{m\,s^{-1}}$.

As the drone has the capability of flying at night, it was necessary to ensure visibility of the drone for other aircraft. Thus, red and green navigation lights are installed on the left and right wing respectively, which are used during cruise. During take-off and landing four white lights, placed at the ends of the rods used for the propellers, are used.

Performance & Sensitivity Analysis To measure the performance of the drone, the drag and power consumption was calculated for different flight phases. By calculating the time spent in each phase, it was possible to express the total power consumption of the drone as a function of mission range and number of packages. This allowed the evaluation of the drone range for different numbers of packages. It followed that if the drone was to deliver a single package, the range it could travel would be over 60 km.

The sensitivity analysis was performed by varying the mass, power consumption, lift, drag, number of packages and hover time. Each variable was changed by a factor of 10% in a way that would negatively impact the overall design in order to test its robustness to uncertainties in the design methods used. The range, number of packages and the maximum weight of the payload would then be varied to generate acceptable, even though sub-optimal design solutions.

RAMS Since the delivery drone is autonomous and consequently unsupervised during operation, it was crucial to ensure that it is safe and reliable. This was done by performing a reliability, availability, maintainability and safety analysis (RAMS) for the final detailed design. First, a reliability criterion was established in which the maximum acceptable probability of failure was derived comparing it to the one for aircraft. This way a value of $P_{CF} = 0.0016\%$ was found. Next, it was investigated which modes of failure there are for the delivery drone and which one is the most critical for the reliability of the system. Since many failures can be detected or predicted due to the redundancy in the system (e.g. a malfunctioning of the sensors can be spotted since the system receives two different kinds of inputs) the critical components could be narrowed down to the control surfaces. However, it could be shown that the reliability criterion could be fulfilled by introducing set maintenance intervals. These included daily checks, check A, checks every 5 weeks, check B, and checks every 30 weeks, check C. The daily checks include the following tasks:

- The propeller blades will be wiped clean and checked to make sure there are no cracks or bents.
- The propeller shafts will be checked for any free play and if they still turn smoothly, to make sure the bearings are still intact.
- The tightness of the attachment between detachable parts will be checked and tightened if needed.
- The sensors and cameras will be cleaned to make sure that the location and attitude determination will not be in danger.
- The landing mechanism will be checked for dirt and dust and it will be cleaned.
- The suction cups will be checked and cleaned to ensure that no leaks develop.
- The onboard sensors will be calibrated.

During Check B all servos and bearings will be tested, lubricated and replaced if necessary. Furthermore, all connections such as hinges etc. will be checked. In Check C the batteries will be replaced by new ones due to their limited lifetime.

Verification and Validation The compliance matrix and the feasibility analysis were created to ensure the design of the drone would be able to comply with the system requirements. The results were positive. In addition, the tests for verification and validation of the design were specified. These include structural tests, integration tests, functional tests and acceptance and qualification tests. Finally, the steps that need to be taken to certify the drone were investigated. Since there are no regulations for the certification of drones as of now, the ones for aircraft were used. To validate an aircraft, the team must apply for the correct type of certification, and wait for the authorities to assign a project number to it. Then the team needs to provide all the technical information and perform several tests on the drone. After a review of the technical information, the authorities will perform their own tests. After receiving a summary of the results, the authorities will issue the type certification if adequate.

The final configuration of the delivery drone, which has a final mass of 13.7 kg, is visible in the rendering in Figure 15.1. A more detailed view, with the dimension of the drone is visible in Figure 15.2.

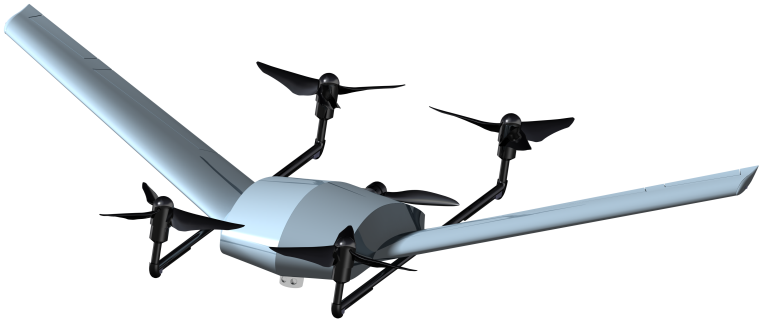

Figure 2: Overall configuration of the silent delivery drone

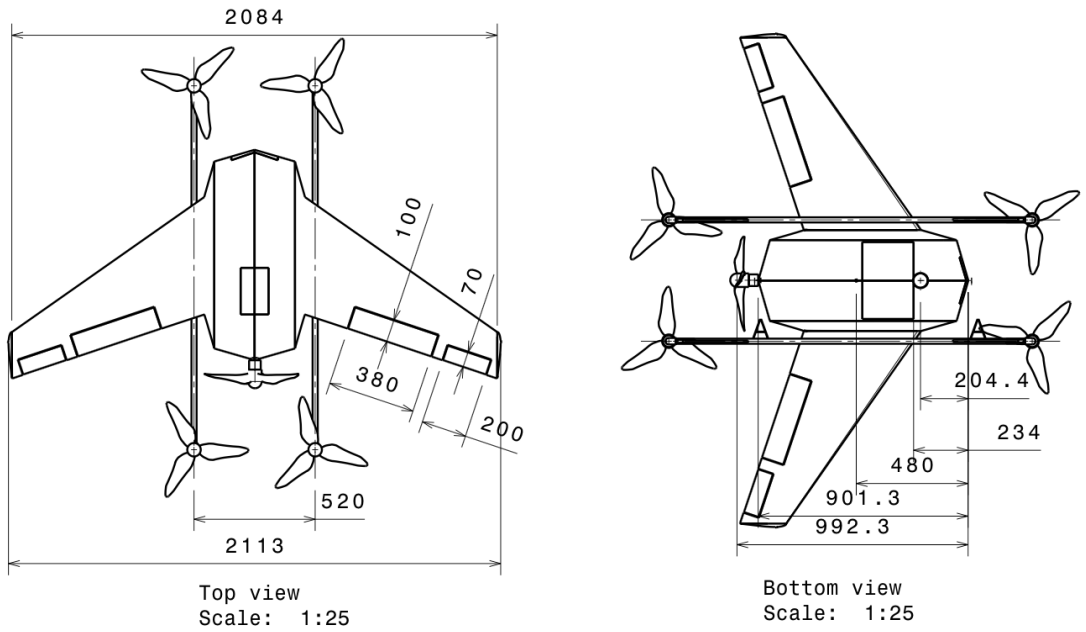

Figure 3: Technical drawing of the silent delivery drone including dimensions in millimetres

Manufacturing, Assembly and Integration Plan With the design finished the Manufacturing, Assembly and Integration Plan could be made. A complete overview of the MAI-plan can be found in Figure 4. One of the user requirements

was to manufacture the main frame using 3D printing, also known as additive manufacturing. The mainframe was divided into three sections. Two being the left and the right wing and the final one being the fuselage including the fairing which connects this body to the wings. It was decided to use the Stratasys Fortus 900mc to print these parts together with nylon 6 as material. Furthermore, it was decided to print the fuselage in two shells to simplify integration and assembly.

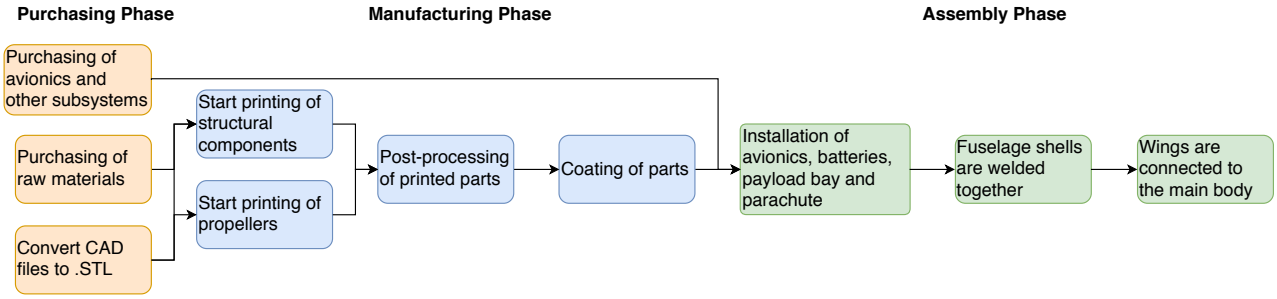

Figure 4: Overview of the MAI-plan

After the parts have been produced, they will be post-processed and finished. This includes removing the part from the base plate in the printer, removing the support material and finally, adding paint as a coating for the nylon 6 parts.

Then, the parts have to be put together. For the assembly of the main wings to the fuselage is was found that a locking mechanism works best. This not only makes the seams waterproof to protect the internals from weather phenomena, it also allows the user to quickly change the wings in case they are damaged.

The shells of the fuselage are connected using welding. Since the material used is a thermoplastic it was found that the sides of the fuselage shells can be reheated and softened using infrared heating which allows the two parts to join together.

Finally, the integration consisted in positioning all the components that had to be placed in the wing. The interference between all the avionics and the respective locations were already established at an earlier stage of the design. The additional structure that was necessary, will become an integral part of the wing.

In particular, the battery system will be integrated using a rail system. This rail system will allow the user to quickly change the batteries between operations. The rail system will also allow the user to quickly access several of the avionics to perform maintenance if necessary. Finally, the rods will be added below the wing. These will be added using round brackets and a pin which prevents it from rotating.

Technical Sustainability With the final design finished, a technical analysis of the sustainability was performed in addition to the previously mentioned project sustainability. This was done by looking into the manufacturing process, end of life solutions, a carbon footprint analysis, energy management and social sustainability.

The use of additive manufacturing has several advantages compared to conventional methods. Less material waste is created and almost no machining is needed, which saves costs, time and resources. Furthermore, the integration of subsystems is easier as cut-outs and brackets can be designed as an integral part of the product.

The components used are classified into two groups, electronics and structure, as the components within these groups have a similar end of life solutions. For the electronics group, the recycling of the lithium polymer batteries is the most important. Currently, a lot of research is being done on the recycling of these types of batteries. For the structure group, the used Nylon 6 material for the skin and structure of the drone, was the most important aspect to consider.

A carbon footprint analysis was done to show the difference in CO_2 emission for drone and truck delivery. The analysis showed that at 100 big packages delivered, the drone emits 57% less CO_2 than a truck, and 72.5% less when delivering small packages. However, when more than 200 packages need to be delivered, truck delivery is more beneficial since the drone has to travel back and forth a lot.

To asses social sustainability, three parameters where used namely equity, social acceptance and quality of life.

Return on Investment and Operational Profit To establish the operating income, a detailed cost break-down was performed. The final design total cost can be decomposed as follows: 842$ to manufacture the structure, 1554$ for the avionics, 577$ for the electric system, 2352$ for the parachute and payload mechanism and 1170$ for the propulsion system. On top of this, there is a maintenance cost of 1550$ per year. This leads to a total cost (including maintenance) of 11145 $. Other sources of expenses for the company include "Sales and Marketing" and "Research and Development" which take respectively 17 % and 18% of the total revenues. Furthermore, a corporate tax of 25% on operating income was taken into account. The final price for the drone is set at 23225 $ which yields a return on investment of 13.3 % in

5 years and a net income of 29 M\$ per 10000 units sold. If the target market volume of sales was met, the net income would be 290 M\$ yearly.

Risk Assessment Regarding management risk, the team took actions to ensure the page limit of the report and its delivery time would be compliant with the requirements. To avoid unexpected delays, safety margins were taken when producing the schedule for the last part of the project. In addition, the risk officer and the team manager have held discussions with departments to ensure that deadlines would be met and the quality of the work was high.

Regarding technical risk, three kinds of risks were identified: risks of the design, risks that have occurred and risks that might happen in the future. For the second kind, the way the team dealt with the problem was explained together with the actions that the team has taken to avoid similar situations in the future. For the other two kinds, the actions to mitigate them were explained.

Project Organisation The last step in the design process was to establish the steps to be taken next if the drone was to actually be produced. They would start by finalising the design, which means revising the design presented in this report. Afterwards, financial resources would have to be acquired from investors to be able to build a prototype of the drone. For this, some parts would have to be 3D-printed and off-the-shelf components would have to be bought. Using the prototype it would be possible to validate the design performing several tests, which were explained in the verification and validation section. Afterwards, the drone would be certified and sold to clients. Once commercial levels would be reached, mass production and distribution could be started.

Contents

Nomenclature

List of Abbreviations

ABS	Acrylonitrile Butadiene Styrene
AM	Amplitude Modulation
BEMT	Blade-Element Momentum Theory
CAD	Computer-Aided Design
CFD	Computational Fluid Dynamics
COMM	Communications subsystem
CONT	Control subsystem
CPU	Central Processing Unit
DSE	Design Synthesis Exercise
EASA	European Aviation Safety Agency
ELEC	ELECtronics subsystem
ESC	Electronic Speed Controller
FBS	Functional Breakdown Structure
FDM	Fused Deposition Modelling
FEM	Finite Element Method
FFD	Functional Flow Diagram
FM	Frequency Modulation
FW	Fixed Wing flight phase
FWIP	Flying Wing with Integrated Propellers
GPS	Global Positioning System
IMU	Inertial Measurement Unit
LIDAR	LIght Detection And Ranging of Laser Imaging Detection And Ranging
MAC	Mean Aerodynamic Chord
MAI	Manufacturing, Assembly and Integration
MISC	Miscellaneous
MTOW	Maximum Take-Off Weight
NA	Not Applicable
NAV	Navigation subsystem
NFC	Near Field Communication
PDB	Power Distribution Board
PID	Proportional Integral Derivative
PROP	Propulsion subsystem
RAMS	Reliability, Availability, Maintainability and Safety
SESAR	Single European Sky ATM Research
SLA	StereoLithography Apparatus
SLAM	Simultaneous Localisation and Mapping
SLM	Selective Laser Melting
SOP	Signals of Opportunity
STRUCT	Structures subsystem
UAV	Unmanned Aerial Vehicle
VTOL	Vertical Take-Off and Landing

List of Subscripts

α	With respect to the angle of attack
β	With respect to the sideslip angle
0.25c	At 25% of the chord
des	Design
geo	Geometrical
i	Induced
L=0_root	At the root when the lift is zero
L=0_tip	At the tip when the lift is zero
LE	Leading edge
max	Maximum
min	Minimum
p	With respect to the roll rate
q	With respect to the pitch rate
r	With respect to the yaw rate
u	With respect to the velocity in x-direction
w	Wing

List of Symbols

α	Angle of attack [°]
α_0	Angle of attack at zero lift [°]
β	Ballistic coefficient [$\mathrm{kg\,m^{-2}}$]
ϵ	Downwash angle [°]
γ	Twist [°]
Λ	Leading edge sweep angle [°]
λ	Taper ratio [-]
μ	Friction coefficient [-]
ω_0	Undamped natural frequency [rad/s]
ω_n	Damped natural frequency [rad/s]
ξ	Damping ratio [-]
A	Aspect ratio [-]
a	Acceleration [$\mathrm{m\,s^{-2}}$]
A_b	Cross-sectional area of the drone [$\mathrm{m^2}$]
A_C	Casualty area where the drone might hit the ground in case of failure [$\mathrm{m^{-2}}$]
b	Span [m]
C_r	Root chord [m]
C_D	Wing's drag coefficient [-]
C_d	Aerofoil's drag coefficient [-]

C_{L_α}	Lift coefficient gradient [-]
C_L	Wing's lift coefficient [-]
C_l	Aerofoil's lift coefficient [-]
C_M	Wing's moment coefficient [-]
C_m	Aerofoil's moment coefficient [-]
D	Drag [N]
F_H	Holding force [N]
i	Incidence angle [°]
I_{ii}	Mass moment of inertia about the ii-axis [kg m°]
L	Lift [N]
L_{GC}	Likelihood of third-party casualties given the loss of control of the drone [-]
M	Mass [kg]
n	Safety factor [-]
N_i	Population density [km^{-2}]
P_{CF}	Maximum acceptable probability of failure for the drone [-]
P_{CM}	Maximum acceptable probability of failure for manned aircraft [-]
q	Dynamic pressure [Pa]
r_h	Horizontal range at which obstacles have to be detected [m]
r_v	Vertical range at which obstacles have to be detected [m]
RPM	Revolutions per Minute [Hz]
S	Wing reference surface area [m^2]
St	Stability factor [-]
t/c	Maximum thickness over chord ratio [-]
$T_{\frac{1}{2}}$	Time to damp half the amplitude [s]
$t_{reaction}$	Reaction time to avoid obstacles [s]
V	Longitudinal velocity of the stream [ms^{-1}]
v_h	Horizontal velocity of the drone [$m\,s^{-1}$]
v_v	Vertical velocity of the drone [$m\,s^{-1}$]
W	Weight [N]
w	Downward velocity [ms^{-1}]
ac	Aerodynamic Centre
C_l	Roll moment coefficient [-]
C_m	Pitch moment coefficient [-]
C_n	Yaw moment coefficient [-]
C_x	Force in the x-direction coefficient [-]
C_Y	Force in the y-direction coefficient [-]
cg	Centre of Gravity
np	Neutral Point

1 Introduction

Major industrial delivery companies like Amazon, DHL and UPS are planning to use small drones for package delivery in the near future with the intention to reduce delays in the delivery due to traffic.[1] The drawback of this, however, is that the high-frequency noise of drones is perceived to be more annoying than car noise as has been found by research carried out by NASA[2]. Subsequently, the following mission need statement can be formulated: There is a need for fast package delivery while fulfilling noise pollution regulations. The enterprise "Silentium", whose objective it is to design a silent delivery drone, has previously established a conceptual design for this drone. In this report the detailed design will be presented.

The purpose of this report is to summarise the steps taken up to the final stage of the project and to give an in-depth description of the detailed design process. Furthermore, more general aspects surrounding the design, such as the current economic market, sustainability, safety and manufacturing will be discussed to show that the enterprise is indeed feasible.

The report can be divided into three major parts corresponding to phases of the project, namely the one preceding the design, the design itself and a post-design part. In the first part, in chapter 2, a market analysis will be performed in order to show how much the drone can cost while still being profitable. Subsequently, in chapter 3 a strategy will be presented showing how sustainability can be accounted for over the course of the design process. After that, the operations of the drone will be discussed in chapter 4 where it will be explained how the drone can find the quickest route, which flight profile it follows and where it will land. This information needs to be known because it influences the design. Finally, the requirements for the delivery drone will be stated in chapter 5.

The second part of the report starts with a summary of the conceptual designs in chapter 6 to provide a starting point for the description of the detailed design. The detailed design begins with the presentation of the data handling and communication in chapter 7 where the interaction between all subsystems will be shown. This is followed by the discussion of the the wing design in chapter 8, the structure in chapter 9, control and navigation in chapter 10, the propulsion system in chapter 11, the payload mechanism in chapter 12 and finally the auxiliary systems in chapter 13. With the help of a sensitivity analysis in chapter 14 it will be shown that the design is robust despite the uncertainties in the tools used. After that, a summary of the detailed design will be provided in chapter 14. It will then be checked if the final design is safe and reliable in chapter 16 and verification and validation will be performed in chapter 17.

Part three of the report starts with chapter 18 where it will be explained how the drone will be manufactured. After that, technical sustainability will be discussed in chapter 19. In chapter 20 it will be checked if the initial assessment for the cost has been correct by comparing it to an estimation based on the final design. A risk assessment will be performed in chapter 21 and finally, in chapter 22 it will be shown which steps would be taken in the future as continuation of this project.

[1] https://theconversation.com/delivering-packages-with-drones-might-be-good-for-the-environment-90997 last accessed 03/05/2018

[2] https://ntrs.nasa.gov/archive/nasa/casi.ntrs.nasa.gov/20170005870.pdf last accessed 26/04/2018

2

Market Analysis

Before the design process of a product is started, a market analysis should be performed in order to establish the demand and the competition for the system. In this chapter a business model for the company Silentium will be presented. In section 2.1 a value proposition and the mission objectives will be shown. In section 2.2 the key partners in the development and sales of the product are listed and in section 2.3 the key resources the company needs and its mission objective are explained. Subsequently, the current and future state of the market will be shown in section 2.4 and the target market will be explained in section 2.5. Possible threats to the project due to competition will be shown in section 2.6 and finally, in section 2.7, the strategy that the company will adopt to make revenue will be explained.

2.1. Objective and Value Proposition

The objective of the company is to design a silent delivery drone which distributes packages faster, at lower cost and lower emissions while complying with noise regulations. The objective partially overlaps with the value proposition: the reduction in cost of delivery per package and faster delivery.

2.2. Key Partners

In order to develop, test and do marketing for the product, it is essential to cooperate with external organisations. Some of the major partners are listed below.

Incubator: An incubator is very useful at the early stages of the enterprise. It increases the trustworthiness of the company and at the same time it facilitates the interaction with investors and other possible partner companies. Finally, it can provide working spaces for a reasonable price.

Shipping company: Shipping companies are the main customer and potential investors, so it is very important for the company to draft a contract with one of them. This way demand and capital can be secured. Furthermore, their collaboration in the feedback on the products design is essential.

Legislators: Noise and safety regulation for drones are not yet finalised. It is therefore important to collaborate with the legislators to provide technical guidance in the drafting of the rules. These rules can decide the fate of the drone since the system will not be allowed to fly in case of non-compliance.

Manufacturing Facilities: While the drone is supposed to be 3D-printed in the early stages of the company, as will be shown in chapter 5, the company might have to switch to mass production in the long run. Subsequently, it makes sense to check available manufacturing facilities and supplies.

2.3. Key Resources

In this section the main resources needed to successfully complete the product will be listed. The first resource is financial help to build and test the first prototype. Once the working prototype is finished, more investments will be needed to bring the concept to the level of mass production. Another important resource is a data-set to train the machine learning algorithms to operate the drone in the delivery environment. Also related to software is computational power, of which a big amount will be needed to perform design simulations (CFD, FEM, ...) and to train the on-board algorithms. Apart from computational power, the algorithms themselves need to be advanced enough to ensure a high level of reliability during the fully autonomous phase of the mission.

2.4. Market Outlook and Prediction

Parcel delivery is a global market which is continuously growing in size. The current total cost of parcel delivery is approximately 70 Billion Euros globally per year. [23], where the US, Germany and China account for 40 % of the market.

2.4.1. Market Growth

The market had growth rates of 7-10 % in 2015 for established markets and up to 300 % for developing markets such as India [23]. However, there are some limitations regarding parcel delivery drones. The size and weight of the parcel largely constrain the use of drones. Between 86 and 91 % of the parcels weigh less than five pounds [22], which is similar to the 2.5 kg payload requirement (see chapter 5) of the drone. Daily 100 million products are sold online, which leads to an estimate of 86 million parcels delivered daily by drones [22].

However, this assumes that delivery drones will eventually account for all small packages to be delivered, which might not be the case. Other competitors and other technical innovations could be a threat to the use of delivery drones. One established competitor which also aims at fast delivery are bike or motorbike couriers. These are used by companies as Deliveroo and Foodora and already take up a very large part of the market for food delivery. Other innovations such as autonomous ground vehicles and droids could have a large stake in parcel delivery in the future. A lower estimate of 8 million packages daily in 20 years time is given by [22]. This shows that even when a pessimistic estimate is used the potential market for the delivery of parcels by drones is very large.

2.4.2. Market Volume

To estimate the value of the drone delivery market the following assumptions were made:

- 50 % of last-mile delivery operations can be performed using a drone. This assumption can be justified by considering that 54 % of the global population lives in urban areas, where drone delivery becomes economically viable.
- On average a drone will deliver 3 packages with an autonomy of 30 km.
- Travel time for deliveries is 1 hour, assuming 30 km/h speed plus extra time for operations.
- 7 hours per day of operational time.

Top-Down Estimate Using these assumptions, a top-down estimate of the market can be performed yielding the number of drones to be 1.5 million with 70,000 of them in the USA. This number is preliminary but the order magnitude should be accurate.

To get a better feeling for the number of drones that can be sold, an estimation of the number of drones necessary for the Netherlands and in particular Delft was made. Using the same heuristics the number of drones needed in the Netherlands, which has a population of 17 million people and specifically in Delft are 3300 and 30, respectively. This means that in Delft the number of packages delivered every day is 900.

Bottom-Up Estimate Next, a bottom-up approach was used. From national statistics, it is known that 500,000 packages are delivered every day in the Netherlands [1]. Considering the population of Delft, it was found that around 3000 packages are delivered in the city every day. This means around 100 drones are necessary to perform the deliveries.

The discrepancy between the top-down and the bottom-up approach can be explained with the assumption that only 50% of deliveries can be performed using a drone. Delft is a densely populated area and virtually 100% of last-mile deliveries can be carried out by drones. Taking this into account, the discrepancy factor remaining is only 1.5 which is acceptable for such a rough initial estimate of the market. To estimate the total value of the market a top-down estimate will be used. In the future, if a more geographically accurate estimate is required, statistics for the respective areas will be researched.

2.4.3. Market Value

In this section, an estimate of the cost of the drone and its related operations will be given. Furthermore, an upper bound on the cost to make the drone delivery system competitive against the common method of delivery will be derived.

[1] `https://www.acm.nl/en/publications/publication/17561/More-parcels-and-less-mail-delivery-in-2016` last accessed 20/06/2018

Cost The current cost for on-demand last mile delivery for shipping companies like UPS and DHL is estimated to be 2.5 $. [22]. This value will be used as a benchmark for the silent delivery drone. Assuming a battery life of 250 hours and a cost per item of 100 $, a motor life of 750 hours with a cost per set of four of 60 $, and including other factors like insurance, taxation, electric usage the values in Table 2.1 were obtained [22].

System Item	Cost [$\$h^{-1}$]
Insurance	0.02
Command and control	0.02
Communication	0.02
Labour	0.02
Maintenance	
Batteries	0.4
Motors	0.08
Rotors	0.01
Electrical	0.03
Battery recharging	0.24
Airspace charges	0.1
Total Hourly Cost	0.94

Table 2.1: Estimated hourly operating costs of the drone delivery system [22]

For the hourly system both the initial cost of the system and its life-span needed to be estimated. The ratio between system cost and lifetime are particularly important, since the system cost per hour is directly proportional to this ratio. To find the upper bound for the ratio it was assumed that the drone will be operational for 30 hours per week, and that the average number of deliveries per hour is 3. Given these constants and 2.5 $ as the maximum cost per package delivery, a value of 7665 $ / year was obtained for the cost-to-lifetime ratio. Furtheremore, assuming that companies want to save at least 5 % on delivery costs and a profit of at least 5%, the ratio becomes 7300$/year. This ratio gives a hard requirement on the cost, and it can be used to perform a trade-off between lifetime and system costs during the design phase.

Operating Income At this stage only a rough estimation for the operating income can be given. A more detailed analysis will be performed after the detailed design in chapter 20. The first step was to calculate the number of drones required and consequently the number that the company should be able to produce. The current business model is focused on creating an exclusive partnership with one of the big companies in the market. UPS has 22 %, FedEx 24 % and DHL 38 % of the market share. For further calculations it was assumed that Silentium partners up with a company that has 20 % of the market share. An optimistic scenario assumes that Silentium is the only company providing drones to, e.g. FedEx. Given that 1.5 million operational drones are required at any time and that they have to be replaced every 3 years, the production rate should be 500,000 per year. Taking the market share of 20 % into account, this leads to 100,000 drones to be produced by Silentium every year. The corresponding operating income with a sale price of 10000$ is 1000 millions $. Using a more pessimistic scenario, in which Silentium only operates in a regional area making up to 2% of the global market, 15,000 drones need to be produced every year. This would lead to an operating income of 150 million dollars per year.

2.5. Target Market

Silentium provides a silent delivery drone, able to deliver in a range of 15 km from the distribution point. (This is an user requirement as will be shown in chapter 5). Apart from the product, services to support operations and maintenance will be provided. From this it can be concluded that most companies having a form of online retail can benefit from the silent delivery drone. Both big shipping companies and small businesses like supermarkets, bakeries and restaurants can use the system to offer home-delivery for their products. This share of the market is generally reachable via direct sales and advertising. Investment in advertisements would probably be focused on social networks like Facebook and search engines like Google Search to increase the awareness level of the public of the company. This market can be considered the Served Available Market for the company Silentium.

Targeting this share of the market, however, seems unrealistic at this stage. Small shops have other, cheaper ways to deliver their products. Furthermore, the associated cost related to the installation of an operations drone centre is too high for these shops. Therefore, the aim lies in being subcontracted by the big players in the shipping sector. These companies can easily absorb initial costs and thanks to their products flow volume, the drone delivery technology can

be very revolutionary in reducing delivery cost and time. The target market therefore includes big retailers and shipping companies. Examples of such companies are Amazon, DHL, UPS, National post delivery etc.

2.6. Competitor Analysis

The number of competitors in the same business as Silentium dictate the difficulty of getting a good market share. For Silentium to be successful, it is necessary to have a reliable and competitively priced product. In this section, the competition Silentium may face will be shown, the business strategies and objectives will be explaied, and the product lifetime and cost will be determined. For that both startups and mature companies will be considered.

Matternet Matternet is a relatively new company that was founded in 2011. It designs, creates and operates a network of package delivery drones which are sold individually or lent to other businesses. Its most recent partner is Mercedes-Benz, with which they are working on integrated drone-delivery trucks. This indicates with high probability that their objective is to target big package delivery carriers. Their main product, the Matternet drone, is set to cost 5000$ a piece, or 1000$ per month when lending as a subscription[2]. The lifetime of the drone is not public, but it was estimated to be 750-1500 flight hours.

Flirtey Flirtey is a company that was founded in 2013. Like Matternet, they too have designed and created a delivery drone. However, their target market seems to be different. Their objective is to reinvent the drone delivery experience for urgent medical supplies, online retail and food delivery. This indicates that instead of targeting the big delivery carriers, they plan on selling directly to institutions and large companies. Their drone's price is unknown at the time of writing.

Amazon Amazon is known for its big market share in the online shopping business. Over the past years, logistics have become a big part of their business due to the increasing number of orders they handle every day. To reduce logistics costs, they have been investigating the usage of drones for package deliveries. Multiple prototypes have already been created and tested successfully. Although Amazon is one of the potential customers of Silentium, they are also a threat to the enterprise. If they are first to bring a delivery drone network to the market, a big chunk will immediately be taken up. The price of their multiple prototypes is unknown.

UPS UPS is an international package delivery multinational which is responsible for 22% of the world's parcel delivery market. Their initiative to work with package delivery drones has been lacking in the past few years, but recently they have decided to work with the company 'Workhorse' to design a new package delivery drone. The product seems to still to be in an early prototype stage, and the price is unknown.

DHL DHL is the global leader in the world parcel delivery market with a market share of 38%. So far, they have already made three different working prototypes for package delivery. The main objective of these drones is to deliver parcels to locations that are difficult to reach by conventional modes of transport. The price of their second prototype, the parcelcopter 2.0, was found to be 55,000 $.

Outlook on competitors Even if the most of the technical details of the competitors is unknown our product specifications appear to be superior. Currently Silentium is only company able to deliver 4 packages, up to 2.5 kg, while still preserving a range of 30 km. Even though, the Amazon drone appears to a bigger range for a payload of 2.2 kg (with the aim of targeting non-urban areas), Silentium can achieve the same or better results by reducing the number of packages.

2.7. Revenue Streams

In this section the main sources of income for the company will be presented. As specified in section 2.5 the aim is selling directly to big shipping companies or more specifically selling the licence of the design to these big shipping companies. This way, the operations are handed over to them, thus reducing the necessary initial investment and therefore the general risk. Other sources of revenues include general operational support, offering training of personnel for maintenance and drone operations, continuous updates of the drones software and design.

Therefore, the expansion and growth of the company are related to its ability to be subcontracted by big companies that dominate the shipping market. The size of the market and buying company would put Silentium in a very good

[2] https://www.nanalyze.com/2015/12/matternet-delivery-drones-that-are-delivering-now/ accessed on 20/06/2018

position to face competitions. Furthermore, the absence of infrastructure and large responsibilities make the company particularly suited to be sold, if a good offer comes.

3

Project Sustainability

Sustainability is important since only a sustainable design can be successful on the market in the long run and naturally no harm should be done to any living being or the environment. This chapter comes before the design since sustainability has to be considered for every design step, which can only be done if the strategy has been established beforehand. Section 3.1 shows how sustainability is taken into account in various steps throughout the last phase of the project.

3.1. Sustainability Approach

For this phase of the project, a new sustainability strategy has been developed. Similar to the previous phases of the project sustainability is a parameter which is often taken into consideration during the project. Therefore, a diagram has been created to provide a complete overview of which work-packages have this parameter taken into account. This figure can be found in Figure 3.1. The number two in the figure indicates the start of this phase of the project.

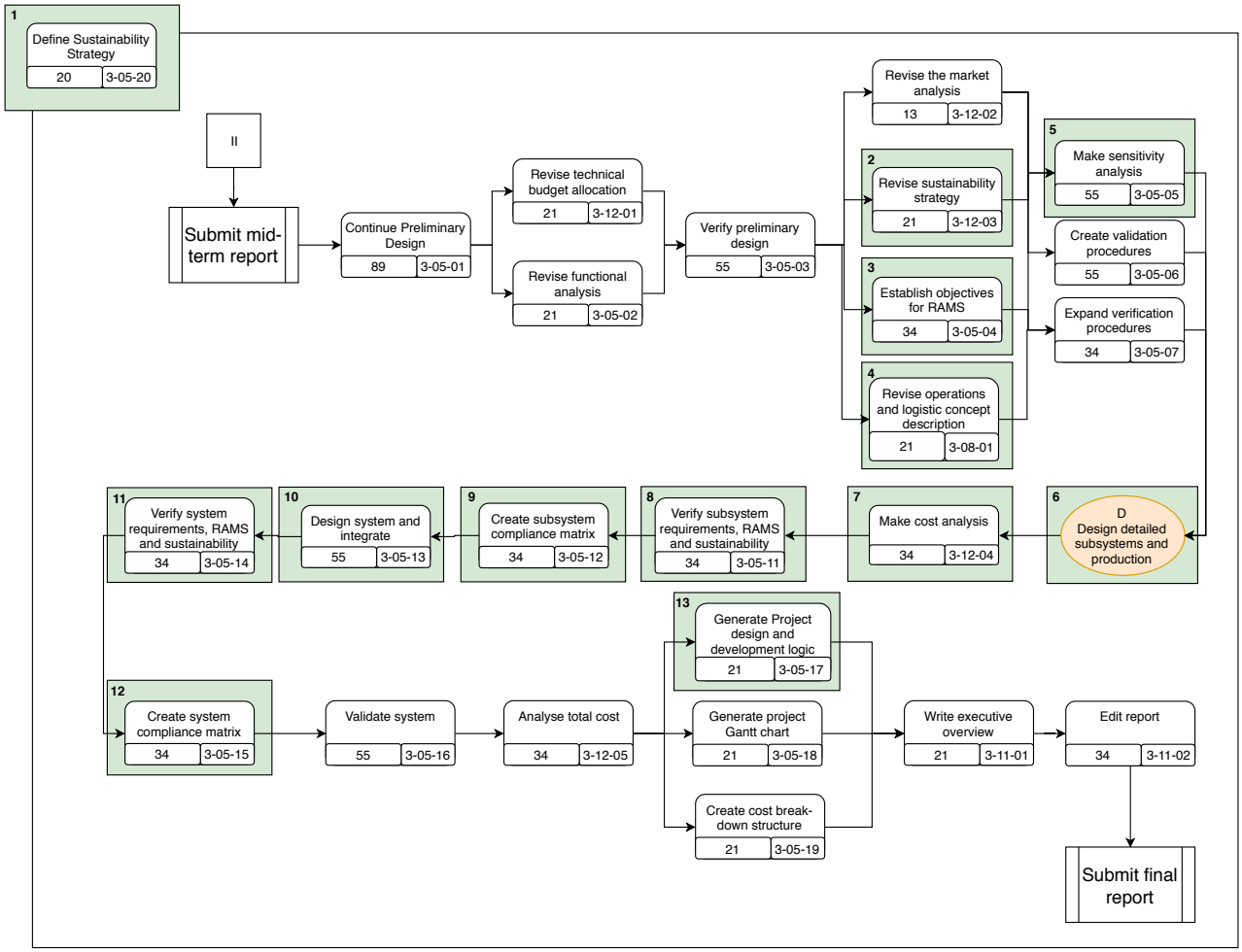

Figure 3.1: Work flow diagram including focus points for sustainability

1. The strategy for the sustainability is often found to be part of several tasks. Hence, before the team started with the final phase of the project, first an overall sustainability strategy has been defined.

2. The sustainability strategy has been revised. This is necessary since the project progresses as well and the sustainability has to be adapted continuously. For this work package, in particular, the strategy has been revised based on the budget allocation and the functional analysis.
3. When the objectives for the RAMS have been designed, sustainability has also been taken into consideration. Especially since maintenance is part of the RAMS, sustainability became a parameter of this work package. How the maintenance of the drone will be handled can severely impact the level of sustainability of the project.
4. The revising of the operations and logistic concept will include several aspects regarding sustainability. It is important to not only analyse sustainability regarding the drone itself but for the complete operation of the drone as well.
5. Depending on the results of the sensitivity analysis, sustainability has been considered as a limiting parameter. For example, if the power usage would increase too much, the design needed to be changed accordingly to reduce the power consumption in order to keep the drone more sustainable compared to truck delivery.
6. The implementation during the detailed design is very important for this phase of the project. All the subsystems will be designed in this work package and if all of them are correctly connected to sustainability the drone can have a significant positive impact on the environment. For example, during the design of the propulsion subsystem, it could be optimised in such a way that sound levels are decreased. By setting up the sustainability strategy beforehand it is made sure that all team members take it into consideration during the final phase of the project.
7. Cost has also been added to the sustainability strategy. To keep the drone affordable compared to its competition is both important for the clients as well as the team.
8. To ensure that the subsystems comply with the set requirements on sustainability they have to be verified. For example, it should be verified that propulsion subsystem does not exceed a certain power consumption. If a requirement is not met, the design should be updated accordingly.
9. This work package comes directly from the verification of the subsystem requirements, here it is shown if each of the subsystems complies with its sustainability requirements.
10. When the subsystems are integrated into the complete design it is important to take into account sustainability. A focus point of this work package is to ensure ease of maintenance which has a severe impact on the sustainability of the project.
11. Similar to the verification of the subsystems, this work package will include verifying if the complete system complies with the set system sustainability requirements. For example, the system should be verified to not exceed a certain set of noise levels.
12. This work package comes directly from the verification of the system requirements, here it is shown if the system complies with its sustainability requirements.
13. For this work package, it is important to include how sustainability will be applied in the post-DSE phases of the project. This important as sustainability is not only part of the design itself, but also in the phases after the design phase.

3.2. Sustainability technical parameters

The sustainability of the drone will be assessed both qualitatively and quantitatively. The manufacturing sustainability, end of life solutions, equity, social acceptance and quality of life will be evaluated in a qualitative fashion. On the other hand, the carbon footprint and energy management of the drone will be assessed quantitatively. Furthermore, the obtained values will be compared to the ones of existing systems to assess the impact of the drone delivery system will have on the environment and human societies.

4

Operations

When designing a system it also has to be considered how it can be operated and if it e.g. requires additional infrastructure as this is essential for the success of the product. This chapter will focus on the operations of drone delivery. The chapter is placed in the beginning of the report since operations can influence the design and its requirements. We started with an analysis of the base station followed by the the routing, the flight profile and the delivery process. Finally, a safety analysis were performed and the current regulations for drones were investigated.

4.1. Base Station

Operating the drone starts with system initialisation and loading the packages to be delivered. This will be done at so called 'base stations' or 'depots', located in package distribution centres. When a drone is needed for operation, the base station is capable of loading the packages, replacing the batteries, and providing operational data to the drone. While loading the packages the order of delivery established by the route needs to be taken into account. It could either be done manually, or by a robot arm, which is up to the costumer. During periods in which no current operations are active, the stations are used as storage facilities for the drones. When empty batteries are replaced, the software inside the base stations keeps track of the number of cycles and their degradation. The batteries each have their own Near Field Communication (NFC) tags, making it easy to manage the stock.

4.2. Routing

This section explains the constraints of the algorithm and its working principle. In addition, a flow diagram shows how the algorithm works. Next, improvements on the algorithm are discussed and finally the results of the routing problem are shown using two cases.

When the drone needs to deliver a large amount of packages, a routing algorithm can be used to determine a path to all addresses. The goal is to minimise the delivery cost and delivery time for each package. Since the drone has limited payload capacity the problem becomes a 'capacitated vehicle routing problem' [1]. In order to find the exact solution for the routing, brute force search could be used. However, this is computationally expensive for a large amount of nodes (delivery points) since there would be $(N-1)!$ possibilities and the search would run in $\mathcal{O}(n!)$ time complexity. Therefore, a more efficient algorithm should be used for the routing.

To develop the algorithm the following assumptions were made:

- The maximum range of the drone is 30 km.
- The drone travels in straight lines to each of the addresses (if regulations allow flying over the area).
- Maximum amount of packages to deliver during a mission is 4.
- Deliveries are represented by nodes, which have been generated with a uniform random distribution, on a circle with a radius of 15 km with the depot in the origin.
- Each node is assigned a package with a given mass and a dimension. The total mass of the packages is constrained by the total payload capacity of the drone, which is 2.5 kg.
- The sizes of packages have been standardised and can consist of units with a surface area of 105 x 74.25 mm and a depth of 105 mm.
- A package can vary from 1 unit up to 8 units in size. The mass of a single unit may not exceed a 500 g, due to constraints posed by the payload mechanism.

The algorithm is a greedy algorithm that searches for the closest node to its current location. From there it will keep going until it has visited all the nodes, or until one of the constraints forces it to go to the depot.

In Figure 4.1 the flow diagram of for the routing can be seen. The algorithm iterates until all nodes have been visited. It outputs the final route, the total distance travelled and a plot of the route. The nomenclature used in the diagram is given below.

[1] `http://neo.lcc.uma.es/vrp/vrp-flavors/capacitated-vrp/` last accessed 17/06/2018

- $Node$: The address of the package recipient.
- Loc_{node}: The (x,y) location of a node.
- W_{node}: The weight of the package that needs to be delivered at 'node'.
- S_{node}: The size (dimensions) of the package that needs to be delivered at 'node'.
- Tot_{dis}: The total distance travelled along the route.
- Tot_{nodes}: The total amount of nodes selected after visiting the depot, with the nearest node added.
- W_{tot}: The total package weight all packages selected after visiting the depot, with the nearest node added.
- Tot_{dim}: The total size of all packages selected after visiting the depot, with the nearest node added.
- Tot_{dis}: The total distance travelled after visiting the depot, with the nearest node and the distance from the nearest node to the depot added.

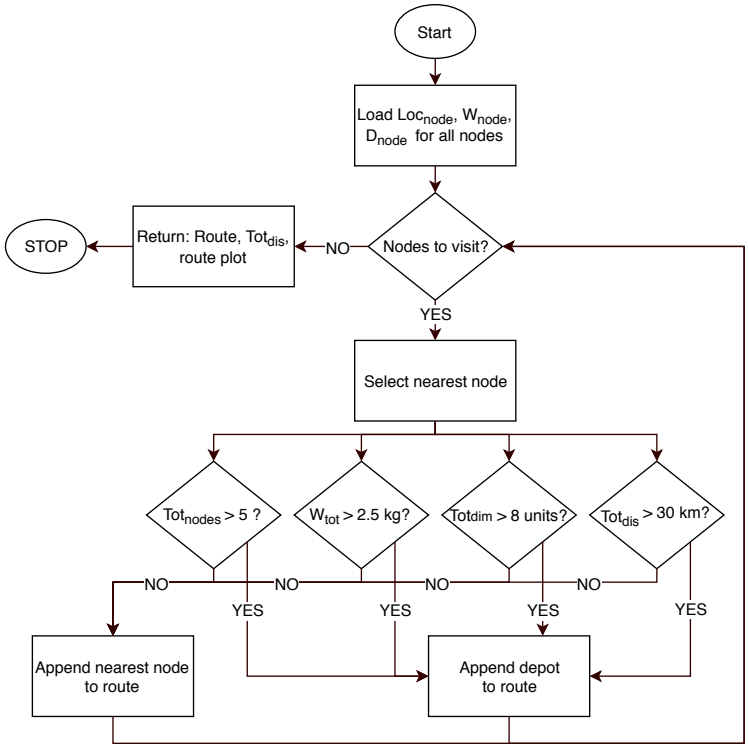

Figure 4.1: Routing algorithm flow diagram.

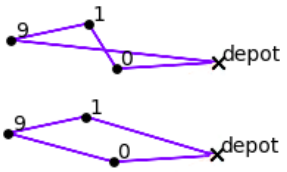

Figure 4.2: Improvement on the algorithm for entangled paths and local optima.

Once the nodes that need to be visited are determined, the algorithm determines the shortest path that passes through all of them. A maximum of 4 nodes per mission can be visited, therefore, brute force is a good solution because there are only 28 (4!) solutions possible. In this way, entangled paths constructed by the algorithm can be mitigated, as shown in Figure 4.2. Another improvement is the implementation of priority, which the customer can give to packages. Those packages will be delivered before others in the routing algorithm.

The way the dimension and the weight are generated has a large influence on what the solution will be for the drone routing. In the algorithm, the package dimensions are assigned using a truncated normal distribution with values in the range of 1 to 8. The weights use a similar normal distribution with the dimension of the package as the mean for the distribution. In this way smaller packages will likely be lighter than big packages.

If the packages then are small and light, the drone will be able to carry more of them and has to go to the base station less often than when the packages would be big and heavy. To show this two test cases have been constructed below. For both test cases, 10 randomly positioned nodes were generated within a 15 km radius of the depot. The specifics of each distribution are mentioned in the test cases.

Case 1. The sizes of the packages are sampled from a discrete normal distribution with mean 3 and variance 1 ($\mathcal{N}(3,1)$) shown in Figure 4.3. The output of the algorithm can be seen in Figure 4.4. The average total distance the drone travelled in this scenario was 104.76 km with an average weight of 625 g.

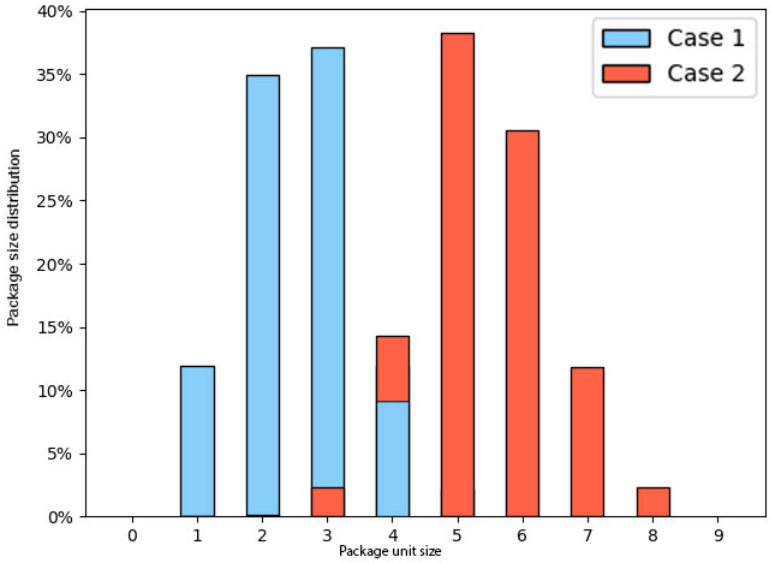

Figure 4.3: Distribution of the package sizes for two different cases

Case 2. The sizes of the packages are sampled from a discrete normal distribution mean 6 and variance 1 ($\mathcal{N}(6,1)$) shown in Figure 4.3. The output of the algorithm, using the same nodes as in case 1 as input, can be seen in Figure 4.4. The average total distance the drone travelled in this scenario was 186.38 km with an average weight of 1250 g. We observe therefore 78% reduction in travel distance compared to the one case 1.

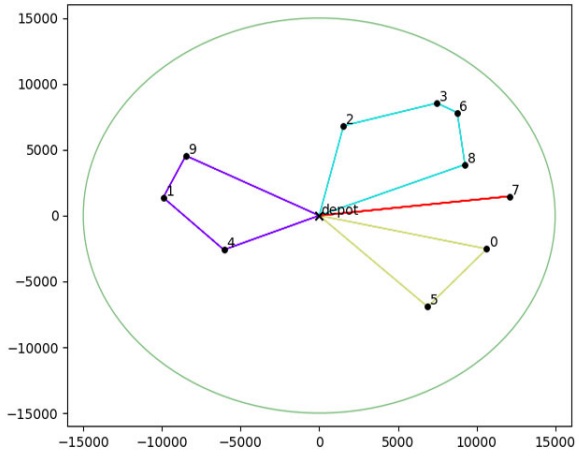

Figure 4.4: Routing algorithm output for small packages

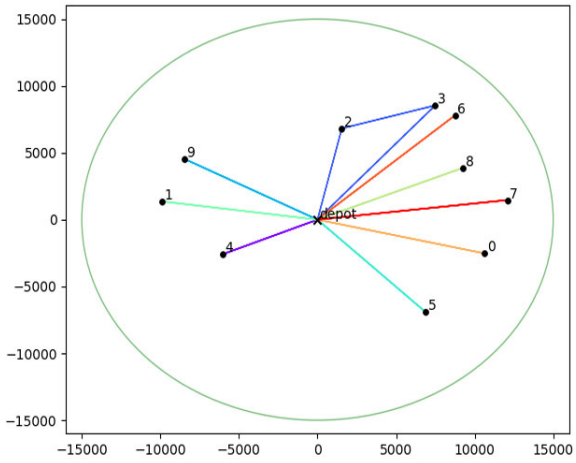

Figure 4.5: Routing algorithm output for big packages

From both cases we can conclude that the efficiency of drone delivery is highly dependant on what kind of packages will be delivered by the drone. Bigger packages constrain the drone, so it has to visit the base station more often. It is up to the costumer to do an analysis on what packages it wants to deliver, as long as the dimensions and weight stay in the limits that the drone is designed for.

4.3. Flight Profile

The flight profile of the system is presented in this section. It stems from the driving performance requirements for range and number of climbs (SYS-DR-7, SYS-DR-30). It was the primary input for the initial sizing and indirectly it was driving for the subsystem design. The elements of flight profile can be categorised in vertical take-off and landing phase (VTOL) and fixed wing flight phase (FW).

A hover and a loiter phase have been introduced to account for contingencies. Note that for emergency cases the battery can be drained beyond the nominal depth of discharge yielding an extra 66% of the nominal battery capacity (60% Depth of Discharge). The resulting flight profile is presented in Figure 4.6.

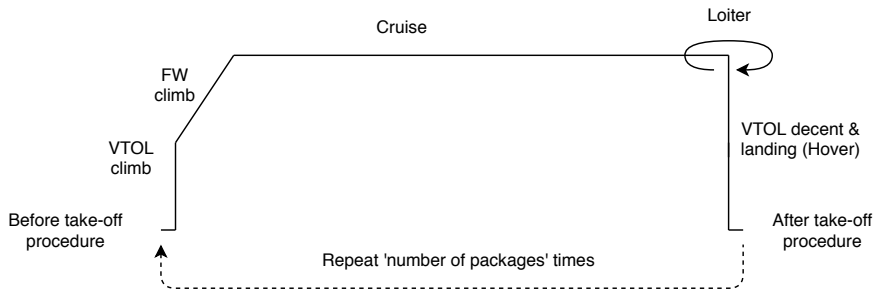

Figure 4.6: General flight profile for various number of packages

The duration of the different phases is as following. The VTOL climb mode shall last 60 m with a speed of 1 $\mathrm{m\,s^{-1}}$, while the FW climb mode shall climb to 120 m with a velocity of 16.5 $\mathrm{m\,s^{-1}}$ and includes the transition from VTOL to FW. The cruise phase shall be 30 km long at most, at a speed of 17.8 $\mathrm{m\,s^{-1}}$. The loiter shall be 5 minutes in total and the hover shall be 5 minutes in total. Furthermore, the flight profile shall be executable with full payload given that there may be issues regarding the delivery.

4.4. Delivery

In a previous phase of the project three types of deliveries were identified. These can be found in Table 4.1.

Density	Garden (y/n)	Example
High	No	Manhattan
Medium	Yes and No	Suburbs
Low	Yes	Country side

Table 4.1: Population Density Categories

High Density Areas Due to many irregularities at the roofs of the majority of the apartment buildings we suggested introducing standardised landing platforms that can be installed on top of them. Designing such a platform is beyond the scope of this project, and could be done by the costumer since the only requirement for delivery is that the drone can land on the platform.

Medium Density Areas This category is more challenging compared to the previous one. In the case the house would have a garden, and the drone has to determine whether the garden is a safe place to land. On the other hand some houses may not have a garden at all or have a garden which is not large enough for the drone to land safely. In these cases, it is advised to install a package delivery system which is incorporated in public space. Another solution that could be used is to reserve the use of existing parking locations for cars to land the drone. Since the drone is not much wider than an average car it should be able to easily land and park in the same places. Then the recipient can collect the package from the drone at the nearest parking location.

Low Density Areas These areas are often located outside urban areas and don't present particular problems for landing. The delivery companies to decide where they would like to position the base stations. This could mean that the people living in these areas will get the possibility for drone delivery later since it is less profitable business.

During the drone delivery process, a system should be implemented which notifies the recipient of a package before the drone arrives. A total of three types of notifications have been defined and are listed below.

1. A message before the drone takes off. The recipient should confirm if he or she is able to receive the package within a given time-frame.

2. A message notifying the drone is within a few minutes of arrival.
3. A confirmation that the package has been delivered.

These messages could be sent using text message or a designated app, just like the apps current taxi services use. This would allow for registration of the recipients. At the moment of signing up, it could be required for the recipient to stand at the location where he or she wants the drone to land. The GPS location and a mapping software could be used to check is the location is suitable for the drone to land.

4.5. Regulations

As of now the regulations regarding UAVs are different for each country and even different per state in the case of the US. However, regulatory proposals are continuously worked on by various authorities. The European Aviation Safety Agency (EASA) has published their opinion, which will serve as a basis for the European Commission to adopt concrete regulatory proposals later this year [35].

Figure 4.7 shows a breakdown of the categories of UAV operation specified in the regulatory proposal by EASA. The diagram shows that Silentium does not fall within the open category as its MTOW will be higher than 4 kg and it will have to fly within close proximity to people. Silentium falls under the category called 'specific'.

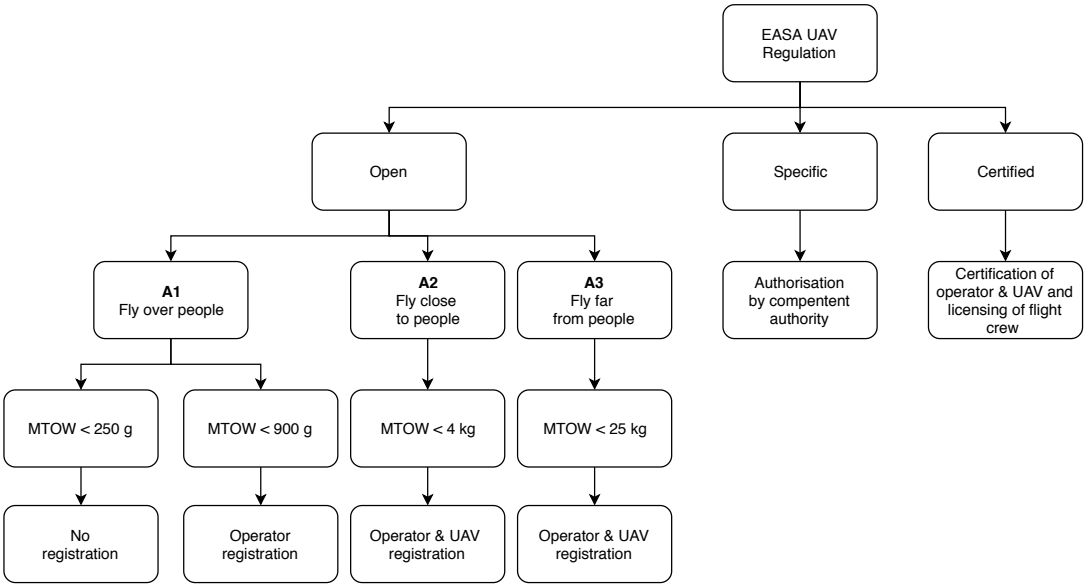

Figure 4.7: Breakdown of UAV categories in EASA opinion No 01/2018 [35]

A proposal by the Single European Sky ATM Research (SESAR) project called U-Space is more applicable to delivery drones [2]. It aims to provide services and specific procedures designed to support safe, efficient and secure access to airspace for large numbers of drones. This is in particular focused on the use of high-density operations with a fleet of autonomous drones.

Since one of the main requirements of the drone is to respect European night noise regulations, it is important to identify these regulations. As European countries have different regulations on noise pollution, the Dutch law will be considered leading in the noise constraints of the drone. Dutch law states a maximum instantaneous noise level of 65 dB(A) at 7.5 m for nightly loading and unloading, and a maximum yearly average night noise level of 40 dB(A) [1].

It is clear that regulations for UAV operations are still in its early stages and are continuously changing. It is therefore very important for Silentium to keep track of the progress on regulations and make sure it respects these regulations.

[2] `https://www.sesarju.eu/u-space-blueprint` last accessed 21/06/2018

5
Requirements

The final step in the pre-design phase was to establish the requirements which will be done in this chapter taking into account the considerations made in the previous chapters. First, the user and stakeholder requirements will be listed in order to ensure that the wishes and needs of our customers and of all stakeholders are taken into account. Furthermore, they will be used to arrive at the system requirements which are the ones that will be used during the design. Subsequently, the Functional Flow Diagram and the Functional Breakdown Structure will be shown which also contribute to the system requirements. Finally, the budget breakdown will be presented which serves as a basis for the subsystem requirements.

5.1. User Requirements

In the list below the final user requirements for the delivery drone are listed. They were taken from the specifications/ agreements given by/ made with the customer.

- The maximum operational speed shall respect European Law.
- The maximum weight of the payload shall be 2.5 kg and its maximum size shall be 210 mm x 297 mm x 105 mm.
- The drone shall respect European night noise regulations.
- The lifetime of the drone shall be at least 2 years.
- The drone shall have an autopilot with proximity sensors.
- The drone shall be designed for home delivery in densely populated areas.
- The drone shall be able to safely continue/abort missions with low or absent GPS signal.
- The drone shall be single point failure free.
- The cost of the final product shall not exceed one of the competitors.
- The drone shall be manufactured with 3D printing.
- The drone shall not get closer than 30 cm from any object while operational.
- A text message will inform the recipient about the delivery.
- The design shall include redundancy to be able to continue/abort the mission safely with 50 % of the propulsive system operational.
- An optimisation software shall optimise the path to deliver up to 4 packages.
- The path shall be defined before take-off. It shall be modified in case of risk.
- The drone components shall be off-the-shelf.

5.2. Stakeholder Requirements

In this section, the stakeholder requirements will be presented. This is important since it has to be ensured that no third-party is harmed in any way by the project. In order to do that, it first had to be established who the stakeholders are.

- **Customers:** (Shipping companies/large retailers) The customers will eventually buy the drone and operate it. Requirements set by the customer are usually key requirements.
- **Package recipients**: The package recipients are the people who receive the packages delivered by the drone.
- **Civilians:** Civilians are all people living in the operating area of the drone, or close to it. They are affected by the system since it operates around them, even though they are not directly involved with the package delivery.
- **Government:** The government includes all official administrations which determine the rules regarding the operation of drones for delivery services. Since the drone has to comply with regulations, it has to be designed in such a way that these requirements are accounted for when possible, or else it would not be able to operate.
- **Environmentalists** Environmentalists include all organisations regarding the environment and wildlife. They could possibly oppose the use of drones for package delivery when (urban) wildlife would be disturbed in a significant way, which could lead to more restrictions from the government.

- **Private and civil aviation:** The airspace in which the drone will be operated might be used by private or civil aviation as well. Since this could result in safety issues this should be accounted for in the design.

The stakeholder requirements can be seen in Table 5.1 where they were categorised into (non-)driving and (non-)key requirements. Driving means that the requirement drives the design to a large extent and key that it is of high importance. Please note that a key requirement is not necessarily a driving one and vice versa. This division was made since it is difficult to take all requirements at once into account when starting the design. Consequently, it was first designed for the driving requirements since these drive the design and subsequently the design was altered to also comply with the remaining ones.

Id	Requirement	Stakeholders	Classification
S1	The drone shall deliver the parcels without causing any damage.	Package recipient, civilians	Driving / Key
S2	The drone shall not cause damage to properties	Civilians, environmentalists	Driving / Key
S3	The drone shall comply to noise regulations.	Recipients, civilians, government	Driving / Key
S4	The drone shall not cause any disturbance to the urban wildlife.	Environmentalists	Driving / Non-key
S5	The cost of the final product shall not exceed that of competitors.	Customer	Non-driving / Key
S6	The operating cost of the drone shall not exceed that of competitors.	Customer	Non-driving /Key
S7	The drone shall deliver packages faster than using conventional truck delivery.	Customer, package recipient	Non-driving/ Non-key
S8	The drone shall be traceable by the company when delivering packages.	Customer	Non-driving / Non-key
S9	The drone shall notify the person to receive the parcel upon its arrival.	Customer, package recipient	Non-driving / Non-key
S10	The drone shall not invade the privacy of the package recipients and civilians.	Package recipients, civilians	Non-driving / Non-key
S11	The drone shall comply with existing safety regulations regarding drones.	Recipients, civilians, government	Non-driving / Non-key
S12	The delivery drones shall leave enough airspace to not disturb the urban wildlife	Environmentalists	Non-driving
S13	The drone shall not cause disturbance for private and civil aviation.	Private and civil aviation	Non-driving
S14	The drone shall be visible for other aircraft	Private and civil aviation	Non-driving / Non-key
S15	The drone shall be able to operate in unfavourable weather conditions.	Customer	Non-driving / Non-key

Table 5.1: Overview stakeholder requirements

5.3. Functional Flow Diagram

In this section, the Functional Flow Diagram (FFD) will be presented, which provides a detailed overview of the functions that have to be performed during the design process in chronological order. From this information it is possible to derive requirements at system and subsystem level for the performance and capabilities of the drone.

Figure 5.1 shows the Functional Flow Diagram. It has been colour coded in the following way: the zeroth level is red, the first level is green and the second level is white. Special blocks that contain an "OR" are purple and they indicate that only one of the two options will be followed. From some blocks, there are two arrows flowing: a red and a green one, with a $\bar{G}$ for NO GO and G for GO, respectively. Their meaning is that the result of the check specified on their parent block might be positive or negative. In the first case, it is a GO and the drone can continue with the nominal flow. In the second case, it is a NO GO and either some intermediate steps are taken or the flow is ended shortly after.

For clarity, some blocks are expanded at a lower level. In those cases, the parent block is repeated with a "REF" sign to indicate that it is a duplicate, and the children blocks follow in chronological order. In some cases the children flow diagram was too big, so expansions A and B were created. They are shown in Figure 5.2 and Figure 5.3 respectively.

The functions of the drone were categorised chronologically into designing it, producing it, distributing it to the companies that will be using it, operating it and finally retiring it at its end of life. The design function is divided into several phases. Phase 0 starts at the beginning of the project and ends with the delivery of the project plan [10]. Phase 1 starts at the end of phase 0 and it finishes with the submission of the baseline report [8]. Phase 2 follows, which is concluded with the midterm report [9]. The last phase goes from the mid-term report submission to the final report.

5.4. Functional Breakdown Structure

The Functional Breakdown Structure (FBS) is closely related to the Functional Flow Diagram in the sense that both of them give a clear idea of what functions the drone needs to be able to perform. However, the FBS does not present them in a chronological order, but in an "AND" tree structure. In addition, the FBS goes into more detail by decomposing the functions into smaller tasks.

The FBS for the silent delivery drone can be seen on Figure 5.4. This figure is also colour coded: the zeroth level is red, the first one is green, the second one is white, the third one is blue, the fourth one is yellow and the fifth level is orange. It should be noted that this colour scheme has not been respected on the lowest level of each branch: these tasks are all white and they are not inside of blocks for clarity purposes.

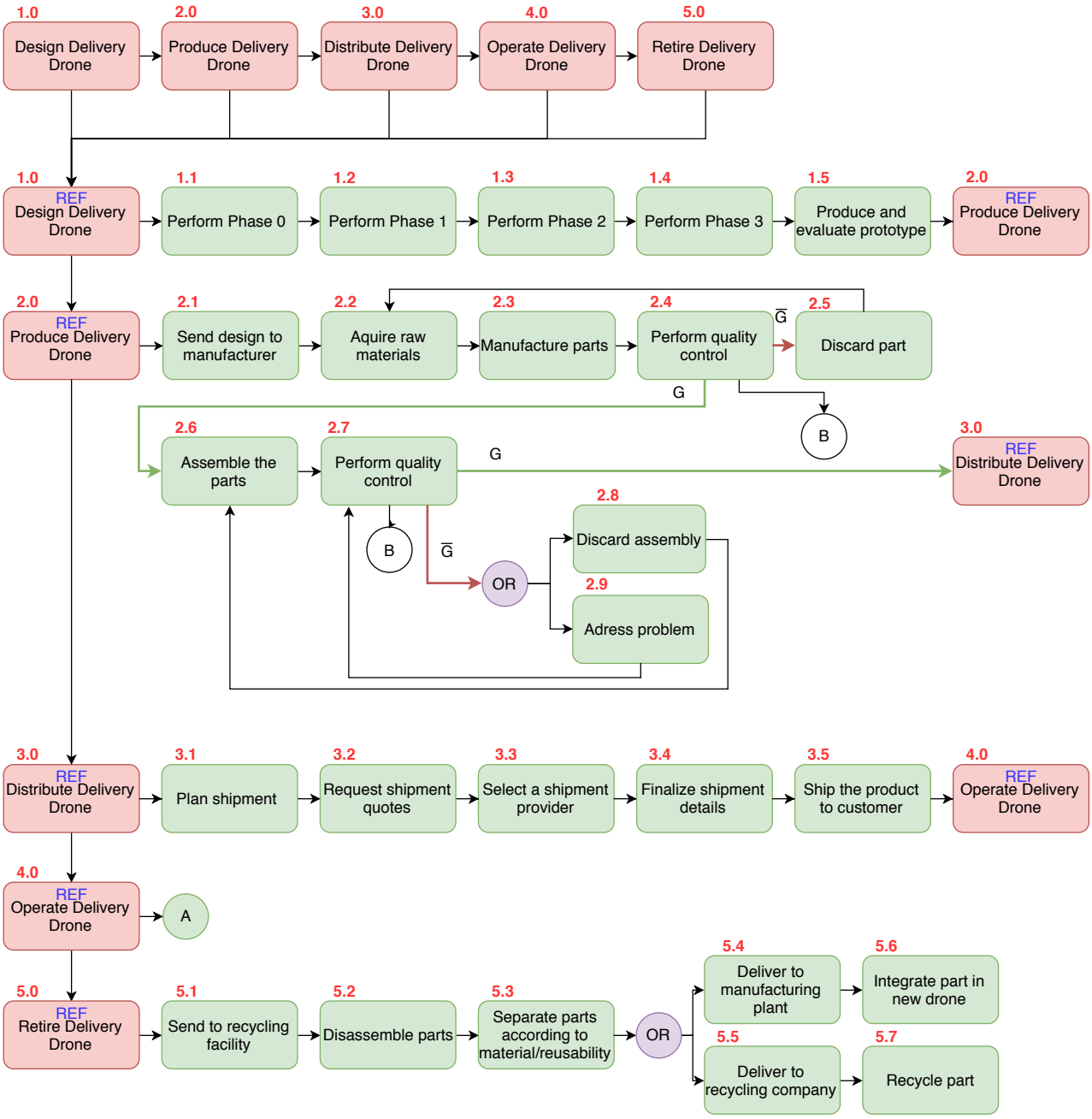

Figure 5.1: Functional Flow Diagram for the silent delivery drone.

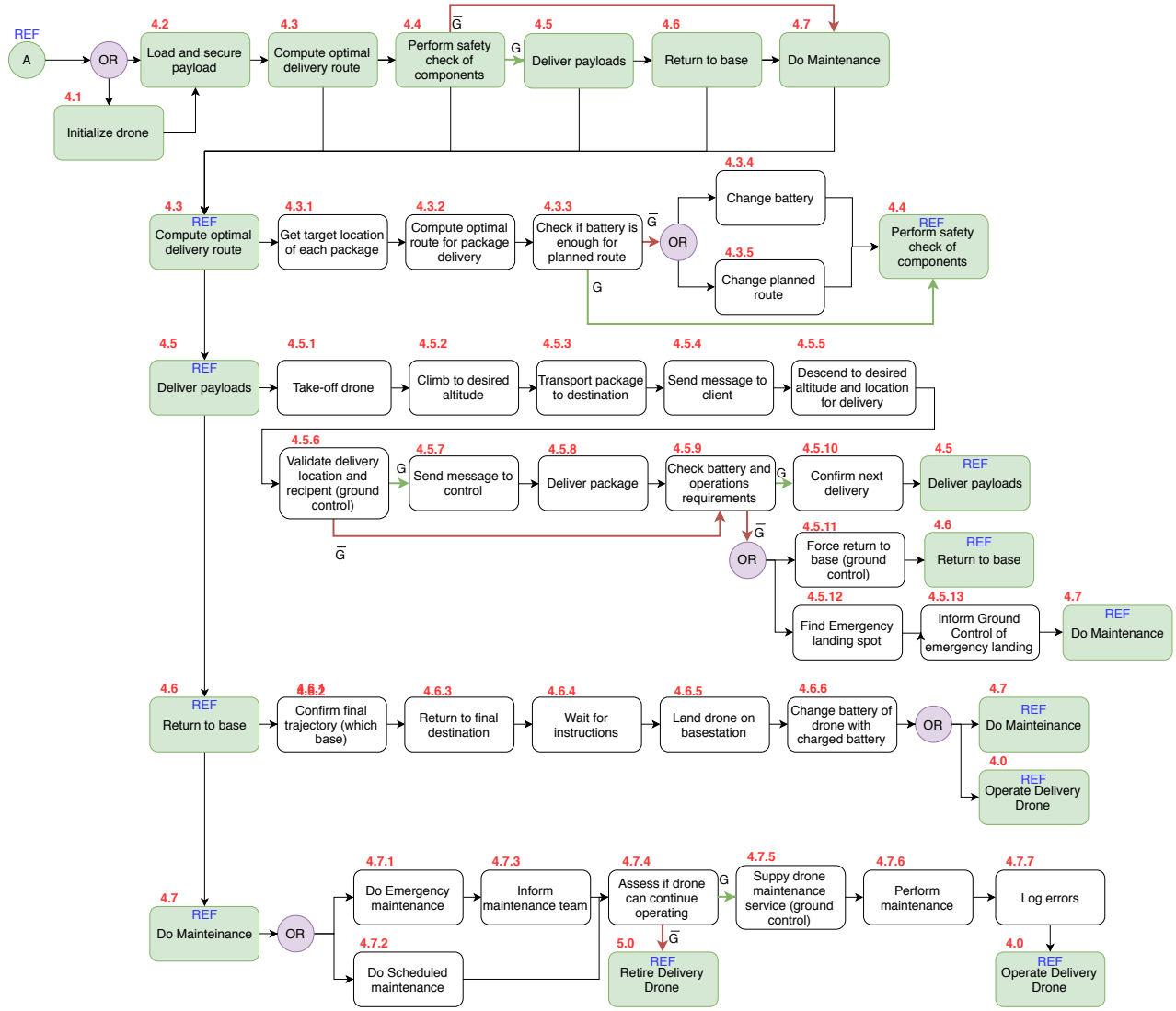

Figure 5.2: Expansion of block A in the Functional Flow Diagram for the silent delivery drone.

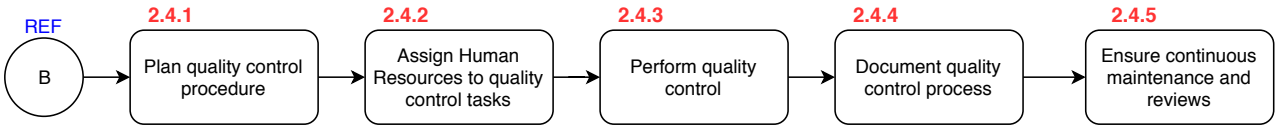

Figure 5.3: Expansion of block B in the Functional Flow Diagram for the silent delivery drone.

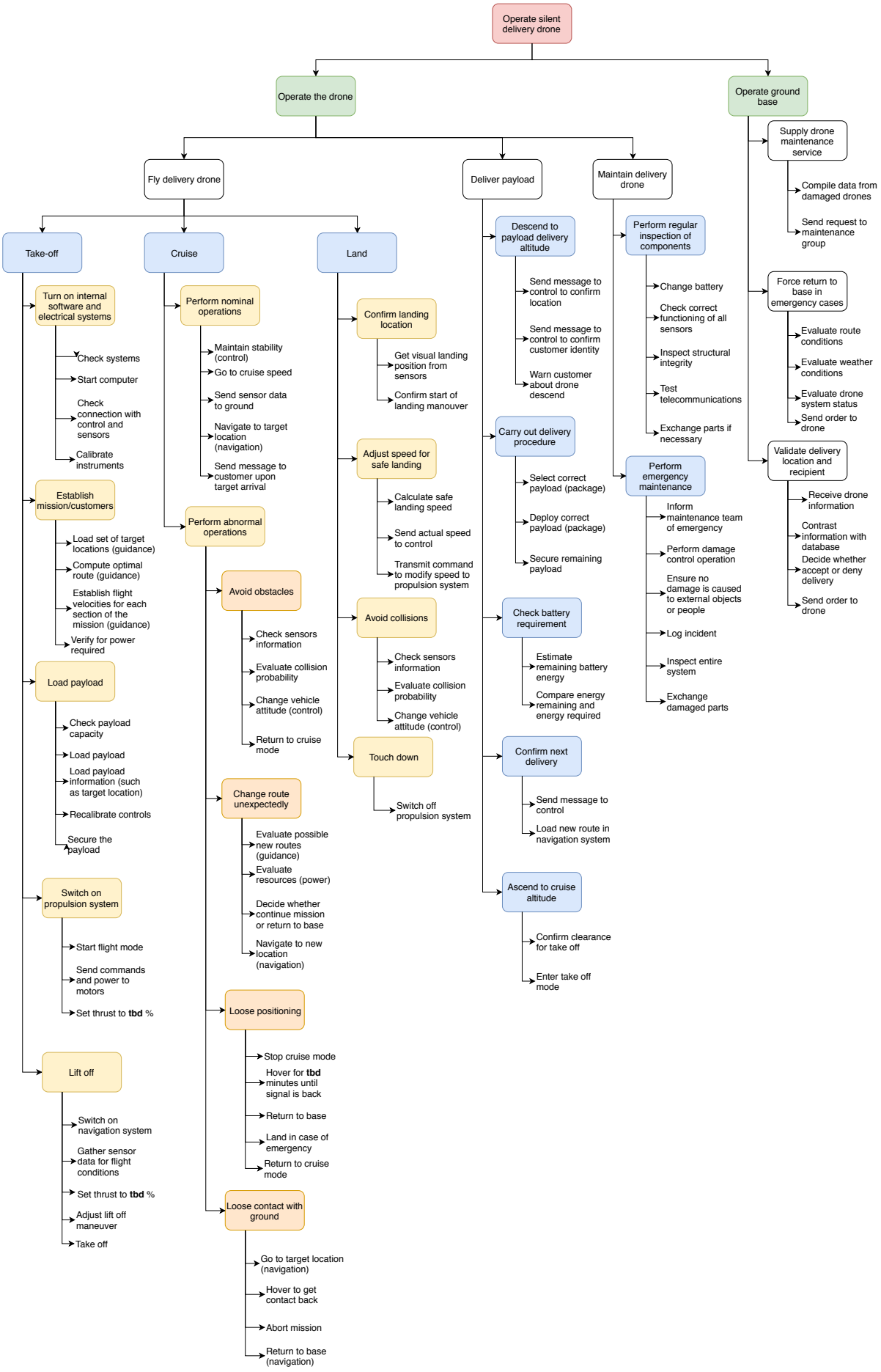

Figure 5.4: Functional Breakdown Structure for the silent delivery drone.

Firstly, the operations are divided into operating the drone itself and the ground station operations. The functions of the ground station are maintenance of the drones, making decisions in case of emergencies or unexpected situations and validating delivery locations and recipients. The operations of the drone are more complex, so they are further divided into flying, delivering the payload and maintenance tasks. In all cases, both nominal and exceptional situations have been considered, in order to minimise the chances of failure.

5.5. System and Subsystem Requirements

In this section, the system requirements will be derived and the technical budget breakdown will be performed which then serves as a basis for the subsystem requirements. Furthermore, the approach used for contingency planning will be explained.

System Requirements The system requirements directly followed from the user and stakeholder requirements as well as technical considerations. Furthermore, the FFD and the FBD were taken into account when establishing the system requirements as these provide a good overview of what the system needs to be able to do. All of the system requirements can be found in chapter 17, where they are listed in the compliance matrix for the overall system.

Subsystem: Budget Break-Down In order to give specifications on the mass and power available per subsystem in the subsystem requirements, a technical budget breakdown had to be performed first. The technical budget was allocated based on the preliminary sizing. From that, the mass of most subsystems as well as their average energy consumption during the different phases of the mission was known. The budget breakdown can be seen in Table 5.2. The values listed indicate how much power and mass each subsystem can use during the detailed design. The structure includes the load carrying structure, the fairings and the actuators necessary for the control surfaces. The propulsion system includes the motors and the electric speed controllers for the motors and propellers. The electric system and battery include the battery and all the necessary subsystems for power distributions. The Avionics include all electric instruments on boards excluding the batteries, power distribution and motor.

Subsystem	Peak power [W]	Average Power [W]	Mass [kg]	Energy [MJ]
Structures	28	28	3.17	0.042
Propulsion	1469	485	1.0	1.316
Electric system and battery	-	-	3.22	-
Payload mechanism and auxilarly systems	20	5	1.75	0.01
Avionics	50	40	0.75	0.072
Payload	-	-	2.5	-
TOTAL:	**1539**	**530**	**12.4**	**1.39**

Table 5.2: Preliminary budget break-down

Subsystem Requirements With the system requirements and technical budget breakdown established, the subsystem requirements could be derived. They are listed in the detailed design chapters of the respective subsystems. The command and data handling subsystem requirements can be found in chapter 7, the ones for the structure in chapter 9, the wing design ones in chapter 8, the ones for control and navigation in chapter 10, the propulsion ones in chapter 11, the ones for the payload mechanism in chapter 12 and finally the ones for the auxiliary system can be found in chapter 13.

Contingency Planning The conceptual technical budgets and mass estimation methods are generally inaccurate throughout the duration of the projects but with decreasing level of uncertainty the further the design progresses. This uncertainty is very dangerous since it might compromise the compliance to requirements. To make up for it, contingency margins for each phase of the design were introduced. To illustrate how the contingency management works consider the following example: a design with a target mass of 20 kg, a 20% contingency at the conceptual design phase, 10% at preliminary and 5% at the detailed design phase. Since the contingency at the conceptual design is 20%, it will be tried to achieve a predicted mass of 16 kg. If the predicted mass is more than that, iterations will be performed until the target is met. At the following stage, the preliminary design, the aim is to get an expected mass of less than 18 kg. Again, if this is exceeded, further iterations are required. This process will be repeated until the design is completed. The contingencies that were chosen for both the mass and the power budget are, 25%, 15%, and 10% for the conceptual phase, the preliminary phase and the current, detailed phase, respectively.

6

Conceptual Design Summary

With the requirements established the actual design process could be started. In this chapter, the approach used for this will be described, briefly summarising the steps taken in previous reports preceding the detailed design. The purpose of this is to provide an overview of the decisions that lead to the conceptual design on which the detailed design was based and to show its robustness.

In order to arrive at a conceptual design, a trade-off between the possible configurations for the delivery drone was made. Based on this, 4 concepts were created which were then sized to determine more of their respective performance characteristics. Comparing these, the most suitable design was chosen which was then used as a basis for the detailed design. In the following section, it will be explained how the concepts were derived and their respective characteristics will be presented. Subsequently, the trade-off used to pick the most suitable one will be explained and finally, the winning concept will be presented and a sensitivity analysis will be performed.

6.1. The Conceptual Designs

Before going into the design details, it makes sense to explain which aspects were considered in the design process. First of all, the range had a big effect on the design of the drone. An increase in range corresponds to an increase in power consumption and subsequently also an increase in weight due to the increased capacity of the batteries needed to perform the mission. Considering competitors and the range of current multicopters, it was decided to make use of lifting surfaces or a combination of lifting surfaces and a propulsive system. This way advantage can be taken of both, the more efficient nature of lifting surfaces during cruise and the possibility to take off vertically with the propellers. Furthermore, it was decided that the payload should be stored within the drone, since having it outside of the main body would increase the drag to an unacceptable extent.

Another important factor is the requirement related to the avoidance of catastrophic failure due to an engine failure. Due to this requirement, extra control surfaces or a configuration of surfaces that allow controlling the aircraft even in case of engine failure are needed. Furthermore, for all conceptual designs, it had to be considered that their main bodies have to be able to accommodate both the payload and the batteries.

From these considerations, it could be derived that all conceptual designs should have lifting surfaces and propellers in order to guarantee the ability to take-off vertically while still complying with the range-requirement. The 4 concepts can be seen in Figure 6.1 to Figure 6.4 and their specific characteristics will be briefly explained hereafter.

- Concept 1: Fixed-wing. This design can be seen in Figure 6.1. It includes 6 propellers positioned parallel to the ground for VTOL (Vertical Take Off and Landing), in addition to a seventh propeller that is positioned perpendicular to the ground. This last propeller is used together with the main wing and horizontal and vertical stabilisers during cruise.

- Concept 2: Flying wing. This design is depicted in Figure 6.2 and consists of one big flying wing that has five propellers attached to it. The biggest one provides horizontal thrust for cruise, while the other four, which are used for take-off and landing, are smaller and are attached to the wing using rods.

- Concept 3: Flying Wing with Integrated Propellers (FWIP). This original design is shown in Figure 6.3. It consists of one big flying wing with one propeller positioned perpendicular to the ground on its back for cruise. The innovative part of this design is the location of the six propellers that are needed for vertical take-off and landing: they are inside of the wing, and they would be shielded during cruise to provide a bigger lifting surface.

- Concept 4: Tilting wing. This design can be seen in Figure 6.4. It is the most similar to a conventional aircraft. It consists of a fixed main wing and a fuselage-mounted wing. The propulsion system consists of two propellers on the main wing and two more on the horizontal stabiliser. These propellers are able to rotate in order to provide vertical take-off and landing as well as thrust during cruise.

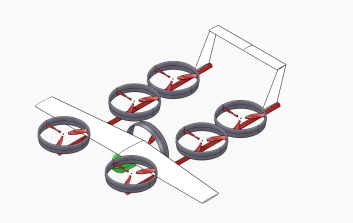

Figure 6.1: Sketch of the fixed wing concept

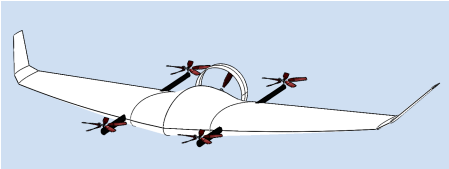

Figure 6.2: Sketch of the flying wing concept

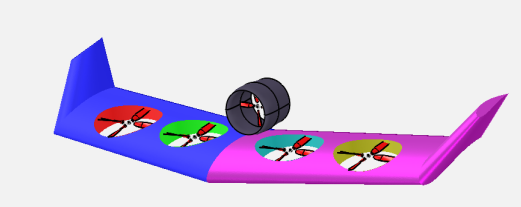

Figure 6.3: Sketch of the flying wing with integrated propellers concept

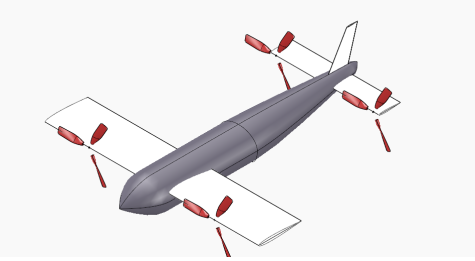

Figure 6.4: Sketch of the tilt wing concept

6.2. Trade-Off Summary

This section will explain how the trade-off between the four concepts was performed. The strategy consisted of selecting a set of criteria and assigning an importance weight γ_i (where $0 \leq \gamma_i \leq 1$ and $\sum_i \gamma_i = 1$) and a compliance score δ_i (where $0 \leq \delta_i \leq 1$) for each criteria. The total score of a concept was determined by the sum of the product of the importance of each criteria and its compliance score.

The importance weight could be *Less Important*, *Neutral* or *Important*, with respective scores of 1, 2 and 4. The weight γ_i was then computed by dividing the score of each criterion by the sum of all scores. The results were scaled in the following way: the most convenient result received a score of 1 and the least convenient a score of 0. Everything in between was mapped linearly. The criteria that were chosen, together with their importance and the estimation method used for each are summarised in Table 6.1. The approach for the determination of the score for these criteria will briefly be discussed and the results will be presented in section 6.3.

Criteria	Absolute Weight factor	Importance Weight	Estimation method
Take-off Mass	Important	12.5%	Quantitative
Aerodynamic Characteristics	Important	12.5%	Quantitative
Stability Characteristics	Important	12.5%	Quantitative
Noise	Important	12.1%	Qualitative and Quantitative
Risk	Important	12.1%	Qualitative
Dimensions	Neutral	6.1%	Quantitative
Reliability	Neutral	6.1%	Qualitative
Safety	Neutral	6.1%	Qualitative
Cost	Neutral	6.1%	Qualitative
Maintainability	Neutral	6.1%	Qualitative
Energy consumption	Neutral	6.1%	Quantitative
Availability	Less Important	2.9%	Qualitative

Table 6.1: Trade-off criteria weight factors.

Sizing: The sizing was done to obtain the scores for the mass and the dimensions of the conceptual designs. It was performed using an adaptation for UAV-VTOL aircraft of the Raymer method for conventional aircraft [42]. The output was several parameters for each concept, for example, the diameters of the propellers, the mass of all the components, wing dimensions and power required. From this, the scores which will be presented in section 6.3 could be derived.

Performance characteristics For each concept, the aerodynamic and stability characteristics were computed to be able to derive the scores for these categories. The aerodynamics characteristics were obtained from XFLR5 and from the sizing parameters, that had been computed earlier. The stability characteristics were computed by estimating the centre of gravity position for each configuration and using standard stability analysis procedures.

RAMS For reliability, availability, maintainability, and safety a qualitative score was given to each concept.

First, reliability was studied. At this point, the reliability analysis was performed based on complexity and redundancy of the concepts. Regarding availability, user requirement E.3 establishes that it shall be possible to construct the drone using off the shelf components. For this reason, the same score was assigned to all the designs. Next, maintainability was considered. Since all components need to be off the shelf, maintainability was expected to be dependent on how accessible and how strongly integrated the parts are. Finally, safety was analysed. Concepts that include a structure that provides some protection for the propellers were deemed safer.

Sustainability For sustainability, noise, social acceptance and energy consumption were considered. Noise production was estimated using a quantitative method based on propeller size, blade configuration and operating conditions. Some other considerations were also relevant, in particular, the interaction with a stator, the duct, shielding or redirection of the noise and active noise cancellation.

Factors that play a role in social acceptance are, amongst others, size and noise. Additional factors included in social acceptance were found difficult to quantify and it was therefore decided to not include it in the trade-off. Finally, the total energy consumption was computed during the sizing and a score was given to each of the concepts.

Cost Analysis It was decided to compare the cost of each component of the concepts separately since no sophisticated cost estimation methods are available for drones and since they have comparatively few components. Furthermore, costs related to manufacturing and maintenance were considered.

Risk The final trade criteria to be determined was the concept risk, which was assessed by looking at the possible technical issues related to each conceptual design, their probability and their impact.

6.3. The Winning Concept

With all trade criteria scores determined, the final trade-off table could be set up using the method described in section 6.2 and the best concept was selected. The results are shown in Table 6.2 where the column width corresponds to the importance weight of the criteria. The colours green, blue, yellow and red represent the scores "Excellent", "Good", "Correctable deficiencies" and "Marginal", respectively. It can be seen that the trade-off was conclusive, with concept 2, the flying wing depicted in Figure 6.2, scoring a full 13 points higher than the second place concept. This was mainly due to its light design, its favourable stability characteristics and its low risk.

Criteria / Options	Take-off Mass	Aerodynamic Char.	Stability Char.	Noise	Risk	Dimensions	Reliability	Safety	Cost	Maintainability	Availability	Energy Consumption	Total score ϕ
Fixed Wing	0	7.62	12.1	0	12.1	0	2.44	4.88	2.44	4.88	2.4	0	48.86
Flying wing	12.1	6.53	9.68	2.18	9.68	6.1	3.66	2.44	4.88	3.66	2.4	5.43	68.74
FWIP	3.99	12.1	2.42	12.1	2.42	2.44	3.66	2.44	2.44	2.44	2.4	6.1	54.95
Tilt-Wing	7.99	0	4.84	7.14	4.84	4.03	2.44	3.66	6.1	3.66	2.4	4.39	51.49

Table 6.2: Final trade-off scores, with the individual $\gamma \cdot \delta$ scores per criterion, and the total score.

6.4. Sensitivity Analysis

The scores assigned in the trade-off table have an uncertainty that stems from both, a lack of information about the system and inaccuracies in the methods used for the trade-off. Consequently, it was analysed how these uncertainties

can affect the choice of the final design. This was be done by varying the assigned weights to simulate the uncertainty of the scores given and then check if the flying wing concept would still obtain the highest score. If that was not the case it was checked if the combinations of weights that led to this outcome is realistic and could actually have occurred this way.

Calculating the scores for all possible combinations, it was found that there are indeed many scenarios for which the flying wing does not win the trade-off. In order to reduce the number of these scenarios, only combinations which had an importance weight of 4 for the mass were considered. The reason for that is that it is certain that the mass is of high importance for the trade-off. Given this constraint only the following set of weights allow another concept to win the trade-off: 1.Mass: $\sigma = 4$, 2.Dimensions: $\sigma = 1$, 3.Aerodynamics: $\sigma = 4$, 4.Stability: $\sigma = 1$, 5.Noise: $\sigma = 4$, 6.Risk: $\sigma = 1$. Consequently, the flying wing will always obtain the highest score if it can be shown that at least one of those weights is unrealistic and would not actually be assigned this way. Since stability is a crucial parameter for safety it will never be assigned a score of only 1 as required to change which concept wins the trade-off. That means that the flying wing will indeed obtain the highest score for all possible, realistic combinations of weights making it a robust choice.

In Table 6.3 one scenario for which the flying wing does not obtain the highest score is shown. It can be seen that the first 6 importance weights do indeed correspond to those stated above and that here the FWIP is the winning concept. The red columns contain values that were adjusted (indirectly) and the blue ones the unweighted scores that stay unchanged. However, only changing the importance weight for the stability to $\sigma = 2$ results in the flying wing being the winning concept again showing that the design is robust.

Criteria	Importance	Weight	Fixed Wing	Flying Wing	FWIP	Tilted Rotors	Fixed Wing	Flying Wing	FWIP	Tilted Rotors
Mass		12.9	0	1	0.33	0.66	0	12.9	4.26	8.51
Dimensions		3.2	0	1	0.4	0.66	0	3.2	1.28	2.11
Aerodynamics		12.9	0.63	0.54	1	0	8.13	6.97	12.9	0
Stability		3.2	1	0.8	0.2	0.4	3.2	2.56	0.64	1.28
Noise		12.9	0	0.18	1	0.59	0	2.32	12.9	7.61
Risk		3.2	1	0.8	0.2	0.4	3.2	2.56	0.64	1.28
Reliability	2	12.9	0.4	0.6	0.6	0.4	5.16	7.74	7.74	5.16
Safety	2	3.2	0.8	0.4	0.4	0.6	2.56	1.28	1.28	3.2
Cost	2	3.2	0.4	0.8	0.4	1	1.28	2.56	1.28	3.2
Maintainability	2	6.5	0.8	0.6	0.4	0.6	5.2	3.9	2.6	3.9
Availability	1	12.9	0.8	0.8	0.8	0.8	10.32	10.32	10.32	10.32
Energy Consumption	2	12.9	0	0.89	1	0.72	0	11.48	12.9	9.29
Total:							39.05	67.79	68.74	54.58

Table 6.3: Table showing sensitivity analysis for a combinations of weights that yields a different winning conceptual design. The red columns contain values that were adjusted (directly or indirectly). The blue columns contain the unweighed scores.

Showing that the flying wing would win the trade-off for all realistic combinations of weights provided enough trust in the design to move it to the detailed design stage. The starting point for that is the parameters presented in Table 6.4. These were obtained during the sizing and were also used for the technical resource budget in chapter 5. This is return was used for the detailed design of the subsystems which will be presented in the following chapters.

Max take-off weight [kg]	12.3
Wing span [m]	1.73
Wing Area [m^2]	0.60
Number of propellers	4 VTOL and 1 FW
cruise speed[ms^{-1}]	23.8
L/D_{cruise}	12

Table 6.4: Overview of technical specifications of the chosen design

7

Detailed Design: Data Handling and Communication

The detailed design part of the report will be started with the data handling, communications and electronic components of the drone in this chapter. Several diagrams will be presented, namely, the Hardware Diagram showing all the components and how they are interrelated, the Electrical Block Diagram which depicts how the power is distributed amongst the components that require it, and finally the Software Diagram which illustrates the working principles of the code that is used to operate the drone.

7.1. Hardware Diagram

The Hardware Diagram is depicted in Figure 7.1 where all components of the drone can be seen. Furthermore, the relations between all the hardware elements are shown and information that is usually included in Communication and Data Handling Diagrams is depicted. This includes the information that is transmitted between the components and the data rate that this information requires. Furthermore, the kind of connection used is specified and important information, such as the commercial model or the memory and processing power (when applicable) is shown. It should be noted that the GPS receiver and the mobile broadband chip as well as the inertial measurement units (IMUs) and the flight controllers are depicted in the same blocks. The reason for that is that they are integrated with the same piece of hardware. In addition, some components appear twice to avoid single point failure.

Each type of component included was depicted using a different colour. The batteries are shown in red, the power distribution board in green, all the sensors in blue, the propulsion system in orange, the communications system in yellow, the processing and storing units in grey and the flight controller in purple.

The data handling and communication subsystem contain most of the electronic components required by the drone. The components needed to ensure a proper functioning of the drone are listed below, and they are shown in Figure 7.1 in bold letters.

1. Batteries to provide and store power.
2. A power distribution board to convert the power from the batteries to the appropriate voltage for each component. A power input of the wrong voltage could seriously damage the parts.
3. A flight controller to take care of the controllability of the drone. It indicates the correct speed to the Electronic Speed Controllers (ESC) and processes the data from the IMU.
4. A processing unit to process the input data from sensors that are not part of the IMU, for example, cameras or LIDAR scanners. It was decided to use a powerful processing unit since image recognition will be used as will be further explained in section 10.2. It will also process commands from the base station, GPS data, and commands for the flight controller.
5. Sensors to ensure safety and proper navigation. The wide range of sensors includes an Inertial Measurement Unit (IMU), composed of accelerometers, gyroscopes, barometers and magnetometers, a LIDAR scanner and ultrasonic sensor for obstacle detection, a pitot tube for airspeed measurements, a GPS receiver for positioning data and a camera for landing spot recognition, and cellular and radio receivers to triangulate the position of the drone in case the GPS signal is lost. These sensors are described in detail in section 10.2.
6. A mobile broadband chip with access to the 4G network to communicate with the base station. It was decided to use mobile broadband instead of radio communication because of the range and obstacle constraints radio communication presents. In addition, it has higher up- and downlink data rate capabilities.
7. A local storage memory card to ensure all the flight data is safe in case of a crash or unexpected circumstances.
8. Electronic Speed Controllers (ESC) to receive the desired rotational speed from the flight controller and transmit it to the motors.

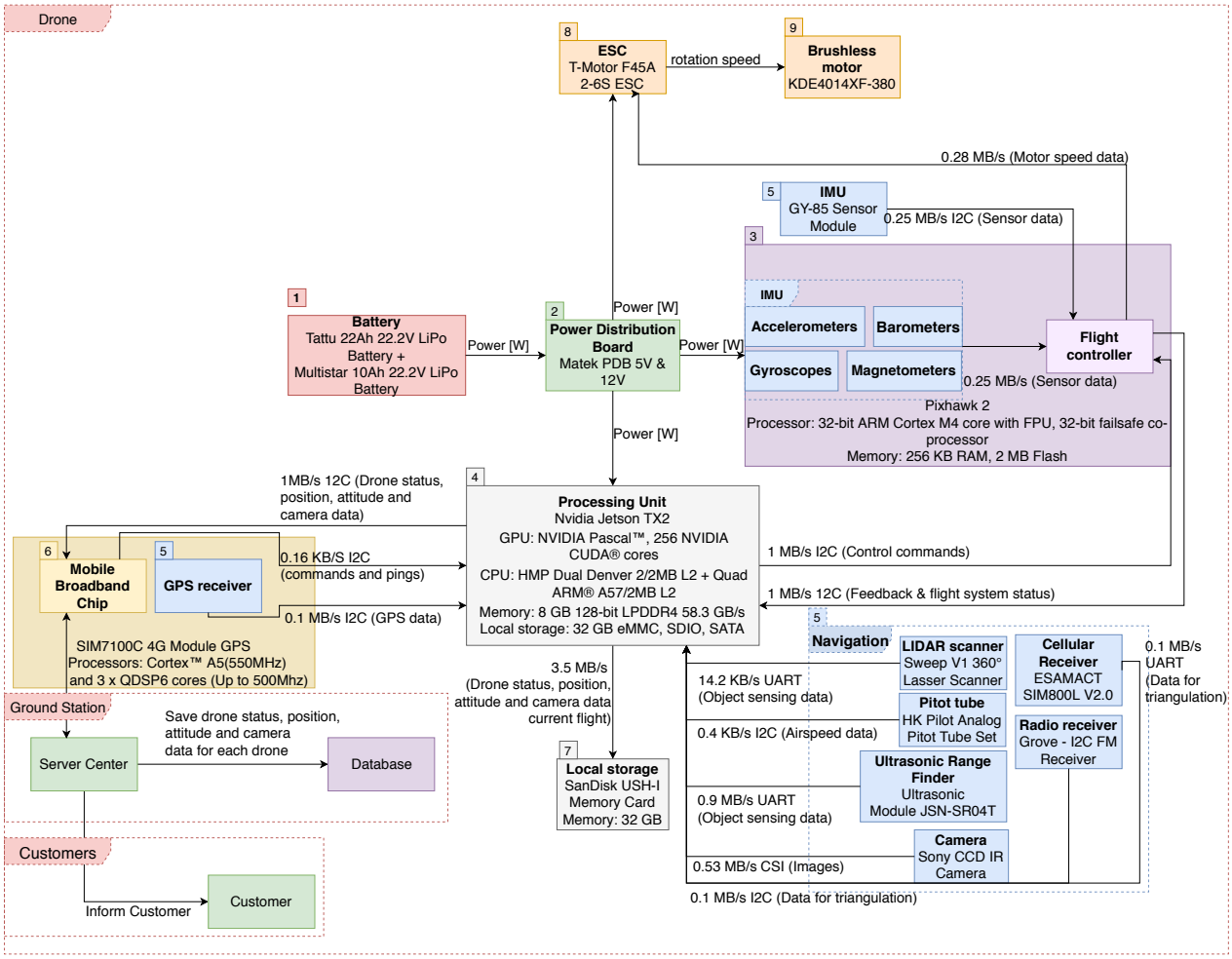

Figure 7.1: Hardware diagram.

9. Brushless motors to provide thrust. It was decided to use outrunner brushless motors because they can provide a higher torque with respect to their weight as compared to another kind of motors. In fact, it is a very common choice for drones that use propellers [1].

7.2. Software diagram

Figure 7.2 shows the software diagram for the delivery drone. The software is mainly used for the autopilot of the drone, the delivery route optimisation and the handling of the payload. This is explained in greater detail in section 10.2 and section 4.2.

The software has two main inputs, namely the GPS coordinates of the destinations to which the packages will be delivered and the sensor data, in particular, whether the GPS signal is available or not. With the list of locations, the software will create a route passing through the destinations in the most efficient order as was explained in chapter 4. On the other hand, if it is possible to use GPS, it will be used together with the IMU to determine the attitude and the position at each moment using a Kalman filter. If it is not available, triangulation will be used with radio and cellular receivers and the IMU. Then, the actual position and attitude and the destination will be compared and commands will be sent to the ESC accordingly, correcting the path if necessary. When the final position is reached according to the GPS, the visual recognition system will find the landing spot and determine if it is safe to land. If the terrain is appropriate, the system will send the commands to the ESC to descend and land. Otherwise, it will be communicated to the ground station that it is not possible to land which will decide what is the best option. After landing, the payload will be delivered and the next delivery point will be set as an objective.

[1] `http://www.thinkrc.com/faq/brushless-motors.php`, accessed on 25/06/2018

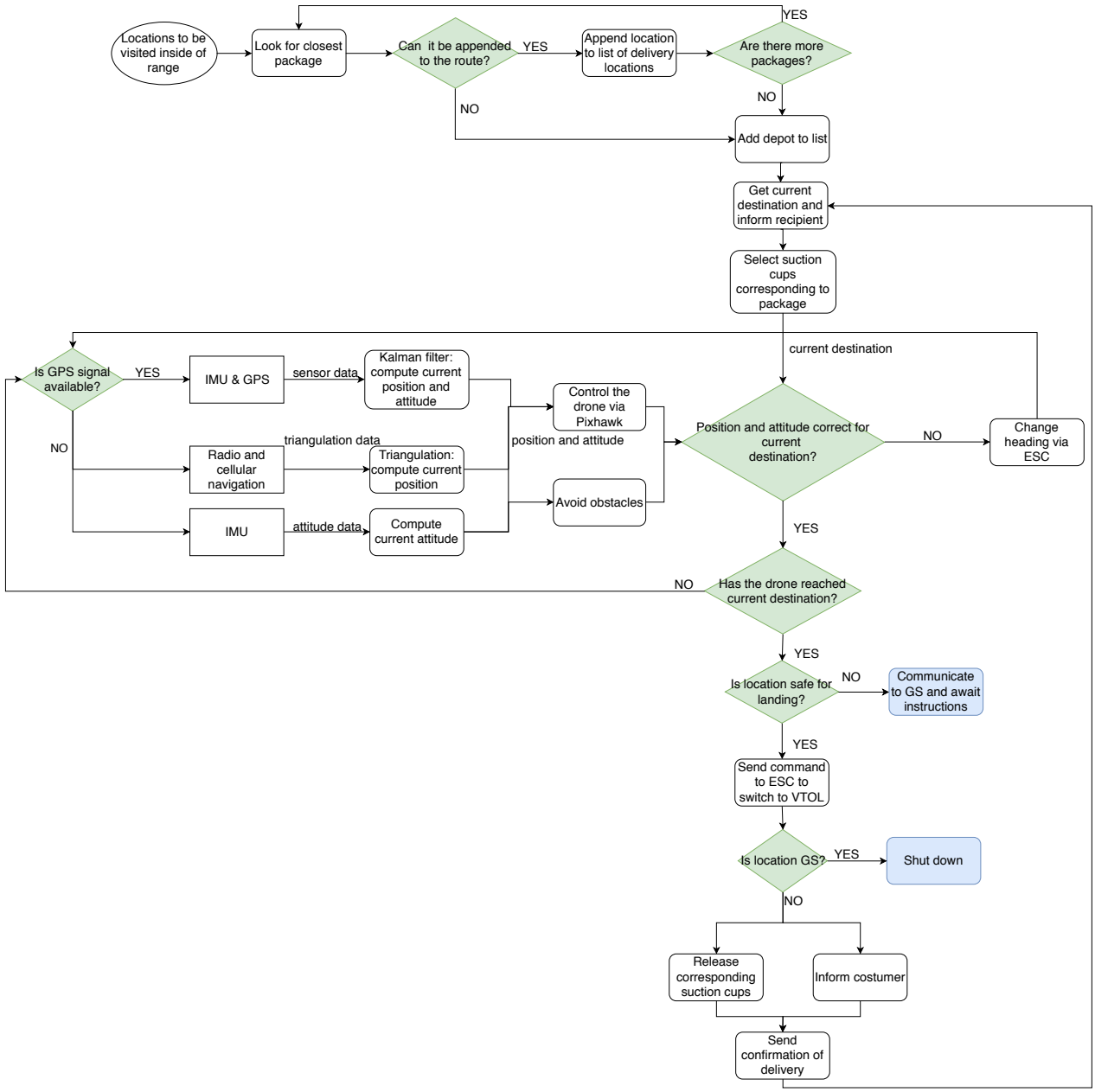

Figure 7.2: Software diagram.

7.3. Electrical Block diagram

Figure 7.3 shows the Electrical Block Diagram for the delivery drone. The power is stored in two batteries to avoid single point failure. They have the same voltage (22.2 V) and they are connected in series. Furthermore, they are connected to the Power Distribution Board (PDB), which has 12V, 5V and 5V (ESC) outputs. Most of the components of the drone have an input voltage of 5V or 12V, so they can be connected directly using a Daisy chain, which is a wiring scheme that allows the components to be connected in sequence. The ESC can be connected directly to the board using the dedicated pints. The pitot tube and the mobile broadband chip require a lower input voltage, so voltage regulators will be used to avoid damaging the components.

7.4. Subsystem budget

In Table 7.1 detailed information about the hardware that is part of the telecommunications and electronics subsystems of the drone is presented. Information about the sensors presented in section 10.2 used for the navigation sub-system

is also presented because they are included on the hardware diagram, and therefore are relevant to this chapter. The technical data sheets and commercial information can be found using the links in the footnotes.

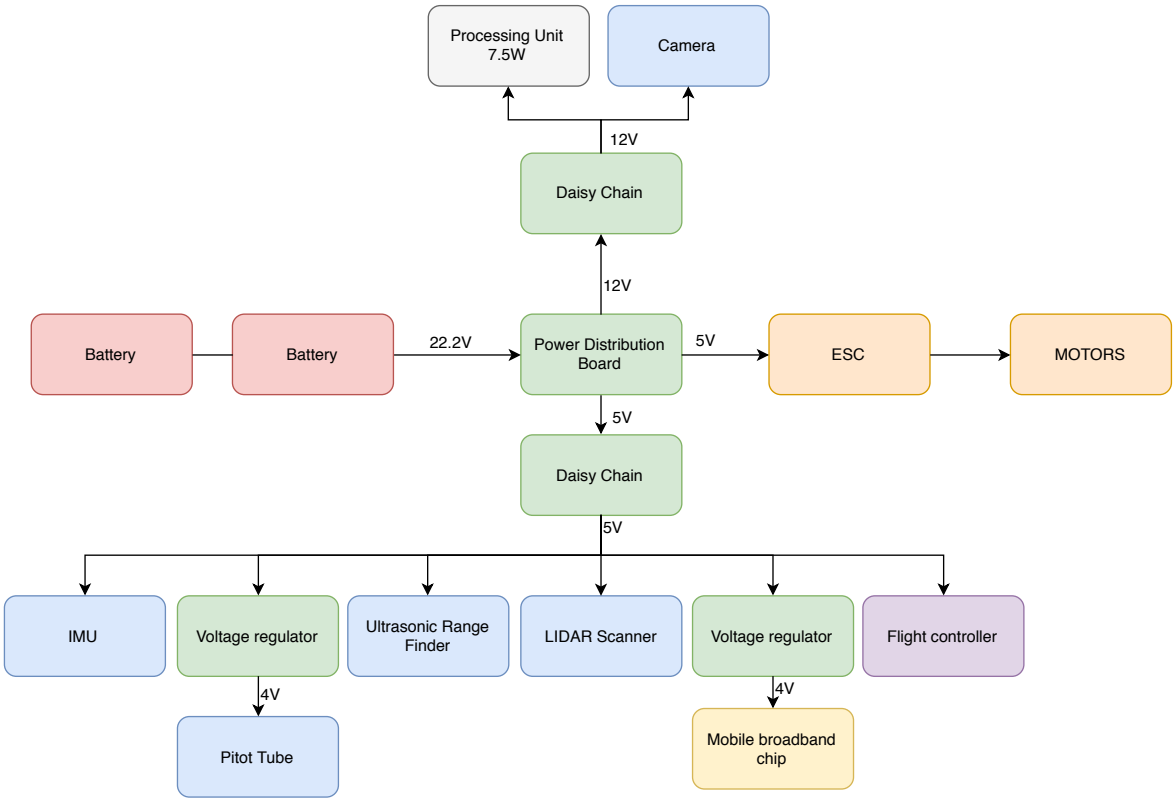

Figure 7.3: Electrical Block Diagram.

Component	Commercial model	Cost [euro]	Mass [g]	Dimensions [mm]	Power [W]
Battery 1	Tattu 22000mAh 22.2V [2]	394	2490	200 x 91 x 64	N/A
Battery 2	Multistar 10000mAh 6S LiPo [3]	70	1189	156 x 53 x 65	N/A
Power distribution	Matek PDB 5V & 12V BEC [4]	10	6	36 x 36	N/A
Flight controller	Pixhawk 2 [5]	260	75	94 x 43 x 31	15
Processing unit	Nvidia Jetson TX2 [6]	460	85	50 x 87	7.5
IMU	GY-85 IMU [7]	9	3	22 x 17	0.5
LIDAR sensor	Sweep V1 360° [8]	300	120	65 x 65 x 62	3.25
Ultrasonic sensor	JSN-SR04T [9]	6.25	5	42 x 29 x 12	0.15
Camera	1/2.5-inch Sony Camera [10]	20	60	100 x 60 x 70	1
Local storage	SanDisk 32GB memory card [11]	25	2	32 x 24 x 2	N/A
Pitot tube	Pixhawk Airspeed Sensor [12]	18	18	120 x 78 x 16	0.16
Mobile broadband	SIM7100C [13]	72	232	150 x 170 x 34	7.6
Cellular reception	SIM800L [14]	15	50	15.8 x 17.8 x 2.4	5
Radio navigation	Grove I2C FM Receiver [15]	8	9	140 x 85 x 10.5	0.6
Total	-	1667.25	4344	-	40.76

Table 7.1: Overview of the cost, mass, dimensions and power of the electrical components of the delivery drone.

7.5. Subsystem Requirement Compliance Matrix

In the final stage of the subsystem design, it is important to ensure that it actually complies with the subsystem requirements. In Table 7.2 a compliance matrix for the telecommunication and electronics subsystem is depicted including the verification method. It can be seen that the subsystem does indeed comply with all requirements.

Requirement	Verification Method	Compliance
SYS-SUB-TC-1 The TC subsystem shall have a range of at least 15km.	Mobile broadband is not restricted by range.	yes
SYS-SUB-TC-2 The TC subsystem shall not use more than 5W of power.	Peak power calculation from product data sheet.	yes
SYS-SUB-TC-3 The TC subsystem shall be able to transmit with a data rate of at least 20 $MB\,s^{-1}$.	Product data sheet.	yes
SYS-SUB-TC-4 The TC subsystem shall be able to receive data at a rate of at least 0.05$MB\,s^{-1}$.	Product data sheet.	yes
SYS-SUB-TC-5 The mass of the TC subsystem shall not exceed TBD kg.	Calculated from products data sheet.	yes
SYS-SUB-TC-6 The cost of the TC subsystem shall not exceed 100 $.	Calculated from the commercial value of mobile broadband chip.	yes
SYS-SUB-TC-7 The TC subsystem shall provide communication in the presence of obstacles.	4G network is not affected by obstacles.	yes
SYS-SUB-PW-1 The mass of the PW subsystem shall not exceed 6kg.	Calculated from products data sheet.	yes
SYS-SUB-PW-2 The PW subsystem shall be able to deliver 2200W.	Calculated from batteries data sheets.	yes
SYS-SUB-PW-3 The PW subsystem shall use a voltage of at least 22.2V.	Product data sheet.	yes

Table 7.2: Compliance matrix for the telecommunications and electronics of the drone.

[1] https://www.genstattu.com/tattu-22000mah-22-2v-25c-6s1p-lipo-battery-pack-with\-as150-xt150-plug.html last accessed 13/06/2018

[2] ttps://hobbyking.com/en_us/multistar-high-capacity-6s-10000mah-multi-rotor-lipo-pack.html last accessed 13/06/2018

[3] https://www.multirotorparts.nl/matek-power-distribution-board-with-5v-12v-bec.html last accessed 13/06/2018

[4] https://drones.altigator.com/pixhawk-21-the-cube-p-42392.html?zenid=pqrq5rv6oua4n8ovq6dfcdopl0 last accessed 13/06/2018

[5] http://www.siliconhighwaydirect.co.uk/product-p/900-83310-0001-000.htm last accessed 13/06/2018

[6] http://www.herdware.com/shop/modules/gy-85-sensor-module-9-axis-6dof-9dof-imu-sensor/ last accessed 13/06/2018

[7] https://www.robotshop.com/en/sweep-v1-360-laser-scanner.html last accessed 13/06/2018

[8] https://www.ebay.com/itm/Ultrasonic-Module-Distance-Measuring-Transducer-Sensor-Waterproof-JSN-SR04T-/172141746411 last accessed 13/06/2018

[9] https://hobbyking.com/en_us/1-2-5-inch-sony-ccd-video-camera-700tv-lines-f2-0-5mp-ir-pal-1.html last accessed 13/06/2018

[10] https://www.sandisk.com/home/memory-cards/sd-cards/extremepro-sd-uhs-i last accessed 13/06/2018

[11] https://hobbyking.com/en_us/pixhawk-digital-airspeed-sensor-w-pitot-tube.html last accessed 13/06/2018

[12] https://hobbyking.com/nl_nl/sim7100c-4g-module-gps-gprs-development-board.html last accessed 13/06/2018

[13] http://www.dx.com/p/esamact-sim800l-v2-0-5v-wireless-gsm-gprs-module-quad-band-with-antenna-cable-cap-51752tc=US&ta=nl&gclid=cj0kcqjw3v3ybrcoarisapklbk57zu8zgq_y_tdqcuyelofzvjf0u6lp7st1y6xl1lgb9cay21drixsaavv2ealw_wcb#.Wx_HJI7peUk last accessed 13/06/2018

[14] https://www.seeedstudio.com/Grove-I2C-FM-Receiver-p-1953.html last accessed 13/06/2018

8

Detailed Design: Wing Design

Following the midterm, the complete wing has been designed. This step is essential since the final wing characteristics will serve as input for the integration of the rest of the subsystems, as well as the operations of the vehicle. For that purpose, first the aerodynamics of the vehicle have been analysed in section 8.1. Then, in section 8.2, an explanation is provided on the stability analysis, including a discussion of both, the longitudinal and lateral stability characteristics. Next, the accuracy and validation of the aerodynamic analysis tool XFLR5 are discussed in section 8.3. Furthermore, the final converged aerodynamic and stability characteristics are briefly summarised in section 8.4. Finally, in section 8.5, the design of the control surfaces is explained in detail.

8.1. Aerodynamics

Here, first the airfoil is selected in subsection 8.1.1 based on the wing characteristic obtained from the sizing process. Then, the fuselage and fairing are discussed in subsection 8.1.2, as well as the performance of the fuselage in subsection 8.1.3. Finally, the aerodynamic interaction of the propeller with the wing is studied in subsection 8.1.4 and a small discussion regarding the boundary layer ingestion (BLI) is treated in subsection 8.1.5.

8.1.1. Aerofoil Selection

To select the best possible aerofoil, a step by step procedure was defined:

1. Determine minimum thickness over chord ratio (t/c) required for holding all systems except the payload and the battery which will be housed in external fairings.
2. Determine the design aerofoil (2D) lift coefficient, namely the aerofoil lift coefficient required at cruise.
3. Select a group of aerofoils which seem suitable for the current flying wing configuration: low Reynolds number aerofoils, aerofoils for flying wings, etc. and perform trade-off with all aerofoils comparing aerodynamic characteristics.
4. Develop a 3D aerodynamic model of the chosen design and check that it meets aerodynamic requirements.

Minimum Thickness First of all, it was determined that the maximum dimension which had to be taken into account for the design of the wing comes from the telecommunication, electronics or navigation element with the largest height. In this case, it would be the flight controller, causing a minimum t/c of the aerofoil of 6%.

Design Lift Coefficient The $C_{l_{des}}$ for an unswept wing can be calculated as follows

$$C_{l_{des}} = 1.1 \frac{\frac{1}{q}\left\{\frac{1}{2}\left[\left(\frac{W}{S}\right)_{start-cruise} + \left(\frac{W}{S}\right)_{end-cruise}\right]\right\}}{\cos^2(\Lambda_{LE})} = 0.92 \tag{8.1}$$

where q is the dynamic pressure given by $\frac{1}{2}\rho V^2$. The variables $\left(\frac{W}{S}\right)_{start-cruise}$ and $\left(\frac{W}{S}\right)_{end-cruise}$ are the wing loadings before and after payload deployment. The factor $\cos^2(\Lambda_{LE})$ corrects for the wing being swept. Finally, an extra safety factor of 10% is applied to account for loss of lift due to the presence of a 'fuselage' and the propellers. Furthermore, from the sizing, due to the stall characteristics, it is required that the maximum lift coefficient ($C_{L_{max}}$) is at least 0.9.

Aerofoil Trade-Off For the trade-off we considered 10 aerofoils from different families, as shown in Table A.1. Their aerodynamic characteristics were calculated with XFLR5, aerodynamic analysis tool for wings flying at low Reynolds numbers. In the conceptual design, a cruise velocity of 23.8 [m/s] was estimated and used for this analysis. Furthermore, the analysis was carried out under a Reynolds number at the Mean Aerodynamic Chord (MAC) of 562328.46 [-] and Mach number of 0.074 [-].

For the trade-off analysis the following points are desired:

1. High thickness to chord ratio since it leads to lower structural weight.
2. C_l for an angle of attack (α) of 0° close to the design lift coefficient, such that during cruise, a high angle of attack is not required.
3. The angle of attack for the aerofoil zero-lift coefficient was not used in the trade-off since its benefits and drawbacks are included in the previous item (C_l for $\alpha = 0$).
4. $C_{l_{max}}$ as high as possible since the wing is required to meet the stall $C_{L_{max}}$ of 0.9 and the translation from 2D to 3D reduces the maximum lift coefficient.
5. The angle of attack required to reach $C_{l_{max}}$ is as high as possible since it is not desired to stall by a slight increase in angle of attack due to, e.g., an air gust.
6. The minimum aerofoil drag coefficient ($C_{d_{min}}$) should be as low as possible.
7. It is desired that C_l corresponding to $C_{d_{min}}$ is as close to $C_{l_{des}}$ as possible, since that is the cruise aerofoil lift coefficient.
8. $(C_l/C_d)_{max}$ should be as high as possible such that the cruise phase is efficient.
9. It is desired that C_l corresponding to $(C_l/C_d)_{max}$ is as close as possible to the design lift coefficient such that, during cruise, the flying wing is as efficient as possible.
10. The cruise C_m should be as low as possible such that the trim required is minimum because it increases drag and complexity.

When carrying out the trade-off, all the variables were normalised to an interval between 0 and 1 and all the parameters were given a weight of 1 since at this stage all of them have equal importance for different departments. As a result, from the trade-off, three aerofoils resulted to have very similar results, namely the SD 7090, E216 and the NACA 2415. In order to select a final candidate, a fair comparison of the 3D aerodynamic properties of the 3 remaining options was carried out using the same planform characteristics specified at the end of the preliminary sizing. The characteristics of the planform used (obtained from the concept-sizing) can be observed in Table 8.1 and trade-off in Table 8.2.

Parameter	Span [m] (b)	Taper Ratio [-] (λ)	Sweep [°] (Λ_{LE})	Root Chord [m] (c_{root})	Twist [°] (γ)	Aspect Ratio [-] (A)
Value	1.737	0.4	35	0.496	-3	5

Table 8.1: Planform characteristics.

	Aerodynamic characteristics			Trade-off		
Name	SD 7090	E216	NACA 2415	SD7090	E216	NACA 2415
Thickness ratio	10 %	10.4 %	15 %	0	0.08	1
C_L for $\alpha = 0$ [-]	0.08	0.45	0.085	0	1	0.014
α for $C_L = 0$ [°]	-1.2	No convergence	-1.2	X	X	X
$C_{L_{max}}$ [-]	1.2	1.5	1.17	0.09	1	0
α of $C_{L_{max}}$ [°]	17	17	16.5	1	1	0
$C_{D_{min}}$ [-]	0.007	0.014	0.008	1	0	0.86
C_L of $C_{D_{min}}$ [-]	0.12	0.13	0.0425	0.89	1	0
$(C_L/C_D)_{max}$ [-]	26	21.4	23.5	1	0	0.46
C_L of $(C_L/C_D)_{max}$ [-]	0.29	0.45	0.33	0	1	0.25
Cruise C_M [-]	-0.395	-0.72	-0.56	1	0	0.49
	Final trade-off scores			4.97	5.08	3.07

Table 8.2: Final aerofoil trade-off.

As can be seen in Table 8.2, the winning aerofoil was the E216. However, due to problems with the analysis not converging in XFLR5 the second best aerofoil from the trade-off was chosen. This is the SD 7090 (which can be observed in Figure 8.1).

The most beneficial aspect of this aerofoil is that it is thicker than required, meaning that the structural weight will be lower. Furthermore, its maximum lift coefficient is higher than the required 0.9 [-] for stall and the moment coefficient during cruise is the smallest between the different options of the last trade-off.

3D Wing Design Once the final aerofoil was selected, an estimation of the twist required for stable flight was carried out. For that purpose, the Panknin method [1] is used. As can be observed in Equation 8.3, the geometric twist angle

[1] `http://www.b2streamlines.com/Panknin/Panknin.html`, last accessed 25/06/2018

(γ_{geo}) equals the total twist angle (γ_{total}) computed in Equation 8.2 minus the difference in zero lift angle of attack between the root and the tip aerofoils, $\alpha_{L=0_{root}}$ and $\alpha_{L=0_{tip}}$ respectively.

$$\gamma_{total} = \frac{(K_1 \cdot C_{m_{root}} + K_2 \cdot C_{m_{tip}}) - C_{L_{des}} \cdot St}{1.4 \cdot 10^{-5} \cdot A^{1.43} \cdot \Lambda_{0.25c}} \quad (8.2) \qquad \gamma_{geo} = \gamma_{total} - (\alpha_{L=0_{root}} - \alpha_{L=0_{tip}}) \quad (8.3)$$

In Equation 8.3, the coefficients K_1 and K_2 were computed using Equation 8.4 and Equation 8.5 respectively. λ and A represent the taper ratio and aspect ratio respectively. Their values can be obtained from Table 8.1. $C_{m_{root}}$ and $C_{m_{tip}}$ are the moment coefficients at the root and the tip during cruise. St is the stability factor, also known as the static margin. This is the distance between the neutral point and the c.g. expressed as a percentage of the MAC, and was assumed to be 5% (0.05). Finally, the sweep at quarter chord $\Lambda_{0.25c}$ was found using Equation 8.6, where C_r, b Λ_{LE} and λ can be found in Table 8.1

$$K_1 = \frac{1}{4} \cdot \frac{3 + 2\lambda + \lambda^2}{1 + \lambda + \lambda^2} \quad (8.4) \qquad K_2 = 1 - K_1 \quad (8.5)$$

$$\tan(\Lambda_{0.25c}) = \tan(\Lambda_{LE}) - 0.25 \cdot \frac{2C_r}{b} \cdot (1 - \lambda) = 31.57° \quad (8.6)$$

Introducing the values corresponding to the chosen aerofoil and the planform characteristics, the angle required for twist according to Equation 8.3 for a single aerofoil wing was -16.96°. The absolute value of the result is very high, causing the 2D aerodynamic analysis tool XFOIL within XFLR5 to not converge. As a result, it was decided to design the wing with two different aerofoils, one for the root and one for the tip with a smooth transition between both. Since the objective was to decrease the absolute twist angle value, the moment coefficient of the aerofoil, as well as the angle of attack at zero lift, had to be as high as possible.

Inspecting the initial trade-off in Table A.1, the best aerofoil for this purpose resulted to be the **Fauvel 14** aerofoil, an option with reflex, which can be observed in Figure 8.2. Using the SD 7090 aerofoil at the root and the Fauvel 14 at the tip, the required twist for stability is reduced to -7.309°. The aerodynamic characteristics for this final wing concept are summarised in Table 8.3.

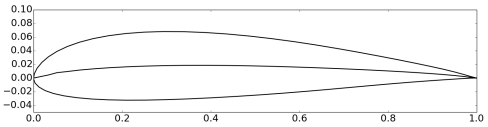

Figure 8.1: SD 7090 aerofoil contour used at the root of the flying wing.

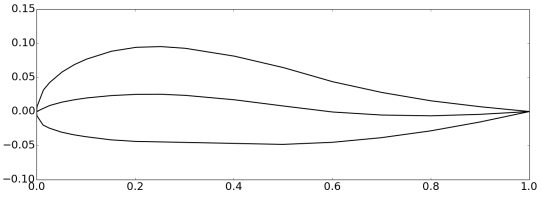

Figure 8.2: Fauvel 14 aerofoil contour used at the tip of the flying wing.

	$C_{L_{\alpha=0}}$	$\alpha_{C_L=0}$	$C_{L_{max}}$	$\alpha_{C_{L_{max}}}$	$C_{D_{min}}$	C_L of $C_{D_{min}}$	$(C_L/C_D)_{max}$	C_L at $(C_L/C_D)_{max}$	$C_{M_{cruise}}$
SD 7090 + Fauvel 14	-0.04	0.6	1.21	19	0.0093	0.07	21.3	0.38	-0.53

Table 8.3: Aerodynamic characteristics of the wing with the SD 7090 at the root and the Fauvel 14 aerofoil at the tip.

If the wing would fly at the design lift coefficient (0.618 [-]), the lift-over-drag ratio would be 18.5, close to the maximum of the current design, namely 21.7. Finally, the moment coefficient during cruise is lower than the aerofoil moment coefficient of the SD7090. This is beneficial since lower forces will have to be generated by the control surfaces to trim the aircraft, meaning lower trim drag.

8.1.2. Fuselage Design

In this subsection, the design of the fuselage that will hold the batteries, the main payload subsystem and avionics are explained. In particular, the batteries will be located in the front and, the payload system will be positioned behind them to allow easy replacement between missions.

The volume of the two LiPo batteries are 200 x 91 x 64 mm and 156 x 53 x 65 mm and they are placed longitudinally. The larger battery was placed in front with its 91 mm side in the longitudinal direction and with a height of 64 mm. Behind this, the smaller battery was placed with 53 mm in the longitudinal direction and 65 mm in height. The payload system has a volume of 220 x 330 x 140 mm. It was decided to position it with the 220 mm side in the longitudinal

direction, which allows the fuselage to become thinner. This is beneficial for the design, as will be explained later. The respective positions and orientations of these systems can be found in Figure 8.3.

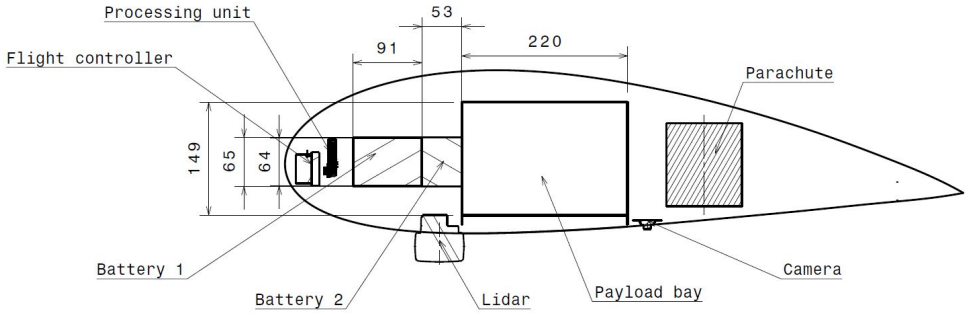

Figure 8.3: Position of the components of the drone that are placed inside the fuselage.

Since the fuselage must provide lift, the selected aerofoil had to be capable of generating the required lift and of holding the payload and batteries. With the current orientation of payload and batteries, it was found that aerofoils with a t/c of approximately 21% would provide a sufficient amount of volume while keeping the chord length at 800 mm. The aerofoils considered for the fuselage are shown in Table A.2.

To select the fuselage aerofoil, an analysis similar to the one presented in subsection 8.1.1 was performed. In this analysis, however, the drag was the most important parameter given that this part of the frame is dedicated to the housing of the subsystems. Therefore, the C_l over C_d plots were analysed in particular to find the aerofoil with a large drag bucket. The aerofoils were analysed at a Reynolds number of 1178218 for a chord length of 800 mm and at a cruise velocity of 23.8 $\mathrm{m\,s^{-1}}$.

From this analysis, it was found that the **NACA 4421** (which can be seen in Figure 8.4) performed best. However, to have space contingency in the centre, the **NACA 4424** (which can be observed in Figure 8.5) was added in the middle of the fuselage. This also provides a better transition in the lateral direction by making the wing more rounded in the centre.

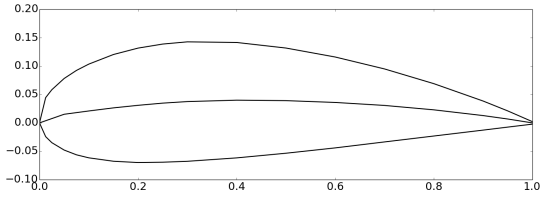

Figure 8.4: NACA 4421 aerofoil contour chosen for the outer part of the fuselage.

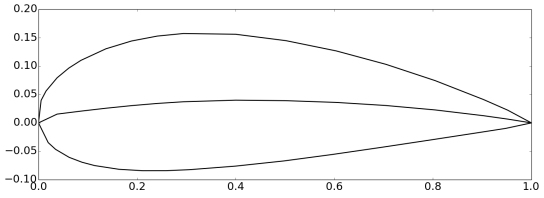

Figure 8.5: NACA 4424 aerofoil contour chosen for the root chord, inner part, of the fuselage.

The next step was to design a connection between the fuselage and the main wing. This meant that an additional fairing was required to connect the sides to the main wing. This shape was determined to occupy 5% of the span m, distributing it equally between both sides of the fuselage. This was done in order to decrease the wetted area (and therefore the drag) and still allow the structure of the wing to follow a smooth transition to the fuselage. This fairing can be optimised further through the use of wind tunnel tests and CFD analysis in the future.

8.1.3. Fuselage performance

Now that the fuselage has been designed it is important to examine what this shape does to the design in terms of performance. The first observation one may make is that it does not look like a conventional fuselage.

One of the important design parameters of this drone is its dimensions. It has to be able to land at several locations. Therefore, the smaller the dimensions of the drone the more flexible it will be during the landing phase. The current

fuselage design helps in that aspect. Instead of becoming a conventional cylindrical shaped fuselage, it was decided to use a lifting body made of aerofoils.

This does not only mean that additional lift is produced, but it also means that less drag is produced. For example, if a conventional cylindrical body would have been used, a minimal diameter of 231 mm would have been required; value determined by the payload dimensions plus a 5% contingency for the structure. This would result in a higher drag force since the total frontal area seen by the free stream flow is larger. Additionally, following Ref. [34] it was found that having a conventional fuselage causes a significant loss in lift between 0 and 20 % of the span of the wing. Including such a body would have meant that, in order to compensate for this loss in lift and additional drag, a larger lifting surface would be required. As a result, this was not the preferred option.

Another reason was for the structure to be able to flow uninterrupted through the wing. With a lifting body instead, the main structure can go from tip to tip without having the necessity of having to cut in the fuselage and therefore, decreasing the complexity.

For these reasons it made sense to use instead a lifting body as a fuselage. The performance decrease that was found by adding this component can be observed in Figure 8.12, Figure 8.13, Figure 8.14 and Figure 8.15.

8.1.4. Propeller Interference

Since two of the four propellers will be installed in front of the wing, the interference on an aerodynamic level between the two structures had to be analysed. This analysis was divided into two parts. First, the additional drag component was estimated, basing the computations on [19]. Then an analysis on the reduction in lift component was made.

Drag To be able to find the interference drag between the wing and the propellers first an estimate had to be made on the drag produced by the propellers during cruise. An estimation of the C_D was made based on existing drag data for stopped propellers in a free stream flow. For this analysis, it was estimated that the blade angle of the propellers (β) was between 40° and 80°. With the following equation, the drag coefficient could then be estimated.

$$C_{D_{\text{propeller}}} = 0.1 + cos^2(\beta) \tag{8.7}$$

From this, it was found that the average $C_{D_{\text{propeller}}}$ of the blade was approximately 0.21. Since the propeller is made up of three blades, a total surface area of 0.096 m^2 was found. The total drag could then be determined using Equation 8.8.

$$D_{\text{propeller total}} = C_{D_{\text{propeller}}} \cdot q \cdot S_{\text{propeller}} \cdot 4 = \left(C_{D_{\text{propeller}}} \frac{S_{\text{propeller}}}{S_{\text{wing}}} 4 \right) q \cdot S_{\text{wing}} = C_{D0_{prop}} q \cdot S_{\text{wing}} \tag{8.8}$$

By rewriting Equation 8.8, it is possible to express the drag and thus C_D of the propeller in terms of the wing surface area. This conversion shows us that the parasite drag coefficient of the wing would increase by $C_{D0_{prop}}$ (equal to 0.0436).

The previously mentioned calculation, however, only covers the drag when the wing is flying at an angle of attack of 0°. For different angles, the following equation was used to find the induced drag component.

$$C_{Di} = 0.0002 \cdot (\alpha)^2 \tag{8.9}$$

This was found to be equal to 0.0313 in the worst case scenario (12.5° angle of attack).

Finally, there is the additional drag caused by the propellers positioned in front of the wing. This type of drag is called interference drag. For the estimation of the extra drag coefficient, the following equation has been used.

$$\Delta C_{Di} = \frac{C_L^2}{\pi A} 15 C_{FH} \tag{8.10}$$

Where (C_{FH}) can be calculated by $C_{FH} = \frac{C_{D_{\text{propeller}}}}{qS}$, resulting in a value of 0.0094 [-]. Furthermore, C_L was 0.74 [-] and the aspect ratio is 5.525 [-]. This computation resulted in an additional drag coefficient of 0.0006 [-]. This drag component, therefore, is not expected to cause a major impact on the total drag based on an analysis of the worst case scenario and has therefore been neglected.

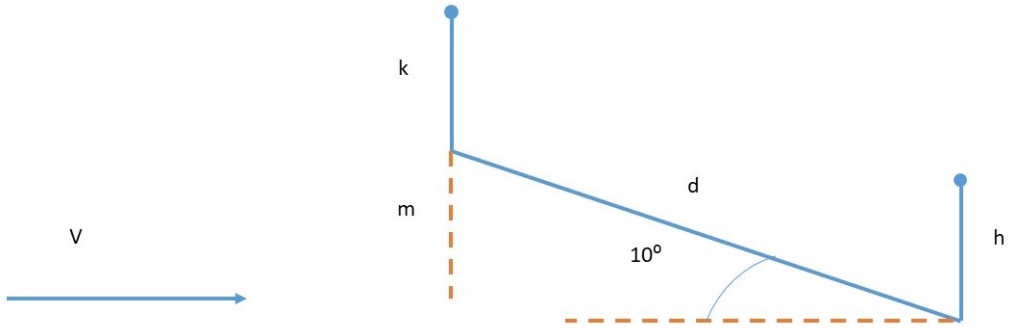

Figure 8.6: Diagram indicating the propellers location against the height of the rod.

Lift Then also the reduction in lift has been examined. The propellers, however, have been positioned in such a way that the wake they cause does not reach the wings at the cruise angle of attack. For this, the required length was found to be 61 mm at and cruise angle of attack of 10°. The diagram used for this computation can be found in Figure 8.6.

The distance of d was found to be 439.4 mm. Then k was found in Equation 8.11. Here h is the thickness of the aerofoil. The value of k was found to be the minimal distance required for the rods to have the wake not interfere with the wing.

$$k = h - m = 137.583 - (\sin(10) \cdot 439.4) = 61[mm] \tag{8.11}$$

8.1.5. Boundary Layer Ingestion (BLI) discussion

In the current drone configuration, it can be noticed that the pusher propeller, which provides thrust during cruise, is located behind the fuselage. Its diameter covers approximately 25% of the vehicle's span and is located behind the wing root, which means that 41.5% of the wetted area is located in front of this propeller.

As a result, it can be observed that the design experiences Boundary Layer Ingestion (BLI). The boundary layer is a layer of slower moving air that builds up along the drone's skin causing additional drag. In the case of the current vehicle, this layer builds along the chord of the fuselage, fairing and wing. However, thanks to the pusher propeller, the air is energised and accelerated behind the aircraft. This means that the total drag created by the boundary layer moving over and dissipating behind the drone is decreased because some of the corresponding air is sped up.

As a consequence, the final product can show a **reduction in drag** and, therefore, a **reduction in the power consumption**. The only disadvantage is that the design of the pusher must take into account that the blades do not see a constant flow, but they experience additional stresses every time they pass through the distorted flow. In the current design, a quantitative analysis has not been carried out since the study of BLI is still in its early stages and most of the results are empirical, focused on a specific aircraft design. It is important to consider and further study the effects of BLI once tests can be performed with the first product prototypes. However, in Reference [17] and Reference [18] it has been concluded that Boundary Layer Ingestion can cause a decrease in power consumption between 5% and 18% depending on the design.

8.2. Stability

In this section, the stability of the vehicle is analysed. These key computations will serve as input for the control analysis and sizing of the different control surfaces. First, in subsection 8.2.1 the location of the c.g of the drone was found by integrating all the subsystems accounting for the longitudinal stability of the vehicle, that is presented in subsection 8.2.2. Second, in subsection 8.2.3, the lateral stability of the vehicle is tested. In the longitudinal and lateral stability analyses, both, the static and dynamic behaviours are reasoned. Finally, in subsection 8.2.4, the vertical stability of the vehicle is discussed.

8.2.1. Centre of Gravity Estimation

In order to verify whether the current design is stable, it is required to determine the location of the centre of gravity and check that it is in front of the neutral point, while also accounting for the required static margin (St) of 5% MAC. The maximum allowable centre of gravity position is given by $x_{cg_{max}}$ (equal to 0.438 m). To calculate the C.G. of the drone, the weights and the location of the c.g.'s of the different components of the system were identified. A CATIA model was generated to verify that all the components would fit given their respective positions. The locations can be

visualised in Figure 8.8 and their mass and location information have been summarised in Table 8.4. The masses of all the components were obtained from their respective technical departments.

The final mass of the complete product is 13.70 kg, 1.4 kg more than the estimated 12.3 kg obtained during the sizing of the preliminary design. However, this should not pose a risk for the design since the aerodynamics and propulsion system have been oversized to account for such difference.

Subsystem	**Component**	Mass per unit [grams]	Amount	Total mass [grams]	x-position [mm]	y-position [mm]	z-position [mm]
COMM. & ELEC.	Battery 1	2490	1	2490	135.5	0	-18.8
	Battery 2	1189	1	870	207.5	0	-18.8
	Processing unit	85	1	85	60	0	-24.1
	Flight controller	75	1	75	35	0	-9.4
	Local storage	2	1	2	35	0	-9.4
	Power Distribution Unit	6	2	12	171.5	±194.5	0
	Mobile broadband chip	12	2	24	171.5	±194.5	0
	Cabling	60	1	60	400	0	0
NAV.	LiDAR 360° scanner	120	1	120	204.4	0	80
	Ultrasonic range finder	5	10	50	490	0	0
	Pitot tube	18	2	36	825	±1054	-256.5
	Camera	60	1	60	480	0	58.1
	Back-up IMU	4	1	4	455	0	0
	Cellular reception	23	1	23	270	0	0
	Radio navigation	11	1	11	450	0	0
PROP.	ESC front	17.5	2	35	-275	±260	-115
	ESC back	17.5	2	35	1284.74	±260	-115
	Propeller front	106	2	212	-275	±260	-115
	Propeller back	106	2	212	1284.74	±260	-115
	Engine front	215	2	430	-275	±260	-115
	Engine back	215	2	430	1284.74	±260	-115
	ESC pusher	17.5	1	17.5	900	0	0
	Propeller pusher	106	1	12.5	900	0	0
	Engine pusher	215	1	215	900	0	0
STRUCT.	Rods	140.12	2	280.24	504.87	±260	18
	Wings	2130	1	2020	450.6	0	-128.54
	Fuselage	466.15	1	466.15	374	0	-0.61
	Landing gear	360	1	360	0	0	18
	Rail mechanism	300	1	300	117	0	0
	Fasteners & integration	200	1	200	600	0	0
CONT.	Actuator of rudder	34	2	68	913	±914.17	-232.456
	Actuator of elevon	34	2	68	794.67	±618.02	-122.63
MISC.	Payload	2980	1	2980	344	0	-26
	Parachute	475	1	475	610	0	-15
	Paint & coating	475	1	475	600	0	0
Total mass [grams]				13703.89			

Table 8.4: Mass and centre of gravity location of all components.

During the mission, the payload mass of the drone will change as packages are delivered. To guarantee stability during the entire mission, the c.g. location may never exceed the value of $x_{cg_{max}}$. The final centre of gravity coordinates with and without payload in x-, y- and z-direction, following the coordinate frame in Figure 8.7, have been summarised in Table 8.5. It can thus be seen that the c.g. location is always in front of the $x_{cg_{max}}$.

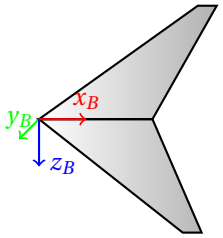

Figure 8.7: Coordinate frame for centre of gravity positioning.

Direction	With payload [m]	Without payload [m]
x	0.368	0.358
y	0	0
z	-0.043	-0.046

Table 8.5: Final centre of gravity location.

8.2.2. Longitudinal stability

The longitudinal stability was analysed in order to understand the behaviour of the aircraft in the presence of an input or disturbance, e.g. an air gust, which changes the dynamic of the vehicle at cruise. It acts as input to the design of the control of the vehicle, as well as the control surfaces; more specifically, the elevator. For that purpose, first, the longitudinal static stability was studied in subsection 8.2.2, including an analysis of the location of the centre of gravity. Finally, in Figure 8.2.2, the dynamic stability of the vehicle was researched.

Static Stability In order to ensure the longitudinal stability of a flying wing, it must be ensured that the aerodynamic centre (ac) is located behind the centre of gravity (cg). The aerodynamic centre is also the neutral point (np) of the aircraft because there is no tail.

The neutral point was assumed to be located at quarter chord length of the Mean Aerodynamic Chord (MAC). Having the origin of coordinates at the nose of the fuselage, the neutral point of the flying wing concept was located at 0.458 m.

$$x_{np} = \frac{C_r}{4} + b \cdot \frac{(1+2\lambda)}{6 \cdot (1+\lambda)} \cdot \tan(\Lambda_{0.25c}) \qquad (8.12)$$

$$MAC = \frac{2 \cdot C_r}{3} \frac{1+\lambda+\lambda^2}{1+\lambda} \qquad (8.13)$$

The maximum aft position of the centre of gravity was assumed to be located 5% of the MAC in front of the neutral point. For that purpose, the MAC was computed with Equation 8.13, resulting in a length of 0.406 m and a maximum aft position of the cg ($x_{cg_{max}}$) of 0.02 m in front of the neutral point, namely at a distance of the nose of the fuselage of 0.438 m.

The location of the centre of gravity before and after the payload is deployed was found to be located in front of $x_{cg_{max}}$ (0.438 m). The shift in centre of gravity with its distance to the neutral point before and after the payload deployment can be observed in Figure 8.9. As can be seen, NP - SM > CG. This meant that the system is considered **longitudinally statically stable** because the slope of the C_M-α curve is negative.

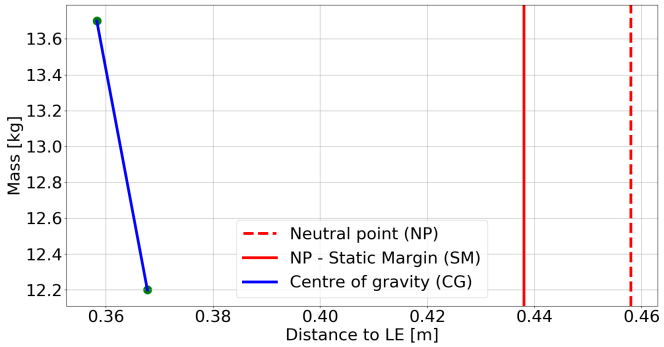

Figure 8.9: Location of the centre of gravity before and after the payload deployment.

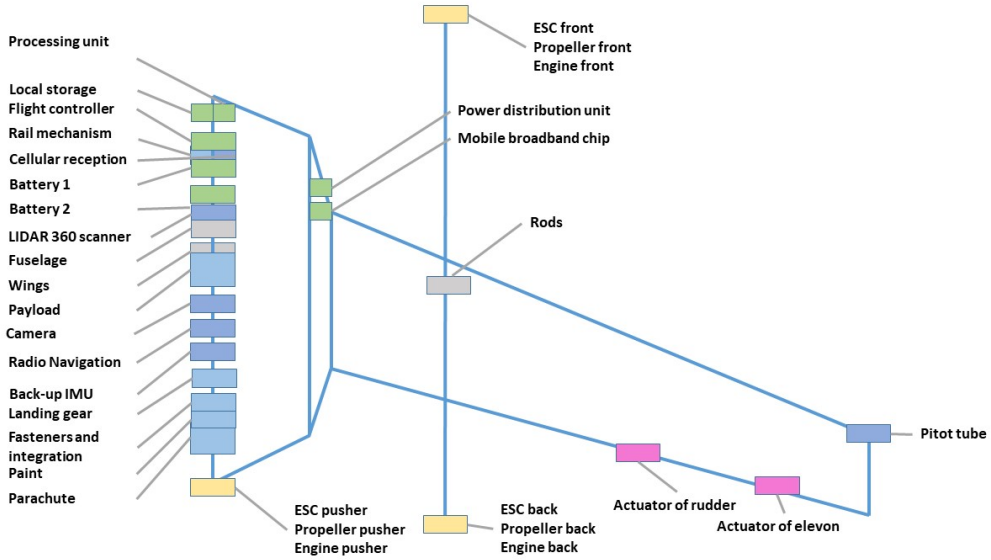

Figure 8.8: Location of all components within the system.

Dynamic stability In order to determine the longitudinal dynamic stability, the team decided to make use of the aerodynamic software tool XFLR5. With this tool, it was possible to obtain the moments of inertia of the system, as well as the stability coefficients and the behaviour of the aircraft with the different longitudinal and lateral eigenmodes.

To stabilize all aircraft longitudinal eigenmodes, namely the short period and the phugoid, the twist of the wing was altered again. During this process, the twist of the fuselage section was kept at a minimum such that the drag increment was as small as possible. The resulting wing twist at the different aerofoil sections has been summarised in Table 8.6.

Aerofoil (spanwise location)	NACA 4424 (0 [mm])	NACA 4421 (173 [mm])	SD 7090 (216 [mm])	Fauvel 14 (1041 [mm])
Twist [°]	1.9	1.9	3.25	-10.9

Table 8.6: Twist distribution along the wing span.

With the new aircraft geometry, the symmetric eigenmotions, namely the phugoid and the short period were analysed.The eigenmodes with their corresponding eigenvalues and stability characteristics can be seen in Table 8.8 while the stability derivatives are presented in Table 8.7. As can be observed, the real component of both eigenvalues is negative, which means that the eigenmotions are damped and, therefore, stable. This means the vehicle is **longitudinally dynamically stable**.

Longitudinal derivatives								
C_{x_u}	C_{x_a}	C_{x_u}	C_{l_α}	C_{l_q}	C_{m_u}	C_{m_α}	C_{m_q}	-
-0.026	0.052	-0.002	3.386	4.188	-0.003	-0.677	-1.629	-

Table 8.7: Stability derivatives.

Eigenmode	Eigenvalue [-] (λ_c)	Period [s] (P)	Time to damp half the amplitude [s] ($T_{\frac{1}{2}}$)	Undamped natural frequency [rad/s] (ω_0)	Damped natural frequency [rad/s] (ω_n)	Damping ratio [-] (ζ)
Phugoid	-6.784 ± 22.98 i	0.273	0.102	23.96	20.29	0.283
Short period	-0.031 ± 0.193 i	35.52	22.20	0.226	0.179	0.160

Table 8.8: Stability characteristics of the symmetric eigenmodes of the system.

8.2.3. Lateral stability

The study of the lateral stability is key for the analysis of the control and the sizing of the lateral control surfaces, namely the rudder and the ailerons. First, in subsection 8.2.3, the lateral static stability is investigated making use of the lateral stability derivatives. Finally, in Table 8.2.3, the lateral dynamic stability of the drone is researched with the lateral eigenmotions of the aircraft.

Static stability When analysing the stability of an aircraft, there exist some desirable behaviours upon a change in sideslip angle (β), roll rate (p) or yaw rate (r).

Lateral derivatives								
C_{Y_β}	C_{Y_p}	C_{Y_r}	C_{l_β}	C_{l_p}	C_{l_r}	C_{n_β}	C_{n_p}	C_{n_r}
-0.334	-0.507	0.101	-0.249	-0.397	0.062	0.030	0.049	-0.013

Table 8.9: Stability derivatives.

The dihedral angle and the sweep have an effect on the roll moment coefficient (C_l) with a change in sideslip angle. In general, it is desired that the C_{l_β} stability derivative has a negative value, meaning that a positive sideslip angle (deviation of the body x-axis to the left of the aerodynamic x-axis) causes a negative roll moment (roll of the vehicle to the left).

Furthermore, when designing the static lateral stability it is highly desired to have a positive weathervane stability, meaning that the change of the yaw moment coefficient with respect to a change in sideslip angle is positive (C_{n_β}>0). This is required such that a change in the alignment between the x-axes of the body and aerodynamic coordinate frames is corrected during flight with a positive yaw moment. This stability derivative can be compared to the change of pitch moment coefficient with respect to the angle of attack (C_{m_α}) discussed in subsection 8.2.2. In the case of the drone, it was found that $C_{n_\beta} = 0.03 > 0$, which is beneficial for the lateral static stability. As a result, it can be said that the aircraft is **statically laterally stable**.

Next, it is important to highlight the high absolute value of the roll damping coefficient (C_{l_p} = -0.397) of the aircraft. This stability derivative shows the roll moment change due to a modification in roll rate, which means that the aircraft generates a higher counteracting roll moment the higher the roll angular velocity. The high value found in the flying vehicle being designed is caused by the high difference in twist between the root and the tip of the vehicle, namely 12.8°. The design trick consists of making the root stall before the tip thanks to a higher incidence angle at the root with respect to the tip. In this manner, once the aircraft reaches the stall angle of attack, the nose will drop first instead of a wing tip, which would cause the undesirable roll motion of the vehicle.

Finally, it is desired that the yaw damping stability coefficient (C_{n_r} = -0.013) has a negative value. It is the case with the drone, meaning that an undesired positive yaw angular velocity is counteracted by a negative yaw moment; beneficial yaw motion damping behaviour. As a result, the aircraft is both **roll and yaw damped**.

Dynamic stability To find the dynamic stability, the eigenmodes in lateral direction were analysed. These include the roll subsidence, the Dutch roll and the spiral. Similar to the previous analysis, the tool XLFR5 was used. From the initial results, it became clear that the wing was unstable in the lateral direction. For this reason, the dihedral angle was increased to satisfy the lateral stability. In theory, this angle could be increased as much as necessary to obtain lateral stability. However, every time the angle was increased, it was found that the drag would marginally increase and the lift would be reduced by a same similar percentage. It was concluded that the dihedral angle needed to have a value of 22° to have stable lateral eigenmodes without having to increase dramatically the weight of the structure due to the presence of higher stresses.

Furthermore, in Table 8.10, the eigenvalues of the modes can be found. The values have a negative real component, which means that the modes are damped. When the modes have an imaginary component, it means that the modes experience an oscillatory motion. Finally, it can be concluded that all modes are stable and therefore, the wing is **laterally dynamically stable**.

Eigenmode	Eigenvalue [-] (λ_b)	Period [s] (P)	Time to damp half the amplitude [s] ($T_{\frac{1}{2}}$)	Undamped natural frequency [rad/s] (ω_0)	Damped natural frequency [rad/s] (ω_n)	Damping ratio [-] (ζ)
Roll subsidence	-50.52	-	0.014	-	-	-
Dutch roll	-0.165 ± 2.144i	2.93	1.43	0.342	0.341	0.077
Spiral	-0.238	-	2.917	-	-	-

Table 8.10: Stability characteristics of the symmetric eigenmodes of the system.

8.2.4. Vertical Stability

Regarding the vertical stability, the goal is to get the centre of gravity as close to the middle between the fore and aft pairs of propellers as possible. In the end, it was found that, while the payload is loaded, the distance between the propeller in the front and the cg is 642.76 mm and between the rear propeller and the cg is 916.98 mm. As a result, additional thrust is required from the front propeller to compensate for this difference in moment during vertical operations, since the difference in distance to the centre of gravity between the pairs of propellers is 274.21mm. After the payload has been delivered, the difference in distance changes to 926.42mm between the propeller in the front and the cg and to 633.33 mm between the rear propeller and the cg. This means a difference of 293.42 mm between the front and aft propulsion groups. Therefore, the vertical stability decreases when the payload is deployed and the difference in thrust required is higher, as can be seen in Figure 8.10. The possibility of increasing the distance of the front propulsion group to the nose of the fuselage was discarded due to the increase in weight and the increase in the drone dimensions.

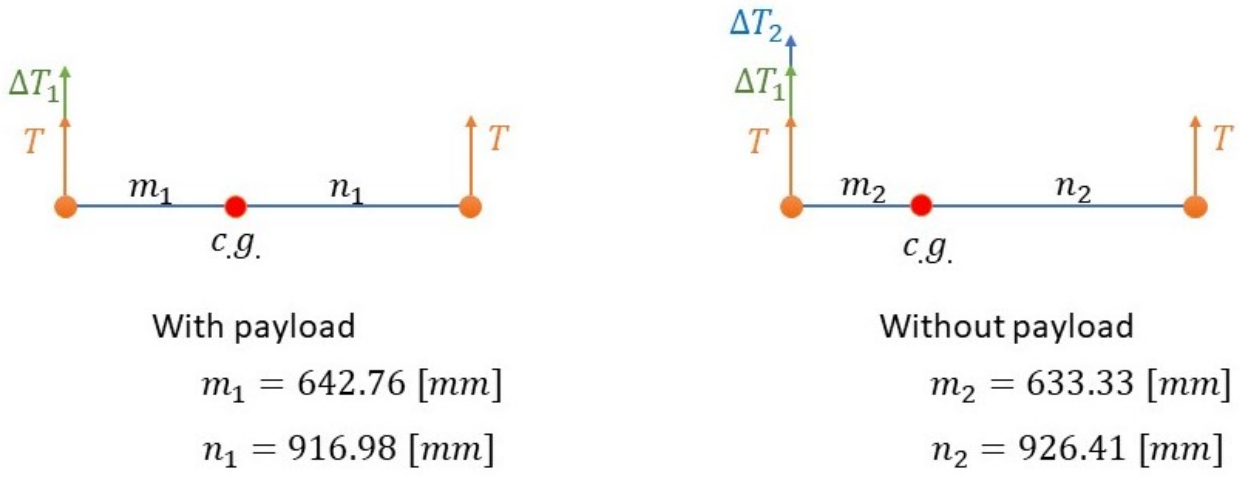

Figure 8.10: Vertical stability change with payload deployment.

Considering the worst case scenario and making use of the sum of the forces in the vertical direction (Equation 8.14) and the sum of moments around the centre of gravity (Equation 8.15), it is possible to compute how much thrust has to be provided by the front (T_1) and aft (T_2) propulsion groups as a function of the total required thrust (T).

$$\sum F_y : T_1 + T_2 = T \tag{8.14}$$

$$\sum M_y : T_1 \cdot m_2 - T_2 \cdot n_2 = 0 \tag{8.15}$$

In the end, once the payload has been deployed, the thrust required by the front propulsion group is 59.39% the total required thrust, while the required thrust by the aft propulsion group is 40.61%. As a result, the front propellers should be able to provide approximately 10% more thrust when compared to the situation where the cg is at the same distance

from the front and aft propulsion groups. The required thrust differential during VTOL operations was taken into account by the propulsion (chapter 11) and control groups (section 10.1).

8.3. Accuracy and validation of XFLR5

As has been explained above for the analysis of the aerodynamics, the software XFLR5 has been used. Compared to conventional methods like CFD, this allows for much quicker assessments of the aerodynamic properties of the wing. By NASA, it is also recommended to use software like XFLR5, also known as potential flow solvers, when less time is available because of the heavy computational power required to solve CFD analysis [39]. Where it took the potential flow solvers several minutes to run it took the CFD solvers several hours. Due to the length of the project, this has not been a sustainable option for the team, especially since several design iterations were made. The results of XFLR5 have to be set in perspective and their accuracy has to be examined.

Following Ref. [39] and a research performed by Purdue University [36], it was found that the potential flow solvers provided good predictions in the linear region. This was also found often in the analyses that have been made. The graphs would converge in the linear region, while they would not after stall, for example.

A common discrepancy in XFLR5 is that it underestimates the drag. Therefore, it is expected that during testing additional power by the pusher propeller is required. Nonetheless, it turns out that all other discrepancies in the lift prediction and moment estimation are negligible.

Having taken all these aspects into consideration, software like XFLR5 are still a great solution to estimate the aerodynamic properties. Once the model is implemented correctly, it allows to quickly put through updates and iterations with a decent enough accuracy to build further on.

8.4. Final Aerodynamic and Stability Characteristics

In this section, the aerodynamic and stability characteristics are summarised. Due to the inherent connection between both fields of expertise, an iterative process has been followed until both analyses converged to the required design characteristics. First of all, in subsection 8.4.1, the final planform geometry is summarised. Secondly, the final aerodynamic characteristics are presented in subsection 8.4.2. Finally, in subsection 8.4.3, the results of the stability analysis are briefly reviewed and the mass moments of inertia are included, given that they will serve as input to the control analysis.

8.4.1. Planform geometry

Due to the need of altering the design in order to include the payload bay with an aerodynamic fairing and the modifications to ensure longitudinal and lateral stability, some characteristics of the planform were altered when compared to the sizing results, and they have been summarised in Table 8.11. The final twist distribution can be observed in Table 8.6 and the final planform can be found in Figure 8.11. It can be noted that the part of the wing located between two aerofoils consists of a smooth linear transition from one to the other.

Parameter	Value
Span [m]	2.08
Taper ratio [-]	0.36
Sweep [°]	35
Root chord [m]	0.556
Tip chord [m]	0.199
Surface area [m^2]	0.786
Aspect ratio [-]	5.504
Dihedral [°]	22

Table 8.11: Final planform geometry characteristics.

8.4.2. Final aerodynamic characteristics

The aerodynamic characteristics of the final wing design with the fairing and the additional drag found from the propellers have been summarised in Table 8.12. These values represent the final design including the geometrical modifications (in twist and dihedral) carried out during the stability analysis. Besides that, four plots representing the aerodynamic characteristics of the final wing with and without the fuselage and including the additional drag have been plotted. More specifically, the drag polar in Figure 8.12, the C_L-α curve in Figure 8.13, the ratio C_L/C_D-α in Figure 8.14 and C_M-α in Figure 8.15. The red line represents the wing optimised without the fuselage, the blue line is the modified wing with

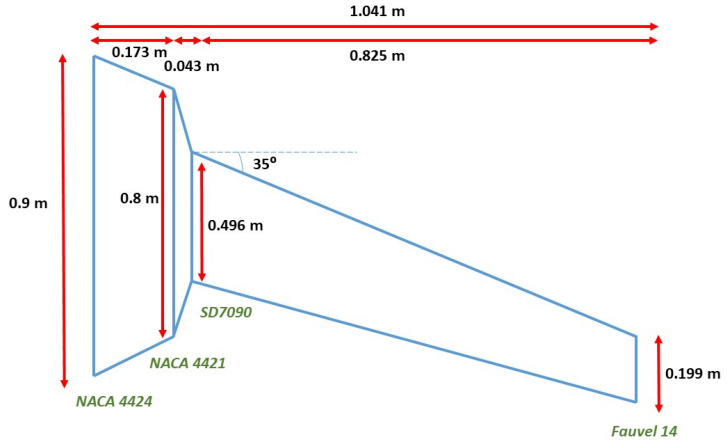

Figure 8.11: Planform of the final flying wing. The different aerofoils are indicated in green at the location where they start along the span.

the payload bay and its corresponding fairing and the green line is the complete wing together with the additional drag found from the propellers.

From Figure 8.12, it can be seen that the presence of the fuselage and the fairing, and the modifications due to stability have increased the drag when compared to the original flying wing and with the additional drag of the propellers it was also found that the total drag increases further. Their relative increases can be compared to this figure.

Furthermore, in Figure 8.13 it was found that the addition of the fuselage does not change the lift curve of the drone since it is located under the red line. However, with the additional drag, it was found that the lift curve becomes less steep and moves upwards. This means that at the same angle of attack, the aircraft generates more lift and a change in angle of attack (e.g., due to an air gust) has a lower effect in the dynamics of the vehicle at cruise. However, the maximum lift coefficient has also decreased when including the propellers in the analysis.

Next, in Figure 8.14 the addition of the propellers has decreased the maximum lift-over-drag ratio, which means that the cruise phase is less efficient.

Finally, in Figure 8.15 due to the propellers, the moment coefficient curve, with respect to the angle of attack, is less negative. This is beneficial since at cruise a lower force will have to be supplied by the control surfaces to trim the aircraft, meaning that less trim drag will be required.

Name	NACA 4424 + NACA 4421 + SD 7090 + Fauvel 14 with drag
C_L for $\alpha = 0$ [-]	0.17
α for $C_L = 0$ [°]	-2.9
$C_{L_{max}}$ [-]	0.9
α of $C_{L_{max}}$ [°]	13.5
$C_{D_{min}}$ [-]	0.06
C_L of $C_{D_{min}}$ [-]	0.064
$(C_L/C_D)_{max}$ [-]	8.14
$(C_L/C_D)_{cruise}$ [-]	7.305
C_L of $(C_L/C_D)_{max}$ [-]	0.873
Cruise C_M [-]	-0.133
$C_{L_{cruise}}$	0.62
Cruise wing Lift [N]	155.35
$C_{D_{cruise}}$	0.084
Cruise wing Drag [N]	21.12

Table 8.12: Final wing and fuselage aerodynamic properties.

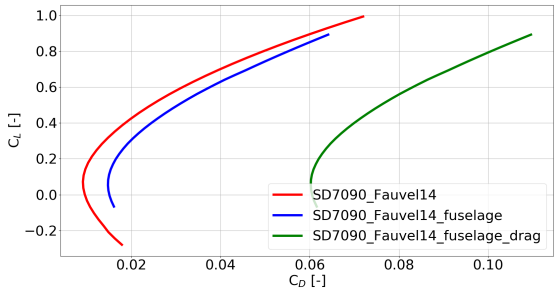

Figure 8.12: Aircrafts' drag polar.

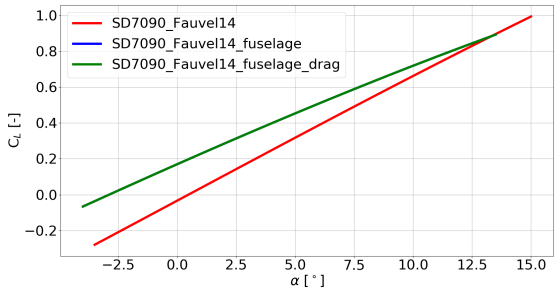

Figure 8.13: Aircrafts' lift coefficient versus angle of attack.

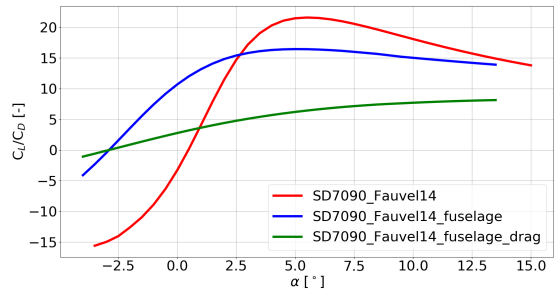

Figure 8.14: Aircrafts' lift coefficient over drag coefficient ratio versus the angle of attack.

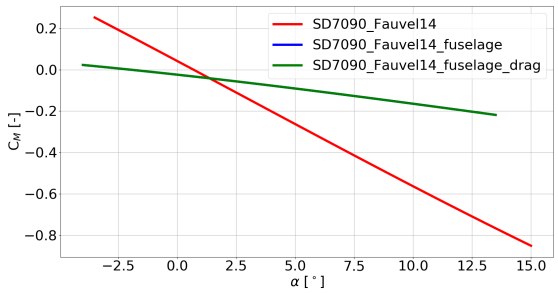

Figure 8.15: Aircrafts' moment coefficient versus the angle of attack.

8.4.3. Final stability characteristics

After all the modifications, the vehicle is longitudinally statically and dynamically stable, and it is laterally statically and dynamically stable. In Table 8.13 the mass moments of inertia of the complete system have been included since they will serve as input to the control analysis.

Mass moments of inertia	**Value [kg·m^2]**
I_{xx}	0.501
I_{yy}	1.436
I_{zz}	1.851
I_{xz}	-0.002

Table 8.13: Mass moments of inertia with the centre of gravity as origin.

Requirement	Verification Method	Compliance
The drone shall have a C_{D0} lower than 0.06	Results from aerodynamic analysis.	yes
The drone shall have a L/D higher than 7.	Results from aerodynamic analysis	yes
The moment coefficient during cruise shall not be lower than -0.2.	Results from aerodynamic analysis	yes
The drone shall provide a lift force higher than 127.5 [N] (13 [kg]).	Results from aerodynamic analysis	yes
The fuselage shall house the electronics subsystem.	Verified with the drone CATIA model	yes
The fuselage shall house the telecommunications subsystem.	Verified with the drone CATIA model	yes
The fuselage shall house the payload subsystem.	Verified with the drone CATIA model	yes
The fuselage shall house the navigation and control subsystems.	Verified with the drone CATIA model	yes
The drone shall be longitudinally statically stable during cruise.	Results from stability analysis	yes
The cg shall not shift more than 5 [cm] with full payload deployment.	Results from stability analysis	yes
The drone's weight shall not be higher than 15 [kg].	Results from integration during stability analysis	yes
The drone shall be longitudinally dynamically stable during cruise.	Results from stability analysis	yes
The drone shall be laterally statically stable during cruise.	Results from stability analysis	yes
The drone shall be laterally dynamically stable during cruise.	Results from stability analysis	yes
The cg shall be located at the same distance from the left and right propeller groups for vertical stability.	Results from stability analysis: subsection 8.2.4	yes
The cg shall be located at the same distance from the front and aft propeller groups for vertical stability.	Results from stability analysis: subsection 8.2.4	no

Table 8.14: Requirement compliance matrix for the drone's aerodynamics and stability.

8.5. Control Surface

To obtain the required roll, pitch and yaw rates during fixed wing flight, it is required to size the control surfaces adequately. In this section, we discussed the sizing procedure for both the elevon and split rudder and presented their design and performance characteristics.

8.5.1. Elevon Sizing

Conventional aircraft make use of both elevators and ailerons to control pitch and roll independently. However, having a total of 4 control surfaces on a flying wing for only pitch and roll would take up a lot of space and is most of the time not feasible, especially on wings with a low span.

A solution to this problem is to combine the elevator and aileron in a new control surface called the elevon. The sizing procedure for this type of control surface is as follows. The elevon will be used as both an elevator and aileron and thus it was also sized independently as such. When the required control surface area for both cases was determined, the most critical case was used as the final design value.

To find the required control surface area in both cases, the following approach was used. First, the change in lift due to a deflection was calculated based on empirical methods. Second, the moment generated by the change in lift could be calculated, using the stability coefficients. Finally, assuming a maximum deflection of 30◦ the required control surface area can be determined.

The first step was to determine how the lift coefficient changed with different elevon deflections ($\frac{dC_L}{d\delta}$). A positive deflection δ was defined to produce a positive change in lift. This can be seen in Figure 8.16.

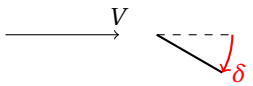

Figure 8.16: Elevon with positive deflection angle.

For determining $\frac{dC_L}{d\delta}$, we made use of Figure 8.17 and Figure 8.18, which illustrates how $\frac{dC_L}{d\delta}$ changes for different relative aileron length $\frac{2a}{b}$ (where a is the elevon length and b is the wing span). The relationship was rewritten to a mathematical expression and can be seen in Equation 8.16.

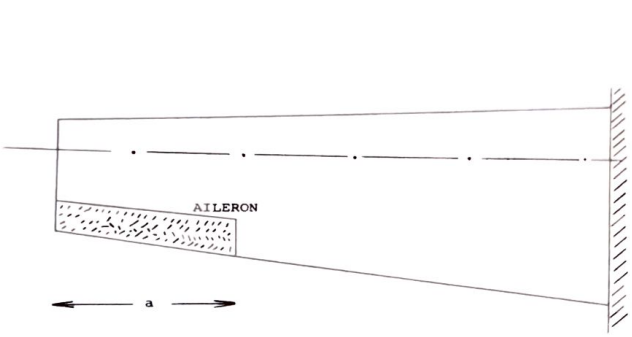

Figure 8.17: Length of aileron a [20].

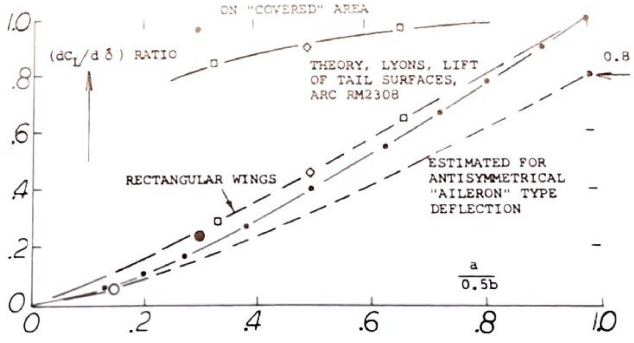

Figure 8.18: $\frac{dC_L}{d\delta}$ for different relative aileron lengths [20].

$$\frac{dC_L}{d\delta}\left(\frac{2a}{b}\right) = 0.8 \cdot \frac{2a}{b} \tag{8.16}$$

Afterwards, the change in lift could be calculated by the general lift equation:

$$\Delta L(\delta) = 0.8\frac{2a}{b}\delta q S_{\text{elevon}} \tag{8.17}$$

Where a is the elevon length, b is the wingspan, q is the dynamic pressure at stall (most critical condition) and S_{aileron} is the elevon surface area ($S_{\text{aileron}} = a \cdot c_{\text{aileron}}$). Based on [20], c_{aileron} is set to be 20% of the mean aerodynamic chord.

The moments generated by deflecting the elevon for roll and pitch could then be expressed mathematically and are shown in Equation 8.18 and Equation 8.19.

$$M_x(\delta) = \Delta L(\delta) \cdot y_{\text{elevon arm}} - \Delta L(-\delta) \cdot y_{\text{elevon}} \tag{8.18}$$

$$M_y(\delta) = -2\Delta L(\delta) \cdot x_{\text{elevon arm}} \tag{8.19}$$

In these equations, the longitudinal and lateral moment arms are given by $x_{\text{elevon arm}}$ and $y_{\text{elevon arm}}$ respectively, using the coordinate system shown in Figure 9.2. Accounting for wing sweep and dihedral, these variables could be expressed as follows:

$$x_{\text{elevon arm}} = x_{\text{elevon}} - x_{\text{cg}} \tag{8.20}$$

$$y_{\text{elevon arm}} = y_{\text{elevon}} - y_{\text{cg}} \tag{8.21}$$

x_{elevon} and y_{elevon} were determined by iteration together with the aerodynamics and structural department.

Finally, the moment required for a given pitch and roll rate was determined by the stability coefficients M_q, L_p and L_r. For a given elevon position, the control surface area can be determined by solving Equation 8.22 and Equation 8.23 for S_{elevon} and taking the largest value.

$$\max(L_p \cdot p_{\text{required}}, L_r r_{\text{required}}) = \Delta L(\delta) \cdot y_{\text{elevon arm}} - \Delta L(-\delta) \cdot y_{\text{elevon}} \tag{8.22}$$

$$M_q \cdot q_{\text{required}} = -2\Delta L(\delta) \cdot x_{\text{elevon arm}} \tag{8.23}$$

A final surface area of 0.039 m with x_{elevon} and y_{elevon} being equal to 0.383 m and 0.579 m respectively. The final dimensions are a length of 0.38 m and a width of 0.1 m. The moment generated at the hinge line can be calculated by taking the change in lift of the elevon and multiplying it by the horizontal distance to the hinge.

8.5.2. Split Rudder Sizing

The absence of a tail in the design of a flying wing poses a problem for yaw control. As no rudder is available, a different method to provide control and stability had to be decided on.

There were multiple types of control surfaces available for yaw. At first, the possibility for having two ordinary rudders positioned on potential winglets was inspected. However, as the moment arm was too small to the centre of gravity, this option proved to not be adequate. Instead, the decision was made to use the split rudder. This type of control surface relies on the generation of drag to yaw the drone. The control surfaces are positioned at the trailing edge of the wing and are able to control the drag generation by changing the deflection angle. A sketch of the split rudder can be seen in Figure 8.19.

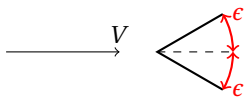

Figure 8.19: Split rudder with deflection angle.

The sizing method for the split rudder is similar to the aileron method. First, a calculation was made on how much drag is produced for a given deflection. Based on a variable position and size along the wing, a yawing moment was found. Finally, using the required yaw rate and the stability moment coefficient for a given yaw rate, the moments were set in equilibrium and a surface area and position could be found by assuming a maximum deflection of 30◦.

To estimate the drag produced by the split rudder, empirical drag measurements for 2D wedges were used, shown in Figure 8.20.

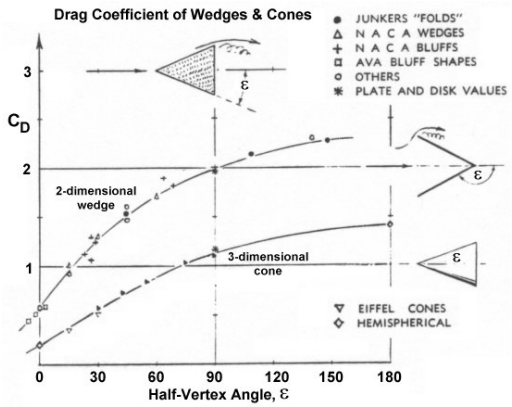

Figure 8.20: Empirical measurements for wedges and cones [19]

A best fit curve for the 2D data was set up and can be seen in Equation 8.24.

$$C_{D_{\text{rudder}}}(\epsilon) = (2.65e-7)\epsilon^3 - (1.337e-5)\epsilon^2 + (2.49e-2)\epsilon + 0.63 \tag{8.24}$$

Using this equation it was possible to find the drag produced for a given deflection angle:

$$D_{\text{rudder}}(\epsilon) = C_{D_{\text{rudder}}}(\epsilon) q S_{\text{rudder}} \tag{8.25}$$

Where q is the dynamic pressure at the most critical flight condition (Stall) and S_{rudder} is the rudder surface area. Next, the yawing moment generated by the two symmetrical rudders could be expressed as following:

$$N_{\text{rudder}}(\epsilon_{\text{left}}, \epsilon_{\text{right}}) = D_{\text{rudder}}(\epsilon_{\text{right}}) \cdot y - D_{\text{rudder}}(\epsilon_{\text{left}}) \cdot y \tag{8.26}$$

Finally, the yawing moment coefficient with respect to the yaw rate N_r and with respect to the roll rate N_p were used to determine the maximum counteracting moment. Setting the moment generated by the split rudders and by the yaw rate equal resulted in:

$$\max(N_r \cdot r_{\text{required}}, N_p \cdot p) = N_{\text{rudder}}(\epsilon_{\text{left}}, \epsilon_{\text{right}}) \tag{8.27}$$

By positioning the split rudders at the tip of the wing, the moment arm y could be expressed by $y = \frac{b}{2} - \frac{l_{\text{rudder}}}{2}$, where l_{rudder} is the length of the rudder along the span. With the area relationship $S_{\text{rudder}} = l_{\text{rudder}} c_{\text{rudder}}$ and the assumption of $\frac{c_{\text{rudder}}}{c} = 0.2$, Equation 8.27 was solved to find a required surface area of 0.0140 m.

9

Detailed Design: Structure

In this chapter, the detail design of the drone's structure is discussed. Firstly, the loads that the drone has to sustain were determined. Secondly, a material was selected given the applied load, price and sustainability constraints. Thirdly, as two structure designs were considered, a trade-off was made between a wing box and rod design. The chapter was concluded with the analysis and optimisation of the selected structure design.

9.1. Flight Envelope and Material Selection

The detail design of the structure of the flying wing was started by first evaluating the flight envelope of the drone. A maximum load factor of 2.5 was selected, as is typical for transport aircraft [37], and maximum gust velocity of 5 $\mathrm{m\,s^{-1}}$. The resulting flight envelope is shown in Figure 9.1.

Since the gust loads are not driving the design and the limit load factor is 2.5, by including an ultimate load factor of 1.5, it was found that the structure needed to be designed for a load factor of 3.75.

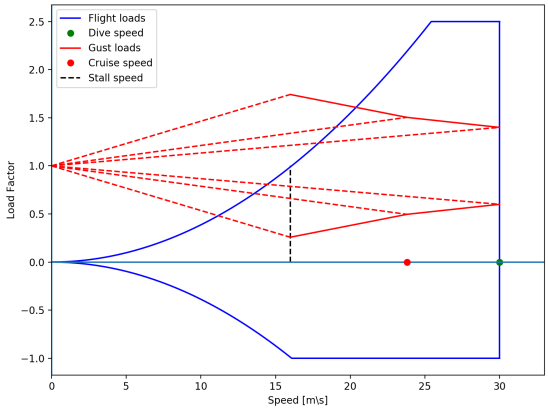

Figure 9.1: Drone's flight envelope.

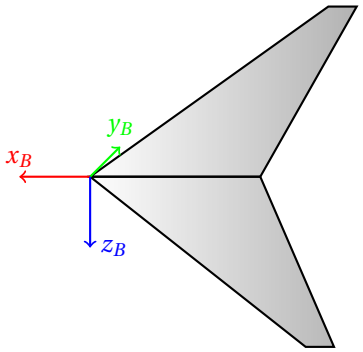

Figure 9.2: Frame of reference.

The materials that were selected have been based on their availability for existing 3D printers on an industry level. Nylon 12CF, Nylon 6, ULTEM 1010, ULTEM 9085 Certified, Antero 800NA, PEEK and PC-ABS are all materials which are available for a fused deposition modelling (FDM) system. Additionally, Scalmalloy has been included which can be manufactured using a selective laser melting (SLM) system. For several of the materials different strengths have been found depending on the orientation in which they have been manufactured using the 3D printer. The different orientations are as found in Figure 9.3.

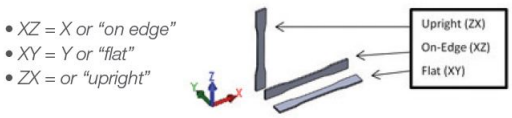

Figure 9.3: Orientation of the specimen during manufacturing.

For the computation of the stability factors for the materials, only the strength in XZ-direction has been taken into account. Since when the main structure will be printed it can be decided how the part is positioned to have the stronger side lining up in the direction which carries the highest stresses yielding the most effective structure.

In Table 9.1 is shown a selection of materials, together with specific material coefficients. To express the efficiency in carrying tensile loads we use the specific strength $\frac{\sigma_y}{\rho}$, for column buckling stability $\frac{E^{0.5}}{\rho}$ and for sheet stability $\frac{E^{0.33}}{\rho}$. Also, in Table 9.2 are shown the column and sheet buckling coefficients normalised over the price of the raw material (not the filament price).

Material	Density	Ultimate Tensile Strength (XZ Axis) [MPa]	Ultimate Tensile Strength (ZX Axis) [MPa]	Young's Modulus (XZ Axis) [GPa]	Young's Modulus (ZX Axis) [GPa]	Raw price per kilo [$/kg]	Specific Tensile Strength	Specific Tensile Stiffness	Buckling Stability	Column Stability
Nylon 12CF	1.15	63.4	28.8	7.52	2.30	140	55.1	6.54	1.70	2.38
Nylon 6	1.15	67.6	36.5	2.23	1.82	4	31.7	1.94	1.14	1.30
ULTEM 1010	1.27	81	48	2.77	2.20	300	63.8	2.18	1.11	1.31
ULTEM 9085 Certified	1.34	77	59	2.60	2.40	320	57.5	1.75	1.03	1.20
Antero 800NA	1.28	93.1	45.9	3.10	3.50	255	72.7	2.42	1.14	1.38
PEEK	1.3	98	N.A.	4	N.A.	80	75.38	3.08	1.22	1.53
PC-ABS	1.10	41	N.A.	1.9	N.A.	4	37.3	1.73	1.13	1.25
Scalmalloy	2.67	520	N.A.	70	N.A.	150	194.8	26.22	1.54	3.13

Table 9.1: Selection of possible materials for the manufacturing of the main frame of the drone.

Material	Buckling stab./price	Sheet stab./price
Nylon 12 CF	0.012	0.017
Nylon 6	0.285	0.325
ULTEM 1010	0.004	0.004
ULTEM 9085	0.003	0.004
Antero 800NA	0.005	0.00613
PEEK	0.015	0.019
PC-ABS	0.285	0.315
Scalmalloy	0.01	0.02

Table 9.2: Column and sheet buckling coefficients normalised over the price per kg of the material.

Since the expected stresses in the structures are relatively low, we gave precedence to the economic aspect of the materials. In follows that the two best material are the Nylon 6 and the PC-ABS. In the end we selected the Nylon 6 since it is less dangerous for the environment than the PC-ABS.

9.2. Trade-off

From the conceptual design a mass for the structure was determined. Including a contingency factor the structure is allowed to weight 2.8 kg. Since the loads that the drone has to sustain are relatively low two different structures were considered: a wing-box and a main frame constituted by one or more rods. In the first case, the skin is load carrying whilst in the second it is not. The frame of reference for the analysis is given in Figure 9.2.

The rod carrying structure has been modelled using simple beam theory while the wing-box has been idealised using booms, which are area agglomerations that simulate the effect of stringers and skin. After performing a trade-off between the two structures we found out that the wing-box design was lighter. In the next section, the modelling, design and optimisation of the structure is presented.

9.2.1. Assumptions

The following lists contain the list of the assumptions for the construction of the wing-box model and their consequences.

- In the wing-box, it is assumed that only the skin and spar are effective in carrying shear stress and that only the stringers and the spar are effective in carrying normal stress. Furthermore, the stringers and spar are modelled as booms, with an area that takes into account the normal stress that can be carried by the skin and spar.
  The main consequences of the assumptions are: the bending stiffness being underestimated, therefore the maximum normal stress being overestimated, and the underestimation of the maximum shear flow. This assumption simplifies the calculation of the moment of inertia.

- The moments distributions $M_z(x)$, $M_y(x)$ and $M_x(x)$ are assumed to be independent of variations of the rotation angle θ around 0°. This assumption is justified since twist angle is usually very small and the location of the centroid is only slightly changed due to rotation around the shear centre due to torsion. This assumption will mainly affect the value of the torque which is dependent on the direction of twist. Consequently, small inaccuracies will be introduced in the shear flows of the structure.

- The wing-box structure will be discretised, by dividing it into sections. Along the section, the twist angle ϕ and all internal forces and moments are assumed to be constant. By discretising the wing-box the problem can be solved numerically by numerically integrating along the span to find values like the deflection and the twist. Additionally, it simplifies the calculations. The main consequence is inaccuracy in the calculated deflection and twist, due to numerical errors. Specifically, the error will be proportional to a power of Δx, the dimension of a section span-wise, depending on the degree of accuracy of the method (i.e. Forward Euler is first order). However, by decreasing the step size until convergence this error can be minimised.
- In order to find the boom areas, it is assumed that the main source of stress is bending in the y-direction. Compressive forces are expected to contribute much less to the normal stress and will, therefore, be neglected. The main consequence will be an underestimated moment of inertia I_{yy} since by assuming the bending to be predominantly in the y-direction, one tends to accurately represent I_{xx} at the cost of sacrificing accuracy in the other moment of inertia. This problem is partially solved by iteratively updating the areas of the booms: after the first simulation is run the values of the normal stresses are used to update the booms areas. This process is repeated until convergence.

9.3. Method and Equations

Here the general method and equations used are explained. Each subsection explains the finding and calculation of some parameter. In the end, a general overview of how the modules interact with each other is given.

Idealisation The wing-box has been discretised, positioning booms in the stringer locations and along the spar. The resulting idealised shape is shown in Figure 9.4, the present booms model either stringers or skin.

Internal Shear and Moment Distribution From the design of the wing it was possible to obtain the lift distribution over the wing shown in Figure 9.5. Together with its own weight, they constitute the two main loads that the wing has to sustain. The lift distribution and the weight of the wing itself generate the internal shear load and moments shown in Figure 9.6 and Figure 9.7

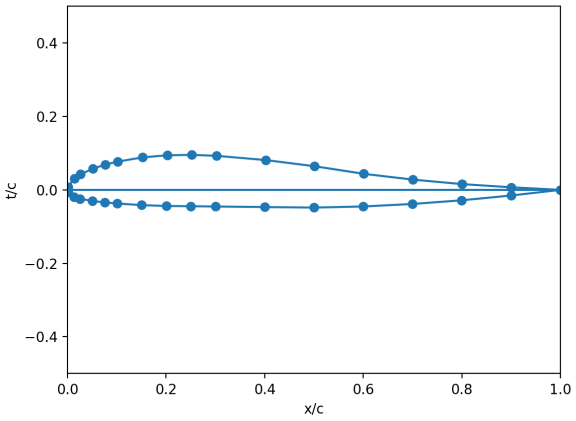

Figure 9.4: Idealised aerofoil, blue booms idealise stringers and skin.

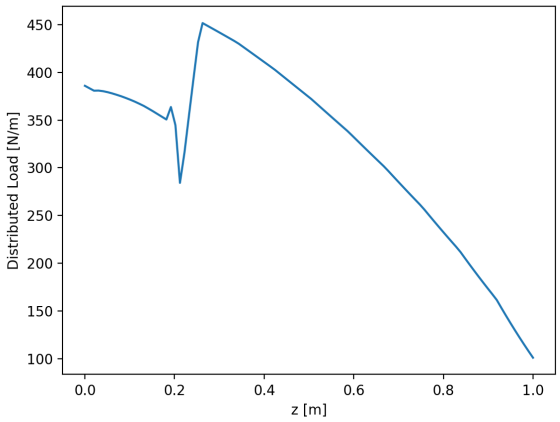

Figure 9.5: Distributed load in the y direction over the wing.

Boom Areas Given two adjacent stringers i and j the area of the equivalent boom is given by Equation 9.1[30].

$$B_i = \frac{t_{sk} \cdot l_{skin}}{6} \cdot \left(2 + \frac{\sigma_j}{\sigma_i}\right) + A_{\text{stringer}} \tag{9.1}$$

Where t_{sk} is the thickness of the skin, l_{skin} its length and σ_i the stress experienced by boom i. In our case stringers are absent, $A_{\text{stringer}} = 0$. At the beginning of the simulation, when the normal stresses are still unknown, it is assumed that the predominant loading causing normal stress is due to bending. Consequently, the ratio $\frac{\sigma_j}{\sigma_i}$ becomes equal to the ratio of the distances from neutral line of the booms. For the spar idealisation, $A_{stringers} = 0$ and $t_{skin} = t_{spar}$. Iteratively, the areas of the booms are updated.

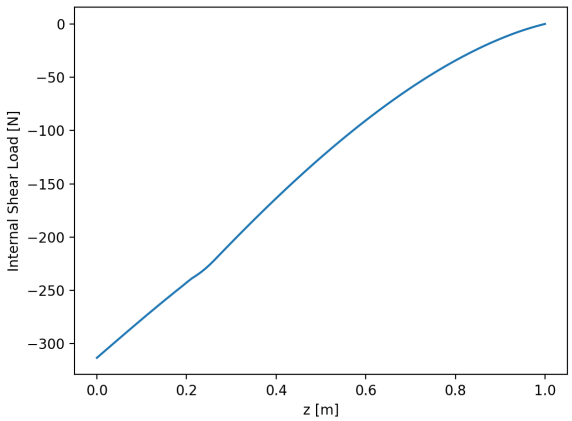

Figure 9.6: Internal shear load over the span, centre to tip.

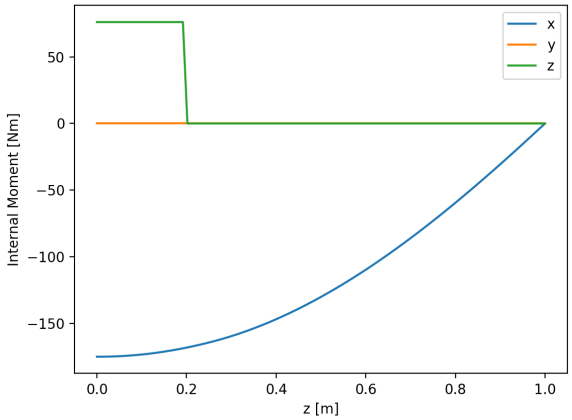

Figure 9.7: Internal moment distribution over the span, centre to tip.

Span-wise Deflection The span-wise deflection in the y-direction and x-direction of the wing-box is indicated by y_s and x_s and it is related to the moment distributions $M_x(x)$ and $M_y(x)$ by [30]:

$$\begin{bmatrix} x_s \\ y_s \end{bmatrix} = \frac{-1}{E(I_{xx}I_{yy} - I_{xy}^2)} \begin{bmatrix} -I_{xy} & I_{xx} \\ I_{yy} & -I_{xy} \end{bmatrix} \begin{bmatrix} M_x \\ M_y \end{bmatrix} \tag{9.2}$$

Unfortunately, since the deflection cannot be calculated analytically since both the moment and the moment of inertia vary along the span we used a simple numerical integrator to compute it.

Normal Stress The normal stress induced on the idealised stringers by both compressive forces and unsymmetrical bending is given by [30]

$$\sigma_x = \frac{M_z(I_{yy}y - I_{zy}z)}{I_{zz}I_{yy} - I_{zy}^2} + \frac{M_y(I_{zz}z - I_{zy}y)}{I_{zz}I_{yy} - I_{zy}^2} - F_x/A \tag{9.3}$$

where F_x indicates the compressive force experience by the structure at a certain location and A the sum of the areas of the booms. Since again the moments of inertia vary along the span, the compressive stresses will be evaluated at a given section i and assumed constant throughout it.

Pure Shear Stress To calculate the shear stress in the aileron skin due to forces not applied through the shear centre, the problem is decomposed into two. The forces are translated to the shear centre and a torque accounting for that is introduced.

Assuming that the forces S_z and S_y are applied at the shear centre. Cutting each cell at one edge there will be an induced shear flow in the cell i at edge n equal to [30]

$$q_{si_n} = \frac{S_y I yz}{I_{zz}I_{xx} - I_{zy}^2} \sum_{j=0}^{n} B_j z_j^{'} + \frac{S_y I_{yy}}{I_{zz}I_{yy} - I_{zy}^2} \sum_{j=0}^{n} B_j y_j^{'}, \tag{9.4}$$

where q_{si_n} is the shear flow due to the shear forces, $z_j^{'}$ and $y_j^{'}$ are coordinates w.r.t. the axis system attached at the centroid. The next step is to find the constant shear flows q_1 and q_2 induced respectively in cells I and II. Since the forces are applied through the shear centre twist rate of the two cells will be equal to zero. Therefore the rate of twist of cell i is

$$\frac{d\phi_i}{dx} = \frac{1}{2A_i} \sum_{j=0}^{n} \frac{(q_1 + q_2)s_j}{Gt} = 0 \tag{9.5}$$

This condition gives two equations to find the values of both q_1 and q_2.

Pure Torsion The superimposed problem consists of solving the shear flow related to a torque applied to the wing-box. Assuming that the torque T applied at location i is known and that our wing-box can be modelled as a single cell system, the following equation holds:

$$T = 2Aq_0 \tag{9.6}$$

From the shear flow q_0 we can obtain the shear stress τ. Now that both the shear stresses and the normal stresses are evaluated it is possible to obtain the Von-Mises stresses which simplify to:

$$Y = \sqrt{\sigma_x^2 + 3\tau_{yz}^2} \tag{9.7}$$

where σ stands for the normal stress and τ for shear.

Buckling For the design of the structure both skin buckling for the wing-box and column buckling for the rods that hold the propellers needs to be considered. The buckling stress for a thin plate is given by [30]

$$\sigma_{sb} = \frac{k\pi^2 E}{12(1-\mu^2)}\left(\frac{t}{b}\right)^2 \tag{9.8}$$

where Poisson ratio $mu = 0.5$ for nylon 6, b is the length and t the thickness of the sheet. To reduce the effective length of the sheet b ribs are introduced across the wing-box. To prevent buckling a rib or a similar support structure is needed every 8 cm. The buckling stress for columns is given by

$$\sigma_{bc} = \frac{\pi^2 EI}{L^2 A} \tag{9.9}$$

where L is the length of the beam and A the cross-sectional area. Using this equation, the hollow rods which sustain the propellers were sized. The rods are 22 mm in diameter with 1 mm thickness.

Fatigue From a qualitative point of view, the flying wing does not present high-stress concentration since the transition from the fuselage to the wings is smooth. Quantitatively, given a maximum stress of 18 MPa as visible in Figure 9.12, the nylon 6 has a lifetime approx. 50000 loading cycles which correspond to a lifetime of more than 3 years[40]. The resistance to UAV, humidity and harmful environmental conditions is enhanced via coating. The coating consists of polyutherane with isophorone disocyanate, which is a well established material for the coating of plastics [6].

9.4. Results

Here the results of the simulation are presented along with commentary on the values obtained. Normal and shear stresses were simulated and the Von Mises stresses computed. The stresses are presented in Figure 9.12. The shear stresses are concentrated at the root. This is due to a change in the sweep angle at the attachment point with the fuselage, which introduces a torque. The normal stresses are equally distributed throughout the span, given a variable thickness. On the top panels, as expected, there is a compressive stress (negative) while on the bottom a tensile one. The normal stresses are concentrated towards the leading edge because the wing is thicker there. Finally, the Von Mises stresses peak at 18 MPa on the top panels of the wing. The stress is well below the yield stress for the material.

Thickness It soon became clear that the stresses were lower than the yield strength of the selected material. Therefore the critical constraints were preventing failure, avoiding buckling of the skin on the top panels and manufacturability for the bottom panels. We have optimised the panel thicknesses to reduce mass and the resulting thicknesses can be seen in Figure 9.8. To further reduce weight the thickness distribution chord-wise has been modified as shown in Figure 9.9.

	Wing-box skin	Ribs	Propellers rods	Fairing	Total
Mass [kg]	1.86	0.27	0.28	0.46	2.87

Table 9.3: Mass Budget

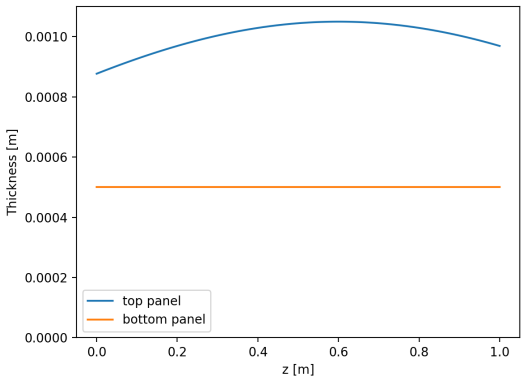

Figure 9.8: Span-wise skin thickness distribution.

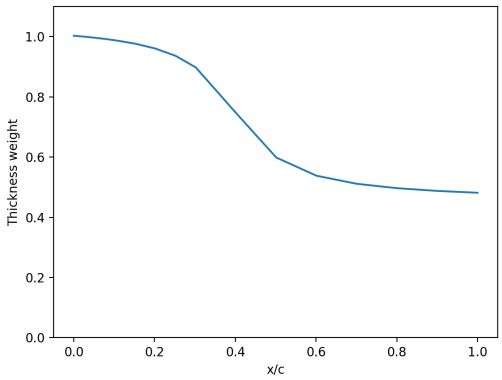

Figure 9.9: Weight applied to the top panel thickness.

9.5. Verification

The verification of the software include system and unit-tests of the following modules:

- Graph module: graph can be represented by adjacency lists for each node. Some nodes of the graph are initialised (booms) and the adjacency lists are checked to ensure they contain the right neighbours. The centroid calculation is verified
- Geometry module: booms areas and moments of inertia calculations are verified using example 20.4 from Megson [30].
- Section Geometry module: all properties related to a single section of the wing-box are tested. This section includes testing of the moment of inertia, and transformation of position around one axis, due to changes of geometric parameters along the span like the twist
- Stress module: the stresses are simulated in the Section object. This section deals with tests aimed at verifying The geometry used to verify the normal stresses is shown in Figure 9.10 and for the shear stress (including torsion) the 2-cell beam is shown in Figure 9.11.

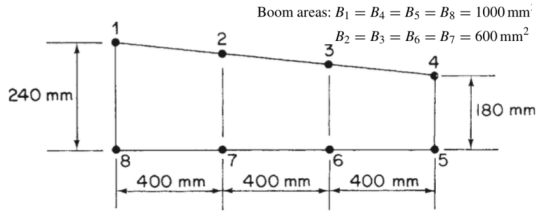

Figure 9.10: Geometry used to test the section geometry and normal stresses due to bending (problem 23.1 Megson [30]).

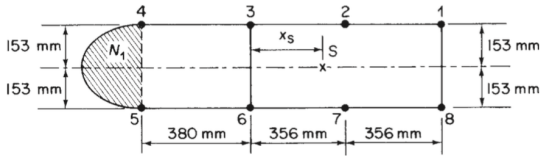

Figure 9.11: Structure used to verify shear flows due to pure torsion and shear.

Requirement	Verification Method	Compliance
SYS-SUB-STR-1: The structure shall be able to sustain all the loads during its lifetime	Analysis by boom idealization	yes
SYS-SUB-STR-2: The mass of the structures subsystem shall not be higher than 3.16 kg.	Inspection in budget	yes
SYS-SUB-STR-3: The structures subsystem shall be able to sustain 8000 loading cycles.	Analysis on empirical data of Nylon 6	yes
SYS-SUB-STR-4: The structures subsystem shall protect the power, telecommunication, payload, and control and navigation subsystems from rain, snow and hail.	Inspection	yes

Table 9.4: Compliance matrix for structure requirements.

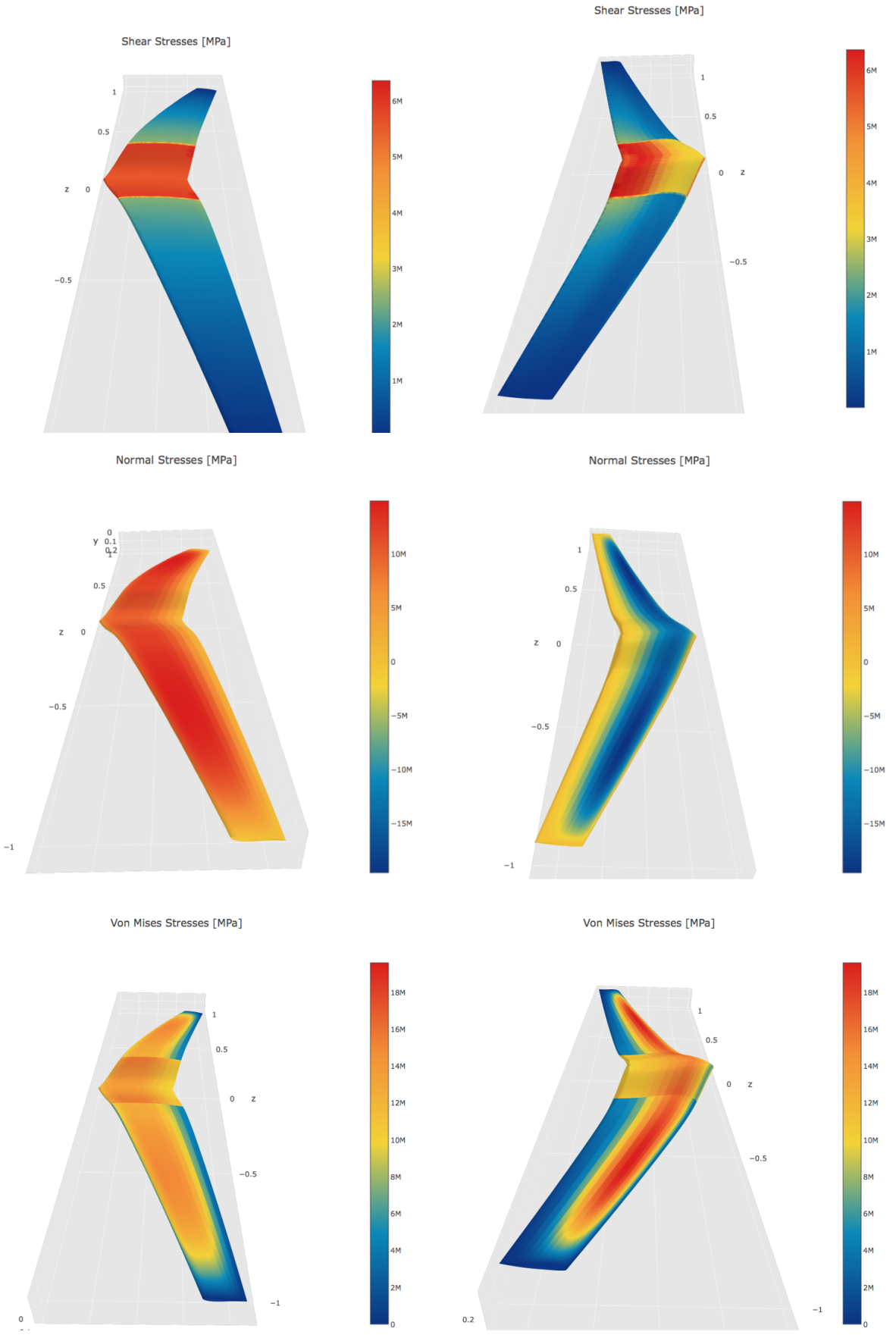

Figure 9.12: Stress distribution in the span.

10

Detailed Design: Control and Navigation

As the delivery drone does not only have to be silent but also autonomous, special attention had to be paid to the control and navigation subsystem. In this chapter the equations of motion will be derived in section 10.1 and subsequently the chosen sensors for autonomous navigation will be presented in section 10.2.

10.1. Control

In this section, the controller is implemented to stabilise and control the drone during different flight phases. Control of any complex system always starts off with the modelling of its dynamical behaviour. Using this model, the user is able to simulate the system and design controllers to obtain the required behaviour.

10.1.1. Equations of Motion

In this subsection, the dynamical model of the drone shall be determined for fixed wing and VTOL flight. First, the coordinate systems for the derivation shall be presented. Next, the free body diagrams for both conditions are discussed and finally, the equations of motion and their simplifications are shown.

The inertial reference frame to be earth-fixed, meaning that the x-axis points north, the y-axis points east, and the z-axis points towards the centre of the earth. As the drone shall not be travelling further than 30 km, the curvature of the earth can be neglected. This coordinate system shall be used to express the position of the drone in x, y, z coordinates and the orientation of the drone ϕ, θ, ψ with respect to the x, y and z axis respectively. The coordinate system can be seen in Figure 10.2. The body axis-system shall be fixed to the centre of gravity of the drone, with the x-axis pointing forward, the y-axis pointing starboard, and the z-axis pointing down. In this coordinate system, the velocity of the drone will be specified as a vector with the velocity components u, v, w along its x, y and z axis respectively. The coordinate system can be seen in Figure 10.1.

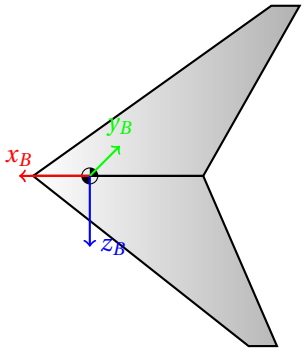

Figure 10.1: Body reference system

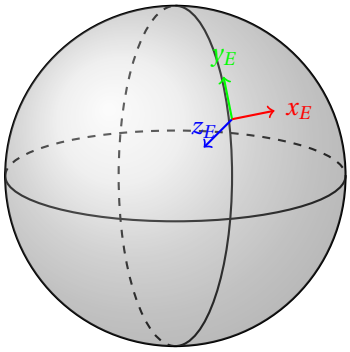

Figure 10.2: Inertial Reference Frame

To convert from the body axis system to the inertial axis system, use is made of the standard 3d transformation matrices.

Next, the free body diagrams for the fixed wing and VTOL conditions were set up, which are seen in Figure 10.3 and Figure 10.4 respectively. In both cases, the forces and moments are drawn with respect to the body coordinate system, as this will simplify the equations of motion. In the fixed-wing free body diagram, the effects of the lift, drag and moment generated by the wing are shown as L, D and M_{ac}. The trust produced by the pusher propeller is given as T. The forces and moments generated by the control surfaces and body are given by $X_c, Y_c, Z_c, L_c, M_c, N_c$ and $X_b, Y_b, Z_b, L_b, M_b, N_b$ respectively. The choice was made to not draw these forces in the free body diagram to reduce visual clutter. The VTOL diagram shows the forces and moments generated by the four horizontal propellers as $T1, T2, T3, T4, M1, M2, M3, M4$ and the drag force D generated during climb.

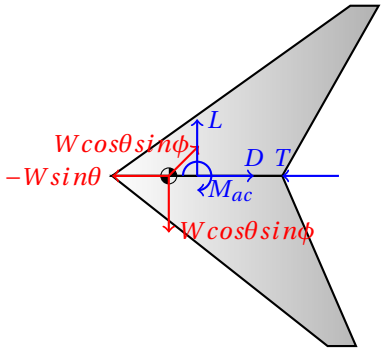

Figure 10.3: FW equations of motion

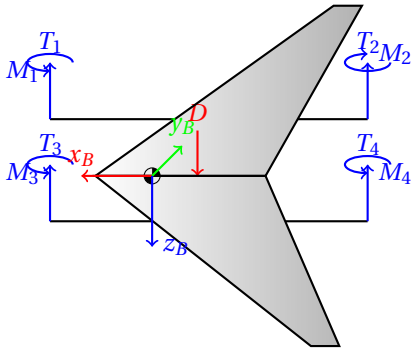

Figure 10.4: VTOL equations of motion

The equations of motion can now be set up based on the forces in the free body diagram and the fundamental equations $F = ma$ and $I\dot{\omega} + \omega \times (I\omega) = M$. For both conditions, it follows that a total of 12 state variables are present. The variables $l_{\text{ms}}, l_{\text{mf}}, l_{\text{mb}}, l_{\text{dc}}$ represent the distance from the cg to the motor rods, to the front propellers, to the back propellers and to the drag centre respectively.

VTOL EOM

$$\dot{u} = rv - qw - gs\theta$$
$$\dot{v} = pw - ru + g(c\theta s\phi)$$
$$\dot{w} = qu - pv + g(c\theta c\phi) + \frac{(-T_1 - T_2 - T_3 - T_4 + D)}{m}$$
$$\dot{x} = w(s\phi s\psi + c\phi c\psi s\theta) + v(c\phi s\psi - c\psi s\phi s\theta) + u(c\psi c\theta)$$
$$\dot{y} = v(c\phi c\psi + s\phi s\psi s\theta) - w(c\psi s\phi - c\phi s\psi s\theta) + u(c\theta s\psi)$$
$$\dot{z} = w(c\phi c\theta) - u(s\theta) + v(c\theta s\phi)$$
$$\dot{p} = \frac{I_{yy}qr - I_{zz}qr + l_{\text{ms}} \cdot (T_3 + T_4 - T_1 - T_2)}{I_{xx}}$$
$$\dot{q} = \frac{I_{zz}pr - I_{xx}pr + l_{\text{mf}} \cdot (T_1 + T_3) - l_{\text{mb}} \cdot (T_2 + T_4) + D \cdot l_{\text{dc}}}{I_{yy}}$$
$$\dot{r} = \frac{I_{xx}pq - I_{yy}pq + M_2 + M_4 - M_1 - M_3}{I_{zz}}$$
$$\dot{\phi} = p + s\phi t\theta q + c\phi t\theta r$$
$$\dot{\theta} = c\phi q - s\phi r$$
$$\dot{\psi} = s\phi sec\theta q + s\phi sec\theta r$$

FW EOM

$$\dot{u} = rv - qw - gs\theta + \frac{(-D + T + X_a + X_c)}{m}$$
$$\dot{v} = pw - ru + g(c\theta s\phi) + \frac{(Y_a + Y_c)}{m}$$
$$\dot{w} = qu - pv + g(c\theta c\phi) + \frac{(-L + Z_a + Z_c)}{m}$$
$$\dot{x} = w(s\phi s\psi + c\phi c\psi s\theta) + v(c\phi s\psi - c\psi s\phi s\theta) + u(c\psi c\theta)$$
$$\dot{y} = v(c\phi c\psi + s\phi s\psi s\theta) - w(c\psi s\phi - c\phi s\psi s\theta) + u(c\theta s\psi)$$
$$\dot{z} = w(c\phi c\theta) - u(s\theta) + v(c\theta s\phi)$$
$$\dot{p} = \frac{I_{yy}qr - I_{zz}qr + Lb + La}{I_{xx}}$$
$$\dot{q} = \frac{I_{zz}pr - I_{xx}pr + M_{ac} - L(x_{ac} - x_{cg}) + Mb + Ma}{I_{yy}}$$
$$\dot{r} = \frac{I_{xx}pq - I_{yy}pq + Nb + Na}{I_{zz}}$$
$$\dot{\phi} = p + s\phi t\theta q + c\phi t\theta r$$
$$\dot{\theta} = c\phi q - s\phi r$$
$$\dot{\psi} = s\phi sec\theta q + s\phi sec\theta r$$

Finally, it is possible to make some simplifications to the equations of motion. First, The motor thrust and torque can be modelled as a quadratic function of motor speed multiplied by a constant ($T = k_t \cdot s^2$ and $\tau = k_m \cdot s^2$). These constants would be obtained by measuring the thrust and torque for different speeds and fitting the curve. The lift and drag force generated by the wing can be calculated by the lift and drag equations as a function of angle of attack ($\alpha = tan\left(\frac{u}{\sqrt{u^2+v^2+w^2}}\right)$).

10.1.2. Controller

The control mechanism for the design can be divided into three different parts. The VTOL controller, the fixed wing controller, and the controller handling the transition phase between VTOL and fixed wing flight. Given the length of this project and the time available, the decision was made to only design controllers for the VTOL and fixed wing part. In this subsection, the process of controller design shall be discussed and some final simulations presented.

To model the system dynamics and design the controllers, the program Simulink since it offers a polished toolbox for the control design of non-linear systems. It allows the user to automatically linearize a system about a given operating point to use well-established control system design methods such as Bode plots, Root locus plots and more.

When all the controllers are designed, they will be rewritten to include an observer such that they make use of the

provided sensor data (accelerometer, gyroscope and GPS). Finally, the controller is exported to the Pixhawk 2 using Simulink's integrated conversion software.

VTOL Controller The VTOL controller must provide lateral and longitudinal stability to the drone during flight, but should not make it so stable that it becomes uncontrollable. The final goal of this controller is provided stability to the drone while still retaining the ability to control and follow a predefined 3D route $(x(t), y(t), z(t))$ while maintaining a specified heading $(\psi(t))$.

The entire control system is made up of 3 parts. The controller, the signal mixer and finally the nonlinear model.

The controller has two main loops. The inner loop, which controls the drone attitude, and the outer loop, which controls the drone position. The outer loop takes the error between the current and required position and heading (x, y, z and psi), and generates output signals for the desired motor and desired drone orientation. The inner loop than calculates the error between the required and determined attitude values, and by use of PID controllers, outputs the required thrust and torque to correct the current drone state. The tuning of the PIDs was done using Simulink's integrated PID Tuner.

Based on the dynamics of the system, and the relationships between thrust, torque and motor speed, the signal mixer converts the values from the controller outputs to motor speeds for the non-linear model.

Finally, the nonlinear model takes as input the motor speed of each of the 4 motors and outputs the integrated state space variables.

Fixed Wing Controller The fixed wing controller is responsible for keeping the drone stable during flight. The user will be able to specify the required speed, heading and altitude (u, ψ and z) during flight. It shall also be able to recognise the eigenmotion for dutch roll and provide control procedures for actively damping this mode.

Just as with the VTOL controller, this system is made up of three parts. The controller, the signal mixed and the nonlinear dynamic model.

The controller is a single loop system which, based on the error between the required and measured speed, heading and altitude (u, ψ and z), uses PID controllers to generate the required roll, pitch and yaw moment, and the required thrust.

This signal mixer converts the previously mentioned moments to elevon and split rudder deflections. The required thrust is converted to motor RPM.

Finally, the control signals are fed into the dynamic system and the resulting state variables can be observed.

10.1.3. Verification

Verification methods of the control system include:

- Equations of Motion Implementation: The equations of motion can be unit-tested to verify that they were implemented correctly. This would be done by using mock variables and comparing the software results with hand-calculated results.
- Dynamic Model Fixed Wing: By simulating the eigenmotions during fixed-wing flight, the model can be verified for correctness (compared to the results found by the stability department)

10.2. Navigation

With the drone being autonomous, it had to be established how it can navigate to its destinations, avoid obstacles and find its landing spots. In this section the approach used to achieve this will be discussed following the division into the 3 main tasks listed above. First, it will be explained how the requirements on the navigation subsystem were derived, then an overview of the possible design solutions will be given. Subsequently, it will be shown which hardware was deemed most suitable for the delivery drone and which software is required. Finally, it will be checked if the derived design does comply to the navigation subsystem requirements.

10.2.1. Return on Subsystem Requirements

The subsystem requirement were established in section 5.5. There were however, some requirements for which it was not yet been explained why the specific values were chosen which will be done in this section.

- **SYS_SUB_NAV – 1** : *The navigation subsystem shall estimate the drone position with a precision of **8m***. For this requirement a "backwards-approach" was used in which it was checked if the accuracy provided by GPS will be

sufficient for the operation of the delivery drone. According to the National Coordination Office for Space-Based Positioning, Navigation, and Timing, the global average user range error is ≤ 7.8 m within a 95% interval.[1] The driving parameter for the required position accuracy is that the drone has to be able to arrive at the correct address and find its landing spot. If this was to be achieved using only GPS, centimetre-accuracy would be required. While there are GPS-systems that can achieve this level of accuracy, they are costly and consequently not ideal. Considering that the drone also has to be able to perform obstacle avoidance, it was decided to use a camera to find the landing spot. As will be shown in subsection 10.2.3, the landing spot can still be found even if the position is off by 7.8 m. From that it was concluded that the accuracy of conventional GPS-systems will be sufficient yielding, after rounding, a required position-accuracy of 8 m.

- **SYS_SUB_NAV – 3** : *The navigation subsystem shall detect any object within a 360 view range and a **37.5 m** distance.* The range is mainly determined by the velocity at which the drone flies since the system needs sufficient time to respond and avoid obstacles. Using the reaction time $t_{reaction} = 2\text{s}$ established in section 10.1 and the horizontal velocity of $v_h = 18.75\text{m}\,\text{s}^{-1}$ during cruise established in chapter 4 the required range is $r_h = 2\text{s} \cdot 18.75\text{m}\,\text{s}^{-1} = 37.5\text{m}$.

- **SYS_SUB_NAV – 4** : *The navigation subsystem shall detect any object above or below it within a **1.5 m** distance.* Using the same reasoning as for the horizontal range and remembering that the vertical velocity of the drone is $1\text{m}\,\text{s}^{-1}$, it can be determined that the vertical range has to be $r_v = 1.5\text{s} \cdot 1\text{m}\,\text{s}^{-1} = 1.5\text{m}$.

10.2.2. Review Possible Design Solutions

In this section the possible options for the navigation subsystem will be summarised to provide an overview before the more detailed discussion about the sensors in subsection 10.2.3. In Table 10.1 and Table 10.2 the options for the position and attitude determination and the obstacle avoidance as well as their advantages and disadvantages are depicted.

Navigation Looking at Table 10.1 it can be seen that in fact none of the solutions by themselves are sufficient for the position and attitude determination. For the inertial navigation the error diverges over time, the magnetometer and the barometer only provide information about attitude and altitude respectively, GPS-signal can be lost in urban areas and visual navigation is difficult to use at night. Signals of Opportunity (SOP) is a collective term for signals that are present in urban areas which are not necessarily meant for navigation but can still be used for it by implementing trilateration as has been shown in [32]. These signals include e.g. WiFi, cellular signals, FM/AM signals etc [32]. While it does provide higher accuracy than GPS when at least 2 kinds of signals are used and when coupled with inertial navigation, it is a rather new technology and consequently has a low technology readiness level. [32]

Consequently, it was decided to use a combination of all these solutions. Since GPS provides absolute position information, has no growing error, and can be used at night, it will be used as a base for the position and attitude determination. To make up for its low accuracy in altitude, additionally a barometer will be used.

Design Solution	Advantages	Disadvantages
Barometers	+ Cheap + High update frequency	- Only provides information about the altitude
Magnetometers	+ High update frequency + Works in all weather conditions + High accuracy	- Only provides information about the attitude
Inertial Navigation	+ High update frequency + Works in all weather conditions	- Error accumulates over time
Visual Navigation	+ High accuracy + Provides postion information without GPS	- Requires high computational power - Requires map of the area with landmarks - Difficult to use at night
Signals of Opportunity	+ Works without GPS + Works at night + No growing error + Higher accuracy than GPS when at least 2 signals available	- High computational cost - Low technology readiness level - Requires more than one sensor
GPS	+ Cheap and simple + Provides information about attitude and position + No growing error	- Signal frequently lost in urban areas - Limited accuracy especially for altitude

Table 10.1: Overview of the possible design solutions for the position and attitude determination of the delivery drone.

[1] `https://www.gps.gov/systems/gps/performance/accuracy/` last accessed on 08/05/2018

As the precision of the GPS is only guaranteed within a 95% interval, it makes sense to use a Kalman Filter (a technique to improve sensor accuracy) to combine data from the GPS and the inertial navigation to improve the location accuracy. This process will be further explained in subsection 10.2.4. Furthermore, a back-up will be required in case no GPS-signal is available. One way to achieve this would be to use visual navigation however, the drone has to be able to operate at night which would require night-vision cameras. While there are affordable infrared cameras for drones, they have short range vision (usually less than 10m) and low resolution which makes them unsuitable for visual navigation. Fortunately, SOP serves as a good back-up since it can operate at night and has a bounded error. As additional back-up, inertial navigation fused with magnetometers using a Kalman Filter can be used as will be explained in subsection 10.2.4.

Obstacle Avoidance Naturally, the drone does not only have to be able to navigate but also to avoid obstacles. The sensors that could be used to do that are listed with their respective advantages and disadvantages in Table 10.2.

Design Solution	Advantages	Disadvantages
Laser sensors	+ Can operate at night + High distance range	- Expensive
Visual object recognition	+ Very high resolution	- Limited use at night
Infrared	+ Can be used at night + Commonly used for drones	- Rather low distance range
Ultrasound	+ Cheap + Light	- Low distance range

Table 10.2: Overview of the possible design solution for the obstacle avoidance of the delivery drone.

The most limiting factor for these sensors is their range since according to the requirement SYS_SUB_NAV-3, the obstacles have to be detected at a distance of at least 37.5 m in the horizontal direction. The only sensors that are able do this at day and night are the laser sensors. Again, affordable infrared cameras have a low range and are therefore not suitable. However, since laser sensors are comparatively expensive it would not makes sense to also use them for the detection of obstacles in the vertical direction since the required range for that is much lower, namely 1.5 m as determined by SYS_SUB_NAV-4. Consequently, the much cheaper and lighter ultrasonic sensors can be used for that. As discussed in subsection 10.2.1, a camera will be needed to find the landing spot due to the limited GPS-accuracy. Since the required range for that is lower (It is sufficient to only see several meters far as the drone is already close enough) an infrared-camera can be used such that the drone is also able to operate at night.

10.2.3. Sensor Selection

In the previous section an overview of the various sensors for the navigation subsystem was provided. In this section it will be explained which exact off-the-shelf sensors were chosen and it will be shown how they will be positioned on the drone. The mass and power consumption of all parts will be summarised in chapter 14 and the cost in chapter 20.

GPS Receiver It was decided to use the GPS receiver that is included in the mobile broadband chip SIM7100C 4G Module GPS GPRS Development Board as this will also be needed for the Telecommunications subsystem. It will be mounted on top of the drone to provide good reception as can be seen in the third top image from the left in Figure 10.5.

IMU The GY-85 Sensor Module 9 Axis 6DOF 9DOF IMU Sensor was chosen containing 3 gyroscopes and 3 accelerometers for the attitude, 2 barometers for the altitude and 2 magnetometers as measurement updates for the attitude. Since it does not have to receive any signals it can be positioned inside the drone body as can be seen in the third bottom image from the left Figure 10.5. An additional back-uo IMU is integrated in the flight controller, as explained in chapter 7.

SOP For this system several sensors are needed since it relies on more than one form of measurement. The strength of surrounding WiFi-signals can be measured using the processor unit which includes a WiFi receiver. To use radio and cellular signals for trilateration, a radio and a cellular receiver are required for which the Grove - I2C FM Receiver and the ESAMACT SIM800L V2.0 5V Wireless GSM GPRS Module Quad-Band with Antenna Cable Cap were chosen, respectively. These are depicted in Figure 10.5 where it can be seen that they will be mounted on top of the flying wing beacouse similarly to the GPS-module they have to be unobstructed, to receive their signals.

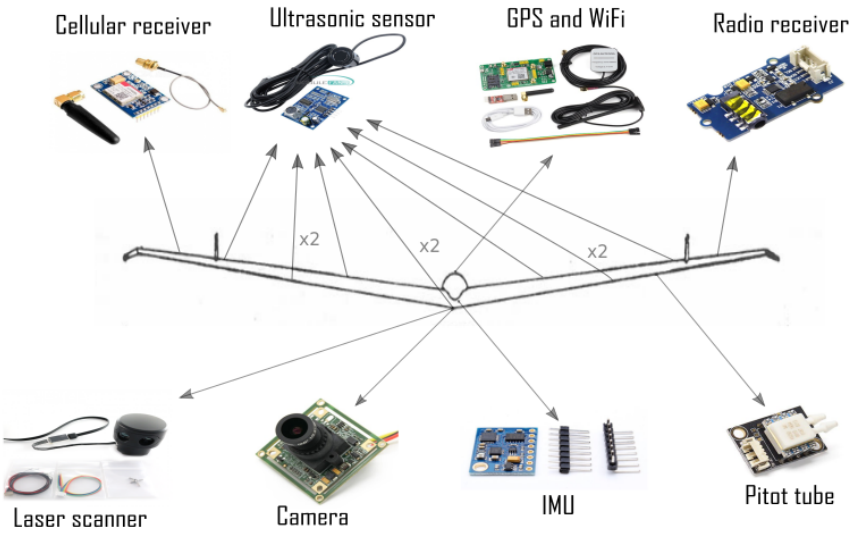

Figure 10.5: The sensors chosen for the navigation subsystem and their respective locations on the drone.

Horizontal Object Detection A laser scanner, namely the Sweep V1 360° Laser Scanner was chosen as can be seen in the first bottom picture from the left in Figure 10.5. The reason for that is that it provides a range of 40m which is just enough to comply to the horizontal range requirement. Since it rotates, it can provide 360° coverage using just one sensor, which makes the design both lighter and cheaper. In order to ensure a clear field of sight this sensor will be mounted in the centre of the drone. It was decided to attach it at the bottom since the most critical obstacles (people) will be located underneath the drone.

Object Detection Above It was decided to use the cheaper and lighter ultrasonic sensors for obstacle avoidance in the vertical direction since a lower range is required. For that the Ultrasonic Module Distance Measuring Transducer Sensor Waterproof JSN-SR04T was chosen as can be seen in the second top image from the left in Figure 10.5. While it is not the cheapest ultrasonic sensor on the market, its price is still significantly lower than that of a laser range finder and unlike its cheaper competitors it is waterproof. This is essential since the sensors will be mounted to the outside of the drone, which is exposed to harsh weather conditions. In total 10 of these sensors will be required with four of them equally spaced spanwise on top of the wing to provide obstacle avoidance in the vertical direction. They will be mounted at a slight angle forward to also cover those areas which are not covered by the laser scanner. The remaining 6 sensors are placed equally spaced below the wing and at the leading edge for redundancy as will be explained in section 5.5 Since each sensor covers an area of about 60 cm and the total span of the drone is 2 m there are stripes of 5 cm for the directions in which there are only 3 sensors which are not covered. However, only very small obstacles as for example insects will not be detected which was considered acceptable remembering that they will only be used if other sensors fail and then at low velocities. Since there are four sensors at the top one of them is redundant.

Object Detection Below For the primary obstacle detection in the vertical direction underneath the drone (the ultrasonic sensors are back-up) , it was decided to use image recognition since the drone will be equipped with a downward-facing camera, that is needed to find the landing spot. For that the 1/2.5-inch Sony CCD Video Camera 700TV Lines F2.0 5MP IR (PAL) was chosen as depicted in the second bottom image from the left in Figure 10.5. It provides day and night vision with a range of up to 8m. Furthermore, it has a very large angle of view (AOV) of 170° enabling it to cover a large ground area. This means that hovering at an altitude h of 5 m (according to the manufacturer the best quality images can be achieved at this distance) the camera can see $r_{camera} = h \cdot \tan \frac{AOV}{2} = 57.15$ m far. This proves that the drone can indeed still get close enough to the landing spot to detect it even using the low accuracy of conventional GPS-signals as stated in subsection 10.2.1.

Velocimeter To determine the horizontal velocity more accurately than it is possible using GPS, a pitot tube is required. To ensure that it can be connected to the flight controller a digital one had to be chosen, as opposed to the analogue ones

usually used for aircraft, resulting in the choice of the Pixhawk Digital Airspeed Sensor w/ Pitot Tube depicted in right bottom image in Figure 10.5.

10.2.4. Required Software

Until now it has only been discussed which hardware was chosen but it was not explained how exactly this hardware can be used to navigate, avoid obstacles and to find the landing spot. Using the division into these 3 main tasks of the navigation subsystem the required software for the drone will be explained in this subsection.

Navigation From section 10.1, it is known that the navigation subsystem has to provide the required velocity, altitude and heading to the control system during fixed wing flight and position and heading during VTOL flight. The current position and attitude of the drone are determined using the GPS, inertial measurements and in case of GPS-signal loss, SOP. This information is then passed on to the processor where the current and desired position are compared. The latter is known from the route obtained from the routing algorithm established in chapter 4. Based on that, a direction vector can be determined towards which the drone has to fly. This in return needs to be translated into the required heading of the drone which can then be fed into the control system together with the desired velocity and altitude which are known from the flight profile established in chapter 4. The exact data flow was discussed in more detail in chapter 7. Furthermore, the software can estimate the travelling time since it knows the distance and the velocity. In case the processor receives no information from one of the sensors it has to activate the sensor serving as its backup. Finally, the drone has a map including all the locations of the landing spots registered with the company such that it can give input to the control system to fly to the closest one in case an emergency landing is required.

As explained in subsection 10.2.2, the accuracy of the attitude and position determination can be improved using a Kalman-filter which fuses the measurements from several sensors to reduce their uncertainty. Its working principle is shown in Figure 10.6 [4]. Prior knowledge of the states of the system (e.g the position using GPS or SOP) $x_{k-1|k-1}$ and their probability distribution function (p.d.f.) $P_{k-1|k-1}$ are available, where the subscripts indicate the time-steps. These can then be propagated forward in time using a physical model that obtains information about the accelerations from the IMU. This introduces new errors increasing the variance of the p.d.f. of the states as indicated by the green p.d.f. in the top right image. From measurements another p.d.f. is available as indicated in red in the bottom right picture which can then be fused with the propagated p.d.f. to obtain an updated state estimation with a smaller variance as indicated in purple in the bottom left picture. This is then the basis for the next iteration.

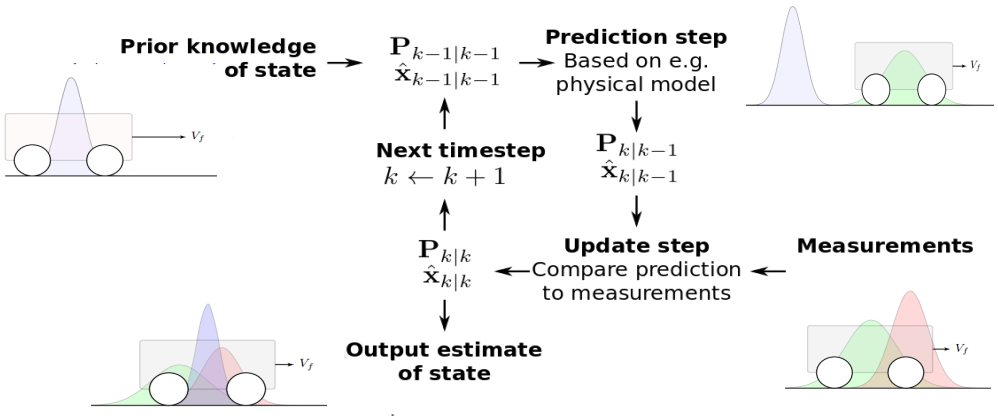

Figure 10.6: Illustration of the working principle of a Kalman filter.

When no GPS-signal is available to provide measurement updates, SOP's can be used. However,the position and clock states of the signals might not be known (since not all of them are actually meant to be used for navigation) which means that they have to be estimated. This requires simultaneous localisation and mapping (SLAM) which describes the process of constructing or updating a map of an unknown environment while simultaneously keeping track of the system's location within it. [32] This can be done using an extended Kalman Filter which does not only estimate the drone's states but also the SOP's. A detailed discussion of the working principles of the extended Kalman filter is beyond the scope of this report.

As mentioned in subsection 10.2.2, the Kalman Filter can not only be used to increase the accuracy of the GPS but

also to decrease the attitude drift (which directly influences the position drift) of the IMU when no GPS is available. Using the magnetometers for the measurement updates the position drift can be reduced to 5 m rather than 150 m after 60 s which is within the acceptable accuracy. [43] This represents another back-up in case the SOP fails providing the possibility to bridge the time for up to 1 minute between GPS-signal loss and getting it back.

Obstacle Avoidance When one of the obstacle avoidance sensors detects an obstacle, information about the location and the distance of the obstacle is sent to the processor. At this point software is required to determine in which direction to avoid such that a new heading angle can be forwarded to the control system. The approach used is to determine the direction perpendicular to the one in which the obstacle was detected and feed this into the control system together with a reduced velocity until the obstacle is no longer sensed. Then the original heading and velocity will be used again to arrive at the destination. If the landing spot is blocked by an obstacle the navigation subsystems sends the command to hover for 20 s to the control system. If the spot is still not clear by then the mission is aborted and the ground station is informed which can then schedule another delivery time. The drone moves on to deliver the next package. High-rise buildings are avoided with the routing algorithm as explained in chapter 4.

Finding the landing spot The software to find the landing spots includes image recognition where the image seen by the camera is compared to the picture obtained from Google Maps as explained in chapter 4. Based on where in the view field the spot was detected, a new heading angle can be determined which is then fed into the control system. This is repeated until the landing spot is in the centre of the view field and the drone can start to descend. For highly densely populated areas where landing spots will have to be built on the roofs, beacons sending radio signals will be installed providing another means of finding the landing spots while also serving as SOP's.

10.2.5. Verification of Subsystem Requirements

With the design finished it is important to verify that the subsystem does indeed comply to the requirements. Since including each sensor twice would lead to a heavy and expensive design, it has to be considered how to meet the single-point failure free requirement which is done hereafter.

- **Laser scanner:**If the laser scanner fails, the ultrasound sensors positioned at the front of the drone take over the obstacle avoidance in the horizontal plane. Since these have a lower range, the drone cannot safely fly fast enough to meet the stall speed and has to hover. Consequently, it will have to perform an emergency landing at the closest safe landing spot as described in subsection 10.2.4.
- **Camera:** In case of a failure of the camera, the ultrasound sensors at the bottom take over the obstacle detection and the drone flies back to the base station where it can land supervised.
- **IMU:** Since an IMU is also included in the flight controller, this one can take over in case the primary one fails.
- **Pitot tube:** The velocity can also be approximated using the the GPS-signal. Since this is rather inaccurate, cruise flight which needs accurate velocity measurements should be avoided and the drone should hover to the closest safe landing spot which it can find using GPS and the camera.
- **GPS:** If the GPS fails, SOP can take over.
- **Ultrasonic sensors:** As explained in subsection 10.2.2 the ultrasonic sensors are redundant meaning that the drone is still able to operate even if one of them fails.
- **SOP sensors:** Since the SOP make use of three different signals, it is still able to perform more accurately than GPS if one fails as was explained in subsection 10.2.2.

The remaining requirements were checked using the compliance matrix depicted in Table 10.3 in which it can be seen that the subsystem design meets all the requirements. The validation of the requirements will be done in chapter 17.

Requirement	Verification Method	Compliance
SYS-SUB-NAV-1 The navigation subsystem shall estimate the drone position with a precision of 8m	Specifications of GPS and SOP	yes
SYS-SUB-NAV-2 The navigation subsystem shall perform real-time object detection	Done using the camera and software	yes
SYS-SUB-NAV-3 The navigation subsystem shall detect any object within a 360 deg view range within 37.5 m distance horizontally	LiDAR sensor has 360 deg view and 40m range	yes
SYS-SUB-NAV-4 The navigation subsystem shall detect any object within 1.5 m distance vertically	Sonar senors have a range of 6m	yes
SYS-SUB-NAV-5 The flying height shall be known within 0.5 m of accuracy.	Barometers have accuracy of 0.3m	yes
SYS-SUB-NAV-6 The navigation subsystem shall provide autonomous flight.	Drone has autopilot	yes
SYS-SUB-NAV-7 The navigation subsystem shall calculate landing speed	Known from mission profile and possible obstacles	yes
SYS-SUB-NAV-8 The navigation subsystem shall send system status and sensor data to the control system	Done by nagigation software	yes
SYS-SUB-NAV-9 The navigation subsystem shall detect sensor malfunction	Done by navigation software	yes
SYS-SUB-NAV-10 The navigation subsystem shall send the command to abort the mission	Done by navigation software	yes
SYS-SUB-NAV-11 The navigation subsystem shall guide toward an emergency landing	Done by navigation software	yes
SYS-SUB-NAV-12 The navigation subsystem shall be able to estimate delivery time	Done by processor based on velocity in mission profile	yes
SYS-SUB-NAV-13 The navigation subsystem shall be single point failure free.	See discussion in subsection 10.2.5	yes

Table 10.3: Requirements compliance matrix for the navigation subsystem.

11

Detailed Design: Propulsion

In this chapter, the propulsion subsystem design is presented. Next to constraints on the design in terms of thrust performance, the propulsion system is the primary source of noise. An approach has been established to optimise for performance whilst reducing parameters driving noise production. Hereby the motors were chosen first and following the propellers were designed second.

11.1. Motor selection

The motors are an essential part of the propulsion system since they provide the torque that makes the propellers rotate. It was decided to use outrunner brushless motors for the propellers. This is the most common choice for drones because of the high torque they can produce compared to their weight. For the choice of motors, the constraints were the total mass of the propulsion system (which was obtained from the preliminary technical budget), the power input and the thrust provided. In addition, they had to be compatible with the choice of batteries.
After researching the off-the-shelf motors available at the moment, it was decided that the best solution for the drone was the KDE4014XF-380 [1]. The reason for this is that at a mass of only 215 grams (cables included) it is able to provide up to 4 kg of thrust using a power input of 500 W, when combined with commercial KDE propellers of 18.5 inches diameter. It is also able to provide a maximum torque of 0.9 $\mathrm{N\,m^{-1}}$ at the maximum current of 36 A during 180 s. With this information it was decided to set the propeller diameter to 18.5 inches: since it was expected that our propeller design would at least equally efficient than a commercial design, it was guaranteed by the empirical data from the technical data sheet [2] that enough thrust would be provided. In addition, a large propeller diameter allows for a lower rotational speed of the propellers, which is beneficial for the noise, as explained in section 11.3. The Electronic Speed Controllers (ESC) were chosen after the motor was selected: the T-Motor F45A 2-6S [3]. The only constraint was the amount of current the ESCs could sustain, which had to be higher than the maximum amount of current the motor could draw to avoid any damage on the parts.

11.2. Propeller Sizing

For the design of low-noise propellers, the method presented by Stoll [41] was employed. In this method, the performance of the propeller is analysed with blade-element momentum theory (BEMT). Blade element theory (BEM) is often used in the design of propellers, rotors, and wind turbines. It relies on breaking down the blade in multiple sections, where each section is assumed to be a 2D wing. The lift and drag of each section are then calculated using the local aerofoil parameters, the local section velocity, and the local chord length. To account for losses near the tip, a Prandtl tip-loss factor is applied. The local thrust and the local power is calculated from the local lift, drag, and inflow angle. Using these local loads, the tangential and axial velocity components can be updated. After this iterative process has converged to within 0.1%, the thrust and power of the propeller as a whole are obtained by integrating over all sections. In this approach, the radial sections are assumed to be independent.

The design of the propeller required the following input variables; the rotational velocity, radius, number of blades, free stream velocity, and section geometry. Then, the chord and twist distributions are optimised for propulsive efficiency following the approach below.

Further noise reduction can then achieved by modifying the blade geometry. The method presented by Stoll is different from other methods in the sense that it concentrates on designing propellers at static conditions, which is makes it especially applicable for the design of the hover propellers.

[1] https://www.kdedirect.com/products/kde4014xf-380, last accessed 24/06/2018

[2] https://cdn.shopify.com/s/files/1/0496/8205/files/KDE_Direct_XF_CF_Brushless_Performance_Testing_-_KDE4014XF-380.pdf?7734511287488513374, last accessed 24/06/2018

[3] https://droneshop.nl/merken/t-motor/t-motor-f45a-6s-esc, last accessed 24/06/2018

11.2.1. Aerofoil Selection

Aerofoil selection of a propeller is fundamental to its performance. Achieving low drag and high lift at the operating conditions is typically the primary concern. However, for a propeller, the operating conditions are wide-ranging, given the different inflow angles as function of inflow velocity and rotational speed. Hence an aerofoil should be selected that has a wide drag bucket (low drag for large angle of attack domain), has a large operational range for the angle of attack and high lift over drag ratio. Furthermore, it should be recognised that the Reynolds number varies significantly over the radial position from ±10,000 to ± 200,000. Given the high dependency of an aerofoils performance and the manufacturing capability, it was decided to select multiple aerofoils for the different regimes. Note that unlike with most propellers the Mach number does not constrain the aerofoil as the Mach number will stay well below the compressibility threshold.

On the basis of a comparison performed across the database of Airfoiltools[4] the GOE225 was selected for Reynolds numbers higher than 75,000 as it has the highest maximum L/D as well as a large angle of attack domain and a low zero-lift drag coefficient. For Reynolds numbers lower than 75,000 the Wortmann FX 60-126/1 was selected as it has the second highest maximum L/D and a large angle of attack domain, the zero-lift drag coefficient is below average. Their lift coefficients is plotted against the angle of attack and drag coefficients in Figure 11.1 and Figure 11.2 respectively. For high Reynolds numbers XFOIL gives a very accurate result compared to experiments[7, 12]. For lower Reynolds numbers (at and below 50000) the simulations starts to deviate from experiments but still within an acceptable margin (<5%)[7]. At stall however XFOIL is not able to approximate well experiments, note that the stall is underestimated meaning that the results are conservative and will yield in a feasible solution[7]. It should be noted that the Wortmann FX 60-126/1 has a smaller angle of attack range than the GOE225 which is why it will not be applied at the root given that the inflow angle varies significantly with operating conditions. At the tip, the transition from GOE225 and Wortmann FX 60-126/1 will be aided by an aerofoil that is the geometric average of the two. The transition was found to be after several design iterations to be for the VTOL blade is at 0.16 m and 0.21 m for the composite aerofoil and the Wortmann aerofoil respectively. The transition for the FW blade is at 0.22 and 0.23 for the composite aerofoil and the Wortmann aerofoil respectively.

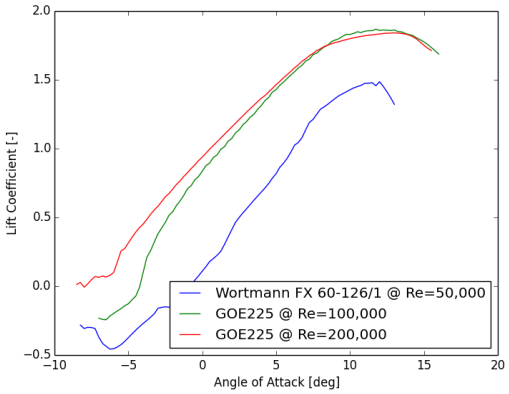

Figure 11.1: C_l-α curve for the selected aerofoils at various Reynolds numbers.

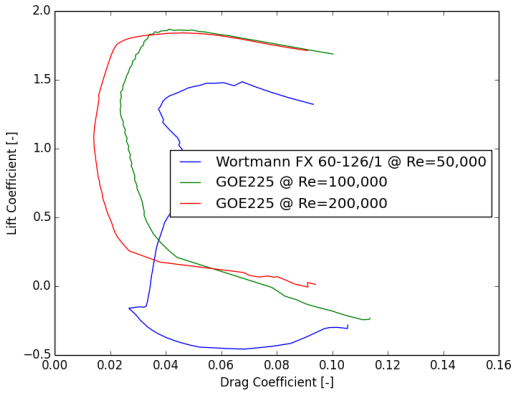

Figure 11.2: C_l-C_d curve for the selected aerofoils at various Reynolds numbers.

11.2.2. Blade Design Procedure

A design procedure based on Blade Element Momentum Theory (BEMT[5]) was proposed by C. N. Adkins and R.H. Liebeck [3]. The method optimises the chord distribution and twist angle for minimum energy loss as given by Reference [5], in other words, minimum power. The main assumption made in the method is that the aerodynamics can be approximated by a sum of sections of aerofoils with the Prandtl loss factor compensation. This assumption and the method, in general, have been found sufficiently accurate when verified with experimental results with the exception of static conditions[3, 29].

First, an initial value for C is estimated from $C = V_\infty^* + \sqrt{2C_T/\pi^3}$. Then, for all blade sections the inflow angle ϕ and the

[4] `http://airfoiltools.com`, last accessed 25/06/2018

[5] The team would like to recognise the support by AWEP-department at TU Delft for providing an in development BEMT code, which has been altered for our purposes.

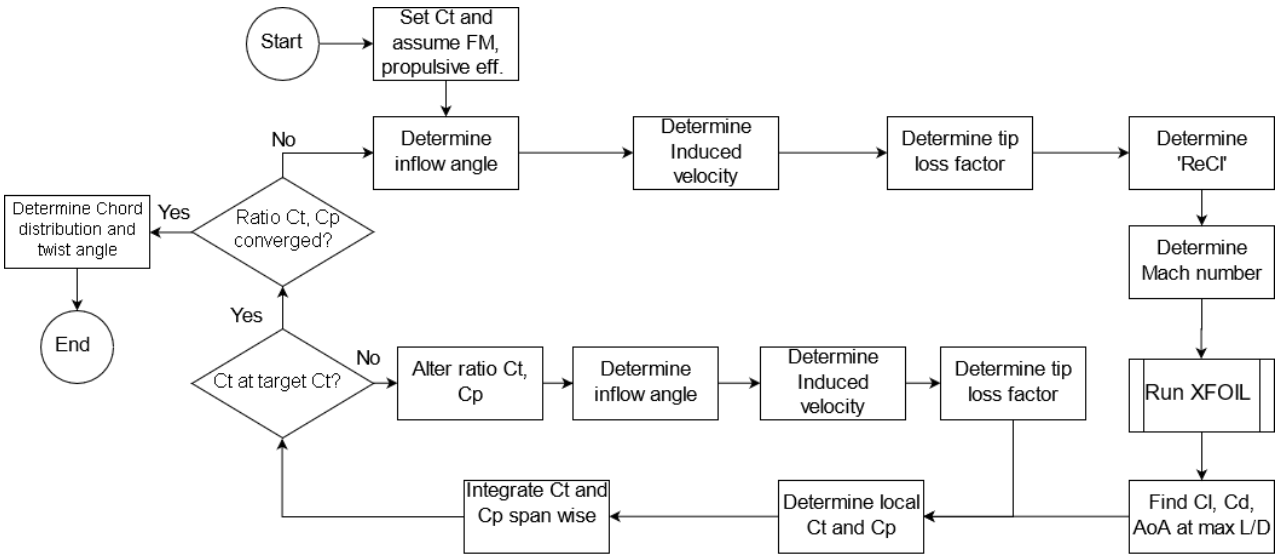

Figure 11.3: Blade design procedure

Prandtl loss factor F are calculated from Equation 11.1 and Equation 11.2, respectively.

$$\tan\phi = \frac{C - \epsilon r^*}{\epsilon C + r^*} \tag{11.1}$$

$$F = \frac{2}{\pi}\arccos\exp\frac{B(r^* - 1)}{2\sin\phi_t} \tag{11.2}$$

Then, the local axial induced velocity V^*_{xi} is calculated from Equation 11.3.

$$V^*_{xi} = \cos\phi\left(r^*\sin\phi - V^*_\infty\cos\phi\right) \tag{11.3}$$

Subsequently ReC_l is found from Equation 11.4.

$$ReC_l = \frac{a_0 M_T R 8\pi F r^* V^*_{xi}\tan\phi}{Bv} \tag{11.4}$$

Then the local Mach number is calculated from $M_b = V^*_b M_T$. Now, using the calculated values of ReC_l and M_b, the C_l and α that minimise ϵ are found using XFOIL. This means that the angle of attack of the blade aerofoil is optimised for maximum lift to drag ratio. Now that a new value is found for C, the process starts over at calculating the inflow angle, until the value converges to within 0.1%. After convergence, the chord distribution is found from $c^* = ReC_l/Re_0 C_l r^*$, and the twist distribution from $\beta = \alpha + \phi$. Finally the thrust and power coefficients C_T and C_P are found from Equation 11.5 and Equation 11.6. This process is visualised in Figure 11.3

$$C_T = \int_{R_{hub}}^{R} \pi^3\left(V^*_\infty + V^*_{xi}\right) F r^* V^*_{xi}\left(1 - \epsilon\tan\phi\right) \tag{11.5}$$

$$C_P = \int_{R_{hub}}^{R} \pi^4\left(V^*_\infty + V^*_{xi}\right) F r^{*2} V^*_{xi}\left(\epsilon + \tan\phi\right) \tag{11.6}$$

11.2.3. Result Sizing

The aforementioned sizing method described generates a planform for a certain number of blades, RPM, diameter, thrust and inflow velocity. The latter two of the parameters are fixed by the required operating conditions, the others are free. As a low RPM and a high diameter correspond to low noise production[13, 16, 24] the diameter will be set to the maximum allowable 0.47 m, where the RPM will be taken as low as possible while still meeting the power consumption requirement including a margin of 10% of 330 W for VTOL climb and 537 W for FW climb. The design space as defined by the VTOL climb and the FW climb (assumed to be most critical) are given in Figure 11.4 and Figure 11.5 for VTOL and FW respectively.

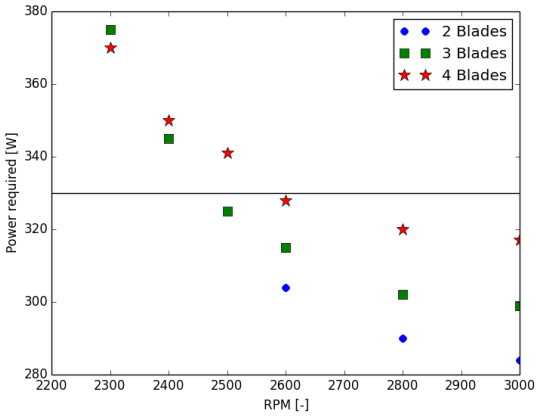

Figure 11.4: VTOL Blade shaft power required for varying design input RPM and number of blades, with fixed thrust setting of 38 N, diameter of 0.47 m and inflow velocity of 3 ms^{-1}.

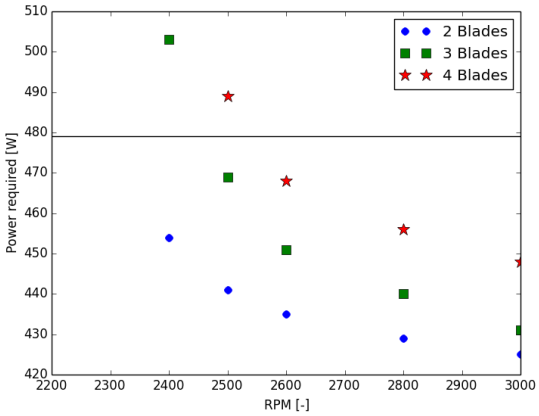

Figure 11.5: FW Blade shaft power required for varying design input RPM and number of blades, with fixed thrust setting of 20 N, diameter of 0.47 m and inflow velocity of 18 ms^{-1}.

The chosen design points are 2500 RPM and 3 Blades for the VTOL propeller and 2400 RPM and 2 Blades for the FW propeller. As the design method does not have a constraint on the chord length the generated planforms have rather large chord lengths. Furthermore, the angle of twist is also unconstrained which leads to high angles of twist at the root. This is to use the aerofoil at the optimal lift coefficient. The baseline geometry, as well as the altered optimized geometry for the blades, are presented in Figure 11.6 and Figure 11.7 for VTOL and FW respectively.

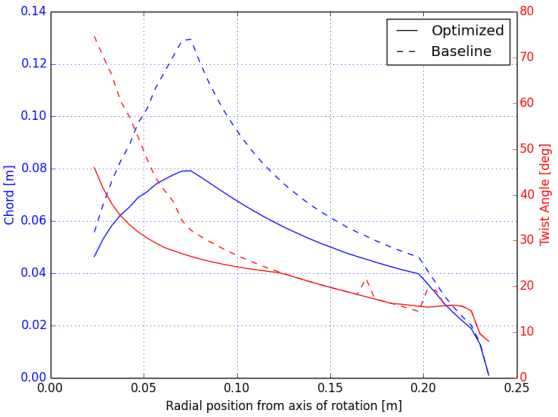

Figure 11.6: VTOL blade chord length and twist angle of the baseline and optimised design.

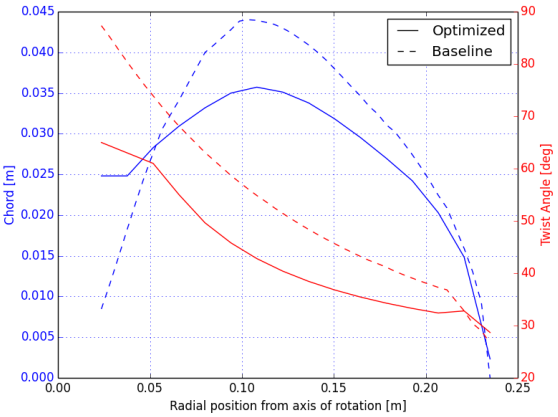

Figure 11.7: FW blade chord length and twist angle of the baseline and optimised design.

An overview of the propeller performance at the operating conditions during the mission is given in Table 11.1.

Flight Condition	VTOL (RPM, power)	Flight Condition	FW (RPM, power)
Descent: -1 ms^{-1}, 31 N	2350, 232 W	Cruise: 18 ms^{-1}, 15.4 N	2450, 319 W
Hover: 0 ms^{-1}, 31 N	2300, 225 W	Climb: 12 ms^{-1}, 15.4N	2600, 454W
Climb: 1 ms^{-1}, 38 N	2475, 330 W		

Table 11.1: Performance of the VTOL propeller during descent, hover and climb and of the FW propeller during cruise and climb

11.2.4. Implementation Verification

Besides unit testing, the implementation of the blade element analysis part of the code was tested against data from McCrink[29]. For the comparison, a blade with a diameter of 25.4 cm with NACA4412 aerofoil, commonly known as a 10x6 propeller, was used. The thrust coefficient (C_t) was computed versus advance ratio J, which is a non-dimensional

term given by $\frac{60V_\infty}{\Omega D}$. To achieve an advance ratio between 0.1 and 0.7 the inflow velocity and the RPM were varied from 3 ms^{-1} to 10 ms^{-1} and from 7090 to 4000 respectively. The results of the analysis are given in table Table 11.2. As can be seen, the discrepancy is small and the method has been successfully implemented.

J	C_t	verification C_t[29]	discrepancy [%]
0.1	0.08	0.075	14.2
0.2	0.070	0.072	2.8
0.3	0.063	0.064	1.6
0.4	0.051	0.051	0
0.5	0.038	0.039	2.6
0.60	.022	0.023	4.3
0.7	NA	0	NA

Table 11.2: Implemented and verification thrust coefficient as a function of advance ratio.

11.2.5. Material Selection

A material for the propeller blades was selected on a rough estimation of the order of the internal stresses. The forces have been modelled as distributed loads in radial and lifting direction and it was found that the bending and tensile stresses are of order 1 MPa. Besides strength, the material should be water resistant, cheap and have a high manufacturing accuracy (± 0.5 mm). From the materials discussed in section 9.1 ABS like material 'VisiJet SL Black' was selected on the basis of these constraints. It has a yield strength of 38 MPa, impact strength 65 Jm^{-1}, cost of 4 \$ kg^{-1} and a accuracy of at least 0.5 mm [6].

11.3. Noise Estimation

The drone is required to comply to the European night noise regulations. However, as no general European law exists on the noise production of drones, or industries in general, the drone was designed to comply with the Dutch noise regulation. The Dutch law allows a maximum instantaneous noise level of 65 dBA during the night, measured at 7.5 metres distance, in the case of loading and unloading businesses in cities while the average noise level during the night should not exceed 40 dBA [1].

The propeller noise is estimated as described in [13]. In this method, the noise of a propeller is estimated using the shaft power, number of blades, propeller diameter, tip Mach number, observer distance, and the number of propellers as input parameters. Lastly, to account for the difference in sensitivity of the human ear to different frequency ranges, A-weighting is applied. The method is expected to have an accuracy of ±10 dB [26]. The noise estimation is obtained by adding the coefficients L_1 through L_6. The noise during hover is then calculated as follows. The coefficient L_1 is given by

$$L_1 = 45.402 + 14.3648 \log_{10} P_{shaft} \tag{11.7}$$

Where P_{shaft} is the shaft power in horsepower. With a shaft power of 225 W, or 0.3 hp , this results in a value of 37.89 dB for L_1.

$$L_2 = 20 \log_{10}(4/B) + 40 \log_{10}(15.5/d) \tag{11.8}$$

L_2 accounts for the number of blades B and the propeller diameter d in feet. This yields a value of 42.59 dB for L_2.

$$L_3 = 37.694 M_t + (14.515 - 10.183 M_t) \log_{10} d \tag{11.9}$$

With L_3 the tip Mach number is accounted for. Given a rotational velocity of 2300 rpm, the tip Mach number will be 0.178. Hence, L_3 equals 8.63.

$$L_4 = 4 \tag{11.10}$$

L_4 represents a correction factor for the directivity. A value of 4 corresponds to the direction with maximum intensity, as can be seen in Figure 11.8.

$$L_5 = -20 \log_{10}(r - 1) \tag{11.11}$$

[6] https://www.3dsystems.com/sites/default/files/2017-05/3D-Systems_SLA_Specsheet_A4_US_2017.05.16_WEB.pdf, last accessed 25/06/2018

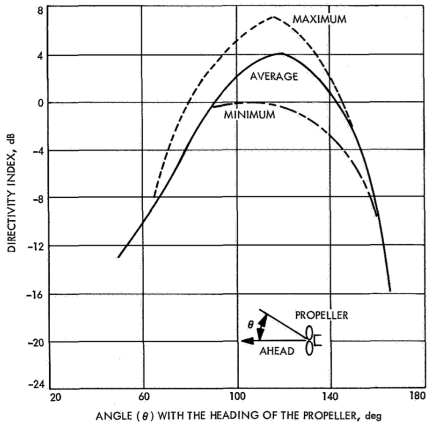

Figure 11.8: Correction factor L_4 that accounts for directivity.

With L_5 the distance of the observer to the propeller is accounted for, assuming uniform spherical propagation, with r is the distance in feet. Given an observer distance of 7.5 meters, L_5 equals -27.46 dB.

$$L_6 = 10\log_{10} N \tag{11.12}$$

Lastly, L_6 accounts for the number of propellers N. Given a propeller number of 4 during take off and landing, L_6 equals 6 dB. Adding L_1 through L_6 results in a noise level of 71.7 dB. For the conversion of unweighted decibels to A-weighted decibels, the following equation is followed.

$$A(f) = 20\log_{10}\left(R_A(f)\right) + 2.00 \tag{11.13}$$

$$\text{where} \quad R_A(f) = \frac{12194^2 \cdot f^4}{(f^2+20.6^2)\sqrt{(f^2+107.7^2)(f^2+737.9^2)}(f^2+12194^2)}$$

For this conversion, the sound pressure level obtained before is assumed to be concentrated at the blade passing frequency. Where the blade passing frequency is as defined below.

$$f = B \cdot \frac{\Omega}{60} \tag{11.14}$$

With a rotational velocity 2300 RPM this gives a blade passing frequency of 115 Hz. Hence, the noise level of 71.7 dB is found to be 55 dBA in the A-weighted spectrum. Following the same procedure for climb, with a rotational velocity of 2475 RPM and a power of 330 W, the noise was found to be 58.2 dBA. During cruise, at an altitude of 120 metres, the noise was found to be 25 dBA.

The supporting structure in the wake of the propeller, used to transfer the thrust from the propeller to the main body, introduces an increase in tonal noise. Each time a blade passes above the strut, there is a fluctuation in loading on the strut. The separation between the propeller and the strut is an important parameter that defines the increase in noise. However, as the separation is more than half the radius of the propeller, the increase in noise is considered negligible.

11.4. Computational Verification

The performance analysis is verified by comparing the results to a simulation in Lattice-Boltzmann Method solver PowerFLOW. To reduce the computation time a single hover propeller was simulated.

To minimise acoustic reflection with the outer boundary, higher viscosity is applied in the outer region of the simulation volume. Pressure measurements were taken at a cylindrical permeable surface around the propeller, where about 15 voxels fit in the acoustic wavelength of sound at 11 kHz. In this way, not only the blade passing frequency and its harmonics are measured, but also the broadband noise. Then, this surface is used as Ffowcs-Williams Hawkings integration surface to find the sound at a location 7.5 meters distance from the propeller. After a settling time of four propeller rotation periods (0.097 sec), measurements were taken during two propeller rotations (0.048 sec).

In order to establish the accuracy of the simulation results, the simulation was performed at four different resolutions, with a refinement ratio of $\sqrt[4]{2}$. Table 11.3 shows the measured thrust and power for the different mesh resolutions, where the number of voxels indicate the number of voxels over the maximum chord length of 7.8 cm. Note that the noise

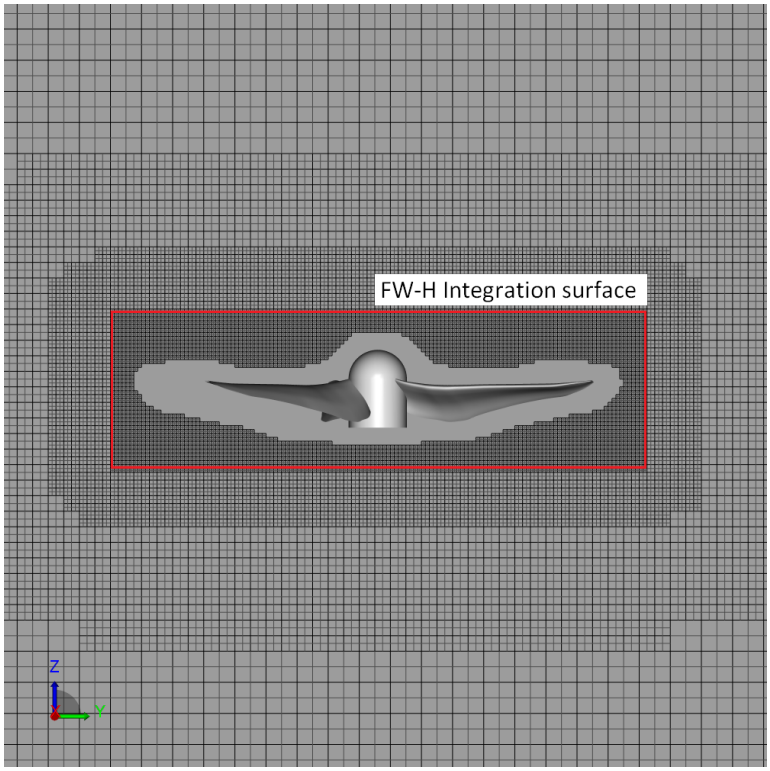

Figure 11.9: Computational grid employed for the simulation. The pressure fluctuations are measured at the cylindrical surface indicated by the red boundary.

Resolution	Thrust	Shaft Power
Coarse 78 voxels	19.5 N	259 W
Medium Coarse 93 voxels	20.2 N	234 W
Medium Fine 111 voxels	20.7 N	235 W
Fine 130 voxels	21.1 N	236 W

Table 11.3: PowerFLOW simulation results per resolution level at 2475 RPM, for a single VTOL propeller.

measurements are excluded because the simulation was not yet time-converged, and therefore not sufficiently accurate to draw a valid conclusion on the noise. The thrust shows a significant discrepancy with the results obtained with the BEMT method. This could be due to the fact that BEMT is generally less accurate at low advance ratios [41]. The reason for a loss in accuracy at low advance ratios could be due to inaccuracies in the way the induced velocity is modelled by the BEMT, as the induced velocity becomes especially important at low advance ratios. To reach the required amount of thrust, the rotational velocity was increased. As the thrust scales with the rotational velocity squared, in order to increase the thrust from 21.1 N to 31 N, the rotational velocity was increased from 2475 RPM to approximately 3100 RPM.

The simulation was run again at the increased rotational velocity of 3100 RPM. To ensure time convergence, the settling phase was increased from four to six rotations. Also, the measurement window was increased from two to four rotations, so that the lowest frequency at which ten wavelengths fit inside the measurement window equals 129 Hz. This defines the lower boundary at which noise can be accurately measured. As it is well below the blade passing frequency of 155 Hz, this length of the measurement window is considered sufficient. The upper boundary still equals 11 kHz. The results are shown in Table 11.4. In this table, the noise levels are given per propeller. As there are four propellers, 6 dBA needs to be added, resulting in a noise level of 59.9 dBA during hover, which is well below the requirement of 65 dBA. The sound spectrum of the propeller at different mesh resolutions is given in Figure 11.10. However, the spectrum does not show the expected behaviour in the tonal region, as there are no peaks at the harmonics of the blade passing frequency. The effect of this unexpected behaviour on the validity of the noise results will have to be further analysed.

Resolution	Thrust	Shaft Power	Noise
Coarse 80 voxels	30.7 N	452 W	58.2 dBA
Medium Coarse 95 voxels	31.8 N	458 W	56.8 dBA
Medium Fine 113 voxels	32.8 N	461 W	55.2 dBA
Fine 135 voxels	33.4 N	463 W	53.9 dBA

Table 11.4: PowerFLOW simulation results per resolution level at 3100 RPM, for a single VTOL propeller.

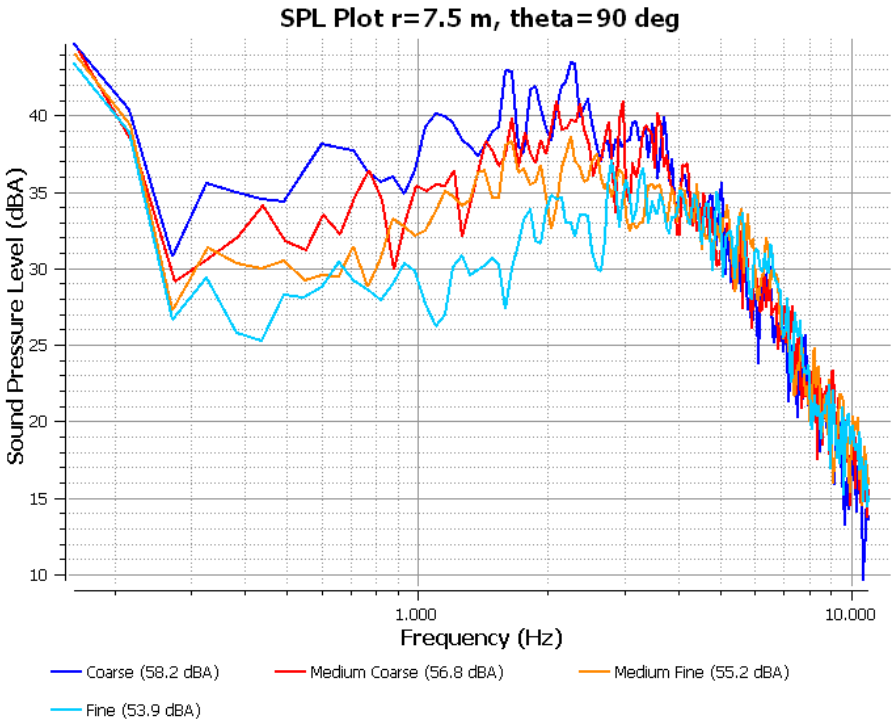

Figure 11.10: Sound pressure level spectrum of a single propeller at 7.5 metres distance, in plane of the propeller.

11.4.1. Compliance to Requirements

The compliance with the subsystem requirements can at this moment not be ensured. The BEMT method confirms that the designs shall be able to operate within the requirements. The method, particularly the performance analysis has been verified. Which gives reason to believe that the results are accurate. However, the large discrepancy with the higher fidelity first needs to be understood before the compliance can be tested. Note that the thrust requirement was easily met by increasing RPM. Doing this resulted in violating the power requirement. The increase in power required means that, with the current design, either the number of packages that can be delivered would have to be reduced, or the depth of discharge of the batteries would have to be increased, which results in a cost increase. Furthermore, the mass estimation of the propulsion system utilised a rubber model for the motors. For the required power output, there are few motors available which mean that a rubber model is not applicable. The mass of the motors is significantly higher than expected. The increased mass has been accounted for in the other subsystem designs. A summary of the requirements and the compliance is given in Table 11.5.

11.5. Future Considerations

In this section, modifications to the current propeller design are discussed, which could lead to a further reduction of noise.

Edge serrations Trailing edge serrations have been shown to effectively reduce both the tonal and the broadband noise of a propeller, as well as a reduction in power [21, 27]. The noise reduction achieved with trailing edge serrations can be attributed to the attenuation of vortex shedding at the trailing edge [33]. This is visualised in Figure 11.11. As the serrations get deeper, the reduction of sound is increased. With a serration depth of 46.67% of the MAC, the noise

Requirement	Verification Method	Compliance
The VTOL Propulsion subsystem shall provide 38 N per propeller at 3 ms^{-1} inflow velocity	BEMT simulation	yes
The VTOL Propulsion subsystem shall provide 31 N per propeller at static condition	See text above	yes
The FW Propulsion subsystem shall provide 15.4 N at 18 ms^{-1} inflow velocity	See text above	yes
The VTOL Propulsion subsystem shall not use more than 367 W per propeller	See text above	no
The FW Propulsion subsystem shall not use more than 526 W	See text above	probable
The diameter of the VTOL propellers shall not exceed 0.579 m	Inspection design	yes
The diameter of the FW propellers shall not exceed 0.488 m	Inspection design	yes
The mass of the propulsion subsystem shall not exceed 1 kg	Inspection motor and ESC mass and mass estimation propellers	no

Table 11.5: Compliance matrix for propulsion subsystem.

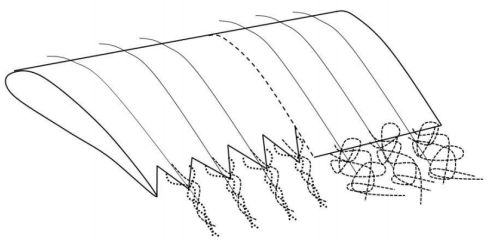

Figure 11.11: Reduction in vortex shedding from trailing edge serrations [21].

decreased by 28%. Thrust levels are maintained within 5%, relative to the unserrated blade design.

Duct Although ducts can reduce the noise of a propeller, the implementation would introduce an unacceptable increase in drag during forwarding flight and hence be unfeasible to reduce the noise of the drone.

Active noise cancellation Active noise cancellation reduces noise by introducing a second source (i.e. a speaker) designed to cause destructive interference with the first source. However, as the phase of the radiated sound differs along the circumference of the propeller, it would become unfeasible to cancel the noise everywhere along the whole circumference.

Proplet Tip vortices are a big contributor to the broadband noise of propellers. To reduce these tip vortices, proplets could be implemented, similar to the way winglets are used to reduce the tip vortices on a wing. However, this would introduce structural difficulties due to the centripetal loading at the tip. In fact reference [21**?**] found an increase in noise when using proplets, which they attributed to uneven wakes created from the flutter of the blade tips.

12

Detailed Design: Payload Mechanism

The parcels have to be delivered in a fast and safe manner, it is, therefore, important to design a mechanism which is able to do this while taking into account the various constraints set on the mechanism, such as mass and cost. An explanation on the aspects to consider is given in section 12.1, the design of the hold and release mechanism is given in section 12.2 and the hatch mechanism is explained in section 12.3. Finally, in section 12.4, a summary of the components used is given including a technical drawing of the payload bay and the compliance of the subsystems with its requirements.

12.1. Overview

There are a set of requirements the payload mechanism should comply with. The maximum power usage shall not be higher than 10 W. The payload shall not exceed a weight of 2.5 kg and shall have a maximum size of 210 x 297 x 105 mm (w x l x h).

In order to design a payload holding mechanism, it is important to first establish what sizes of packages will be delivered. The main concern for the holding mechanism is that it should be able to hold a grid of smaller thicker packages as well as letterbox sized packages stacked on top of each other (shown on the left and right respectively in Figure 12.1). A study by Barclays showed that in the UK in 2013, 35% of the delivered packages, no larger than a standard shoe box, were letterbox packages [1]. The market for letterbox sized parcels is thus a significant part of the small package market. Unfortunately, due to weight and volume constraints on the payload mechanism, it was deemed unfeasible to design a system which can both handle stacked packages and smaller sized packages. At this point, it was decided to design a mechanism for the grid of packages, as it would allow for a larger range of packages to be delivered. In post-DSE activities, a system can also be designed for stacked packages which can then be easily swapped within the drone.

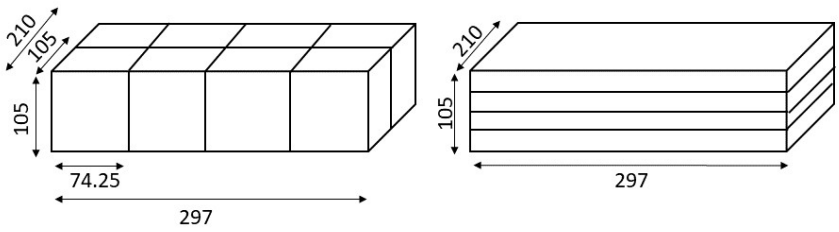

Figure 12.1: Payload bay options (all dim. in mm)

The payload layout shown in the left of Figure 12.1 allows for a wide range of different sized packages while keeping the complexity of the holding mechanism relatively low. The maximum size is divided into 8 equal units of 105 x 74.25 x 105 mm (w x l x h), with each unit only allowed to carry 500 g, which allows for small heavy packages. A package is allowed to consist of multiple units.

Two possible solutions for the holding mechanism were found in the midterm report [9], a grid of grippers with custom tape and active suction cups. After further analysis, it was found that the grid of grippers is not a feasible solution, as additional material has to be applied to the packages itself which is not preferred from a sustainable and cost point of view. Another option that was considered was a system of independent hatches which open when necessary. However, in this case, an additional mechanism is needed to hold the packages in place during flight to prevent sliding. As the suction cup system combines both it considered more feasible than the other options and is further worked out in section 12.2.

[1] `https://www.home.barclays/content/dam/barclayspublic/docs/BarclaysNews/2014/September/the-last-mile-report.pdf`, last accessed 22/06/2018

12.2. Hold & Release Mechanism

To ensure that a range of package sizes can be delivered, a mechanism that can release individual packages has to be designed. Therefore a grid of eight suction grippers, one per unit, is an option as a payload holding mechanism. To select the right suction cups and vacuum pump it is important to first calculate the required holding force per suction cup.

$$F_H = m \cdot (g + a) \cdot n = 0.5 \cdot (9.81 + 1.5) \cdot 2.5 = 14.14N \tag{12.1}$$

$$F_H = m \cdot (g + \frac{a}{\mu}) \cdot n = 0.5 \cdot (9.81 + \frac{2}{0.5}) \cdot 2.5 = 17.26N \tag{12.2}$$

Equations 12.1 and 12.2 show the calculation of the required holding force per suction cup for vertical and horizontal movement respectively. In the equation, m is the maximum allowable mass per unit, n is a safety factor taken to be 2.5 (a minimum of 2 is required for porous or rough surfaces such as cardboard [2]). It is important to note that the necessary standardisation of the packages includes the material, in this case, cardboard which is most commonly used in packaging. The friction coefficient (μ) is 0.5 [1] and a is the acceleration of the system.

The required pressure difference needed can be calculated as follows:

$$P = \frac{F_H}{A_{\text{cup}}} \tag{12.3}$$

Where F_H is the required holding force per cup and A_{cup} the effective suction cup area. This calculation has been done for a range of diameters, from 10 mm to 40 mm and the most critical holding force of 17.26 N. A pressure difference between -0.2 and -0.4 bar is needed for cardboard [3], a 30 mm diameter gave a required pressure difference of 0.244 bar. Suction cups have been selected from `www.festo.com` shown in Figure 12.2. The cups are made of silicone as this material allows better sealing of rough surfaces [4]. They have mass of 9 g and volume of 0.867 cm^3, the holders have a mass of 27 g and a volume of 0.646 cm^3.

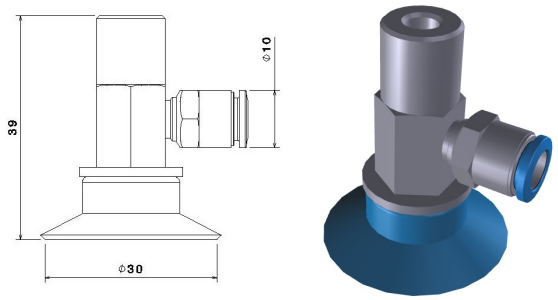

Figure 12.2: Suction cup including holder [5](dim. in mm)

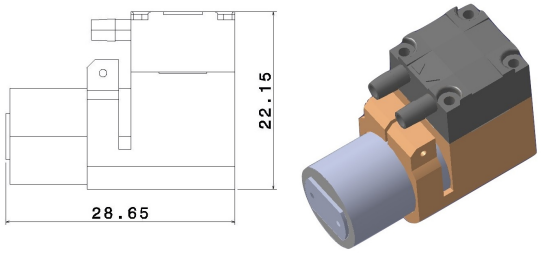

Figure 12.3: Schwarzer SP 100 EC micro pump [6](dim. in mm)

Two options could be used to enable the suction cups to be operated independently, one vacuum pump together with solenoid valves or for each suction cup a separate vacuum pump. After research, it was found that the mass of a solenoid valve system with 8 valves is similar to having 8 separate micropumps. As the system with multiple vacuum pumps allows the mechanism to operate even when one fails, it was chosen to use this option.

In order to select a vacuum pump the required volume to be displaced had to be calculated. This volume consists of the volume of the suction cup, its holder and tubing. The volume of the tubing (V_t) can be calculated as follows:

$$V_t = \pi \cdot \frac{D_{in}^2}{4} \cdot L = \pi \cdot \frac{4^2}{4} \cdot 80 = 1005.3mm^3 \tag{12.4}$$

The tube inner diameter (D_{in}) is 4 mm from the suction cup holder and the length of the tube is taken to be 80 mm as the vacuum pumps can be placed directly next to the suction cups reducing the required length of the tubes. The total

[2] `https://www.festo.com/net/SupportPortal/Files/286804/Basic_Vacuum_Technology_Principles.pdf`, last accessed 25/06/2018

[3] `https://www.pneumatictips.com/size-vacuum-cup/`, last accessed 25/06/2018

[4] `http://fluidpowerjournal.com/2013/03/vacuum-cup-materials/`, last accessed 25/06/2018

[4] `www.festo.com`

[5] `http://www.schwarzer.com/pages_en/produkt.php?id=189`, last accessed 25/06/2018

volume to be displaced is thus 2.52 cm^3, including 0.867 cm^3 for the suction cup and 0646 cm^3 for the holder. Micro vacuum pumps from Schwarzer can be used which have a mass of only 15.5 g and a maximum achievable vacuum of -400 mbar [5] (specifications shown in Table 12.1).

Specification	Value
Mass	15.5 g
Dimensions	28.15 x 22.15 x 13 mm (w x l x h)
Free flow	450 $mL\,min^{-1}$
Max vacuum	-400 mbar
Voltage	3 V DC
Max. nominal current	100 mA
Power	0.3 W

Table 12.1: Schwarzer SP 100 EC micro pump specifications [5]

12.3. Hatch Mechanism

When the drone arrives at its destination the payload bay should open and the package is released. The mechanism should also act as a backup holding system if the holding mechanism fails and a package is dropped within the payload bay.

Several mechanisms for opening the hatches have been investigated, such as plug sliding doors used in busses and trams, however, this was found to be too complex and heavy for use in a drone. A simpler design with two hatches opened with two linear actuators is chosen as can be seen in Figure 12.5. The actuators are free to rotate around the two connection points and they extend to open the hatches.

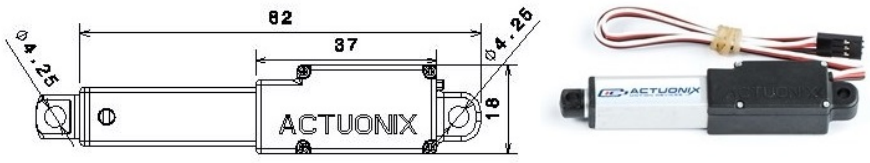

Figure 12.4: L12-R Micro Linear Servo [6](dim. in mm)

Simple micro linear servos from "Actuonix" (shown in Figure 12.4) are selected as they provide a high lifting force for low power consumption (specifications shown in Table 12.2). The actuators have a stroke of 30 mm, an extending speed of 25 $mm\,s^{-1}$ at zero load and 10 $mm\,s^{-1}$ at maximum load (22 N). Thus closing and the opening of the hatches takes between 1.2 and 3.0 seconds depending on the weight of the hatches. The actuators can handle a maximum static force of 200 N each, well exceeding the applied force in case a package is released within the bay due to a failure of the holding mechanism.

Specification	Value
Mass	34 g
Dimensions retracted	18 x 91 x 15 mm (w x l x h)
Dimensions extended	18 x 121 x 15 mm (w x l x h)
Max. lifting force	22 N
Max. static force	200 N
Voltage	6 Vdc
Max. nominal current	460 mA
Power operating	2.76 W
Power standby	0.043 W

Table 12.2: L12-R Micro Linear Servo specifications [7]

[6] https://www.actuonix.com/L12-R-Linear-Servo-For-Radio-Control-p/l12-r.htm, last accessed 25/06/2018

12.4. Summary Components & Compliance Matrix

This section gives an overview of the used components for the payload mechanism including their cost, mass and power consumption shown in Table 12.3. Furthermore, Table 12.4 gives the compliance of the payload mechanism subsystem with the set requirements for the baseline report [8].

Component	Commercial model	Cost [euro]	Mass [g]	Power [W]
Suction cups (8x)	Festo ESG-30, flat, silicone [4]	15.72 (125.76)	9 (72)	N/A
Cup holders (8x)	Festo ESG QS-6 port, M6 thread [4]	-	27 (216)	N/A
Vacuum pumps (8x)	Schwarzer 100 EC [5]	60.97 (487.76)	15.5 (124)	0.3 (2.4)
Actuators (2x)	Actuonix L-12R [6]	59.40 (118.80)	34 (68)	2.76 (5.52) while operating

Table 12.3: Summary payload mechanism components

The several components are placed within the payload bay as shown in Figure 12.5.

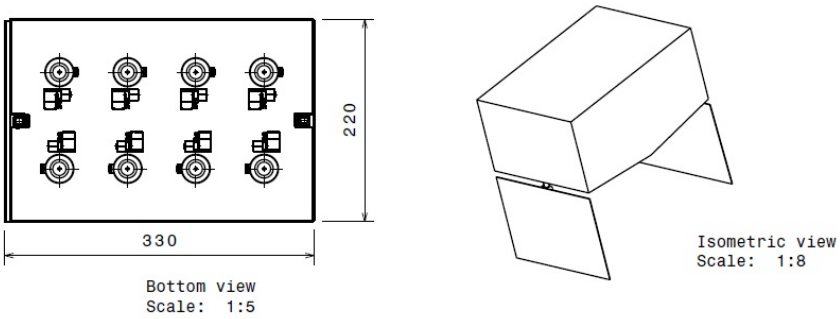

Figure 12.5: Techinical drawings of the payload bay (dim. in mm)

Requirement	Verification Method	Compliance
SYS-SUB-PAY-2 The payload subsystem shall be able to carry a payload of maximum 2.5 kg	Analysis of the holding force calculations	YES
SYS-SUB-PAY-3 The payload subsystem shall be able to carry a payload with the maximum size of 210 mm x 297 mm x 105 mm	Inspection of CAD drawing	YES
SYS-SUB-PAY-4 The payload subsystem shall be able to carry the payload without causing destructive damage	Use of soft suction cups & low pressure difference	YES
SYS-SUB-PAY-5 The payload subsystem shall be able to carry a maximum of 4 packages	Grid of 8 suction cups	YES
SYS-SUB-PAY-6 The payload subsystem shall be able to drop a single package at a time	Inspection of suction cup system shows an independently controllable system	YES
SYS-SUB-PAY-7 The payload subsystem shall protect the payload from adverse weather conditions	Inspection of the technical drawings of the payload bay show that the payload is enclosed, made weather proof by seems	YES
SYS-SUB-PAY-8 The payload subsystem shall not consume more than 10 Watts of power	Inspection of the specifications of used components	YES
SYS-SUB-PAY-9 The mass of the payload subsystem shall not be higher than 0.75 kg	Inspection of the specifications of used components	YES

Table 12.4: Requirements compliance matrix for the payload mechanism subsystem

13

Detailed Design: Auxiliary Systems

This chapter describes the detailed design of several auxiliary systems which do not belong to one specific subsystem. The landing gear is described in section 13.1 and the design of an emergency landing system is explained in section 13.2. Furthermore, the implementation of navigation lights is discussed in section 13.3.

13.1. Landing Gear

The landing gear ensures that the drone is stable when grounded in the most extreme cases, fully loaded and no payload. The most forward and aft cg locations where found in chapter 8, thus the drone needs to remain stable for a cg range from 0.358 m to 0.368 m. It is important to note that the landing gear does not need wheels as the drone is designed for vertical take-off and landing.

The landing gear has to prevent tip-over of the drone when grounded, it is therefore important to establish a limit on the inclination of the landing area. As a first reference the maximum slope angle for a typical helicopter is taken: the Eurocopter AS350 AStar has a maximum lateral inclination of 8° [1]. Unfortunately, the drone needs to be capable of landing in gardens, which may have slopes higher than 12°. This does put some constraints on the design of the landing gear, because the drone has to take-off vertically and thus the drone needs to level itself before ascending (visualised in Figure 13.1). Enough ground clearance for this can be achieved by either moving the landing gear outwards towards the wingtips or increasing the height. This constraint is somewhat relieved due to the 22° dihedral. Similarly, in the longitudinal direction this problem arises due to the propellers placed on the rods. Furthermore, the landing gear should provide enough ground clearance for the forward propeller and opening payload hatches.

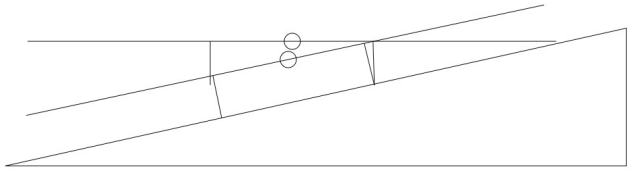

Figure 13.1: Schematic representation of take-off on a slope

Three options were considered at first: landing gear placed within the wing of the drone, wingtips that could rotate and serve as landing gear, and lastly a system that would connect to the already existing rods of the propulsion system. At first the conventional method of retractable gear into the wing was chosen, however after it further analysis it was found to not fit within the slender body of the drone. The rotating wing tips were deemed unfeasible as this would severely impact the structural integrity of the the main frame.

The last option was considered as the best option for several reasons: the rods used for attaching the VTOL propellers to the main body are already capable of sustaining higher loads than necessary for the grounded drone. It also allows for a light weight design using simple retracting servos often used for model aircraft [2] (shown in Figure 13.2). The required minimum landing gear height is 250 mm due to the pusher propeller, a margin is added to ensure enough ground clearance. This results in the use of 280 mm long carbon fibre rods which together with the placement of the servos result in a ground clearance of 78 mm.

The force per rod with a safety factor (n) of 2 and total weight (W) of 134.44 N can be found as follows:

[1] `https://blog.aopa.org/aopa/2012/09/26/slope-limits/`, last accessed 25/06/2018

[2] `https://hobbyking.com/en_us/servoless-retract-with-metal-trunion-for-large-models-51mm-x-43mm-mount-2pcs.html`, last accessed 25/06/2018

[3] `https://hobbyking.com/en_us/servoless-retract-with-metal-trunion-44mm-x-41mm-mount-2pcs.html`, last accessed 25/06/2018

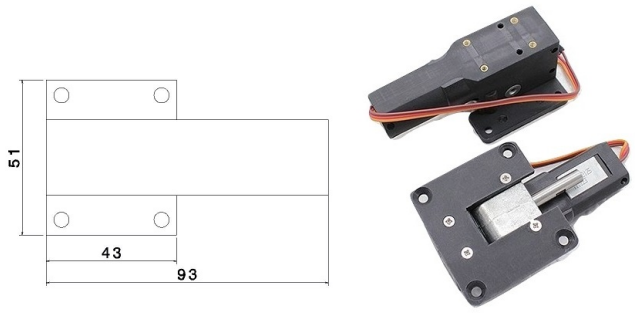

Figure 13.2: Servoless Retract with Metal Trunion [3](dim. in mm)

$$F = n \cdot \frac{W}{4} = 67.22N \tag{13.1}$$

The maximum buckling load is calculated as follows:

$$F_{buck} = \frac{\pi^2 EI}{L^2} \tag{13.2}$$

$$I = \frac{\pi r^4}{8} \tag{13.3}$$

With an E-modulus of 70 GPa for carbon fibre [4], length of 280 mm and a radius of 2.5 mm this leads to a maximum buckling load of 135.18 N. The compression stress is calculated with:

$$\sigma = \frac{F}{A} \tag{13.4}$$

$$A = \frac{\pi r^2}{2} \tag{13.5}$$

This results in a compression stress of 8 MPa, which is is significantly lower than the maximum allowed stress of 100 MPa for carbon fibre [5]. Low cost and light weight off-the-shelve rods[6] are used together with easily replaceable rubber feet [7] at the ends of the rods to ensure enough grip on slippery surfaces. Technical drawings of the complete landing gear system are shown in Figure 13.3 and a summary of the used components is given in Table 13.1.

Component	Commercial model	Cost [euro]	Mass [g]	Power [W]
Servoless retract (4x)	Servoless Retract with Metal Trunion large models	12.70 (25.40)	72 (288)	2.76 (11.04)
Landing rods (4x)	Round Carbon Fibre Rod R2.5 X 280 mm	0.87 (3.50)	3.64 (14.56)	-
Rubber feet (4x)	Tarot small landing gear feet	0.70 (2.80)	3 (12)	-

Table 13.1: Summary landing gear components (total values between brackets).

13.2. Emergency Landing System

Since the drone will be operated in urban areas, there should be a safety mechanism in place to reduce the risk of harming people or animals on the ground in case of failure. Currently, the European Aviation Safety Agency has no regulations regarding the use of such a mechanism.

The user requirements for the drone state that it should be single point failure free. However, for the propeller used in horizontal flight there is no back-up, and there might not be enough time for the horizontal propellers to stabilise the drone while it is in an emergency situation. Also, in case of total power failure there should be a back-up system to guide the drone to the ground. Therefore, it was decided to install a ballistic parachute which takes only one second to open [8]. It has been chosen to look for off-the-shelf parachute systems since they are widely available and reliable. For the given drone weight of 13.7 kg there were two options which both seemed suitable. In Table 13.2 a comparison is shown between the parachute specifications.

[4] http://www.performance-composites.com/carbonfibre/mechanicalproperties_2.asp, last accessed 25/06/2018
[5] http://www.performance-composites.com/carbonfibre/mechanicalproperties_2.asp, last accessed 25/06/2018
[6] http://www.carbon-shop.eu/modified/Carbon-Fibre-Rods/Half-Round-Rods/Round-Carbon-Fibre-Rod\
-R2-5-x-1000-mm::97.html?language=en, last accessed 25/06/2018
[7] https://hobbyking.com/nl_nl/tarot-small-landing-gear-rubber-feet-8mm-2pcs.html, last accessed 25/06/2018
[8] https://galaxysky.cz/multicopters-s71-en, last accessed 25/06/2018

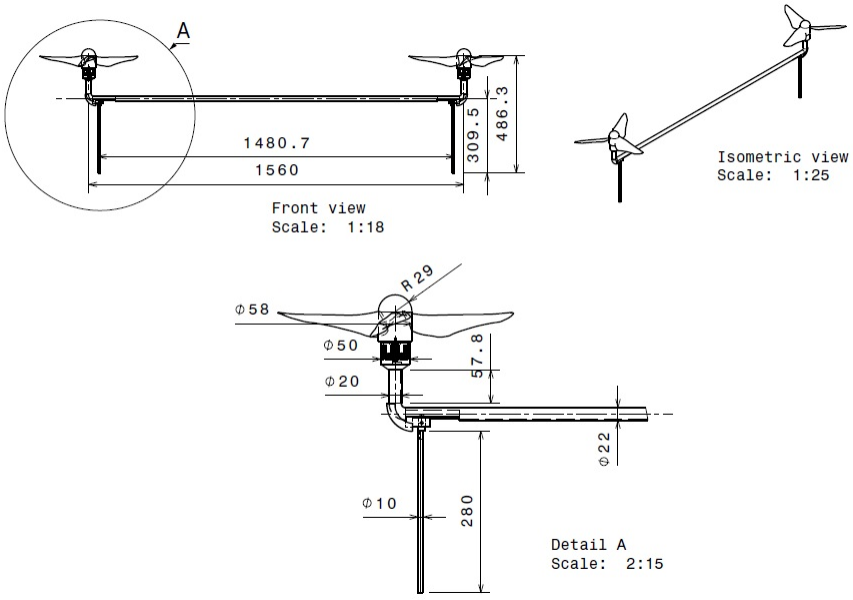

Figure 13.3: Technical drawings of the landing gear including propulsive system (dim. in mm)

	Skycat X68 Pro Series 4-20 [9]	**Galaxy Sky GBS 10/150** [10]
Weight [kg]	790	405
Diameter [mm]	68	100
Length [mm]	229	110
Cost	€1052,-	€1044,-
Suitability range [kg]	4 - 20	5 - 15
Descend speed (with 12kg drone) [m/s]	5.0	4.8
Impact energy (with 12kg drone) [J]	149.5	139.1

Table 13.2: Ballistic parachute comparison

It can be seen that the specifications are quite similar, except for the weight and the dimensions. The Skycat system has a smaller diameter and longer total length than the Galaxy Sky system. However, the weight of the Skycat system is almost double the weight of the Galaxy Sky system. Of course, the total weight of the drone should be minimised. Therefore, the Galaxy Sky GBS 10/150 is the best option for the drone.
According to the manufacturer the minimum rescue height is in the range of 5-8 above the ground, making it suitable for the VTOL phase as well. By using the voltage sensors, the parachute can be installed such that when power drops, the parachute will be deployed within 1 second. However, the pyro-generator will need a backup-guard (a small spare battery) in order to operate in case of total power loss. For this a Scorpion back-up guard [11] of 38 grams with 5V 500 mAh can be used, which is only €25,-. Also, by using the accelerometer, the drone can detect an unexpected drop of altitude and respond by deploying the parachute. In Figure 13.4 the whole parachute system can be seen including the Scorpion back-up guard on the middle right. When the parachute system is used for an emergency, it is reusable by simply reloading the parachute and putting it back to operation state according to the manufacturer [12], which is favourable from a sustainability point of view. In case of parachute deployment, power to all engines will be cut for safety.

In section 18.3 it can be seen that the parachute is placed in the back of the drone. The parachute itself is attached to the structure through the components delivered by the parachute manufacturer, seen in Figure 13.4. For the maintainability of the components a hatch is installed in the back of the drone, beneath which the parachute is installed. In case of an emergency the hatch is unlocked and opens, through which the parachute is deployed. If the hatch does not swing open by itself, the force of the ballistic parachute will open it. However, this system should be tested extensively.

[11] `https://www.scorpionsystem.com/catalog/accessories/backup_guard/S_Backup_Guard/`, last accessed 25/06/2018
[12] `https://galaxysky.cz/multicopters-s71-en`, last accessed 25/06/2018

Figure 13.4: The parachute system which is installed in the drone.

13.3. Navigation Lights

As the delivery drone has capabilities for flying at night it is important to be visible for other aircraft, drone operators, etc. During cruise, the conventional navigation light system for aircraft is used, on the port side (left wing) at the leading edge of the wing tip a red light is installed and on the starboard side (right wing) a green light. During take-off and landing white lights, placed at the end of the rods for the VTOL propellers, are activated as indicated in Figure 13.5. All lights used are light emitting diodes (LED) which have a very low power consumption and low weight. A good option is are UAV strobe locators which weight only 15 grams [13].

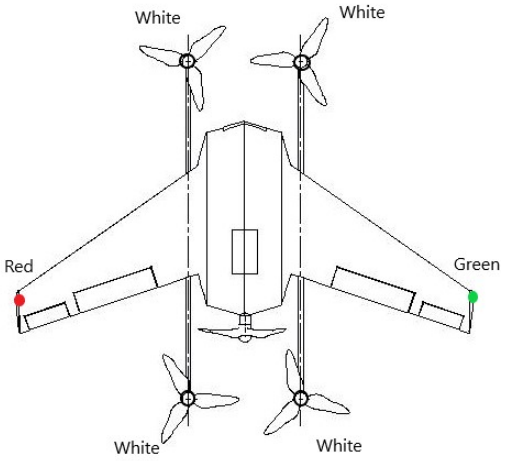

Figure 13.5: Placement of navigation and safety lights

[13] https://www.amazon.co.uk/DS-30-White-Drone-Strobe-Locator/dp/B01CRAQ2CA, last accessed 25/06/2018

14

System Performance and Sensitivity analysis

With the detailed design now finished, the overall performance of the drone can be evaluated, and afterwards, a sensitivity analysis performed.

14.1. General Performance

This section shall discuss the performance of the drone during fixed wing and VTOL flight. Furthermore, the performance calculations for the power consumption of the drone will also be presented.

14.1.1. Flight Performance

Flight performance is a parameter that is very broad and can be difficult to measure. In this subsection, we shall discuss performance regarding the flight phases defined in Figure 4.6.

FW cruise, climb and loiter performance In chapter 8, it was discussed that the drone has a cruise velocity of 18.75 $\mathrm{m\,s^{-1}}$. This is however not the optimum speed at which the maximum $\frac{L}{D}$ occurs. Due to the additional drag caused by the VTOL propellers during fixed-wing flight, the $\frac{L}{D}$ decreased and moved to an angle of attack that occurs after the maximum angle of attack. As this posed an issue, the maximum angle of attack during cruise had to be set by a hard requirement. This was set to 10 degrees by assuming a maximum allowable vertical gust speed of 5 $\mathrm{m\,s^{-1}}$. The same hard requirement had to be set for climbing and loiter flight, as the optimum angle of attack was outside of the feasible range. This was able to be brought up to 12.5 degrees using also a maximum vertical gust speed of 5 $\mathrm{m\,s^{-1}}$. In the case that the drone experiences a gust speed higher than 5 $\mathrm{m\,s^{-1}}$ and stalls, the VTOL propellers can be turned on to stabilise.

During cruise, the drone experiences a total drag of 16.77 N and consumes a power of 350 W. During climb and loiter, when the required power is minimum, the drone flies at a speed of 17.2 $\mathrm{m\,s^{-1}}$. At this speed, the required power is equal to 500 W and 312 W respectively. A slightly more detailed explanation of how the required power values were found can be found in subsection 14.1.2.

Climb behaviour With the drone having a maximum operational altitude of 120 m with respect to the ground height, it can be shown that the change in air density is only 1% over the entire flight envelope. It can thus safely be assumed that the required rate of climb shall not change over the flight envelope for both FW and VTOL mode and stay equal to 1 $\mathrm{m\,s^{-1}}$.

Mission Time analysis The mission time can be derived both from the requirements and from the flight profile given in Figure 4.6. The required loiter time is 60 seconds per package and thus 240 seconds in total (4 packages). The hover time was also specified by the requirements and is set to 60 seconds per package plus another 60 for the final landing (300 seconds total). The climb time in VTOL and FW mode is specified by the required rate of climb (which is 1 $\mathrm{m\,s^{-1}}$ in both cases). Since the drone will first climb to 60 m altitude in VTOL mode and continues to 120 in FW mode, 60 seconds per mode will be spend climbing per package, plus another 60 for initial takeoff. Finally, the FW cruise mode time is determined by dividing the required range by the cruise velocity. It has, however, to be taken into account that some range is already covered during FW climb flight. By subtracting this range from the required range, the time spent in cruise phase can be determined.

The final mission time for a given amount of packages and a given range can be calculated using Equation 14.1. This gives a value of 35.7 minutes for a range of 30000 m and 4 parcels.

$$t(\text{range}, \text{parcels}) = \frac{\text{range} - \frac{60}{ROC_{\text{FW}}} \cdot V_{\text{climb}}(\text{parcels}+1)}{V_{\text{cruise}}} + \frac{60}{ROC_{\text{FW}}}(\text{parcels}+1) + (60(\text{parcels})) + (60(\text{parcels}+1)) + \frac{60}{ROC_{\text{VTOL}}}(\text{parcels}+1) \tag{14.1}$$

14.1.2. Energy Consumption

The energy consumption of the drone can be determined by calculating the various power usages throughout the mission profile and the respective lengths of each section. As was shown in Figure 4.6, there are a total of five mission segments which will have to be analysed. Cruise, climbing and loiter power requirements for fixed wing sections and hover and climb for VTOL sections. In this subsection, most of the equations to calculate the power required will be left out. However, a short method shall be presented on how one can go about coming to the same results.

First, the required power for hover and climb in VTOL flight were determined to be 1119 W and 1645 W respectively. These values were obtained from the propulsion department.

Next, the power during different fixed-wing flight phases can be calculated. The power during cruise phase is determined by first obtaining the lift coefficient C_L. This value can then be used to calculate the drag of the drone using the drag polar, and finally the cruise velocity. This results in a power value (including 90% motor inefficiency) of 350 W.

The power during the climb phase is calculated in much the same way as the cruise phase, except that first the optimum velocity is found for which the required power is minimum. Then, the lift coefficient C_L is determined, the total drag is calculated, and finally $ROC_{\text{FW}} = \frac{P_a - P_r}{W}$ is solved for P_a with $ROC_{\text{FW}} = 1$. This gives a power of 500 W. The loiter power can be determined similarly by setting ROC_{FW} equal to 0, which gives a power of 312 W.

With all the required values calculated, the total energy consumption can be computed using Equation 14.2.

$$f(\text{range}, \text{parcels}) = P^{\text{FW}}_{\text{cruise}} \frac{\text{range} - \frac{60}{ROC_{\text{FW}}} \cdot V_{\text{climb}}(\text{parcels}+1)}{V_{\text{cruise}}} + P^{\text{FW}}_{\text{climb}} \frac{60}{ROC_{\text{FW}}}(\text{parcels}+1) + P^{\text{FW}}_{\text{loiter}}(60(\text{parcels})) + P^{\text{VTOL}}_{\text{hover}}(60(\text{parcels}+1)) + P^{\text{VTOL}}_{\text{climb}} \frac{60}{ROC_{\text{VTOL}}}(\text{parcels}+1) \tag{14.2}$$

This equation is solved for a range of 30000 m and 4 parcels. Correcting for the power loss in the distribution board (95%), it can be found that a total required energy for a single mission is 441 Wh. The depth of discharge of the battery was set to 65%, which results in the battery being able to provide 441 Wh, and thus the drone is able to successfully complete its mission on a single battery charge. The final results for the required power during different flight phases can be seen in Table 14.1

Condition	Power [W]	Time [min]
FW Cruise	350	21.6
FW Climb	500	5
FW Loiter	312	4
VTOL Hover	1119	5
VTOL Climb	1645	5
Total	N/A	40.7

Table 14.1: Required power and time for different flight phases

14.2. Sensitivity Analysis

The detailed design has been completed but there is still some uncertainty that could affect the drone's overall performance. It was decided to perform a sensitivity analysis with the aim of assessing the robustness of the design and finding critical parameters that affect it.

Changed and Free Variables To make sure that the drone is robust with respect to mass, power consumption, lift, drag, number of packages and hover time changes, a sensitivity analysis was performed having those as variables. To estimate the range of variation of the selected parameters, a contingency factor of 10% was used as is used by NASA at

the stage of the design where the layout is determined and the subsystems initial design determined[15]. We considered only changes that would negatively impact the design. Furthermore, if the changes critically impact the design we varied range, the number of packages and the maximum weight of the payload to generate acceptable, even though sub-optimal design solutions.

Increase in Mass In this section, the effects of an increase in overall mass are analysed. The avionics and electric system are selected from off-the-shelf components. Therefore, only the structure, payload mechanisms and propulsion system have a contingency margin of 10 %. Increasing the mass of these subsystems of 10% yields a total increase of 0.7 kg.

Increase in Power Consumption The consequences of a 10% increase in the power consumption of the propulsion system were explored next. The new power used for VTOL hover is 1231 W, VTOL Climb 1810 W, FW cruise 385 W, FW climb 550 W and for FW loiter 343 W.

Decrease in Lift The consequences of a decrease in lift of 10% during the entire mission were also explored. Causes for such a reduction include the lift interference due to the propellers or imperfection on the surfaces of the wings. The decrease in lift corresponds to a downward shift of the C_L curve of the aircraft and a decrease in the L/D curve.

Increase in Drag An increase in drag of 10% was also examined during the mission. Causes for the increase in drag can be the underestimation of the drag generated by the VTOL propeller and/or inaccuracies in the drag modelling program. This translates into an upward shift of the drag polar and a decrease in L/D.

Increase in the Number of Packages Delivered The consequences of an additional delivery on top of the 4 packages specified by the design were determined.

Increase in hover time The consequences of an increase of 1 minute in VTOL hovering time were explored. This could be caused by obstacles present in the landing spot or difficulties in the landing manoeuvres.

Method and Results For each of the changed parameters (mass, power, lift, drag and hover time) the range, the number of packages delivered and max payload mass was changed. The cases are run independently and they do not affect each other since in practice it is improbable that all the prescribed changes happen at the same time. The methodology to find the new range/number packages/payload mass in the same as the one shown in subsection 14.1.1. From Table 14.2, it can be observed that the most critical changes are power and mass variations since they heavily affect the VTOL phase of the drone. Nonetheless, by reducing the number of packages delivered to 3, the drone is able to reach its required range of 30 km.

Change	Num. Packages & Range [km]	New Max Payload Mass at 4 packages, 30 km range [kg]
Power req. up 10 %	(4, 24), (3, 32), (2, 43), (1, 54)	1.8
Lift down 10 %	(4, 29), (3, 38), (2, 46), (1, 55)	2.1
Drag up 10 %	(4, 27.5), (3, 36), (2, 45), (1, 54)	2.15
Mass up 10 %	(4, 19), (3, 30), (2, 40.5), (1, 51)	1.1
Num. Packages + 1	(5, 20)	1.7
Hover Time + 1 min	(4, 26.5), (3, 36.5), (2, 46), (1, 56)	2.2

Table 14.2: Variation of number of packages, range and max. payload mass given a change in one of the performance parameters

15

Detailed Design Summary

In chapter 7 to chapter 13 the detailed subsystem design of the silent delivery drone was described. In this chapter, the overall configuration will be presented showing how the several subsystems were integrated and summarising the established dimensions in chapter 15. Furthermore, it will be checked if the design complies with the budget breakdown in Figure 15.

Overall Configuration In this section, the overall configuration of the silent delivery drone will be presented as can be seen in Figure 15.1. In Figure 15.2 technical drawings of the system are provided summarising the dimensions of the wing body, the propellers and the control surfaces. In chapter 18 the integration of the subsystems as well as the internal layout will be explained in detail.

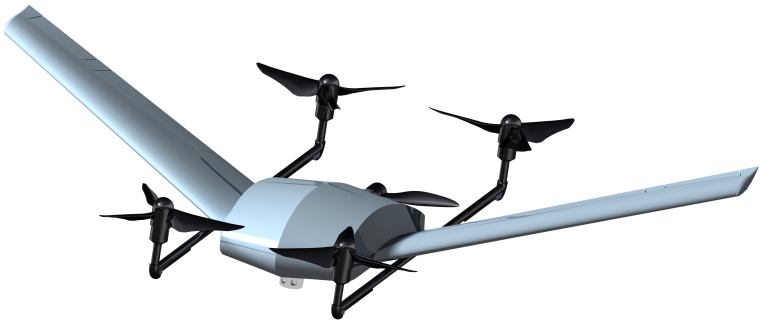

Figure 15.1: Overall configuration of the silent delivery drone

Budget Breakdown Here it was being checked if the power consumption and mass of the several subsystems comply with the technical budget break-down established in chapter 5. In Table 15.1 the values for the budget and the actual values of the peak power, the average power, the energy and the mass for each subsystem are depicted. The subsystems not complying with the mass requirements are the propulsion system, electric system and payload mechanism and auxiliary systems. Since the masses of the first two, cannot be further reduced, the non-compliance is due to the low fidelity of the conceptual design. The mass of the auxiliary systems is higher than expected due to the weight of the coating, parachute and integration parts that were not included in the conceptual budget. The rest of the subsystem are below their allocated budgets. Note that ability to execute the mission is not compromised by the change in mass as is discussed in chapter 14.

	Peak power [W]		Nominal Power [W]		Energy [MJ]		Mass [kg]	
Subsystem	Budget	Actual	Budget	Actual	Budget	Actual	Budget	Actual
Structures	-	-	-	-	-	-	3.17	2.87
Propulsion	1469	1116	485	349	1.316	1.476	1	1.7
Electric system and battery	-	-	-	-	-	-	3.13	3.69
Payload mechanism and auxiliary systems	20	16.56	5	2.4	0.01	0.006	1.75	2.25
Avionics	50	33.75	50	33.35	0.072	0.072	0.75	0.626
Payload	-	-	-	-	-	-	2.5	2.5
TOTAL:	1539	1166.31	540	384.75	1.398	1.554	12.3	13.7

Table 15.1: Return on technical budget break-down

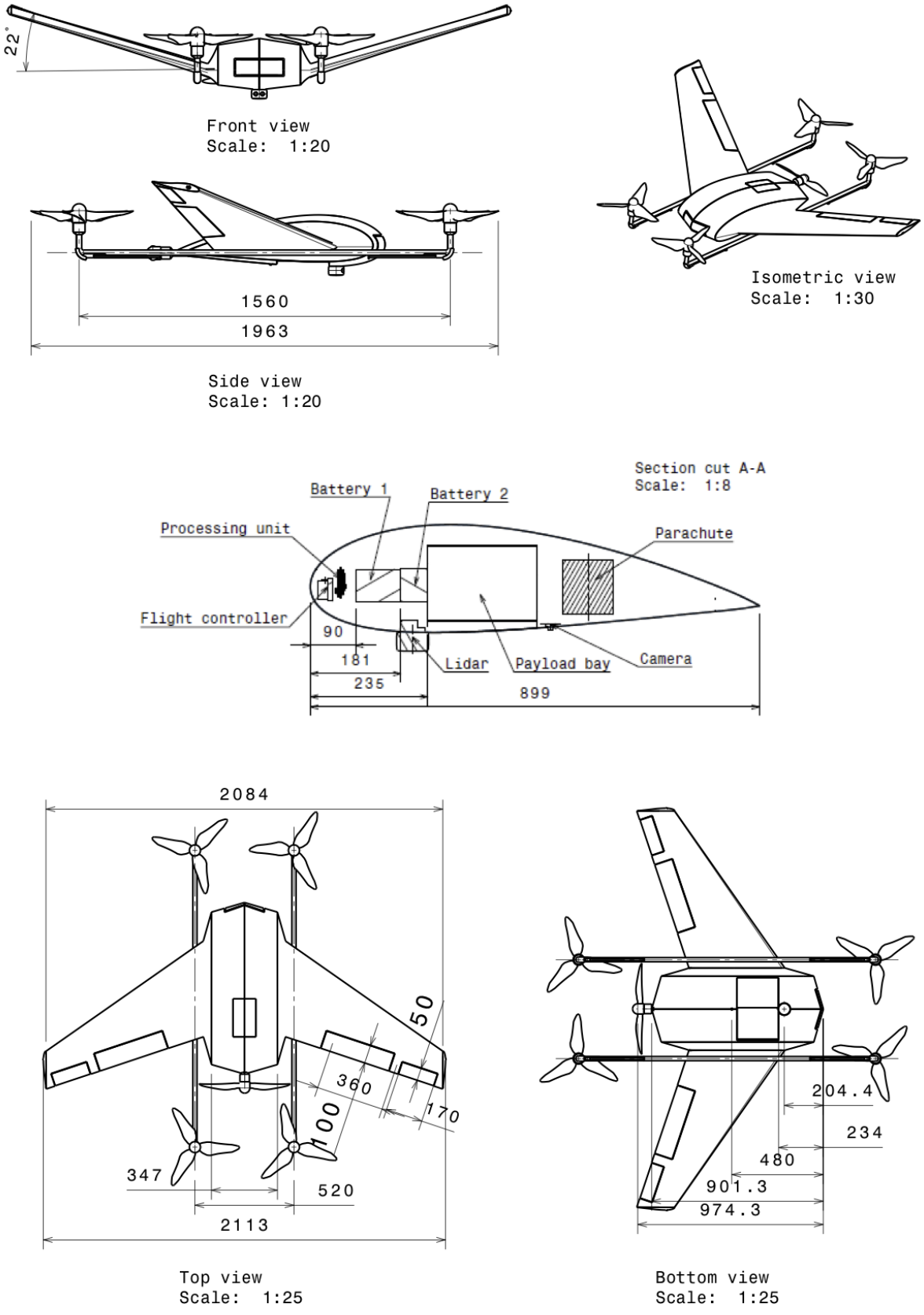

Figure 15.2: Technical drawing of the silent delivery drone including (dim. in mm)

16

RAMS

Since the delivery drone is autonomous and consequently unsupervised during operation, it is crucial to ensure that it is safe and reliable. In the midterm report [9] parameters related to reliability, availability, maintainability and safety (RAMS) have been used for a qualitative comparison of the 4 conceptual designs as has been explained in chapter 6. In this chapter a quantitative analysis regarding those parameters will be performed for the detailed design.

First, the design philosophy with respect to safety will be explained and the maximum acceptable probability of failure will be established in section 16.1. Subsequently, in section 16.2 the failure modes and the reliability of the components will be discussed. Based on that, the required maintenance intervals will be derived in section 16.3 and finally the availability will be discussed in section 16.4.

16.1. Safety

Safety is an important aspect that has been considered during the entire design process. In chapter 17 it was shown that the drone can avoid obstacles and that it can perform emergency landings in case of a component failure. It was decided to print the drone body in several parts as this can prevent cracks from propagating further. In chapter 13 it was explained that a parachute will be added to the system to avoid it from falling from the sky and generally a fail-safe approach was used meaning that the system is single-point failure free.

Estimation Failure Rate As of now there are no regulations for the maximum acceptable probability of failure for UAVs. Consequently, it was decided to use the approach presented in [25] where the failure probability is derived based on the one specified for aircraft, namely $P_{CM} = 1x10^{-7}$. However, contrary to the crash of a manned aircraft, the failure of an UAV does not necessarily injure people. Therefore, the maximum acceptable probability of failure for aircraft was divided by the likelihood of third-party casualties given the loss of control of the drone, L_{GC}, to arrive at the maximum acceptable probability of UAV loss of critical function, P_{CF}. This relationship is depicted in Equation 16.1

$$P_{CF} = \frac{P_{CM}}{L_{GC}} \tag{16.1}$$

The likelihood of third-party casualties given the loss of control can be estimated using Equation 16.2 where A_C is the casualty area where the drone will hit the ground and N_i the population density of the area above which the drone is operating.

$$L_{GC} = A_C \cdot N_i \tag{16.2}$$

The casualty area in return could be looked up in [25] based on the ballistic coefficient β which can be calculated using Equation 16.3 where M is the mass of the drone, C_D its drag-coefficient and A_b the cross-sectional area.

$$\beta = \frac{M}{C_D \cdot A_b} \tag{16.3}$$

In Table 16.1 the values used to calculate P_{CF} are presented. The population density of Amsterdam [1] was used and it would have have to be adjusted accordingly if the drone was to operate somewhere else. The remaining parameters were established during the detailed design. This yields a maximum acceptable failure rate of $P_{CF} = 1.6x10^{-5}$. If this is fulfilled the drone has a safety level equivalent to that of a commercial aircraft.

[1] https://www.ucl.ac.uk/ineqcities/atlas/cities/amsterdam, last accessed 20/06/2018

P_{CM} [-]	M [kg]	C_D [-]	A_c [m^2]	A_b	N_i [km^{-2}]
$1x10^{-7}$	12.9	0.073	13.75	0.89	4439

Table 16.1: Overview of the parameters used for the computation of the maximum acceptable probability of failure.

16.2. Reliability

The required reliability of the drone is directly connected to the maximum acceptable probability of failure established in the previous section. In this section it will be shown how the reliability of the system can be modelled such that the maintenance intervals needed to comply to the safety requirement can be determined.

Assuming that components fail independently, it was decided to use a Poisson-distribution which has a flat probability density function since no information about the failure behaviour of the system is known. Using the Poisson distribution, the reliability of a system over a period of time t and a failure rate λ can be estimated using $P(X = 0) = e^{-\lambda t}$ where X is the number of failures.

Next, it had to be determined which subsystems have to fail for the entire drone to crash. An overview of that is depicted in Figure 16.1 where the green circles imply that all events below have to occur for the failure and the red rectangle that only one of them has to happen. A failure of the communication and payload system is not included since these would hinder the drone's operation but not make it fail. It can be seen that most failure modes include circles meaning that more than one component has to fail for this to occur. Only for the structure, the vertical propeller and the motors this is not true. However, all of these components are expected to last for at least the operational time of the drone. Furthermore, the parachute would still have to fail for a complete system failure. It can be concluded that the drone is indeed single-point failure free.

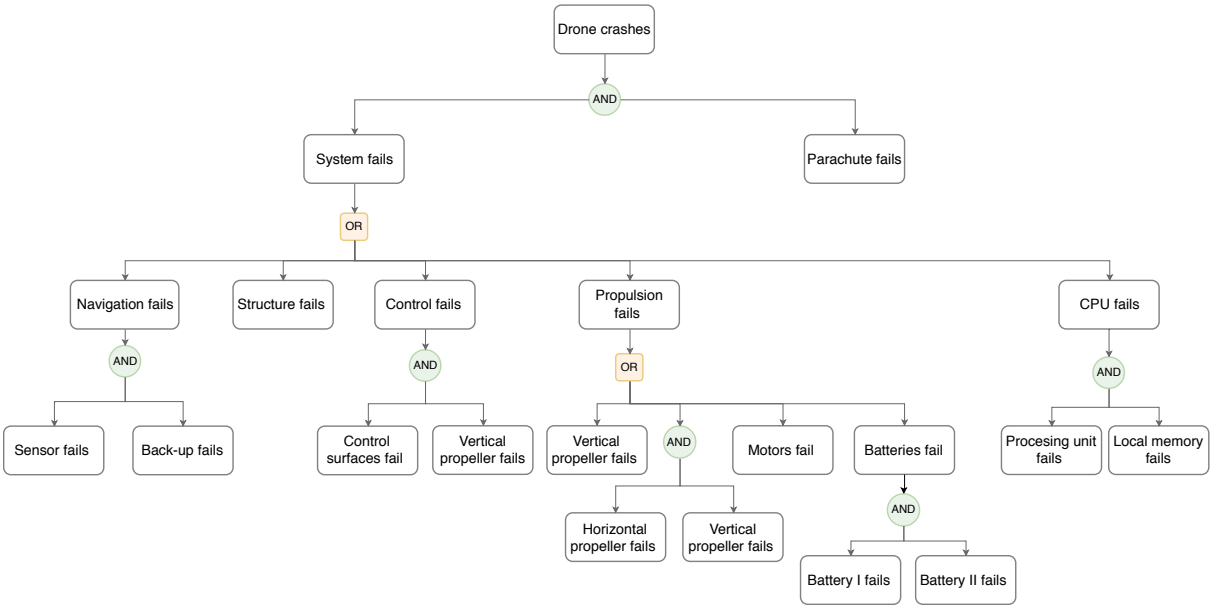

Figure 16.1: Breakdown of the possible failure modes

Up to now it has not been taken into account that some failures can be detected/predicted for sensors and the CPU, the propellers and motors and the battery. As will be explained in the following section, the structure will be inspected visually before each cycle which, looking at Figure 16.1 only leaves a failure of the control system as a cause for an unexpected system failure.

Consequently, the reliability criterion is fulfilled if Equation 16.4 holds, i.e. the probability of the system failure is below the acceptable failure probability P_{CF}.

$$(1 - e^{-\lambda_{cs} t_l}) \cdot (1 - e^{-\lambda_{vp} t_l}) \cdot P_{fp} \leq P_{CF} \tag{16.4}$$

where t_l stands for the lifetime of the drone, λ_{cs} and λ_{vp} are failure rates for the control surfaces and vertical propellers, while P_{fp} is the probability of failure for the parachute. Their values are specified in Table 16.2 [2]. The failure rates for

[2]The failure rate for parachutes was retrieved from `https://www.cirruspilots.org/copa/safety_programs/w/safety_pages/`

the control surfaces and the propellers were retrieved from [38][3].

P_{fp} [-]	λ_{cs} [h^{-1}]	λ_{vp} [h^{-1}]	t [h]
0.1125	0.0032	0.0034	3500

Table 16.2: Overview of values used for the reliability calculation.

Plugging these values into Equation 16.4 shows that the reliability requirement is not fulfilled. However, this can be changed by introducing maintenance intervals as will be explained in the next section.

16.3. Maintainability

Most of the components in the drone are non-moving and have a lifespan that exceeds the operational life of the drone. The electric motors do consist of moving parts, but as they are brushless they still have a lifespan that exceeds the operational life of the drone[4]. Furthermore, the structure will be printed in 3 parts which hinders cracks from propagating which in return makes it easier to maintain it.

However, there are some parts that require maintenance to ensure the safety of the drone. Scheduled and unscheduled maintenance will be performed. The unscheduled checks will be executed if e.g the drone detects a sudden increase in power required for flight, which means that the propeller or the motor could be damaged. In that case it will fly back to the base and the problem will be investigated. There will be three kinds of scheduled maintenance; a daily one, check A, one with a 5-week interval, check B, and one with a 30-week interval, check C.

Check A The daily visual inspections are necessary to prevent possible failure at an early stage. In these daily inspections, the following issues will be checked for and it is expected to take about 15 minutes.

- The propeller blades will be wiped clean and checked to make sure there are no cracks or bents.
- The propeller shafts will be checked for any free play and if they still turn smoothly, to make sure the bearings are still intact.
- The tightness of the attachment between detachable parts will be checked, and tightened if needed.
- The sensors and cameras will be cleaned to make sure that the location and attitude determination will not be in danger.
- The landing mechanism will be checked for dirt and dust and it will be cleaned.
- The suction cups will be checked and cleaned to ensure that no leaks develop.
- The on-board sensors will be calibrated.

Check B In the previous section on reliability it was shown that the drone does not fulfil the reliability requirement if no maintenance is performed. However, solving Equation 16.4 for the time t_l equal to the maintenance interval of 5 weeks, and assuming 30 hours of flight time per week, it can be shown that the probability of system failure is lower than specified in section 16.1. Specifically, in check B all servos and bearings are tested, lubricated and replaced if necessary. Furthermore, all connections as e.g. hinges will be checked. This check is estimated to take about 1 hour.

Check C The Lithium-Polymer batteries degrade rather quickly. Considering the depth of discharge of 65% of our drone, the life expectancy of the batteries is 1500 cycles[5]. This means that the batteries needs to be replaced every 30 weeks which will be done in check C.

16.4. Availability

After showing that the drone is safe and reliable it finally has to be considered what to do in case it becomes unavailable due to e.g. scheduled or non-scheduled maintenance. Since the system is comparatively inexpensive (when comparing it to e.g. an aircraft) it will be possible for companies to buy more than required such that they will have "back-up drones". Furthermore, the manufacturers will provide drones that can be rented to companies in case they happen to have a shortage.

723.cirrus-caps-history.aspx last accessd 20/06/2018.

[3]The values include a scaling factor of 25, as opposed to 1 for military aircraft, since they were meant for hobby UAVs. Since the delivery drone lies between military and hobby applications a factor of 12.5 was used.

[4]https://drive.tech/en/stream-content/brushed-vs-brushless-dc-motors last accessed 21/06/2018

[5]http://batteryuniversity.com/learn/article/how_to_prolong_lithium_based_batteries, last accessed 21/06/2018

17 Verification and Validation

While the subsystem requirements have been verified in the respective detailed design chapters, it still has to be checked whether the individual systems work together in such a way that they comply with the system requirements. Firstly, an overview of the requirements is given and the compliance of the system to the requirements will be checked. The justification is given throughout the report and is referenced accordingly. If the system does not comply with a requirement, a feasibility analysis is presented on the probability of meeting it. Furthermore, validation tests for certification are described.

17.1. Compliance Matrix and Feasibility Analysis

In Table 17.1 the compliance matrix for the system requirements is shown. The requirements were grouped into those concerning the drone itself, the ground control system, the base station system and environmental protection. For each requirement, it is briefly stated how it was verified and it is indicated whether or not the system does comply with it. Looking at the compliance matrix, it can be seen that some requirements "probably" fulfil the requirements. That means that it cannot yet be said for certain if they will comply but it is assumed that they will. Further tests would be required in order to make a definite statement about their compliance. In the following paragraphs, a brief feasibility analysis will be performed for the requirements for which the system received a "probable" in the compliance matrix.

Weather Resistance The weather resistance of the system cannot be confirmed yet. However, it is likely that the system will be weatherproof. First of all, the materials used that are exposed to the outside are either waterproof or in case of the wing, coated with a weatherproof laminate. Secondly, the number of seems has been limited. Furthermore, the seems will be sealed with a rubber sealant in case of a hatch or with Mylar tape (sealing tape used in General aviation) elsewhere. This makes meeting requirement SYS-DR-11 and requirement SYS-DR-36 probable.

Ground Control Interaction The system shall be able to send information like video, sensor data and the current operations via a 4G network. This network is capable of sending this information with high reliability. The drone will operate autonomously in nominal and also in emergency situations. A loss of signal is hence not a major issue and the intent behind requirements SYS-DR-10, SYS-GC-1, SYS-GC-2, SYS-GC-3 and SYS-GC-4 is met.

Drone Autonomy The system has all the sensors and computational power for positioning and analysis of its surrounding including a visual analysis, as described in chapter 7 and section 10.2. With this, it is assumed that the drone will be able to operate autonomously. As the required software is not developed yet the requirements SYS-DR-17, SYS-DR-24 and SYS-DR-27 can only be considered probable.

Table 17.1: Compliance matrix for the system requirements

Requirement	Verification Method	Compliance
Requirements Drone		
SYS-DR-1 The drone shall not cost more than 13780$.	The cost was estimated to be 11,145$.	yes
SYS-DR-2 The drone max. take off weight shall not be more than 16 kg.	The mass was estimated to be 13.7 kg.	yes
SYS-DR-3 The drone shall not be bigger than 1.8x 2.2 m.	Inspection of Technical drawings in chapter 15.	yes
SYS-DR-4 The drone shall be able to fly at a maximum velocity of at least 20 $\mathrm{m\,s^{-1}}$.	The maximum speed was found to be $\mathrm{m\,s^{-1}}$) in chapter 8.	yes

SYS-DR-6 The drone shall not use more than 2200 W of power at any time.	Analysis of the subsystem peak power consumption.	yes
SYS-DR-7 The drone shall be able to fly for 30 km without recharging or changing batteries.	Flight profile performance analysis .	yes
SYS-DR-8 The drone battery shall be replaceable.	A mechanism that allows for quick replacement is used for the batteries as explained in chapter 18.	yes
SYS-DR-10 The drone shall not lose connection to the control centre during normal operations.	See feasibility analysis ground centre interaction.	yes
SYS-DR-11 The drone shall be able to able to carry a maximum payload of 2.5 kg.	Performance analysis and payload mechanism analysis.	yes
SYS-DR-13 The drone shall be IP44 certified.	See weather proofing feasibility analysis.	probable
SYS-DR-15 The drone shall be able to transmit a live video image.	Inspection of average 4G uplink speed and video size.	yes
SYS-DR-17 The drone shall be able to autonomously deliver the payload to the client.	See autonomy feasibility analysis.	probable
SYS-DR-19 The drone shall have a hovering endurance of minimum 5 minutes.	Mission profile performance analysis.	yes
SYS-DR-20 The drone shall have an electric propulsion system.	Inspection of components; electric motors used.	yes
SYS-DR-21 The drone shall be able to transmit all data required by the ground control.	Inspection of average 4G uplink speed and data size as well as specifications CPU.	yes
SYS-DR-22 The drone shall notify the customer upon arrival at the delivery point.	Inspection of the operations plan and communication flow.	yes
SYS-DR-23 The drone shall not damage the packages during nominal mission.	Inspection of the payload mechanism indicates a fail-safe system.	yes
SYS-DR-24 The drone shall not get closer than 30 cm to any object while in flight mode.	See autonomy feasibility analysis.	probable
SYS-DR-25 The nominal life of the drone shall be more than 7500 flight hours.	RAMS analysis.	yes
SYS-DR-26 The drone shall be free of single point critical failure.	RAMS analysis.	yes
SYS-DR-27 Drone shall be able to deliver the package without GPS.	See autonomy feasibility analysis.	probable
SYS-DR-29 The drone shall be able to carry a payload of size 210 x 297 x 105 mm.	Inspection of the technical drawing.	yes
SYS-DR-30 The drone shall be able to deliver up to 4 packages in a nominal mission.	Mission profile performance analysis.	yes
SYS-DR-31 The drone shall load delivery paths for up to 4 packages in a nominal mission from the ground station.	Operations chapter describes verified routing algorithm, for communication with the drone see feasibility analysis ground centre interaction.	yes
SYS-DR-33 The drone shall safely abort or complete the mission with 1 unit of the propulsion system not working.	A parachute will be deployed in case of failure.	yes
SYS-DR-34 The drone shall have a plug-and-play structure.	All electrical components are off the shelf connected with of the shelf wires.	yes
SYS-DR-35 The drone shall store all sensor and flight data from the last operation on its local storage.	Data handling and communications analysis.	yes
SYS-DR-36 The drone shall operate with precipitation up to 7.6 $\mathrm{mm\,h^{-1}}$.	See weather proofing feasibility analysis.	probable

SYS-DR-37 The drone shall operate with gusts up to 5 $m s^{-1}$ of wind speed.	Aerodynamic analysis	yes
Requirements Ground Control System		
SYS-DR-32 The system shall calculate paths before take-off.	Operations chapter describes verified routing algorithm.	yes
SYS-GC-1 The command & control system shall be able to know the positions of all the currently operational drones within a 10 m error.	See feasibility analysis ground centre interaction.	yes
SYS-GC-2 The command & control system shall be able to take over complete control of a drone.	See feasibility analysis ground centre interaction.	yes
SYS-GC-3 The command & control system shall read out and save drone status for all drones continuously.	See feasibility analysis ground centre interaction.	yes
SYS-GC-4 The command & control system shall read out sensor data for all drones continuously.	See feasibility analysis ground centre interaction.	yes
Requirements Base Station System		
SYS-BS-1 The base station shall be able to replace the drone batteries.	Operational analysis.	yes
SYS-BS-2 The base station shall be able to charge empty batteries.	Operational analysis.	yes
SYS-BS-3 The base station shall communicate with Ground Control to track the lifetime of the batteries.	Operational analysis.	yes
SYS-BS-4 The base station shall be able to accept packages and prepare them for loading.	Operational analysis.	yes
SYS-BS-5 The base station shall be able to load packages efficiently in the drone package bay.	Operations chapter describes verified routing algorithm including grouping of packages.	yes
Requirements Environmental Protection		
SYS-SY-1 The delivery of a package by drone shall have a smaller carbon footprint than conventional delivery.	Analysis was performed on a sample delivery route test case comparing the emissions.	yes
SYS-SY-2 Toxic materials in the drone shall only be used in a closed loop system.	No toxic materials used.	yes
SYS-SY-3 The main structure of the drone shall be reused.	Fatigue life analysis.	yes

17.2. Validation and Certification

In this section the methods for the validation of the design will be explained, followed by the steps that need to be taken in order to certify it. This is important because it has to be proven that the design works and that it is safe in order to certify it and to be able to fly it legally.

Verification Four methods can be used to validate the design: review of design, inspection, analysis and test. When possible, test and analysis will be avoided because they are more costly to perform.

At this stage of the project, analysis has been used to verify the subsystems of the drone, like structures, control and

propulsion. The verification for the structures is explained in chapter 9, and consisted of verifying the code by running tests on the different modules of the code. The method was finding similar examples on textbooks where the solution was provided. Then they were implemented on the program and the solutions were compared. The verification for the control was explained in chapter 10 and was performed by checking the implementation of the equations of motion, compared to results computed by hand. In addition, the eigenmodes were simulated and compared to the results obtained by the stability department, explained in chapter 8. Finally, the propulsion department validated their work by comparing their results with those obtained on a simulation using PowerFLOW, as explained in chapter 11.

Validation In the future, several tests should be performed on the drone to validate the design and ensure it is able to fulfil its mission objective. They are listed below:

- Software verification and validation: all of the software used has already been verified using unit and module tests, specific for each subsystem. Furthermore, there is software that still needs to be written, such as the obstacle avoidance or the visual recognition of the landing spot. For example, in order to validate the visual recognition software there exist several open-source databases like CIFAR10 [1] that will allow us to ensure the convolutional neural network performs with the expected accuracy.

- Structural tests: Firstly, in order to validate the code simple tests should be performed on simple structures. A simple load, like uniform loading, will be applied to a simple wing-box structure. Then the stresses would be measured and compared to those predicted by the software. In order to validate the structural design of the drone, its parts need to be tested. The entire frame will be printed in only two parts, namely the fuselage and the wings, as explained in chapter 18. Since there will be no small components such as stringers, spars or ribs printed separately, only three kinds of tests will have to be performed on the structure. These will include tests on the wing, tests on the fuselage (the two parts of it) and tests on the entire assembled structure. The tests need to include bending, torsion, stiffness, shock loads, fatigue, vibrations and flutter tests. These will be used to evaluate the performance of the design under critical loads and ensure that it will be robust enough to fulfil its mission. Of course, it is also critical to ensure proper joining of all the parts that make up the frame, and that is why these tests are performed also on the assembled parts. Special attention must be paid to this because since a big percentage of the drone is 3D printed, it must be ensured that 3D printing tolerances allow proper integration of the design.

- Electronic tests: The components of the electrical and data handling system, shown in chapter 7, need to be tested and assembled together. Since the components are off-the-shelf, it is expected that they will not need to be tested individually. Instead, they will be connected together one by one in order to validate all the interactions and to ensure the data rate outputs and inputs to each component corresponding to the expected ones. In this way, if there is a faulty connection it will be easier to detect. It is always important to ensure the power input for each component is adequate to avoid damage on the parts. Finally, the telecommunication system will be tested to ensure that the up- and downlink capabilities of the mobile broadband chip are appropriate for the mission. The validation of the integration of this subsystem is strongly connected to the validation of the navigation software. Following the example introduced on the software verification bullet point, in order to validate the visual recognition software the processing unit and camera will be connected. Then the camera will be pointed to images of safe or not safe landing spots, and the results from the processing unit will be evaluated to ensure the accuracy is as required.

- Control surfaces tests: as explained in chapter 10, the wing has elevons and split rudders for controllability. It is important to ensure that the deflection of these surfaces can be set to the desired value within the accepted tolerances and within the expected time. In addition, it is essential to ensure that the integrity of these surfaces will not be compromised in critical cases. Therefore, first, it will be tested that they can be deployed as expected, and afterwards that their integration in the wing is strong enough to guarantee no damage in critical load cases.

- Payload bay tests: The payload system, explained in chapter 12, needs to be reliable. To ensure its proper functioning, first, the suction cups will be tested to check the weight they can hold. It will also be tested, as an integration test, that it is possible to release the desired suction cups independently of others cups. In addition, it will be tested that the hatches can withstand the weight of the packages in case the suction cups fail.

- Auxiliary system tests: The auxiliary systems consist of the landing gear, the parachute and the lights. The landing gear is the most important one in terms of testing. First, it will be tested that it can withstand the load of the drone and the impact of landing. The deployment of the landing gear will be tested as well, and finally, it will be checked that the drone is stable when relying on it, even if the ground has some inclination. Regarding the

[1] `https://www.cs.toronto.edu/~kriz/cifar.html`, last accessed 3/7/2018

parachute and the lights, since they are off the shelf extensive testing is not necessary, but it is important to check their integration with the rest of subsystems. For example, the time it takes to deploy the parachute in case of an emergency situation will be measured.

- Wind tunnel testing: A prototype will be placed on a wind tunnel to test several parameters. Firstly, the aerodynamic analysis of the drone will be validated. This will be done by measuring the drag and the lift, and special attention will be paid to the interaction of the propellers and the sensors placed on the wing. The propulsion analysis explained in chapter 11 will also be validated by measuring the thrust and power of the propellers and its structural integrity under a high rotating speed. Finally, the stability of the propellers under situations like wind gusts will be evaluated. The noise estimations will also be validated by the wind tunnel, together with the effect of the interference of the noise of the different propellers.

- Environmental and thermal tests: Since the drone will be operating in open air, it has to be checked that it can withstand the environmental conditions it will have to fly in. Firstly, the coating will be tested, and the drone will be inspected to ensure that no leakage is present when operating in the rain. It is important as well to ensure the components and the frame can operate under the temperature range it will be subjected to. Environmental tests will be performed first on the separate parts and then on the assembly.

- Flight test: The flight test is one of the most important parts of the validation plan because several subsystems designs will be validated during this test. Firstly, the stability analysis will be validated by measuring the stability coefficients (by performing the eigenmotions in flight) and comparing them with the calculated ones. In addition, the performance of the control surfaces will be evaluated to measure how much rotation rate a certain deflection can achieve, for each of them. In addition, the navigation system will be validated. The autonomous flying capabilities of the drone need to be validated, as well as the performance of the sensors. Finally, the performance calculations will be validated. For example, the range with different payload weight will be measured and compared with the expected one.

- Acceptance and qualifying: Acceptance tests will test the design during normal operating conditions, while the qualification test simulates less optimal conditions.

Aircraft certification As of now, there are no fixed regulation and procedures for the certification of drones, as explained in section 4.5. However, it is expected that the procedures defined in the future will not diverge significantly from the existing ones for aircraft. Therefore, the steps taken for the certification of aircraft will be explained considering that the one for drones will be similar.

1. The certification process starts by applying for the correct type of certification and supplying a specification report together with a certification plan to the corresponding authorities. In the case of the Silent Delivery Drone, the regulations are still subject to changes, but the certification would fall under the 'specific' category defined by EASA as explained in section 4.5.
2. After the airworthiness authorities have assigned a project number to the drone, a compliance outline and a personnel roster, will have to be provided and the authorities will hold a type board meeting.
3. The team will provide the authorities with all the technical information about the drone, including the technical drawings and all the results of the relevant analysis performed so far.
4. While the authorities review the technical information, several tests on the drone, including material, structural and flight tests described in the verification tests paragraph will be performed.
5. The authorities will perform a type inspection authorisation (TIA) and hold a meeting to discuss the case and the results that have been provided so far. Afterwards, they will perform their own flight test.
6. The team will provide the authorities with a summary of all the results and a final design package.
7. If the results are satisfactory, the authorities will issue the type certification and the team can operate the drone legally.

18

Manufacturing, Assembly and Integration

From the finished design, it can be decided on how all parts will be manufactured, if necessary assembled together and how all the subsystems are integrated into the main system. A complete overview of the MAI-plan is provided in Figure 18.1. Note that the integration phase has been taken up into the assembly phase due to the size of the product.
The following chapter will provide the plan that was designed to produce the drone. First in section 18.1 the manufacturing plan will be explained. This is followed by another explanation on the assembly plan in section 18.2. Finally, a summary of the integration is presented in section 18.3.

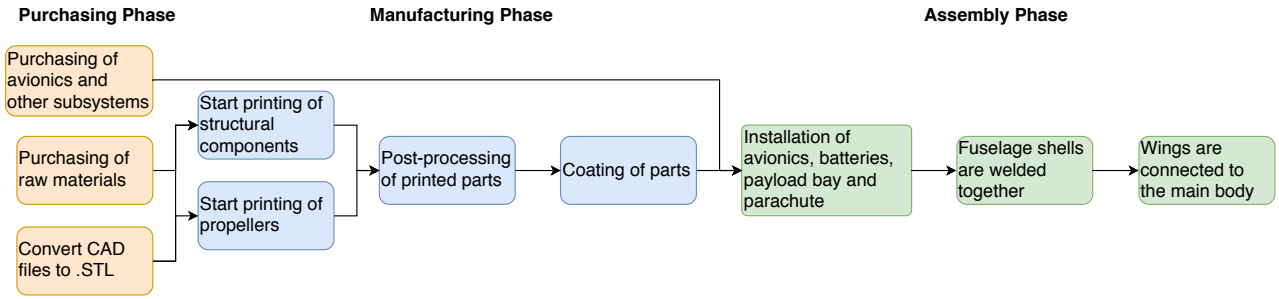

Figure 18.1: Overview of the MAI-plan.

18.1. Manufacturing

One of the user requirements states that the mainframe has to be manufactured using 3D printing, also known as additive manufacturing. In the previous report [9], the majority of benefits, found by implementing additive manufacturing in the production process, have already been explained in depth. These include benefits which would reduce the cost as well as improve the sustainability of the project. A summary of these advantages and disadvantages can be found in Table 18.1.

	Advantages	**Disadvantages**
Product Design	- The complexity of product can be increased overtime - Time to market can be decreased significantly - The product can be optimized to meet specific customer needs - The part count can be reduced allowing for a more integral design - The part can be optimised for strength/weight ratios without having an impact on machineing cost	- Requires post processing - Limited materials are available
Supply Chain	- Purchasing of the raw material is simplified as only one type is needed - A smaller production facility is required	
Sustainability	- Material waste is reduced	
Cost	- By reducing parts count the assembly, purchasing and inventory expenses are reduced - Less manhours are required	

Table 18.1: Overview of all the advantages and disadvantages of implementing additive manufacturing in the production process.

In the previous report [9], several materials had been proposed which all could potentially be used to manufacture the

drone. Now in section 9.1, the final material selection has been made. This selection has been based on the material properties and it was found which materials fit the structural design best. It was found that Nylon 6 performs optimally. With the material known it is now possible to go more in-depth into the actual manufacturing plan.

18.1.1. Manufacturing Process

In the following paragraphs, the complete manufacturing process will be explained further in depth. This description, however, will mainly cover the manufacturing of the parts that will be produced by Silentium itself. The remaining systems that will be ordered from other companies will be covered in the integration section of the MAI-plan.

Production The main structure of the drone will be manufactured using fused deposition modelling (FDM). The printer that will be used for this process is the Fortus 900mc, from Stratasys, with a maximum building volume 914 x 610 x 914 mm. Its minimum layer thickness can be set to 0.254 mm depending on the surface roughness that is required and the printing speed. The structure itself, however, cannot be manufactured in one piece since the building volume is too small. The easiest solution is to divide the structure up into 3 parts. First, there will be wings that will be manufactured independently and finally, there is the fuselage which will include the fairing as well. The fuselage, however, will be printed in two separate parts. The cut will be positioned at the chord line of the aerofoil causing there to be two different shells. How the parts will be connected will be further explained in the following section.

By printing the aforementioned parts, the number of connection points can be minimised. Additionally, the internal structure of the wings can be printed in such a way that they become an integral part of the structure and therefore reduce the weight of the structure. The individual sizes required of the parts are 900 x 216 x 189 mm for the fuselage including the fairing and 825 x 777 x 49.6 mm for the wing.

Before the parts can be printed, the CAD files will first have to be processed. This will be done using the software from Stratasys which comes with the printer. Sometimes, however, depending on the part complexity, manual repairs will have to be made during this process. Additionally, printer parameters such as layer thickness, part orientation and support design will have to be set. These potential problems will be solved during the test phase of the project since these actions only need to be determined once. Additional software provided by Stratasys will automatically create the required support structures.Then the process can almost be started after the spools of Nylon 6 and the support material have been loaded in the printer.

Furthermore, the propellers will also be manufactured using additive manufacturing by Silentium. For aerodynamic reasons, a much better surface quality is required. This led to the decision to choose a different 3D printing method, namely stereolithography (SLA). The printer Projet 6000 HD, created by 3D systems, was chosen as the final candidate. It is able to print with a resolution up to 0.1 mm with an accuracy of 0.05 mm. SLA printers obtain the best surface among all printer types available. The material selected for the propellers is Visijet SL Black.

During the manufacturing process, it is estimated that less man hours are required compared to conventional manufacturing methods. The printers will be able to operate automatically. Depending on the demand the production volume can easily be increased to fit accordingly. The printers themselves depending on the capital available within the company will either be bought or the manufacturing process will be outsourced.

Post-processing After the printing process is completed the parts, depending on the type of printer used will have to be post-processed and sometimes post-cured. In this case the main structure that has been produced using the FDM printer will first have to be removed from the base plate. The first layer can sit on a sheet which does not adhere well to the printed material. This way, when the part is finished it can easily be taken from the printer.

After the part has finished printing, the support structure is to be removed. For the wings and fuselage, it has been decided to use the support material that is soluble in water, which is faster and less likely to damage the part than mechanically removing the support. In later stages, it is possible to optimise the support design based on test runs with the printer. This way the material waste would be reduced further.

For the propeller, a different process is required. Since these parts have been built up by solidifying a liquid resin the excess resin has to be removed from the part. It is important that the correct solvent is used to clean the part to avoid damage. Finally, the parts can be sanded to smooth out the surface roughness.

Part Finishing Since nylon 6 parts are sensitive to moisture, it is necessary to apply a coating, to protect them against the environment. Such a coating could be a simple layer of paint which is water repellent and adheres to the nylon. The addition of a primer will further increase its resistance against water. For this several solutions exist.

Startups such as qlayer[1] provide coating solutions which can reduce the skin drag as well. Their layers are printed on a micro-structure level based on the architecture of shark skin. The company claims that the reduction in skin friction drag can go up to 6%. Unfortunately, this technology is still under development. Experiments have already been performed, which show that the product works as advertised. Once this technique is released on an industrial level, the team would like to incorporate this into the design.

The total surface area of the drone was found to be 1.88 m. Recommended paint layers range between 70 - 90 µm. Assuming that one layer of primer and a colour are needed, a total thickness of 0.18 mm was found. Assuming a density of 1.40 $\mathrm{kg\,dm^{-3}}$ this give a total additional weight of 475 g.

18.1.2. Manufacturing space

To estimate the space required for production it is important to examine the footprint required which the printers will occupy. Additionally, storage facilities will be required to store parts between the phases. As has been described above the first printer that is used is the Fortus 900mc from Stratasys. This printer has a footprint of 2772 x 1683 x 2027 mm. Compared to conventional machines this is a relatively small machine since only one is needed to complete the whole drone's structure. The other printer that is required (Projet 6000HD) has a footprint of 787 x 737 x 1829 mm. Finally, depending on the demand additional printers can be installed and then the factory size can be increased accordingly.

The coating of the parts will have to be applied before they are stored. This can be done in a dedicated painting room which should be at least twice the planform size of the drone.

Finally, space is taken up by the assembly line. Here it is expected that several actions need to be taken to assemble the drone. In total there are 10 processes. Assuming that for each process, an area is required of at least the planform of the wing including a 10% margin, the total line would take up 17.4 x 2.29 m which is approximately 39 $\mathrm{m^2}$. These dimensions should indicate the required size of the factory.

18.2. Assembly

The two wings and the fuselage have to be assembled after they have been manufactured.

The main connection which will take place is between the wings and the fuselage. Since they are manufactured separately, it was found that a fast connection and release system was important to reduce maintenance times. Two different connection methods will be proposed and based on their performance the most appropriate system will be chosen.

Joint Mechanism The first system includes the more conventional way of joining the wing to the fuselage. The complete overview of this structure can be found in Figure 18.2. There the wing is displayed on the right which connects to the red beam. Important to note here is that the connection is not to scale compared to the wing and the fuselage. The red beam will slide into two beams which are connected to the main structure of the fuselage. These are then connected using bolts which are manufactured from the same material as the main structure. Other types of joints can be used as well.

Lock Mechanism The second system shows a more complex construction. However, in practice this would allow for a much quicker locking and release of the system. As can be seen from Figure 18.3 instead of having bolts and nuts there will be a locking mechanism. To fasten the wing to the fuselage the wing will be first rotated to a 90° in the lateral direction. Then the red bar can be shifted within the lock by applying force since the elastic bands, indicated as the green blocks in the figure, will compress. While exerting this pressure the wing is rotated to its normal position and the force is released. Then the elastic band will exert a pressure by pushing the wing away. It cannot move, however, because the locking mechanism keeps it from doing so.

Based on the simple trade of the wing connection method found in Table 18.2 it was found that the locking mechanism is better for the design. Additionally, the drone becomes waterproof since a constant pressure is exerted by the rubber band which also seals the seam. This concept, however, will first have to be tested to see if it works as expected. This

[1] `https://www.qlayers.com/`, last accessed 27/06/2018

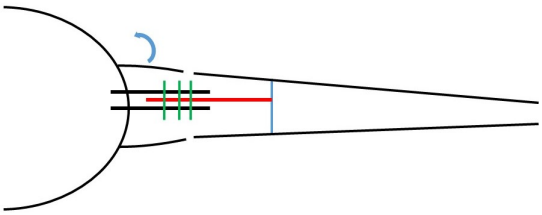

Figure 18.2: Cross section of the drone showing the conventional joining method for the wing with the fuselage. The arrow indicates the direction to which the hatch will open to access the bolts.

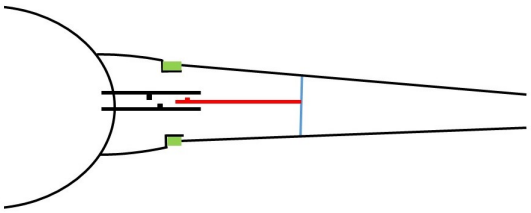

Figure 18.3: Cross section of the drone showing the more complex joining method for the wing with the fuselage. The green blocks show the location of the elastic band following the contour of the aerofoil.

has to be done using a real prototype. If it were to be found that it does not operate optimally the more conventional mechanism would be chosen instead. This mechanism will be made waterproof by adding a rubber seal around the edges of the hatch. Then by applying pressure, you can close the lid since a spring will resist this. A mechanical lock will keep it in place and the pressure will make the rubber seal fit properly making it waterproof. This concept has also been applied to for example the GoPro Hero Session which is waterproof up to five meters. Therefore, the drone should be able to operate during heavy rain as well.

	Level of Complexity	**Integral Design**	**Number of Parts**	**Changing Time**	**Total**
Weight	0.2	0.2	0.2	0.4	1
Conventional Design	0.8	0.4	0.7	0.6	0.62
Complex Rubber Band	0.6	0.8	0.8	0.8	0.76

Table 18.2: Trade-off for the wing connection.

Another permanent connection has to be made between the fuselage shells because the bottom and the top part will be printed separately. This would allow for the easy installation of the subsystems. Following [31] thermoplastics can actually be welded together since the polymers can be softened through the application of heat and by applying pressure. Four major types of welding exist to adhere two polymers. These are hot plate welding, hot gas welding, infrared heating and resistance welding. For this particular case, infrared heating is expected to perform best since this process is often used for polymers like nylon that have strong polar molecules.

18.3. Integration

All of the individual components presented in Table 8.4 have already been integrated into their respective locations within the fuselage and the wing. However, now that all their connections, as well as their physical locations, are known it has to be decided on how all the components are fitted within the wing.

Subsystem Installation Before the shells will be connected, as has been explained in the previous section, all the subsystems have to be installed in the lower shell. All the avionics will have dedicated holes which will be connected to the internal structure of the lower shell. All these additional systems will be fastened using bolts made from the same material as the main structure. Not only is it stated by [31] that this is possible, also the loads on these fasteners are relatively low. Hence, weight is saved since no metal fasteners are needed. The additional structure will be manufactured as an integral design in the fuselage. The orientation and location of the subsystems can be seen in Figure 18.4. For the additional weight of the fasteners needed, an additional 200 g was estimated. This takes into account all the fasteners needed to attach all the subsystems as well as the wings to the fuselage.

Battery Changing System First of all, the batteries were indicated as the component which is changed most often. Therefore, it was decided to add a rail system in the front of the drone where the batteries are located. This rail system allows all components which are positioned in front of the payload system to be pulled out from the front of the drone. The rails can be extended by first pushing the hatch towards the drone after which the mechanical switch releases and then the drawer comes out of the drone. This will allow the user to quickly change the batteries. Since some delicate electrical components are positioned in front of the battery system these will be added in a special case to protect them in

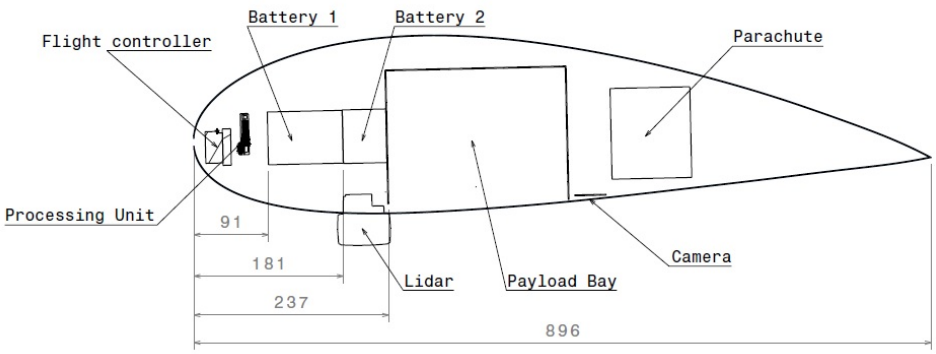

Figure 18.4: Cross section of the fuselage of the drone. The location of all the internal components is indicated.

case one misplaces the battery during the changing process. The wires connected to the flight controller will be guided along the sides so that the batteries can easily be changed with no wires in the way. Finally, the wires will be extended according to the distance that is required for the drawer to extend to easily be able to change the batteries. It was found that the rail system weight is 340 g [2].

Rod integration The rods will have to be connected to the wing. It was decided to add them under the wings to make sure that no extra holes had to be designed through the wing structure. The rods will be attached using two simple round brackets. Additional to this a fastener will be used to go through the rod and connect it to the fuselage to withstand the rod from rotating in the brackets.

[2] https://www.amazon.com/Prime-Line-7210-Drawer-Tracks-Powder/dp/B00E8AF0P8/ref=lp_511238_1_6?s=hardware&ie=UTF8&qid=1529759534&sr=8-6, last accessed 25/06/2018

19 Technical Sustainability

In chapter 3, the design approach regarding sustainability was described. Now that the final design is finished, an analysis will be performed to see how the design performs from a sustainability point of view. This chapter will do this analysis by looking into the manufacturing process, the end of life solutions and by a carbon footprint analysis. Finally, in the last section, the social sustainability will be analysed.

19.1. Manufacturing

Generally speaking, the way a product is manufactured will have a major impact on the level of sustainability of the project. As was briefly stated in Table 18.1, the material waste using additive manufacturing is greatly reduced. Development time and cost are also reduced significantly, resulting in the use of fewer resources. Hence, making the project more sustainable.

The complete manufacturing process only requires electricity as its main energy source. Depending on how the electricity is generated the process could potentially be made more sustainable compared to more conventional manufacturing techniques, where often much higher temperatures are required which are obtained by burning fossil fuels.

19.2. End Of Life Solutions

As discussed in the market analysis performed in chapter 2, the drone should be manufactured at a rate of 300 units per week. This amounts to more than 15500 potential drones per year, of which the frame should have a lifespan of 3 years. Because of the high production rate and the relatively short lifespan, the End Of Life planning has a very significant impact on the sustainability of the project: if it is not handled appropriately, an unreasonable amount of waste will be generated. Therefore, the objective of the team is to recycle as many components as possible.

The components can be classified into two main groups for recycling: electronics and structures. The former includes all electronic components aboard: sensors, processing units, flight controller, batteries, chips, wires and motors. The latter is made up by the frame, the propeller and the payload mechanism. This separation is convenient because the groups are composed of very different materials and therefore the recycling and disposal procedures differ greatly.

Electronics The most important component regarding sustainability are the batteries. The battery that will store and provide power to the drone is a Lithium Polymer battery. At the end of life, these batteries can be safely disposed. For the rest of electronic components, the most common procedure is to separate them into the smallest possible items and reuse them if possible or recycle the material they are made of [11]. At the moment, electronic components and Printed Circuit Board recycling is an active research topic.

Structures The recycling methods that will be used for the components of this group are dependent on the material. The material used for the skin and structure of the drone is Nylon 6. By granulating it in a regrinding mill the material could be re-used with injection moulding up to 10 times, with only a 10-15% decrease in material properties [28]. The skin structure of the drone can be cleaned, chipped, extruded and manufactured into a new product [14].

19.3. Carbon Footprint Assessment

In this subsection, the CO_2 emissions of drone and truck delivery will be compared. This comparison will be done for two test cases, similar to the cases in section 4.2, with large packages and small packages. To mimic a real-life delivery day, the comparison between CO_2 emissions of drone and truck delivery will be done for the range between 100 and 200 packages. This range represents packages delivered by one truck in one day and has been chosen using the following analysis. In Figure 19.2 and in Figure 19.3 are shown examples delivery paths of the drone and the truck, respectively, that have been used in this analysis.

Number of Packages Delivered per Day The largest package delivery service in the Netherlands, which is PostNL, [1] has stated in their annual report (Reference [2]) that in 2016 they operated 1897 small trucks and vans, with an average carbon emission of 237 grams per kilometre. The number of yearly domestic parcels is approx. 130 million. This results in a daily delivery volume of about 356 thousand parcels, which means each truck should carry about 187 parcels per day. Note that the assumption has been made that all trucks are in use, which in reality would probably not be the case. This would result in a higher amount of packages per truck. However, not all packages will be delivered by truck, since PostNL also uses delivery bicycles for package delivery.

Truck Carbon Footprint It is assumed that each truck delivers the packages within a circle with radius 15 km. It is assumed that delivering a package to the doorstep takes on average 1.5 minutes, the rest of time the truck will be driving. Using the total time per package mentioned in the previous paragraph, it can be computed that the truck will be driving for 5.5 hours when delivering 100 packages and 3 hours when delivering 200 packages. The speed limits in residential areas in the Netherlands are either 30 and 50 $\mathrm{km\,h^{-1}}$, therefore it is assumed that the truck will drive 40 $\mathrm{km\,h^{-1}}$ on average. This results in a total of 220 km driven for 100 packages, and 120km for 200 packages. Finally, using the value of 237 grams of $C0_2$ per kilometre the emissions for the trucks are found.

Drone Carbon Footprint For the first case (small packages, as described in section 4.2) it is calculated that for 100 and 200 packages, the drone visits the depot 45 and 84 times on average. For a different number of packages, the number of depot visit is found by interpolation. The energy consumption for the package delivery has been computed using the estimations mentioned in subsection 14.1.2 Also, to use a worst case scenario estimate it is assumed that the electricity used to charge the batteries is generated using coal, gas and nuclear plants. From [2] it has been determined that 0.649 kg of CO_2 is emitted for generating 1 kWh of electricity.

Results The results of the simulations are presented in Figure 19.1. It can be seen that at 100 packages, the drone emits 57% less CO_2 per package than the truck when delivering big packages (case 2). If the packages are small (case 1), however, the drone emits 72.5% less CO_2 per package. For case 2, at 165 packages, the drone becomes less efficient than the truck. For case 1 the drone becomes less efficient when delivering 201 packages. From this, it can be concluded that on average drone has a lower carbon footprint. However, it can be seen that when bigger packages are distributed, truck delivery might be beneficial for a big amount of packages.

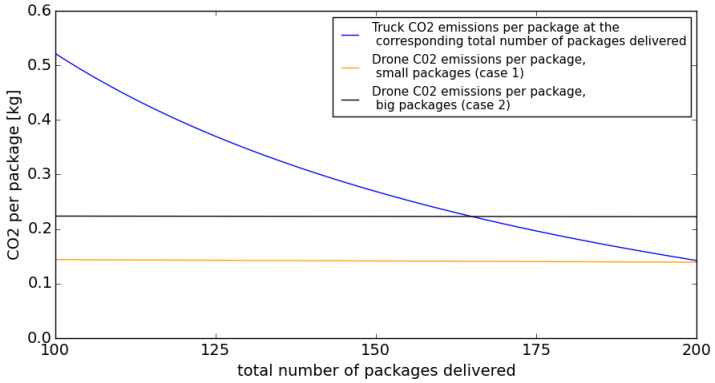

Figure 19.1: CO_2 emissions for truck and drone delivery per package, within a specified range of total amount of packages delivered.

19.4. Drone Energy Management

Since the drones are electric, there is only one way in which they might indirectly generate pollution: in the way the energy that they use is produced. The ideal case would be to operate the drone using only renewable energy. For this, it was decided that the best option was to use solar panels, which could be installed on the base station. After an exhaustive

[1] `https://www.postnl.nl/en/about-postnl/about-us/our-organisation/mail-in-the-netherlands/`, last accessed 25/06/2018

[2] `https://www.co2emissiefactoren.nl/lijst-emissiefactoren/`, last accessed 25/06/2018

Figure 19.2: Routing for a drone delivery case in Los Angeles

Figure 19.3: Routing for a truck delivery case in Los Angeles

analysis, it was concluded that 674 solar panels would be needed, which spans a total surface area of 828 m^2 (or around 29x29 m), assuming that the drones at each base station deliver 1508 packages per day. This numbers were obtained using Solar Frontier solar panels [3], which have an efficiency of 13.8%. In addition, the Tesla Powerpacks could be used for energy storage. Therefore, it is possible to operate the drones in a completely sustainable and environmentally friendly way, without producing any pollution.

19.5. Social Sustainability

Social sustainability is defined as the ability to meet the needs of current members of society as well as supporting the ability of future generations to maintain a healthy community [4]. Unfortunately, this form of sustainability is not easily quantifiable. The social sustainability of this project will be evaluated using three parameters; equity, social acceptance and quality of life [5].

Equity For equity, the question should be asked if the target group gets more control over their lives economically. This question can be answered by looking at the market analysis in chapter 20, in which it was found that delivery by drone will be cheaper than current truck delivery. However, as not all packages can be delivered by drone, this decrease in price is only applicable small packages.

Social Acceptance With social acceptance comes the opinion and needs of diverse groups, their background, cultures and circumstances. Since the drone is quite big, people might find it scary, or think it is unsafe. For this reason, they might not only want it to land in their garden but also not want it to fly in their neighbourhood. Even though it is hard to cope with such opinions, they should be heard and a solution should be thought of. Abundant publicity might be needed to educate people on how people feel about drone delivery and how it might affect their lives (positively and negatively). Examples of such publicity could be on how the drone is designed for safety (using a parachute, for instance) and how the drone will not be as annoying as current drones.

Quality of life The last aspect, quality of life, is more easy to evaluate. Since the drone will make delivering packages faster, cheaper and more sustainable, quality of life will be improved. By being more sustainable than regular truck delivery as it is now, it will not only benefit the current generation but also future generations. The noise of the drone and pollution of the visual sky, however, might decrease the quality of life. But since the core of this project has been to make it as silent as possible, this aspect has been accounted for as much as possible. And as for the pollution of the visual sky, this is hard to quantify and even to put a qualitative analysis on it, since one might find a truck in front of their house more visually disturbing than a drone landing and taking off.

[3] `https://www.zonnepanelen.net/nl/pdf/panels/SF-Datasheet-CIS-modules.pdf`, last accessed 25/06/2018
[4] `http://www.businessdictionary.com/definition/social-sustainability.html`, last accessed 25/06/2018
[5] `http://esg.adec-innovations.com/about-us/faqs/what-is-social-sustainability/`, last accessed 25/06/2018

20

Return on Investment and Operational Profit

After the initial cost estimate performed in chapter 2, a more detailed one will be done based on the detailed design in this chapter. This is important to ensure the economic feasibility of the project. Furthermore, an estimate for the return on investment of the project will be given. In section 20.1 a cost break down for each subsystem will be given and in section 20.2 the return on investment and operational profit will be elaborated. The return on investment is defined as the ratio of the net income over the amount of investment.

20.1. Cost Break-Down Structure

In this section, the cost for all subsystems will be estimated including the cost of all components and processes necessary to produce the drone. In Figure 20.1 is shown the cost break-down of the company.

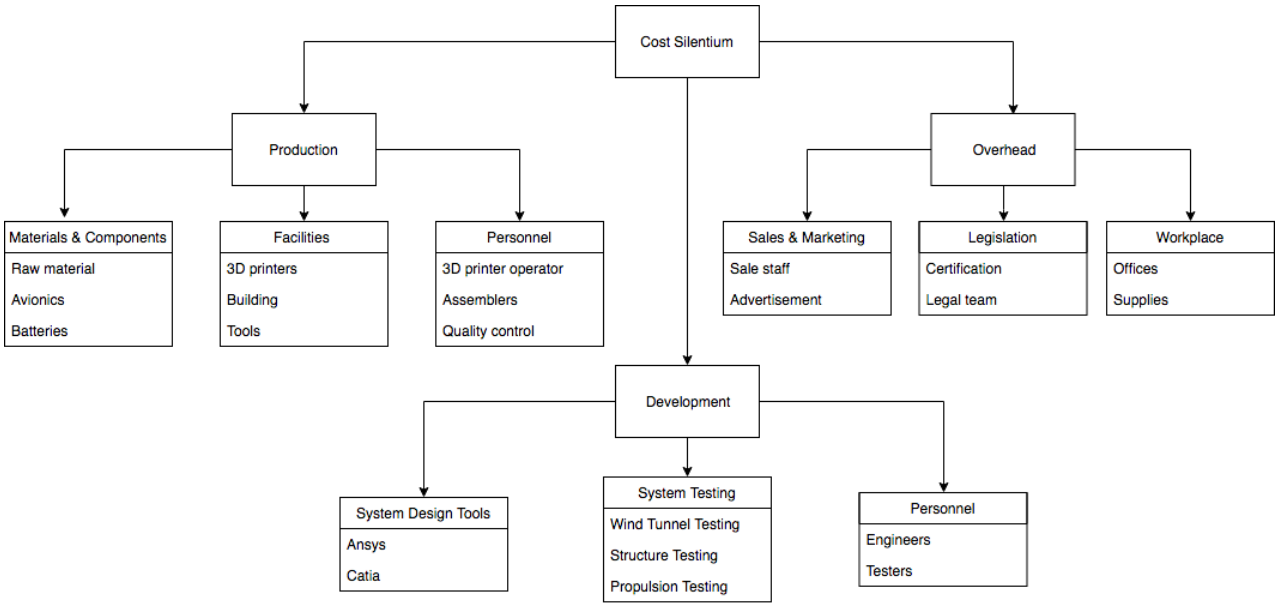

Figure 20.1: Cost break-down scheme for the company Silentium

Structures For the structures, direct, indirect and labour cost had to be estimated. Furthermore, it was assumed that about 5% of the manufactured parts might be faulty, which increases the cost. Direct costs include the cost of the power required for the 3D printer and the cost of the material. A common power consumption for industrial 3D printers is 2 kWh [1]. Since the filament cost for nylon 6 is 90 \$/kg [2] and the mass required is 2.6 kg, the raw material cost for a unit drone is 233 \$. To get the hourly rate of the direct cost, the speed of the manufacturing had to be assessed. An estimate for that is $8.64 \cdot 10^{-5}$ m^3/h [3], which translates into $26h$ of production time. This is a safe estimate since it's based on a rather low-level industrial 3D printer. This gives a direct cost rate of $c_d = 14.9$ \$/h.

The indirect costs include the cost of the 3D printer and its maintenance. A mid-upper range 3D printer from Stratasys (same company that provides the material) costs around 250000 \$ [4]. The expected lifetime is 5 years and the yearly cost

[1] http://www.stratasys.com/3d-printers/objet260-connex3, last accessed 23/06/2018
[2] http://3dinsider.com/3d-printing-filament-cost/, last accessed 23/06/2018
[3] https://ultimaker.com/en/products/ultimaker-3, last accessed 23/06/2018
[4] https://www.cati.com/3d-printing/3d-printer-price/, last accessed 23/06/2018

of maintenance is estimated to be 5% of its value, i.e 5000 $. Assuming that the machine will be operated for 20 h/day throughout the year, the operational hours per year are h_y = 7300 h/year. Based on that, the indirect cost rate was estimated to be c_i = 3.6 $/h.

The labour cost includes the cost of supervision and management of the 3D printers. It was assumed that one person can monitor 10 3d printers at a time and that their salary is 40000 $ per year. Furthermore, the labour cost includes the cost of assembly and testing. Assembly time has been estimated to be 10 h and the testing cost to be 100 $. These values combined with the production speed yielded a labour cost rate of c_l = 13.8 $/h. The total number of drones produced in one year with this work unit (10 3D printers + supervisor) is 2000.

The cost per drone and the rate values are summarised in Table 20.1.

	Direct Costs	Indirect Cost	Labour Costs	Total
Cost Rate [$/h]	14.9	3.6	13.82	32.3
Cost per Drone [$]	388.4	93.96	360	842

Table 20.1: Structure and manufacturing estimates summary.

Electric System and Battery For this subsystem, the components have been selected directly off-the-shelf. The cost of the sub-components can be seen in Table 20.3.

Avionics Similarly to the electronic components, the avionics components have been selected directly off-the-shelf. A detailed cost breakdown is shown in Table 20.2.

Table 20.2: Break-down cost of avionics sub-components

Component	Cost [$]	Amount
LiDAR 360° scanner	342.9	1
Ultrasonic range finder	7.23	10
Pitot tube	54.45	1
Camera	23.17	1
Back-up IMU	9.59	1
Cellular reception	17.33	1
Radio navigation	8.64	1
Mobile broadband chip	96.7	2
Flight controller	301	1
Processing unit	531.8	1
Total	1554.58	

Table 20.3: Break-down of sub-components of the electric system

Component	Cost [$]	Amount
Main battery	456	1
Secondary batter	81	1
Local Storage	28	1
Power Distribution Unit	12.5	1
Total	577.5	1

Payload and Auxiliary Systems Again, the components used for this subsystem were off-the-shelf and their cost is summarised in Table 20.4.

Propulsion While the motors of the propulsion system will be bought, the propellers have to be 3D printed. To estimate the manufacturing cost of the propellers, the same method as the one used to estimate the cost of the structure was used. The 3d printer used for the propellers is Projet 6000 HD. An estimate of the cost is presented in Table 20.5.

Maintenance cost The maintenance procedure planned for the delivery drone was explained in chapter 16. It was established that there is a daily check, which takes approx. 15 min every day. It is estimated to cost 1$ daily per drone with the help of automation to check the integrity of propellers, suction cup and calibration of the onboard sensors. Check B, which is conducted approximately every month for 1 hour was estimated to cost approximately 25$ each time, depending on the salary of the inspector (Here assumed to be $25\$/h$). Finally, during Check C, which is performed every 30 weeks, the battery is replaced for a total cost of approximately 500$ as shown in chapter 7. This results in a maintenance cost of 1550$ per year.

Total cost Summing up the cost contributions of all subsystem and assuming a lifetime of 3 years, the total cost of the drone, including maintenance, is assumed to be 11145$.

Table 20.4: Break-down cost of payload and auxiliary systems

Component	Cost [$]	Amount
Parachute	1205	1
Suction cups	10.43	8
Holders	31.28	8
Pumps	70.64	8
Actuators	68.82	2
Landing rods	17	2
Propeller rods	25	2
Actuators	13.5	2
Total	2352.44	- N/A

Table 20.5: Cost-break down for the propulsion system

Component	Cost [$]	Amount
Motor	120	5
ESC	30	5
Propeller	84	5
Total	1170	

Delivery Related Costs As mentioned in chapter 2, the delivery related costs amount to approximately 0.94$ per delivery. Given a lifetime of three years, the total delivery cost amounts to 11964$.

20.2. Return on Investment and Operational Profit

In this section, the revenue, gross and operating income for the company as well as the return on investment that it is possible to achieve will be estimated.

Company expenses To establish the operating income, the gross income had to be subtracted from the cost that the company has to sustain. The two main expenses for the company are "Research and Development" and "Marketing and Sales". Each department needs money to pay employees (and taxes), rent, equipment and requested services from external companies. Since it is very difficult to estimate these costs, the corporate report of the drone company "Parrot" [5] was used, which has a revenue in the same order of magnitude as the silent delivery drone. From the report, a cost of 17% for "Research and Development" and of 18% for "Sales and Market" of the revenue was estimated.

Pricing Given its mission profile, a single drone is able to deliver an average of 14 packages per day by making 7 trips with an average of 2 packages. Therefore, the total number of packages it can deliver during its 3 years lifetime (assuming continuous deliveries throughout the years) is 15300. In the market analysis in chapter 2 it was found that the last mile delivery costs 2.5$. Consequently, it would cost 38220$ to deliver 15300 packages. To make the delivery system switch from truck to drone delivery, the price was set in such a way that it is 10% more economical to use a drone. Therefore, the price is 23225$ since the delivery costs amount to 11964$. This price includes the handling of operations and maintenance. A discounted price can be discussed with the clients if they want to take over maintenance and operations.

Operating income To simplify the estimation of the operating income, it was assumed (as for the estimate of the structure cost) that the minimum working unit is 10 3D printers, 1 supervisor and as many drone assemblers as needed. This unit can produce one drone for 11445$. Furthermore, it was assumed that all the products produced are immediately sold. The gross income, which is given by the difference in revenue and product cost, is 12080$ per drone. The operating income is given by the gross income minus the operational costs including the research and development department's costs and the sales and marketing's cost. This gives an operating income of 3951$. Finally, cooperate taxes had to be subtracted from the operational income. Taking into account that those taxes are set at 25 % for the Netherlands, this yielded a net income of 2963$ per drone.

Break-Even point and return on investment Now that the net income was calculated, the break-even point could be determined. This was done in terms of units produced and the return on investment. The initial investments is calculated assuming that a period of 6 months is necessary to finalise the validation and set up the manufacturing facility. Including the cost of the workplace, manufacturing building, 10 3d printers, engineering labour (10 engineers) and general workers labour (3), marketing (50 k$) the initial investment sums up approx. to 5 M $. Continuous further investments are needed once production is started to cover manufacturing and operation expenses. In particular, for the production volume shown

[5] `https://corporate.parrot.com/en/financialpublications/2015financialpublications/pressreleaseparrotq42015earnings`, last accessed 23/06/2018

in Figure 20.2 an investment of 46 M $ is needed to sustain the first year (from full production capability) expenses of the company. Assuming the production rate specified in Figure 20.1, it can be seen that the break-even point is at 1200 drone units in Figure 20.2.

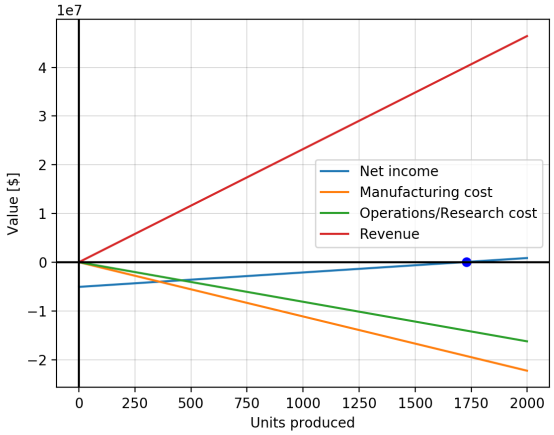

Figure 20.2: Company's expenses and profit in function of the drone units produced.

Using one working unit at full production speed, the break-even point will occur within approximately 10 months, excluding the 6 months to set it up. If more production volume is needed, the number of working units can be increased. After 1 year, the return on investment is 1.9 % while after 5 years the return on investment is 12.4 %. Averaging the net income throughout the working life of one working unit, a net operating income of 29.6 M\$ per 10000 drones sold was found. The original estimated market volume per year of 100000 drones could therefore directly be translated into a net income of 269 M\$ per year.

21

Risk Assessment

In previous chapters, the final design has been designed and evaluated. The aim of this chapter is to analyse risks surrounding the final design and to develop a plan to decrease their probability or consequence. The chapter starts with a short description of the management risks within the project and will continue with identifying technical risks for both, the design phase as for the future phases of the project. This chapter will be concluded by the technical risk mitigation with its corresponding pre- and post-mitigation risk maps.

21.1. Project Management Risk

Project risk management was taken into account when drawing the final schedule for the last period of the project. The risk officer held a discussion with the team manager in order to assess the feasibility of the schedule previously drawn with the system engineers. It is important to take into account the possibility that all team members could take their absence days at the same time in the final weeks of the project and that it is required to finalise the content of the report at least a day in advance such that a full working day can be dedicated to the format and structure review of the report.

The risk officer together with the team manager has held multiple meetings with some technical departments (especially with the noise group) in order to ensure that deadlines were met, quality was according to high standards and enough resources were assigned to the different groups. This would ensure that possible internal problems are identified on time and mitigated accordingly.

Finally, in order to avoid the risk of exceeding the maximum allowed number of pages, a strategy was developed by the team editors. At the beginning of this final phase of the project, the structure of the complete report was predefined taking into account all the phases of the product design process and the deliverables closely related to the project management. Besides that, each of the chapters was assigned a certain page budget, such that the maximum number is not exceeded close to the deadline. If any team member considers that he or she requires more pages, that person would have to request it to the editors. Apart from that, 5% of the maximum 150 pages (namely 8 pages) was reserved as a contingency.

21.2. Technical Risk Identification

Each risk has been assigned an id, probability of occurrence (listed below on the left), severity of consequences (listed below on the right) and related measure taken by the company.

1. Almost Impossible
2. Unlikely
3. Somewhat Likely
4. Likely
5. Almost certain

1. Negligible
2. Marginal
3. Critical
4. Catastrophic

Finally, a general mitigation scheme has been developed in order to classify the different risks depending on the type of action that has to be taken. Such scheme contains five options which are described as follows:

1. **Accept**: No risk management/mitigation action needs to be taken. The combination of the probability and the consequence of the risk is not high enough such that resources have to be destined to mitigate it.
2. **Watch**: Observe and keep track of key parameters representing the risk. The watch plan can trigger risk management activities at a later stage or a plan B.
3. **Mitigate**: Direct mitigation in order to decrease their consequence and/or their probability of occurrence.
4. **Research**: Research activity aimed at a better estimation of the risk probability and/or consequences.
5. **Elevate**: Transfer risk to other entities. It happens when the risk cannot be managed by the company alone or the effect of the risk involves multiple stakeholders.

Having established the method, the major technical risks for the project will be enumerated. These have been divided into risks that have occurred, risks that could still happen and risks that might occur in the future phases of the project.

Table 21.1: Risk associated with the chosen concept and related aspects.

Id	Explanation	Probability	Consequences	Correction
	Possible risks			
1	Propeller drag is too high and drone cannot cruise	Likely	Catastrophic	Mitigate
2	Noise does not comply with regulations	Almost certain	Critical	Mitigate
3	Propellers cannot generate enough thrust for VTOL	Likely	Catastrophic	Mitigate
4	Propellers are not safe to fly in densely populated areas	Likely	Critical	Mitigate
5	Sensors interfere with aerodynamics of the wing	Almost certain	Marginal	Research
	Occurred risks			
6	Technical budget is inaccurate	Almost certain	Critical	Mitigate
7	Preliminary sizing is not accurate	Almost certain	Marginal	Research
8	Noise estimation methods give unreasonable results	Almost certain	Catastrophic	Mitigate
	Future risks			
9	Certification of the drones takes longer than planned	Somewhat Likely	Critical	Research/Elevate
10	3D printing is not accurate enough	Unlikely	Marginal	Watch
11	Not enough financial resources are obtained	Somewhat Likely	Catastrophic	Research
12	Structure is not suitable for certain environments	Likely	Critical	Mitigate
13	Off-the-shelf components stop being produced	Likely	Critical	Mitigate
14	The demand is underestimated and cannot be met	Unlikely	Critical	Watch
15	The demand is low and break even point is not reached	Somewhat Likely	Critical	Research
16	Product does not pass validation tests	Somewhat Likely	Catastrophic	Research
17	Electronic components become outdated	Likely	Marginal	Research

21.3. Technical Risk Mitigation

In this section, we decided on the activities and corrective measures that are necessary to mitigate some of the risks.

1 - Mitigate: If the drag increase and reduction in lift generated by the propellers make it impossible for the drone to fly, the design has to be changed. This can be achieved either by changing the design of the propulsion system, to reduce propeller size, or modifying the configuration so that the propellers do not interact with the aerodynamics of the wing; for example, by tilting the propellers forward during cruise such that they also produce thrust during this phase or by tilting and folding the propellers within the rods such that their contribution to drag is minimised.

2 - Mitigate: Perform an accurate noise estimation with the final design. If the results do not comply with the requirements, the design would require an iteration. This might include changing the propeller design and adding active and/or passive noise cancellation mechanisms, such as well-designed ducts.

3 - Mitigate: Together with the noise estimation, an accurate thrust and power estimation should be performed on the propulsion system. If they are not high enough, the design has to be altered. However, the entire team should first make an effort to decrease the weight of their corresponding subsystems in order to avoid the snowball effect. In addition, the propulsion system design would need to be iterated.

4 - Mitigate: The drone contains proximity sensors to avoid any entity. If the unprotected propellers are still deemed too unsafe, ducts, guards or another kind of protection will be added to the design, causing a new iteration.

5 - Research: The sensors placed on the outer surface of the drone might compromise its aerodynamics. The final aerodynamic characteristics of the complete final design will be validated using an accurate CFD tool during future project phases, and measures will be taken if necessary. These might include changing the sensors, their location within the system or adding an aerodynamically shaped fairing.

6 - Mitigate: An inaccurate technical budget led to a wrong estimation of the power required. As a result, the batteries had to be re-sized at a late stage of the design process, causing an iteration in the stability, aerodynamics and control departments. As a lesson, the group has included contingency margins in the new iteration in order to avoid the later repetition of the complete design cycle.

7 - Research: The preliminary sizing of the drone carried out during early stages of the design process generated results which do not perfectly match the outcomes of the detailed design. This was expected due to the assumptions and statistical relationships used during the sizing. Since the detailed design is based on the sizing, the results obtained

during the detailed design, of parameters such as the weight or the L/D, have to be kept close to the sizing results.

8 - Mitigate: Perform a grid resolution study to ensure the simulation has been performed correctly. Check all the input parameters have been added properly and use the correct units. In addition, read the documentation of the software to ensure the results should be valid for the design and validate with experimental data. If the error can not be found, use a different tool to estimate the noise, even if it has a lower accuracy. Several meetings were held between the noise department, risk manager and project manager to mitigate the risk of this event.

9 - Research/Elevate: An unexpectedly long certification time might mean market or technology changes. We will study the requirements and ensure during the verification and validation processes that the system complies with them. In addition, some small changes can be added to the design if it is seen as convenient for a better market demand and social acceptance. Finally, if the problem lays with a slow process of the certification authorities, the risk would be elevated since the risk involves multiple stakeholders and the bottleneck relays on an entity outside of the company.

10 - Watch: Inaccuracies in 3D printing can lead to a rearrangement of some of the sensors if they do not fit in the fuselage as predicted. With the current tolerances for 3D printing, this event is considered to be unlikely. For the placement of the components inside the drone, the team has applied safety margins to account for possible manufacturing constraints and the process will be constantly monitored.

11 - Research: Without financial resources, the prototype cannot be built. The team will participate in promotional events and technology fairs to attract investors and will observe their response. If necessary, the team will research the need for creating advertisement material or asking for a loan from a financial entity.

12 - Mitigate: The weather conditions might affect the conditions of the drone, which can cause unexpected behaviours or premature failure. Coating and/or cooling systems will be applied to the structure. In the future, if the drone has to operate in extreme conditions, special treatment can be added to the material depending on the region where it will operate or a possible re-design will be required.

13 - Mitigate: If the components stop being produced the team will find another manufacturer for a similar product and will adapt the design to include it.

14 - Watch: The drone might attract too many costumers and the production might not be fast enough to meet the demand. The team will observe the demand increase in time and will subcontract a manufacturer accordingly or increase its production ability

15 - Research: If the demand is too low, the team might not be able to cover the costs of the drone. The team will always keep the costs to a minimum, while ensuring functionality, and negotiate with clients when deemed necessary. Agreements can be made with clients, such as reducing the cost per unit for large orders, if necessary.

16 - Research: Failing the validation tests would lead to a design iteration, which would delay the project. In addition, after the correction of the design, another prototype would have to be built. To avoid such waste of resources, the team will ensure the use of accurate simulation tools during the revision of the final design and research will be carried out to understand the fidelity of the aforementioned tools.

17 - Research: New, more efficient electronic components will become available in a few years. The team will study the development of new technology and adapt the design to include it when it is beneficial in terms of cost.

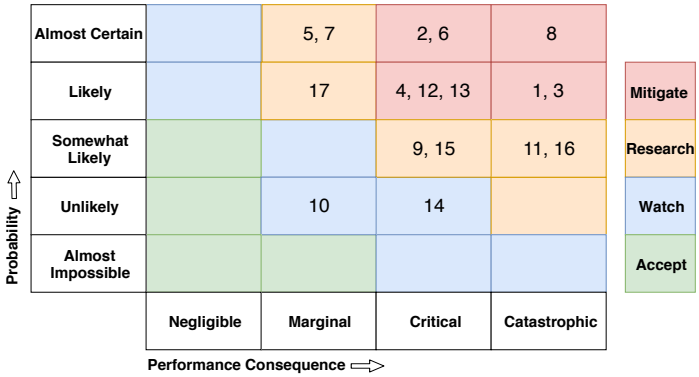

Figure 21.1: Technical Risk Map

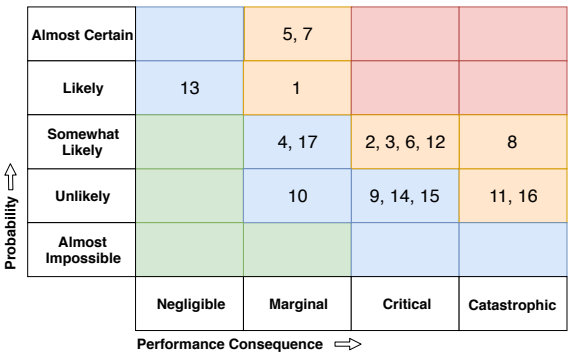

Figure 21.2: Post-Mitigation Technical Risk Map

22

Project Organization

With the detailed design completed, several actions still need to be completed to make the drone a reality. This chapter will present an overview of the activities that would be performed in the future as a continuation of the Silent Delivery Drone project. They will be presented on the form of a Work Flow Diagram (section 22.1) and a Gantt chart (section 22.2).

22.1. Project Design and Development Logic

In this section, the project design and development logic for the future is presented. As seen in Figure 22.1, there are 8 main blocks. The first one consists of finalising the design, which includes design actions that were out of the scope of the project up to this point in time, such as software and electronic configuration design. This is followed by acquiring financial resources, which are essential to build a prototype and continue the project. The plan is to create promotional material for the project, such as a website, flyers or posters and present them at events such as technology fairs to attract the attention of investors. Afterwards, it will be possible to reach an agreement with the investors. With these financial resources, it would be possible to build a prototype and validate the design using it. The validation of the design would consist of several tests, which can be divided into groups: electronic system tests, structures, wind tunnel tests, payload system and landing gear tests. Finally, a flight test would be performed to ensure proper functioning of the remaining subsystem and to validate the stability and control subsystem. All these tests are presented in more detail in Figure 22.2.

During validation it is possible that some errors in the design are discovered, therefore we might have to iterate the design. Once the design complies with all the requirements, it will be certified, and then it can be sold to costumers. For this, the plan is to create advertising material and calculate the optimal selling price to maximise the profit. Afterwards, an agreement must be reached with the costumers. Once the order is placed, mass production can start. While a detailed MAI plan can be found in chapter 18, Figure 22.1 shows a small, generalised summary of the mass production activities. Finally, the drone has to be distributed to the clients. This will be done using a shipment company.

The colour scheme and design of the diagrams are consistent with the one used throughout the report: the first level is red, the second is green and the third is white. Expansions are denoted with a round block with a capital letter on it (for example, "A"), and round blocks with an "OR" and an "AND" represent OR and AND gates, respectively. All the other style details are explained in section 5.3.

22.2. Project Gantt Chart

Figure 22.3 shows the Gantt chart for the activities related to the silent delivery drone. In the figure, the final date is set for December. However, if the project was successful and the costumers were satisfied, the project would continue and keep growing after that period. The blocks are the same as in the flow diagram shown in section 22.1. The block that takes the longest time is the certification of the drone since this has to be done in collaboration with EASA [1], and therefore the exact duration is unknown.

During the first block, a part of the team will focus on creating the necessary software for navigation. The architecture of this program is defined but it needs to be written and verified. In the meantime, the electronics department will create a detailed electronic configuration diagram, including all wires that are necessary and ensuring their length is adequate for the relative position of the components. The rest of the team will be divided in two: one sub-team will review the detailed design of the aircraft and implement improvements if necessary. The rest will create promotional material to catch the attention of investors on the project. The entire team will participate in promoting the drone, while the business manager will be in charge of negotiation with investors.

Once the team has enough financial resources, the production of the drone can start. The drone parts can be divided into two kinds, that can be produced separately: the 3D printed parts (frame and propellers), and the off-the-shelf components (electronics). The two can be prepared simultaneously and assembled at the end. After the prototype is built, it will be validated using the tests described in Figure 22.2.

[1] `https://www.easa.europa.eu/easa-and-you/aircraft-products/aircraft-certification`, last accessed 21/06/2018

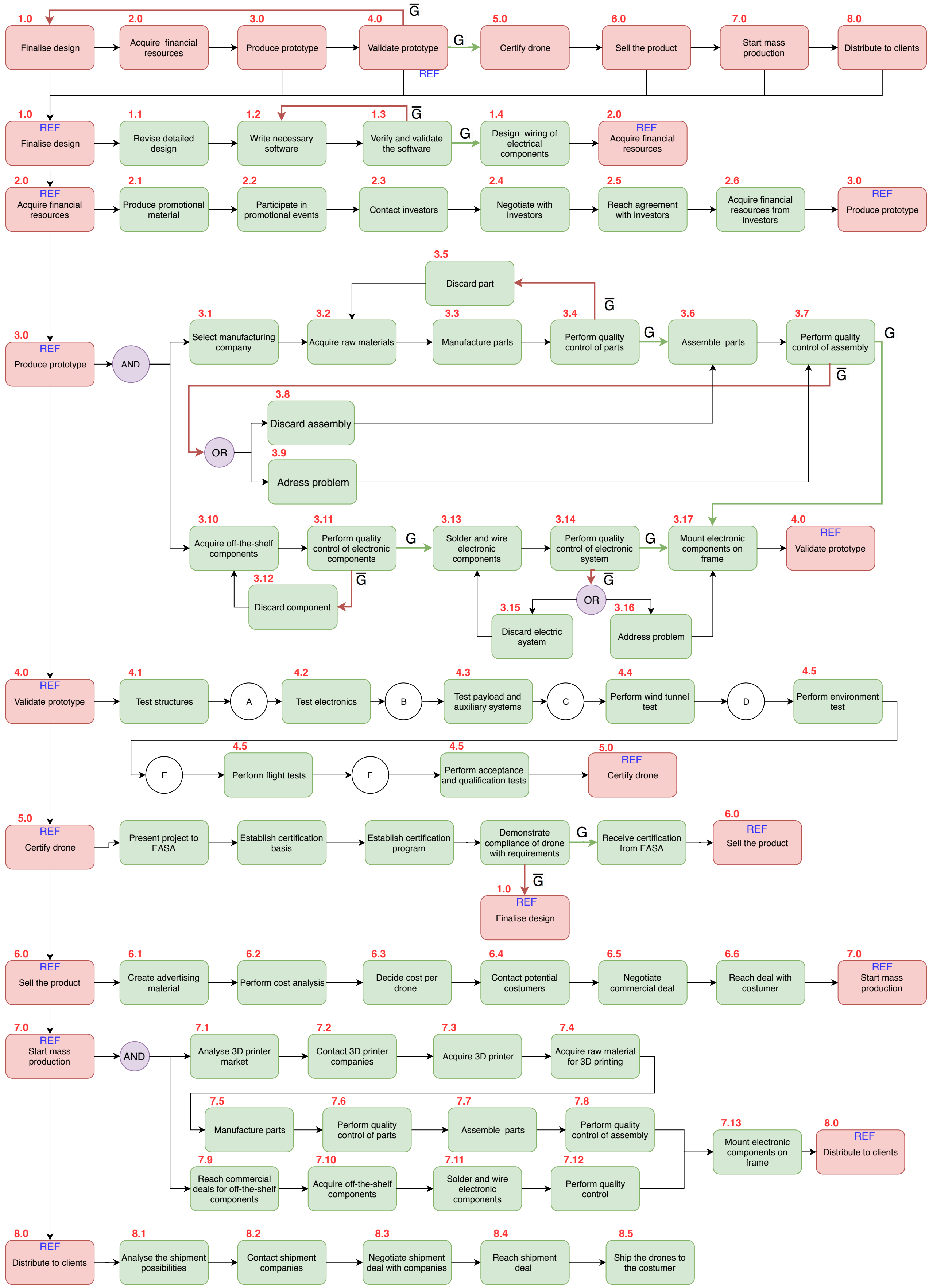

Figure 22.1: Post-DSE work flow diagram.

Since the different tests cannot be conducted simultaneously because there will be only one prototype, the expected time of the validation procedures is one month. After it has been validated, it is possible that the entire design has to be iterated. If this is not the case, the drone will be certified following the steps explained in section 17.2, which can be summarised as shown in Figure 22.3. If the drone is certified, it can be sold and distributed to clients. The team will start creating advertising material at a later stage of the certification procedure. This is because in case the drone is not given the certification and the design needs to be iterated, the advertising material would not be useful. Potential clients will be contacted and agreements will be reached with them. Production can be started slightly before the agreement is finalised since the team will have an idea of the production rate that is necessary to meet the demand. Finally, the drones will be shipped to the client. These last steps will be repeated indefinitely if the drone is successful.

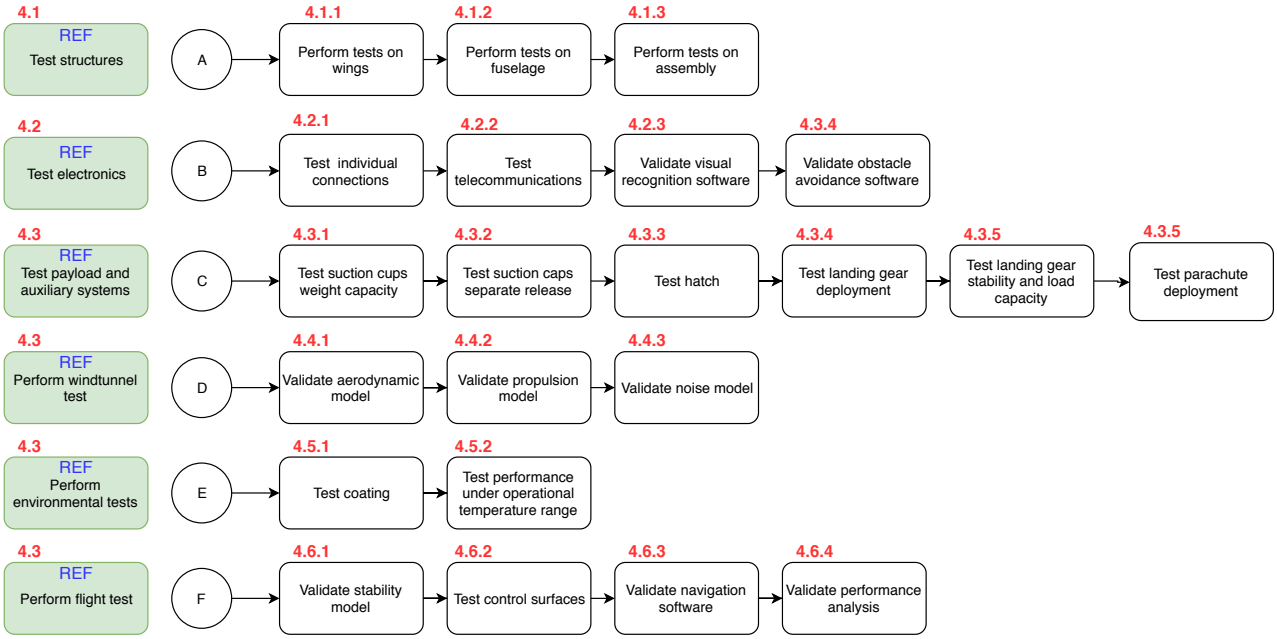

Figure 22.2: Expansions of Figure 22.1

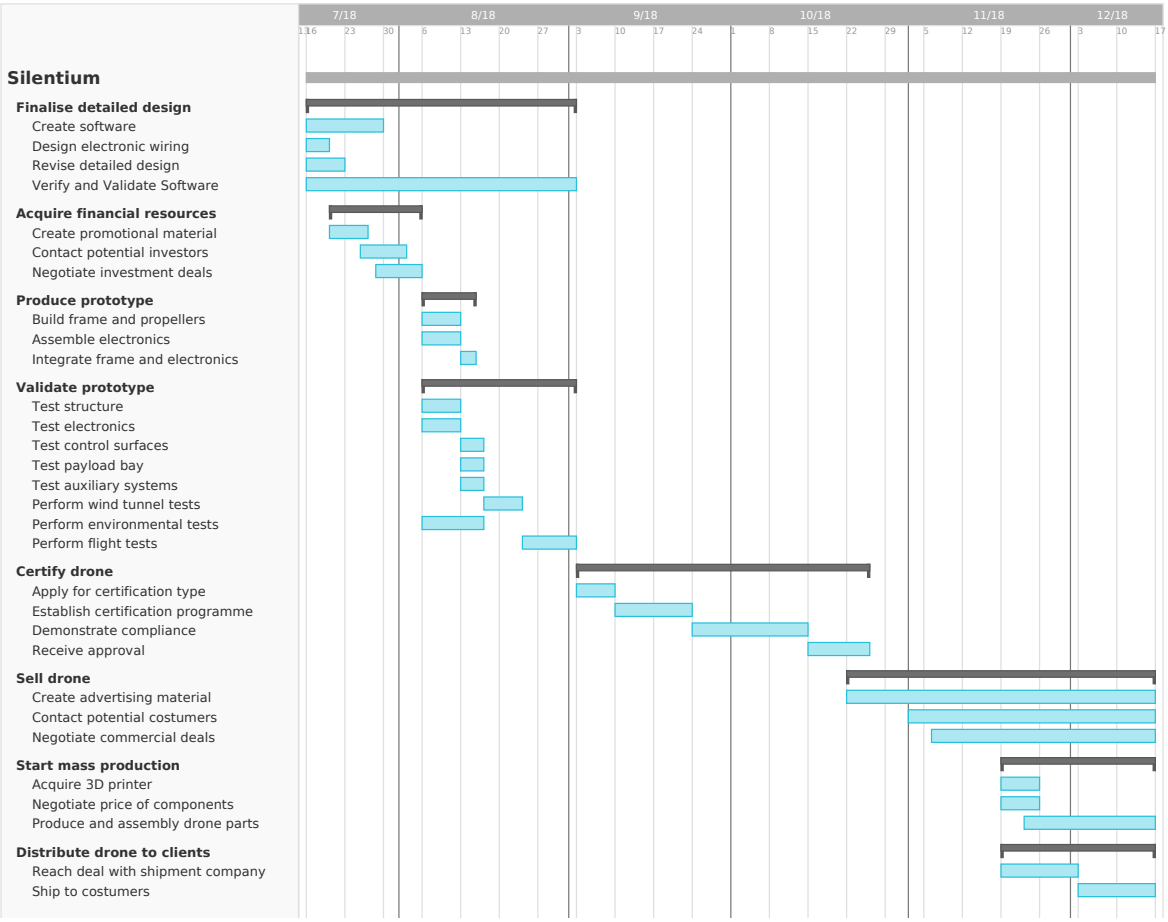

Figure 22.3: Project Gantt chart.

23

Conclusion

This report presents the detailed design of the winning conceptual design for a silent delivery drone from the midterm report. Furthermore, general aspects surrounding the drone, such as a market analysis, operations, sustainability and manufacturing were updated and further worked out.

The final design is a flying wing/blended wing body configuration with four propellers used during vertical take-off and landing and one pusher propeller used during cruise flight (shown in Figure 23.1). The batteries, payload bay, avionics and computer systems are located within the centre body.

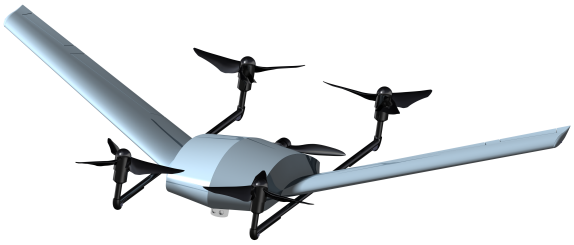

Figure 23.1: Final design of the silent delivery drone.

The main parameters of the final design were identified and shown below.

- Max take-off weight: 13.7 kg
- Number of propellers: 4 VTOL and 1 FW
- Cost: 23,225 $
- Return on investement : 13.3 %
- Cruise speed: 18.75 m/s
- Wing span: 2.08 m
- Surface Area: 0.79 m^2

Furthermore, the following most important aspects of each subsystem are given:

- **Data handling and communication:** A flight controller is used to process data and send commands to the various subsystems. Mobile broadband is used for communication with the base station.
- **Structure:** The main structure of the wing is a wing-box design with an expected lifetime of 3 years. Both the structure and skin are made of Nylon 6.
- **Wing Design:** The wing uses four different aerofoils, with thicker aerofoils used in the fuselage and thinner aerofoils at the tips of the wings. It has a sweep angle of 35° and dihedral of 22°.
- **Control:** Simulink is used to simulate the complete system. The desired position and heading as a function of time are used as an input for VTOL flight, and velocity, altitude and heading for fixed-wing flight.
- **Navigation:** GPS is the primary means of position determination with Signals of Opportunity as a backup. A laser scanner is used for obstacle avoidance and a camera for landing during the day and at night.
- **Propulsion:** For VTOL propellers with three blades operating at 2500 RPM are used, and for FW two propellers operating at 2400 RPM.
- **Payload Mechanism:** The payload bay is divided into eight units of 105 x 74.25 x 105 mm (w x l x h). The payload is held by a suction mechanism with one suction cup per unit.
- **Auxiliary Systems:** For the landing gear four retracting rods are used. A parachute is installed in case of failure of the propulsive system.

A

Wing Design

Table A.1: Aerodynamic characteristics of trade-off wing aerofoils

Name	Eppler 330	N-11	SD 7090	E 216	S 8036	WASP	NACA 2415	AG 37	Fauvel 14	MH 60
Thickness ratio	11 %	10.9%	10 %	10.4 %	16 %	9.4 %	15 %	7.7 %	14 %	10.1 %
C_l for $\alpha = 0$ [-]	0.02	0.65	0.22	0.835	0.18	0.4	0.24	0.38	-0.01	0.09
α for $C_l = 0$ [°]	-0.1	-5.9	-2.2	-5.9	-1.7	-3.2	-2.3	-3.5	0.09	-0.7
$C_{l_{max}}$ [-]	1.29	1.47	1.42	1.69	1.32	1.4	1.42	1.4	1.35	1.28
α of $C_{l_{max}}$ [°]	12	11	14	12.5	18	12.5	15.5	11	12.5	13
$C_{d_{min}}$ [-]	0.007	0.0066	0.0056	0.0066	0.0080	0.0058	0.0072	0.0050	0.0077	0.0056
C_l of $C_{d_{min}}$ [-]	-0.15	0.6	0.22	0.78	-2	0.4	0.29	0.2	-0.01	0
$(C_l/C_d)_{max}$ [-]	85	105	86.5	141	90.5	100	90	88	93.5	86
C_l of $(C_l/C_d)_{max}$ [-]	1.06	0.85	0.77	1.05	0.87	0.95	0.89	0.76	1.14	0.79
Cruise C_m [-]	0.014	-0.098	-0.04	-0.2	-0.034	-0.069	-0.055	-0.043	0.02	-0.009

Table A.2: Aerofoils considered for the fuselage

Name	NACA 0021	NACA 2421	NACA 4421	NACA 64(4) 221	GEO 777 aerofoil
Thickness ratio	21%	21%	21%	21%	22%
C_l for $\alpha = 0$ [-]	0	0.24	0.47	0.17	0.53
α for $C_l = 0$ [°]	0	-2.3	-4.5	-1.5	-4.9
$C_{l_{max}}$ [-]	1.36	1.43	1.40	0.93	1.24
α of $C_{l_{max}}$ [°]	16.5	15.4	12.2	7.0	6.2
$C_{d_{min}}$ [-]	0.0073	0.0077	0.008	0.007	0.0099
C_l of $C_{d_{min}}$ [-]	0.8	0.9	1.08	0.91	1.2
$(C_l/C_d)_{max}$ [-]	80.7	89.8	112.9	112.3	117.4
C_l of $(C_l C_d)_{max}$ [-]	0.99	0.85	0.99	0.90	1.20
Cruise C_m [-]	0.015	-0.033	-0.061	-0.002	-0.041

Bibliography

[1] Activiteitenbesluit milieubeheer (BWBR0022762) (artikel 2.17, lid 1) [Activity decision environmental management (BWBR0022762) (section 2.17, clause 1)].

[2] Annual report 2016. *Post NL*.

[3] Adkins, C. N. and Liebeck, R. H. . Design of optimum propellers. *Journal of Propulsion and Power*, 10(5): 676–682, 1994.

[4] Anderson, D. . Presentation on Integrated Navigation. *University of Glasgow*.

[5] Betz, A. . Screw propellers with minimum energy loss. *Gottingen Reports*, pages 193–213., 1919.

[6] Chen, A. T. and Wojcik, R. T. . Polyurethane coatings for metal and plastic substrates. *Metal Finishing*, 98(6):143 – 154, 2000. ISSN 0026-0576. doi: 10.1016/S0026-0576(00)80405-5.

[7] Chen, W. and Bernal, L. . Design and performance of low reynolds number airfoils for solar-powered flight. In *46th AIAA Aerospace Sciences Meeting and Exhibit*, page 316, 2008.

[8] de Alvear Cárdenas, J.I., Eggers, Y., van Hoorn, F., Jou Ferrer, L., Oosterhof, E., Stikker, R., . . . van der Waals, M., . A silent delivery drone: Baseline, May 2018.

[9] de Alvear Cárdenas, J.I., Eggers, Y., van Hoorn, F., Jou Ferrer, L., Oosterhof, E., Stikker, R., . . . van der Waals, M., . A silent delivery drone: Midtermn, May 2018.

[10] de Alvear Cárdenas, J.I., Eggers, Y., van Hoorn, F., Jou Ferrer, L., Oosterhof, E., Stikker, R., . . . van der Waals, M., . A silent delivery drone: Project plan, April 2018.

[11] Debnatha, B. , Roychowdhuryb, P. , and Kunduc, R. . Electronic components (ec) reuse and recycling – a new approach towards weee management. *Procedia Environmental Sciences*, 35:656 – 668, 2015.

[12] Gnel, O. , Yavuk, T. , and Koç, E. . CFD vs. XFOIL airfoil analysis at low reynolds numbers. *International Conference on Renewable Energy Research and Application*, 2016.

[13] Gray, L. , Magliozzi, B. , Metzger, F. B. , and Towle, G. B. . A study of propeller noise research. 1961.

[14] Grigore, M. E. . Methods of recycling, properties and applications of recycled thermoplastic polymers. 2017.

[15] Guerra, L. . Space systems engineering margins and contingency module. *NASA Exploration Systems Mission Directorate, Washington, DC*, 2008.

[16] Gutin, L. . Uber das schallfeld enier retierenden luftschraube. *Physikalische Zeitschrift der Sowjetunion*, 9, 1936.

[17] Hardin, L. , Tillman, G. , Sharma, O. , Berton, J. , and Arend, D. . Aircraft system study of boundary layer ingesting propulsion. 2012.

[18] Hartuc, T. . Boundary layer ingestion, theoretical and experimental research. 2015.

[19] Hoerner, S. . *Fluid-Dynamic Drag*. By the author, 1965.

[20] Hoerner, S. F. and Borst, H. V. . *Fluid-dynamic lift*. Hoerner, 1992.

[21] Intravartolo, N. , Sorrells, T. , Ashkharian, N. , and Kim, R. . Attenuation of vortex noise generated by uav propellers at low reynolds numbers. In *55th AIAA Aerospace Sciences Meeting*, page 2019, 2017.

[22] Jenkins, D. , Vasig, B. , Oster, C. , and Larsen, T. . Forecast of the commercial uas package delivery market. 2017.

[23] Joerss, M. , Schröder, J. , Neuhaus, F. , Klink, C. , and Mann, F. . Parcel delivery: The future of last mile. 2016.

[24] Kemp, C. F. B. . Some properties of the sound emitted by airscrews. *Proceedings of the Physical Society*, 44(2): 151, 1932.

[25] King, D. W. , Bertapelle, A. , and Moses, C. . UAV failure rate criteria for equivalent level of safety. September 2005.

[26] Kurtz, D. and Marte, J. . A review of aerodynamic noise from propellers, rotors, and lift fans. 1970.

[27] Lee, H. M. , Lu, Z. , and Lee, H. P. . Quieter propellers. 2017.

[28] Lozano-González, J. . Physical–mechanical properties and morphological study on nylon-6 recycling by injection molding.

[29] McCrink, M. and Gregory, J. W. . Blade element momentum modeling of low-re small uas electric propulsion systems. In *33rd AIAA Applied Aerodynamics Conference*, page 3296, 2015.

[30] Megson, T. . *Aircraft Structures for Engineering Students*. Elsevier Aerospace engineering series, Oxford (UK), fifth edition, 2012.

[31] Messler, R. J. . *Joining of Materials and Structures - From Pragmatic Process to Enabling Technology*. Elsevier, Oxford, 2004.

[32] Morales, J.J. and Roysdon, P.F. and Kassas, Z.M., . Signals of opportunity aided inertial navigation, 2016.

[33] Moreau, D. , Brooks, L. , and Doolan, C. . On the noise reduction mechanism of a flat plate serrated trailing edge at low-to-moderate reynolds number. In *18th AIAA/CEAS aeroacoustics conference (33rd AIAA aeroacoustics conference)*, page 2186, 2012.

[34] Mulder, J. , van Staveren, W. , van der Vaart, J. , de Weerdt, E. , de Visser, C. , in t' Veld, A. , and Mooij, E. . *Flight Dynamics*. TU Delft, Delft, 2013.

[35] Opinion No 01/2018. Introduction of a regulatory framework for the operation of unmanned aircraft systems in the open and specific categories. *EASA*, 2018.

[36] Purdue, . XFLR5 Analysis of foils and wings operating at low reynolds numbers. 2009.

[37] Raymer, D. P. . Aircraft design: a conceptual approach. In *3.4.4 L/D Estimation*, page 40, 2012.

[38] Reimann, S. , Amos, J. , Bergquist, E. , Cole, J. , Phillips, J. , and Shuster, S. . UAV for reliability. December 2013.

[39] Shafer, T. , Lynch, C. , Viken, S. , Favaregh, N. , Zeune, C. , Williams, N. , and Dansie, J. . Comparison of computational approaches for rapid aerodynamic assesment of small uavs. 2018.

[40] Stinskas, A. V. , Antropova, N. I. , Korobov, V. I. , Ratner, S. B. , Samokhvalov, A. V. , and Sharova, A. V. . Fatigue properties of kapron (nylon-6) and kaprolon. *Polymer Mechanics*, 1(2):90–92, Mar 1965. ISSN 1573-8922. doi: 10.1007/BF00860690.

[41] Stoll, A. M. . *Design of quiet UAV propellers*. PhD thesis, Stanford University, 2012.

[42] Tyan, M. , Nguyen, N. V. , Kim, S. , and Lee, J.-W. . Comprehensive preliminary sizing/resizing method for a fixed wing – VTOL electric UAV. *Aerospace Science and Technology*, 71:30 – 41, 2017. ISSN 1270-9638. doi: 10.1016/j.ast.2017.09.008.

[43] Woodman, O. J. . An introduction to inertial navigation. August 2007.